DEPARTMENT OF
CIVIL AND ENVIRONMENTAL ENGINEERING

HETEROGENEOUS PHOTOCATALYSIS, SONOLYSIS AND SONOPHOTOCATALYSIS FOR THE REMOVAL OF SELECTED PHARMACEUTICAL COMPOUNDS FROM AQUEOUS MATRICES

Antigoni Achilleos

« A Dissertation Submitted in Partial Fulfillment of the Requirements for the Degree of Doctor of Philosophy at the University of Cyprus »

May, 2011

In memory of my mother

and to my husband Spyros

UNIVERSITY OF CYPRUS

DEPARTMENT OF EDUCATION

Dissertation Acceptance

This is to certify that this dissertation prepared

By Antigoni Achilleos

Entitled Heterogeneous Photocatalysis, Sonolysis and Sonophotocatalysis for the Removal of Selected Pharmaceutical Compounds from Aqueous Matrices

Complies with University regulations and meets the standards of the University for originality and quality

For the degree Doctor of Philosophy

This dissertation was successfully presented and defended to examining committee on Monday 30th of May 2011

Major Professor Dr. Despo Fatta-Kassinos

Advising committee Professor Michael Petrou

Professor Dionissios Mantzavinos

Assistant Professor Konstantinos Kostarelos

Assistant Professor Fatone Francesco

Ph.D. examination committee

Scientific/Academic Advisor

.....

Dr. Despo Fatta-Kassinos

Assistant Professor

Department of Civil and Environmental Engineering

University of Cyprus

Members of the committee

.....	.....
Dr. Konstantinos Kostarelos	Dr. Michalis Petrou
Assistant Professor	Professor
Department of Civil and Environmental Engineering	Department of Civil and Environmental Engineering
University of Cyprus	University of Cyprus
(President of the committee)	
.....	.....
Dr. Dionissios Mantzavinos	Dr. Francesco Fatone
Professor	Assistant Professor
Environmental Engineering Department	Department of Biotechnology
Technical University of Crete	University of Verona

AKNOWLEDGEMENTS

Pursing a Ph.D. was sometimes stressful, complicated, tyring and even sometimes disappointing; however at most times it was challenging and I would say enjoyable. I have been writing, rewriting and re-rewriting new texts and old texts. A lot of experimental work to do and a lot of elaboration.

However none of this work would have seen the daylight without the fantastic network of people who surrounds and supports me – colleagues, family and friends.

This research work has been carried out at the GAIA- Laboratoty of Environmental Engineering of the Department of Civil and Environmental Engineering of the University of Cyprus, between the years 2005 and 2011.

I would like to express my thankfulness to my research supervisor Assistant Professor Dr. Despo Fatta-Kassinos for giving me the opportunity to join her research group, for her continuous guidance, support and advices through all these years for opening to me so many opportunities and for helping me achieving my goal.

I would like to thank warmly my Ph.D. examination committee members Professor Dionissios Mantzavinos, Professor Michael Petrou the Assistant Professor Fatone Francesco and the assistant professor Konstantinos Kostarelos.

I would also like to express my deepest gratitude and appreciation to Dr. Mira Petrovic, Dr. Sandra Perez Solsona, Aleksandra Jelik and Victoria Osorio Torrens from CSIC, Spain for their prompt response to all my requests and for so generously sharing their knowledge on mass spectrometry and elucidation of pharmaceutical transformation products.

I am thankful to Dr. Dimitra Lambropoulou lecturer in the Aristotle University of Thessaloniki for her willingness to help me through the elucidation of pharmaceutical transformation products.

I also appreciate the help provided by my colleagues of the Gaia- Laboratory of Environmental Engineering of the Department of Civil and Environmental Engineering of the University of Cyprus. Especially I would like to thank Dr. Evroula Hapeshi and Marlen Inez Vasquez Hatzylira for the valuable collaboration on the heterogeneous photocatalysis and toxicity studies.

I would also like to express my gratitude to the staff and the Director of the State General Laboratory of Cyprus for their collaboration in the analysis of total organic carbon and especially the chemists Mrs Christiana Frangopoulou and Dr. Eleni Loizou.

My co-workers/friends from the State General Laboratory Mrs Evgenia Paraskeva Vatyliotou and Mrs Nektaria Varnava for their encouragement.

Also I would like to thank Dr. Costas Michael and Dr. Stella Kanna Michaelidou ex- directors of the State General Laboratory for supporting this thesis. I would always carry with me their advices.

Last but not least, I would like to thank my husband Spyros for his love and firm support for making my dream coming true.

ABSTRACT

In Cyprus, due to the severe water scarcity problem, the government turned its attention towards the utilization of every drop of water through the reuse of treated wastewater for irrigation

Pharmaceuticals constitute one category of xenobiotic compounds that raises a lot of concern because they are designed to be biologically active and most often escape urban wastewater treatment plants (WWTPs) intact. There are two main routes for pharmaceuticals to enter the environment. The first route is through WWTPs after excretion, unchanged through urine and faeces or as metabolites. The second route is through the disposal of unused and expired medication via toilet/sink seems. These molecules are later released into the environment mostly through WWTPs effluents or landfill leachates.

The accumulation of pharmaceuticals in the environment raised the need for further advanced treatment for their removal from natural waters. Advanced chemical oxidation processes like heterogeneous photocatalysis, sonolysis and sonophotocatalysis have turned out to be a promising tool for water and wastewater treatment, and have gained considerable attention due to their ability to degrade a wide class of pollutants. The effort and necessity to remove such pollutants stem from the potential of various chemicals or of their mixtures to induce adverse effects to environmental organisms even in very low concentrations during long-term exposure. TiO_2 photocatalysis is an emerging treatment technology for the destruction of various micropollutants found in effluents with key advantages including no mass transfer limitations (when TiO_2 is in slurry form), operation at ambient conditions and the possible use of solar irradiation.

Among the groups of pharmaceutical compounds of greatest environmental interest are the nonsteroidal anti-inflammatory drugs (NSAIDs) such as diclofenac (DCF) and ibuprofen (IBP) and the antiepileptic pharmaceutical compound carbamazepine (CBZ). These compounds were chosen to be further investigated in this thesis because they belong among the top ten pharmaceuticals mostly consumed on national level (DCF and IBP) and also being detected in high concentrations in the final effluents of Urban Wastewater Treatment Plants (WWTPs) of Cyprus (DCF, IBP and CBZ).

The aim of this thesis was to study the conversion/mineralization of DCF, IBP and CBZ, in ultrapure water, urban wastewater and groundwater by means of photocatalysis using UV-A and simulated solar irradiation, sonolysis and sonophotocatalysis, in respect to the operating conditions at bench scale, the toxicity potency developed during and after treatment and the elucidation of the transformation products.

The main innovative activities and aspects of this thesis can be summarized as follows:

- The quantities of pharmaceuticals consumed on annual basis in Cyprus were calculated in collaboration with the Pharmaceutical Services of Cyprus.
- Through an algorithm, the concentrations of the pharmaceuticals that are expected to end up in the sewage treatment plants were determined (this was done for the compounds mostly consumed on national level).
- A heterogeneous photocatalysis process was developed and applied for the removal of the above active pharmaceutical ingredients using an ultra pure water and an actual wastewater matrix and groundwater via artificial UV-A and simulated solar light.
- A sonochemical oxidation process was developed and applied for the removal of selected active pharmaceutical ingredients from aqueous solutions.
- A combined sonolytic-photocatalytic process (sonophotocatalysis) was developed and applied for the oxidation and removal of selected active pharmaceutical ingredients from aqueous solutions.
- The performance of the three methods was evaluated on the removal of total organic carbon, the reduce in the absorption of the solutions with UV-Vis, and the quantification of the initial concentrations of the three pharmaceutical substances with HPLC / ESI-QqLIT-MS at the optimum combination with catalyst loading.
- Identification and quantification of metabolites by UPLC/ESI-QqToF-MS was carried out.
- A toxicity method was applied (*Daphnia magna*) in order to evaluate the toxicity of selected pharmaceutical compounds and to evaluate the toxicity of the various intermediate oxidation products that are formed during the application of the advanced oxidation methods.

ΠΕΡΙΛΗΨΗ

Στην Κύπρο λόγω του έντονου προβλήματος έλλειψης νερού η κυβέρνηση εδώ και αρκετά χρόνια έχει στρέψει την προσοχή της προς την εκμετάλλευση κάθε σταγόνας διαθέσιμου νερού και κυρίως προς την επαναχρησιμοποίηση των επεξεργασμένων αστικών λυμάτων για αρδευτικούς σκοπούς.

Η ύπαρξη ξενοβιοτικών ενώσεων στα αστικά λύματα αποτελεί σήμερα ένα νέο πεδίο έρευνας αλλά ταυτόχρονα ακόμα μία ανησυχία αναφορικά με τις επιπτώσεις που μπορεί οι ενώσεις αυτές να επιφέρουν τόσο στο περιβάλλον αλλά και την ανθρώπινη υγεία μέσω της διοχέτευσης των επεξεργασμένων λυμάτων σε υδάτινα σώματα, στη θάλασσα ή προς άρδευση.

Οι ξενοβιοτικές ενώσεις όμως, δηλαδή οι ενώσεις που είναι ξένες προς τον άνθρωπο και τη φύση, δεν αποικοδομούνται εύκολα και ούτε απομακρύνονται σε ικανοποιητικό βαθμό με τις 'παραδοσιακές' μεθόδους που εφαρμόζονται. Μια νέα κατηγορία χημικών ουσιών που εξετάζεται σήμερα σε νερά και υγρά απόβλητα διεθνώς είναι αυτή των φαρμακευτικών καταλοίπων.

Οι σταθμοί επεξεργασίας λυμάτων είναι οι κύριες πηγές απόρριψης τέτοιων ουσιών στο περιβάλλον. Στην πραγματικότητα μετά τη χρήση των φαρμακευτικών ουσιών τα ενεργά τους συστατικά αποβάλλονται από τον ανθρώπινο οργανισμό είτε σε μεταβολισμένη είτε σε μη μεταβολισμένη μορφή με αποτέλεσμα να εισέρχονται στα αποχετευτικά συστήματα και στη συνέχεια στους σταθμούς επεξεργασίας αστικών λυμάτων.

Η έρευνα αυτή επικεντρώθηκε στην ανάπτυξη τεχνολογιών προχωρημένης χημικής οξείδωσης (ετερογενούς φωτοκατάλυσης, εφαρμογή υπερήχων και σονοφωτοκατάλυσης) για την διερεύνηση της ικανότητας διάσπασης / οξείδωσης / απομάκρυνσης της δικλοφαινάκης (DCF), ιβουπροφαίνης (IBP) και καρβαμαζεπίνης (CBZ) σε εμβολιασμένα υδατικά δείγματα αλλά και πραγματικά λύματα. Κατά την ετερογενή φωτοκατάλυση εφαρμόστηκε τόσο τεχνητό φως UV-A όσο και ηλιακό μέσω ηλιακού προσομοιωτή. Οι πιο πάνω φαρμακευτικές ουσίες επιλέγηκαν καθότι δύο από αυτές (DCF και IBP) συγκαταλέγονται μέσα στις πρώτες σε κατανάλωση στην Κύπρο ουσίες τόσο στον ιδιωτικό τόσο και στον κρατικό τομέα.

Επιπλέον και οι τρεις προσδιορίσθηκαν σε αστικά λύματα στους κυριότερους σταθμούς επεξεργασίας λυμάτων της Κύπρου (DCF, IBP και CBZ) σε σημαντικές συγκεντρώσεις.
Μέθοδοι εκτίμησης της τοξικότητας, εφαρμόσθηκαν τόσο για να εξετασθεί η τοξικότητα των επιλεγμένων φαρμακευτικών ουσιών (DCF, IBP και CBZ) όσο και για να εκτιμηθεί η τοξικότητα των ενδιάμεσων ενώσεων που δημιουργούνται κατά την εφαρμογή των διαφόρων τεχνολογιών οξείδωσης έτσι ώστε να διαφανεί εάν η προχωρημένη χημική οξείδωση μέσω κατάλυσης, υπερηχοβόλησης και σονοφωτοκατάλυσης μπορεί να απομακρύνει τόσο τις ίδιες τις ενώσεις όσο και την πιθανή τοξικότητα τους.

Η πρωτοπορία της παρούσας έρευνας, έγκειται στα ακόλουθα:

- για πρώτη φορά στην Κύπρο με τη βοήθεια των Φαρμακευτικών Υπηρεσιών του Υπουργείου Υγείας, προσδιορίστηκαν οι ποσότητες των φαρμάκων που καταναλώνονται στην Κύπρο σε εθνικό επίπεδο.
- υπολογίστηκαν οι συγκεντρώσεις των ουσιών που καταναλώνονται περισσότερο και οι οποίες αναμένεται να καταλήγουν στους σταθμούς επεξεργασίας αστικών λυμάτων μέσω ενός αλγόριθμου πρόγνωσης των ποσοτήτων αυτών.
- Σχεδιάστηκε και εφαρμόσθηκε ετερογενής φωτοκατάλυση για την απομάκρυνση επιλεγμένων φαρμάκων τόσο με τη χρήση τεχνητού φωτός UV-A όσο και ηλιακού προσομοιούμενου φωτός.
- Σχεδιάστηκε και εφαρμόσθηκε τεχνική υπερηχοβόλησης για την απομάκρυνση των επιλεγμένων φαρμάκων από διάφορα υδατικά διαλύματα.
- Εφαρμόσθηκε συνδυασμένη υπερηχο-φωτοκατάλυση (ή διαφορετικά σονοφωτοκατάλυση) με στόχο και πάλι την απομάκρυνση επιλεγμένων φαρμακευτικών ουσιών από διάφορα υδατικά διαλύματα.
- Η απόδοση των τριών μεθόδων που αναπτύχθηκαν και εφαρμόσθηκαν αξιολογήθηκε με βάση την απομάκρυνση του ολικού οργανικού άνθρακα, τη μείωση της απορρόφησης UV-Vis από τα διαλύματα, καθώς και με βάση την ποσοτικοποίηση με τη μέθοδο HPLC/ESI-QqLIT-MS μέσω χρωματογραφίας των αρχικών συγκεντρώσεων των τριών ουσιών.
- Έγινε ταυτοποίηση και ποσοτικοποίηση οξειδωμένων παραπροϊόντων μέσω UPLC/ESI-QqToF-MS και για τις τρεις μεθόδους επεξεργασίας.

- Εφαρμόσθηκαν έλεγχοι τοξικότητας όπως *Daphnia Magna* για να εξετασθεί η τοξικότητα των επιλεγμένων φαρμακευτικών ουσιών και των ενδιαμέσων ενώσεων που δημιουργούνται για όλες τις μεθόδους επεξεργασίας.

Contents

List of Tables

List of Figures

List of Acronyms

AOPs	Advanced Chemical Oxidation Processes
APIs	Active Pharmaceutical Ingredients
ATC	Anatomical Therapeutic Chemical Classification code
BOD_5	Biological Oxygen Demand
CBZ	Carbamazepine
CE	Capillary Electrophoresis
CID	Collision Induced Dissociation
COD	Chemical Oxygen Demand
DCF	Diclofenac
DDDs	Defined Daily Doses
DO	Dissolved Oxygen
DOC	Dissolved Organic Carbon
DOM	Dissolved Organic Matter
D_{ow}	Octanol/water distribution coefficient
EDCs	Endocrine Disrupting Compounds
EMEA	European Agency for the Evaluation of Medicinal Products
EPI	Enhanced Product Ion
GC	Gas Chromatography
GW	Groundwater
HPLC	High Pressure Liquid Chromatography
HRT	Hydraulic Retention Time
IBP	Ibuprofen
IC	Inorganic Carbon
IDA	Information Dependent Acquisition
IT	Ion-Trap
KHP	Potassium Hydrogen Phthalate
K_{ow}	Octanol/water partition coefficient
LOD	Limit of Detection
LOQ	Limit of Quantitation
MCM	Million Cubic Meters

MECs	Measured Environmental Concentrations
MS	Mass Spectroscopy
NPOC	Non Purgeable Organic Carbon
NSAIDs	Non-steroidal anti-inflammatory drugs
PAHs	Polyaromatic Hydrocarbons
PC	Photocatalysis
PCBs	Polychlorinated Biphenyls
PECs	Predicted Environmental Concentrations
Pop	Population
PPRIs	Photochemically Produced Reactive Intermediates
QqLIT	Quadrupole Linear Ion Trap
QqQ	Triple Quadrupole
QqTOF	Hybrid quadrupole-Time-Offlight
S	Solar
SPC	Sonophotocatalysis
SRM	Selected Reaction Monitoring
SRT	Sludge Retention Time
TC	Total Carbon
TOC	Total Organic Carbon
TPs	Transformation products
TSS	Total Suspended Solids
UHPLC	Ultra-High Performance Liquid Chromatography
UNEP	United Nations Environmental Programme
UV-Vis	Ultraviolet- Visible
WFD	Water Framework Directive
WWTPEf	Effluent of a local urban Wastewater Treatment Plant
WWTPs	Urban Wastewater Treatment Plants
UNEP	United Nations Environmental Programme

CHAPTER 1

PHARMACEUTICALS IN AQUEOUS MATRICES AND ADVANCED OXIDATION PROCESSES

1.1 Wastewater as a non-conventional water resource and the presence of xenobiotics

Water scarcity and water pollution pose a critical challenge in many parts of the world. In urban areas, in various countries, it is becoming difficult for the authorities to manage efficiently water supply and demand. According to various water strategies, wastewater reuse can improve the overall urban water management (UNEP, 2000). At the same time, water-related problems are increasingly recognized as one of the most immediate and serious environmental threats to human kind. Water use has more than tripled globally since 1950, and one out of every six persons does not have regular access to safe drinking water. Lack of access to safe water supply and sanitation affects the health of 1.4 billion people annually (WHO and UNICEF, 2010). The latest Global Environment Outlook of the United Nations Environmental Programme (UNEP), reports that about one third of the world's population currently live in countries suffering from moderate-to-high water stress. Figure 1.1 shows the trends of water scarcity according to the International Water Management Institute (2009).

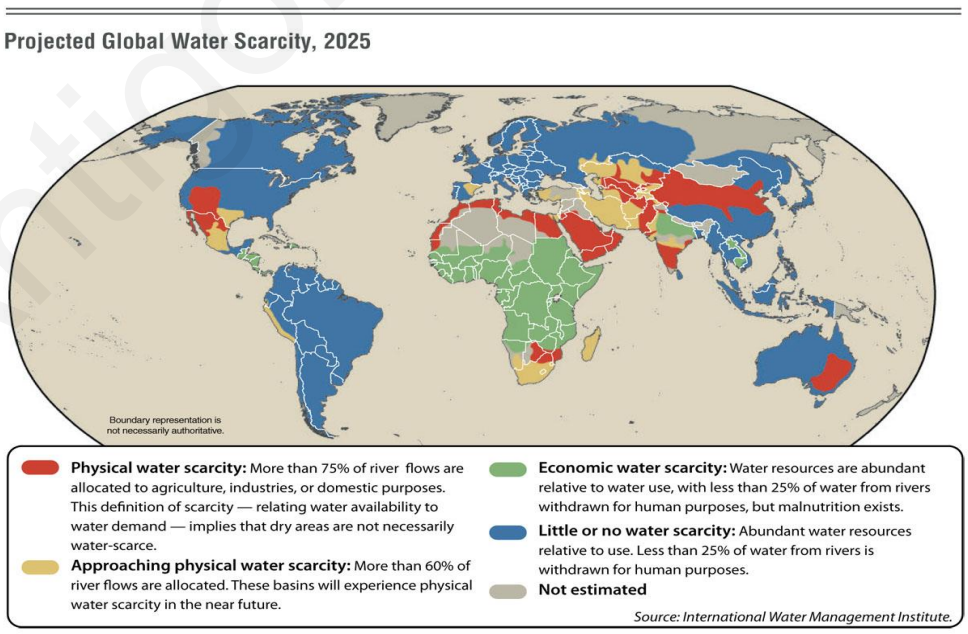

Figure 1.1: Water scarcity trends (International Water Management Institute, 2009)

Approximately half of the European countries are facing water stress issues today (Hochstrat et al., 2003; Bixio et al., 2006). In arid and semi-arid regions, such as Cyprus, there is scarcity of water and the use of treated wastewater for irrigation is an efficient way of conserving fresh valuable water resources. The amount of water, which corresponds to the total surface of the Cyprus Government-controlled area, totals 2,804 MCM whereas only 10% or 280 MCM is considered as inflow since the remaining 90% returns to the atmosphere through evapotranspiration. The mean annual quantity of 280 MCM of water is distributed as 30% surface water and 70% ground water. On average 61 MCM is lost to the sea every year mainly as groundwater seepage.

Agriculture, domestic use and industry are the main economic sectors of water demand. The water demand for agriculture is 168 MCM (65%), and for domestic and industrial use is 92 MCM (35%). It is estimated that the water demand in the Cyprus Government controlled areas will increase from 260 MCM in 2010 to 275 MCM in 2020 (Cyprus Water Development Department, 2011).

Concerning surface water, the average annual inflow to the main dams is about 80 MCM, while the total of all the main dams is 290.8 MCM. During the dry year of 2008 the contribution to irrigation of all dams was only 8.0 MCM. The average annual surface water used for irrigation is 35 MCM, for domestic use (after treatment) is 21 MCM, and for recharge is 9 MCM. Groundwater extraction is estimated to be about 146 MCM on an average annual basis. This figure does not correspond to the sustainable yield of the aquifers, which is much lower. From this amount, 120 MCM are used for agriculture and 26 MCM for domestic demands. Springs contribute very little, mainly for the domestic use of mountainous villages. Desalination units at present contribute up to 50 MCM per year. In Cyprus, to alleviate water shortages, serious consideration has been given to wastewater reclamation and reuse. There are six main urban wastewater treatment plants serving the big urban centers (>1000 p.e.) of the island while another six plants exist serving municipalities with p.e. between 2000-10000, five plants serving communities with p.e. below 2000, five plants serving hospitals and finally nine plants serving military campus. Most of the plants apply tertiary treatment (sand filtration) and disinfection. In order to control the treatment and use of wastewater and thereafter to safeguard the environment and public health, very strict guidelines have been established. These guidelines are stricter than those proposed by the World Health

Organization. In addition the guidelines are followed by a code of practice intended to ensure protection of public health. Reuse is applied only at plants located in big urban centers. Sewage Boards are responsible for the collection and treatment while the Water Development Department undertakes the management of reclaimed water. Tertiary treated wastewater is used to satisfy part of the existing irrigation needs. It is estimated that 59 m^3 of treated effluent will be produced by 2012, (46 m^3 from urban wastewater treatment plants and 13 m^3 from rural wastewater treatment plants) that will be available for agriculture and landscape irrigation. Wastewater reclamation and reuse is a reliable source of water even in drought years and has been the subject of many studies whose main purpose has been the determination of quality criteria for reuse focusing mainly on conventional pollution parameters like Biological Oxygen Demand (BOD_5), Chemical Oxygen Demand (COD), pH, total suspended solids (TSS), heavy metals and microbiological load (viruses, bacteria and protozoa), (Kassinos et al., 2010). Also for plants > 10000 PE a toxicity test should also take place. The acute toxicity inspection must take place once a year and the Gene-toxicity inspection once a year. 75% of the samples must comply with the following limits of toxicity: (i) Microtox, Daphnia and Algae, TU50< 1, (ii) Mutatox, the treated wastewater must not be positive in S9 Mutatox test. It must be mentioned that the existing national guidelines on wastewater reuse tend to focus mainly on risks from pathogens and there is no mention of other trace pollutants such as organic xenobiotics (Kassinos et al., 2010).

The existence of xenobiotic compounds in urban wastewater is nowadays one of the most important research fields in the domain of water management. This is because the presence of xenobiotic compounds constitutes one of the most serious concerns with regard to the possible effects that these compounds may induce on the environment and human health through their introduction via the sewage in the aquatic and terrestrial environment.

The xenobiotic compounds, such as pesticides, alkylphenols, steroids, bisphenols, phthalates, Polychlorinated Biphenyls (PCBs), Polyaromatic hydrocarbons (PAHs) etc, are most often not degradated by conventional treatment processes (Achilleos et al., 2009). During the last several years there has been a growing level of concern related to the hypothesis that various chemicals released through sewage in the environment may exhibit endocrine disrupting effects. This is due to increased incidences of endocrine-related diseases in humans, including declining male fertility, and more significantly, to adverse physiological effects observed in

wildlife where cause and effect relationships are more evident. In fact, the evidence from these incidences suggests that the changes in the reproductive health of humans, including breast and testicular cancer and birth defects could be linked to exposure to Endocrine Disrupting Compounds (EDCs).

Pharmaceuticals constitute one category of xenobiotic compounds that raises a lot of concern because they are designed to be biologically active and most often escape urban wastewater treatment plants (WWTPs) intact. There are two main routes for pharmaceuticals to enter the environment (Bound et al., 2005). The first route is through WWTPs after excretion, unchanged through urine and faeces or as metabolites (Doll et al., 2003). The second route is through the disposal of unused and expired medication via toilet/sink seems. These molecules are later released into the environment mostly through WWTPs effluents or landfill leachates (Sorensen et al., 1998; Ternes et al., 1998; Koplin et al., 2002; Kümmerer et al., 2004; Williams et al., 2005; Cunningham et al., 2006; Nikolaou et al., 2006). Many chemical, physical and biological factors may affect the fate of these molecules in WWTPs, including adsorption/desorption on biosolids (sludge), pH, the ionic strength of the sewage, microbial decomposition rates and the physical and chemical properties of these compounds such as polarity, photostability and volatility (Miao et al., 2005). Therefore WWTPs play an important role in the life cycle of human pharmaceuticals because they act as point sources of these compounds to the environment (Jones et al., 2006). In Figure 1.2 the routes of pharmaceutical compounds in the environment are shown.

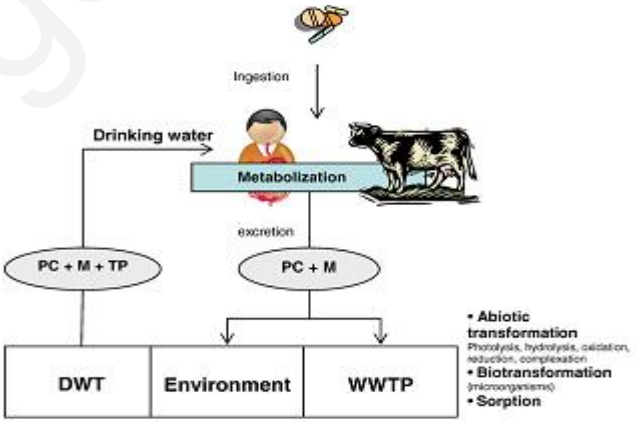

Figure 1.2: Fate of pharmaceuticals in the environment, (Mompelat et al., 2009)

PC: parent compound, M: metabolite(s), TP: transformation products, WWTP: wastewater treatment plant, DWT: drinking water treatment

1.2 Pharmaceuticals' characteristics related to their environmental fate

The characteristics of pharmaceuticals differentiate them from other industrial chemical compounds and this is why they are regarded as special micropollutants (Kassinos et al., 2011). These characteristics include among others polymorphism, their introduction into the environment after human metabolism, their chemically complex structure, and the fact that they can be ionized and have multiple ionization sites spread throughout the molecule (Cunningham, 2008; Kassinos et al., 2011).

1.2.1 Polymorphism

Pharmaceutical compounds exist as solid forms, often as salts and form polymorphs. Polymorphs arise when molecules of a compound are found in the solid state. In addition, solids may form solvates and hydrates also called pseudopolymorphs. Polymorphs including pseudopolymorphs usually differ in bioavailability, solubility, dissolution rate, chemical and physical stability, melting point, colour, filterability, density and flow properties. Active pharmaceutical compounds do exist in these different solid state forms. These forms have different physical chemical properties. The varying water solubility of the various polymorphic forms of pharmaceuticals should always be taken into account. Also, the solubility should be connected with the pH of the matrix in which it is present. These issues may affect not only fate or transport but also assessment of environmental effects (Cunningham, 2008; Kassinos et al., 2011).

1.2.2 Metabolism

Pharmaceuticals are metabolized by a variety of mechanisms. Active pharmaceutical compounds are metabolized and form more polar and water-soluble derivatives that have reduced pharmacological activity compared to the active pharmaceutical compounds and are rapidly excreted. A pharmaceutical compound may contain a group such as -OH, -COOH, -NH_2, - SH which is suitable for combining with a natural compound provided by the body to form water-soluble polar metabolites. Because of glucose availability in biological systems glucuronide formation is one of the more common routes of drug metabolism. Several kinds of drugs tend to form glucuronides, including alcohols, phenols, carboxylic acids, amines and

certain thiols as well as normally occurring substrates such as steroids. Conjugates may also be formed with sulfate.

A parent compound may be excreted:

- Unchanged
- As a glucuronide or sulfate conjugate
- As a major metabolite
- As a complex mixture of many metabolites

It must be noted that there is evidence that glucuronides are capable of being deconjugated to the parent compound during municipal sewage treatment (Cunningham, 2008; Kassinos et al., 2011).

1.2.3 Molecular structure

Pharmaceuticals are not a homogeneous group of compounds. They vary widely in molecular weight, structure, functionality, salt forms, polymorphs, etc. (Roig, 2010)**.** The molecular weights of the chemical molecules range typically from 200 to 500/1000 Da. These are the ones, which are currently being researched and detected in the environment. They are part of the compounds called ‘‘micro-pollutants’’ because they are often found in the mg/L or ng/L range in the aquatic environment (Kümmerer, 2009).

1.2.4 Ionization

The chemically complex character of the molecules and the multifunctional composition of pharmaceutical compounds make them polar, ionizable molecules, and these properties are dependent and influenced by the solution pH. The octanol/water distribution coefficient (D_{ow}) and the octanol/water partition coefficient (K_{ow}) need to be carefully evaluated with regard to multiple ionization sites (Cunningham, 2008; Kassinos et al., 2011).

1.2.5 Dissociation constant

The dissociation constant is an equilibrium constant that describes the degree of ionization of a compound at a known pH.

$$HA \leftrightarrow H^{+} + A^{-} \tag{1.1}$$

$$K_{\alpha} = \frac{[H^{+}].[A^{-}]}{[HA]} \quad (1.2)$$

If there is more than one ionizable functional group in a pharmaceutical compound, then several equilibrium constants can be written for a compound and each must be considered separately. The degree of ionization is controlled by the pH of the solution containing the compound, and the ionized and un-ionized species may have very different properties. The significance of the dissociation constant is the relationship between pka and pH and the resulting distribution of the pharmaceutical in the environment. The ionization degree of a pharmaceutical compound at a particular pH will affect its availability to biological organisms, its chemical and physical reactivity and its ultimate environmental fate (Cunningham, 2008; Kassinos et al., 2011).

1.2.6 Octanol/Water distribution coefficient

The octanol/water distribution coefficient (D_{ow}) is defined as the ratio of the concentration of a chemical in two phases, n-octanol and water when the phases are in equilibrium with one other. The n-octanol water distribution coefficient indicates the tendency of an organic chemical to:

- Partition into lipids or fats
- Sorb to particulates such as soils or sediments
- Sorb to biomass and sludges
- Distribute among the various environmental compartments

The n-octanol/water distribution coefficient is given by:

$$D_{ow} = \frac{\text{concentration in n - octanol}}{\text{concentration in water}} \quad (1.3)$$

It can also be used to predict the bioconcentration potential in aquatic and terrestrial organisms and to estimate the amount of sorption to soils, sediment, biomass and sludges. This is very important for the movement of chemicals in the biosphere (Cunningham, 2008; Kassinos et al., 2011).

1.2.7 Sludge sorption/desorption

The ability to estimate the sorption of a pharmaceutical to solids in various media is critical to understand its environmental fate. The biosolids/water distribution coefficient, $K_{biomass}$ or K_p is the ratio of the concentration of a chemical in two phases, biosolids and water, when the solid phase is biomass and the phases are in equilibrium with each other and the test chemical is a dilute solution in both phases.

Due to all these characteristics, pharmaceuticals are characterized as special pollutants.

1.3 Relevant Legislative Framework

1.3.1 Pharmaceuticals

Policies presented in this part address the framework for issues of authorization of pharmaceutical compounds, water pollution prevention, wastewater treatment as well as monitoring the environmental water quality.

At European level, regulations referring to pharmaceutical compounds and to the environmental risk assessment in relation to their authorization process include: Directive 2004/72/EC on human medicine and Directive 2004/28/EC on veterinary medicine (Roig, 2010). Although separate regulations exist for human medicinal and veterinary compounds these two categories of pharmaceuticals are based on the same principles and are highly similar in content. According to Directive 2004/72/EC on human pharmaceuticals, for all new authorizations the environmental effects must be examined and this assessment must accompany the authorization application. For veterinary pharmaceuticals the situation is different. Contrary to human pharmaceuticals market authorization for veterinary pharmaceuticals can be denied due to an unacceptable risk for the environment (Roig, 2010).

In addition to Directives, specific guidelines are available which recommend the scope and the actual procedure for the environmental impact assessment of medicinal compounds. The environmental risk assessment of human pharmaceuticals is based on the Guidelines of the European Agency for the Evaluation of Medicinal Products (EMEA, 2006). The current EMEA guidance document for human medicinal compounds came into effect in the end of 2006. According to this guidance an environmental risk assessment is required for all new pharmaceutical marketing authorization applications as well as for applications requesting major changes or extensions to existing authorizations which would result to increase of the environmental exposure to pharmaceuticals. In the EMEA guidance document, the environmental risk assessment follows a two-phase assessment. In phase I the drug concentration expected to occur in the aquatic environment is calculated (predicted environmental concentration, $PEC_{surface\ water}$). If the PEC is below a defined action limit of 0.01 μg/L, it is assumed that this specific pharmaceutical compound is unlikely to represent a risk for the environment. Thus the assessment procedure does not continue. If the calculated PEC

is equal or above this action limit, a Phase II environmental fate and effects analysis is required (EMEA, 2006). In Phase II information on the physical, chemical and toxicological properties are obtained and assessed in relation to the extent of the environmental exposure. The phase I is calculated, based on the maximum daily dose (Bound et al., 2004; Bound et al., 2006; Grung et al., 2008).

$$PEC_{surface\ water}(ug/L) = \frac{DOSEai \times Fpen}{WASTEWinha\,b \times DILUTION \times 100} \quad (1.4)$$

where $Dose_{ai}$ is the maximum daily dose, F_{pen} is the market penetration, the proportion being treated daily with a specific drug substance; set to 1%, $WASTEW_{inhab}$ is the volume of wastewater per inhabitant per day, 200 L/inh/d and the DILUTION is 10.

The guidelines suggest that any drug exceeding 0.01 μg/L in surface water should progress to Phase II. Phase II is divided into two tiers. Phase IIA (Tier A) involves the estimate of the PEC to include specific commercial information about the geographical distribution of the drug. The PEC is then recalculated using this new F_{pen}.

$$Fpen = \frac{\text{Total mass of activated ingredient sold} \times 100}{DDD \times \text{Population} \times 365} \quad (1.5)$$

The result is compared with the PNEC using an assessment factor of 1000. According to the guidelines, the risk assessment can be concluded for any drug with PEC: PNEC ratio below 1. The PECs of active substances in surface water is calculated according to the following equation, which is a simplified form of the EMEA algorithm (Stuer-Lauridsen et al., 2000; Jones et al., 2002; Castiglioni et al., 2004; Grung et al., 2008):

$$PEC = \frac{A \times (100 - R)}{365 \times P \times V \times D \times 100} \quad (1.6)$$

where A is the predicted amount used per year (kg/yr) and R (%) is the removal rate. The R is due to loss by adsorption to sludge, by hydrolysis, by volatilization, by biodegradation and etc. P is the number of inhabitants of the geographic area considered, V is the volume of wastewater per day per capita (m^3) and D is the dilution factor (average factor 10).

Accordingly PECs are derived by the first-tier procedure. In second-tier procedure the PNEC (at which a chemical produces adverse effects on organisms) for the aquatic compartment is

estimated from EC_{50} values obtained with acute toxicity tests and by application of an assessment factor. When risk is suspected from this comparison, further considerations on case-by-case bases are subjected to third tier-procedure, including chronic toxicity tests, micro-organism specific test, bioaccumulation study, PEC revision or assessment factor reduced with additional test. When ratio (exposure concentration) equals or exceeds (the effect concentration) to 1, then an ecological risk is suspected (MEC/PNEC≥1). Common criteria for interpreting the ratio or RQ (PEC or MEC/PNEC) establishing different risk levels are as "low risk" from 0.01 through 0.1; "medium risk" from 0.1 through 1, and "high risk" >1 (Hernando et al., 2006).

Based on the concepts and fundamentals, another algorithm was proposed (Ternes et al., 2007), for the calculation of PECs in raw sewage, since sewage treatment plants are the main contributing factors governing the occurrence of pharmaceuticals in the environment. The main emission pathway of pharmaceuticals into wastewater systems is mainly due to the excretion after consumption by patients. The formula applied allows the prediction of the PECs in raw sewage.

$$PEC_{STPin} = \frac{F_{API} \times 10^{12} \times E}{365 \times Pop. \times AWW} \quad (1.7)$$

Where, PEC_{STPin} is the predicted concentration in the raw sewage (ng/L), F_{API} is the consumption of an active pharmaceutical ingredient per year in the area (kg/a), E is the fraction excreted without metabolization in urine, Pop is the population within the area [cap] and AWW is the amount of wastewater per capita and day (L/cap/d). The unchanged excretion rate in urine is the most important factor for calculating the predicted concentration of pharmaceutical in sewers. A commonly used measure of the relative organic solvent solubility is the octanol-water partition coefficient K_{ow}, which is defined as the ratio between the concentrations of the compound in the equal parts of octanol and water. K_{ow}, a key parameter in studies of environmental fate of chemicals, has been found to be related to water solubility, soil and sediment adsorption coefficients. Chemicals with low K_{ow} values, i.e. less than about 10, have high water solubilities and chemicals with high K_{ow} values, i.e. greater than about 1000, are very hydrophobic with low water solubilities.

The value of pka ($pka = -\log Ka = pH - \log(\frac{[A^-]}{[AH]})$) is the negative logarithm of the acidic

dissociation constant for the weak acids. It is an important physico-chemical constant for all processes because the neutral and the ionic forms of the drug typically behave differently. In addition, the organic compounds with low value of pKa can more readily dissociate at the low pH. Pharmaceuticals consumption for 2005 and 2007 and PEC values for Cyprus have been calculated and are shown in Chapter 3.

1.3.2 Water related Policies

Concerning environmental water protection regulations and EU policies, no pharmaceutical compounds are included in the priority list of substances of particular interest to control and monitor. The main reason for this can be seen in the selection process for the first list of priority substances, which dates back almost 10 years and was based on an already existing official list of pollutants. Pharmaceutical compounds are often referred to as emerging pollutants, which means that their presence in and impact on the aquatic environment is just being discovered and researched.

On European level there are no legislative regulations concerning wastewater reuse so far, apart from the Urban Wastewater Treatment Directive (91/271/EEC) which advises to reuse wastewater whenever appropriate (Hochstrat et al., 2006). The Directive 2000/60/EC Water Framework Directive (WFD), requires reaching good status in EU waters by 2015. For surface water good status is defined as the status achieved by a surface water body when both its ecological status and its chemical status are at least good. The requirement of the WFD for good chemical status for water refers to the concentration of substances that are harmful to the ecosystem. A final list of priority substances was published (2455/2001/EC) which became Annex X of the Directive. Annex X of the WFD lists 33 priority substances (mostly organic pollutants) but also some heavy metals and others for which the Commission has to define environmental quality standards. In recent discussions on the proposed Directive of environmental quality standards amending the WFD three pharmaceutical compounds (carbamazepine, diclofenac and iopamidol) were proposed as subject to identification as possible priority substances. However in the final compromise between the European Parliament and Council of Ministers, these pharmaceuticals compounds as well as several other proposed substances were dropped from the finally agreed list of substances to be subject to environmental quality standards under the new Directive (Roig, 2010).

Currently the OSPAR convention is the only regulatory body to consider pharmaceuticals as a threat and this refers to the marine environment. The pharmaceutical compounds clotrimazole (antifungal agent) and diosgenin (steroid) have been listed for priority action, and other drugs have been recognized as being of possible concern (Kassinos et al., 2010).

In conclusion, little has been done so far to prevent pharmaceuticals from entering the environment in the first place; various approaches have been discussed and applied including the control of pharmaceuticals at source, segregation of sources and improvement of disposal systems for expired medicines. However, as there is much uncertainty about the possible detrimental effects of pharmaceuticals on aquatic and terrestrial ecosystems, the precautionary principle should be considered and applied (Kassinos et al., 2010).

1.4 Occurrence of pharmaceuticals in surface waters and wastewater

The concentrations of pharmaceuticals in surface waters and the effluent from WWTPs have been shown to lie in the ng/L to mg/L range. The findings of recent years have been confirmed for different countries and different environmental matrices (Heberer et al., 2001; Ollers et al., 2001; Calamari et al., 2003; Bendz et al., 2005; Miao et al., 2005; Gros et al., 2006; Moldovan et al., 2006; Vieno et al., 2006; Gros et al., 2007; Vieno et al., 2007; Choi et al., 2008; Peng et al., 2008, Kümmerer, 2009; Alder et al., 2010; Fernandez et al., 2010; Munoz et al., 2010; Steene et al., 2010; Yoon et al., 2010).

Pharmaceutical residues measured in surface water have prompted public concerns worldwide. Pharmaceutical compounds as mentioned before are biologically active by design and hence might affect certain keystone species potential leading to disturbance of the ecosystem (Choi et al., 2008). Chronic exposure to certain pharmaceuticals could elicit changes in sex ratio and fecundity of *Daphnia magna* for example (Flaherty et al., 2005; Choi et al., 2008). Pharmaceuticals, which are made to interact with living organisms, can also have acute effects on fauna and flora but due to low concentrations this is not considered as the biggest concern (Jones et al., 2004; Steene et al., 2010). Continuously low inflow of pharmaceuticals could cause subtle chronic changes, which are difficult to detect (Daughton et al., 1999; Steene et al., 2010).

In Tables 1.1 and 1.2, examples of the occurrence of pharmaceutical compounds in surface waters and wastewater are shown.

Table 1.1: Occurrence of pharmaceutical compounds in surface water

a/a	Pharmaceutical compound	Location	Conc. (ng/L)	Reference
1	Acetaminophen	Henares-jarama-tajo river (Spain)	0.1- 43.3	Fernandez et al., 2010
		Han river (Korea)	< 5(LOD)	Choi et al., 2008
2	Atenolol	Henares-jarama-tajo river (Spain)	1.9 - 334.3	Fernandez et al., 2010
		Han river (Korea)	83	Yoon et al., 2010
		Vantaa, Luhtajoki river (Finnland)	25	Vieno et al., 2006
		Vantaa river (Finnland)	55	Vieno et al., 2007
		Ebro river Basin (Spain)	< LOQ – 250	Gros et al., 2006

		Ebro river Basin (Spain) Po and Lambro river (Italy) Warta river (Poland) Hoje river (Sweden) Glatt river (Switzerland)	465 42, 241 3- 22 10-60 < 10 (LOQ)	Gros et al., 2007 Calamari et al., 2003 Kasprzyk-Hordern et al., 2007 Bendz et al., 2005 Alder et al., 2010
3	Atorvastatin	Han river (Korea)	2.6	Yoon et al., 2010
4	Bezafibrate	Henares-jarama-tajo river (Spain)	0.3-46.0	Fernandez et al., 2010
5	Caffeine	Henares-jarama-tajo river (Spain) Han river (Korea) Donana park, watersheds (Spain) Somes river (Romania) Han river (Korea)	12.2 - 417.7 94 < LOD – 0.02 430 - 9700 < 10 - 373	Fernandez et al., 2010 Yoon et al., 2010 Munoz et al., 2010 Moldovan et al., 2006 Choi et al., 2008
6	Carbamazepine	Henares-jarama-tajo river (Spain) Han river (Korea) Donana park, watersheds (Spain) Greifen Lake (Switzerland) Somes river (Romania) Han river (Korea)	0.3-104 44 < LOD – 0.002 35 - 60 65 – 75 < 5 - 36	Fernandez et al., 2010 Yoon et al., 2010 Munoz et al., 2010 Ollers et al., 2001 Moldovan et al., 2006 Choi et al., 2008
7	Chlorpromazine	Henares-jarama-tajo river (Spain)	0.9-2.6	Fernandez et al., 2010
8	Cimetidine	Han river (Korea)	< 20-1338	Choi et al., 2008
9	Clofibrate	Henares-jarama-tajo river (Spain)	0.9-4.9	Fernandez et al., 2010
10	Clofibric acid	Lake Greifen (Switzerland) Peng river Delta (South China)	5- 10 22 - 248	Ollers et al., 2001 Peng et al., 2008
11	Clotrimazole	Tyne river (UK)	6-34	Roberts et al., 2006
12	Codeine	Somes river (Romania)	26.5-53.6	Moldovan et al., 2006
13	Dextropropoxyphene	Tyne river (UK)	< 8-98	Roberts et al., 2006
14	Diazepam	Han river (Korea) Somes river (Romania)	< 0.25 - 0.65 < 30	Yoon et al., 2010 Moldovan et al., 2006
15	Diclofenac	Henares-jarama-tajo river (Spain) Han river (Korea) Donana park, watersheds (Spain) Lake Greifen (Switzerland) River (Switzerland)	0.7-156.0 15 < LOD < LOD – 10 20 – 150	Fernandez et al., 2010 Yoon et al., 2010 Munoz et al., 2010 Ollers et al., 2001 Ollers et al., 2001
16	Diltiazem	Han river (Korea)	< 5-13	Choi et al., 2008

17	Diphenyl hydantoin	Henares-jarama-tajo river (Spain)	0.2-107.4	Fernandez et al., 2010
18	Domperidone	Surface water (Belgium)	< LOQ-297.0	Steene et al., 2010
19	Erythromycin	Surface water (Belgium)	< 4-70	Roberts et al., 2006
20	Flubendazole	Surface water (Belgium)	< LOD-20.2	Steene et al., 2010
21	Fluoxetine	Henares-jarama-tajo river (Spain) Han river (Korea)	0.6 - 66.1 0.78	Fernandez et al., 2010 Yoon et al., 2010
22	Fluphenazine	Henares-jarama-tajo river (Spain)	3.8 - 4.5	Fernandez et al., 2010
23	Gemfibrozil	Han river (Korea) Donana park, watersheds (Spain) River Delta (China)	ND - 7.0 < LOD – 1020 ND	Yoon et al., 2010 Munoz et al., 2010 Peng et al., 2008
24	Hydro chlorotiazide	Henares-jarama-tajo river (Spain)	4.2-960.3	Fernandez et al., 2010
25	Ibuprofen	Henares-jarama-tajo river (Spain) Han river (Korea) Donana park, watersheds (Spain) River Delta (China) Lake Greifen (Switzerland) River (Switzerland) Tyne river (UK) Somes river (Romania)	6.3-2784.0 23 < LOD - 1560 ND - 1417 5 – 15 ND – 80 350 < LOQ - 115	Fernandez et al., 2010 Yoon et al., 2010 Munoz et al., 2010 Peng et al., 2008 Ollers et al., 2001 Ollers et al., 2001 Roberts et al., 2006 Moldovan et al., 2006
26	Iopromide	Han river (Korea)	1013	Yoon et al., 2010
27	Ketoprofen	Henares-jarama-tajo river (Spain) Donana park, watersheds (Spain) Lake Greifen (Switzerland) River (Switzerland)	0.3-991.0 < LOD ND ND - 5	Fernandez et al., 2010 Munoz et al., 2010 Ollers et al., 2001 Ollers et al., 2001
28	Metoprolol	Henares-jarama-tajo river (Spain) Vantaa, Luhtajoki river (Finnland) Vantaa river (Finnland) Hoje river (Sweden) River (The Netherlands) Warta river (Poland) Glatt river (Switzerland)	1.8-26.0 116 107 60 -70 25 – 100 51 – 155 < LOQ - 36	Fernandez et al., 2010 Vieno et al., 2006 Vieno et al., 2007 Bendz et al., 2005 Stolker et al., 2004 Kasprzyk-Hordern et al., 2007 Alder et al., 2010
29	Naproxen	Henares-jarama-tajo river (Spain) Han river (Korea) Donana park, watersheds (Spain)	1.8-640.4 57 0.16	Fernandez et al., 2010 Yoon et al., 2010 Munoz et al., 2010

		Lake Greifen (Switzerland) River (Switzerland) Peng river Delta (China)	ND – 10 10 – 400 ND - 328	Ollers et al., 2001 Ollers et al., 2001 Peng et al., 2008
30	Paraxanthine	Henares-jarama-tajo river (Spain)	0.3-27.8	Fernandez et al., 2010
31	Pipamperone	Surface water from different locations in Belgium	< LOD-961.3	Steene et al., 2010
32	Propiconazole	Surface water from different locations in Belgium	1.9 - 178.3	Steene et al., 2010
33	Propranolol	Henares-jarama-tajo river (Madrid, Spain) River (Germany) River in Southeast England Ebro river Basin (Spain) Hoje river (Sweden) Glatt river (Switzerland) Donana park, watersheds (Southern Spain) Tyne river (UK)	0.1-7.3 590 115 63 10 < LOQ – 8 80 60	Fernandez et al., 2010 Ternes et al., 2001 Ashton et al., 2004 Gros et al., 2007 Bendz et al., 2005 Alder et al., 2010 Munoz et al., 2010 Roberts et al., 2006
34	Salicylic acid	Henares-jarama-tajo river (Spain) Donana park, watersheds (Spain) Somes river (Romania) Peng river Delta (China)	0.1-63.1 0.45 28 – 37 9 - 2098	Fernandez et al., 2010 Munoz et al., 2010 Moldovan et al., 2006 Peng et al., 2008
35	Sotalol	River (Germany) Glatt river (Switzerland)	950 < LOQ - 52	Ternes et al., 2001 Alder et al., 2010
36	Sulfadimethoxine	Henares-jarama-tajo river (Spain) Han river (Korea)	0.4-7.0 < 10 - 13	Fernandez et al., 2010 Choi et al., 2008
37	Sulfamethoxazole	Henares-jarama-tajo river (Spain)	0.1-23.7	Fernandez et al., 2010
38	Sulfamethoxazole	Han river (Korea) Han river (Korea)	31 < 5 - 82	Yoon et al., 2010 Choi et al., 2008
39	Tamoxifen	Tyne river (UK)	31 - 212	Roberts et al., 2006
40	Triclosan	Han river (Korea) Somes river (Romania) Peng river Delta (China)	17 38 35 - 1023	Yoon et al., 2010 Moldovan et al., 2006 Peng et al., 2008
41	Trimethoprim	Henares-jarama-tajo river (Madrid, Spain) Han river (Korea) Tyne river (UK)	0.4 – 23.3 8.9 9 – 12	Fernandez et al., 2010 Yoon et al., 2010 Roberts et al., 2006

		Han river (Korea)	< 10 - 26	Choi et al., 2008

ND- not detected, LOD- limit of detection, LOQ: limit of quantification

As it is shown, the highest concentrations are for caffeine (430-9700 ng/L) in Romania, cimetidine (< 20-1338 ng/L) in Korea, ibuprofen (6.3-2784 ng/L) in Spain and triclosan (35-1023 ng/L) in China. Due to the inability of existing conventional treatment steps currently applied at WWTPs the occurrence of pharmaceuticals is now widely confirmed.

Table 1.2: Occurrence of pharmaceutical compounds in wastewater

a/a	Pharmaceutical compound	Country	Wastewater influent concentration (ng/L)	Wastewater effluent concentration (ng/L)	Reference
1	Acebutolol	Finland	335	140	Vieno et al., 2007
		Greece	-	50	Andreozzi et al., 2003
		France	-	80 – 130	Andreozzi et al., 2003
		Italy	-	20 – 110	Andreozzi et al., 2003
		Sweden	-	< 10	Andreozzi et al., 2003
2	Acetaminophen	USA	960	ND	Yu et al., 2006
		Spain	29000-246000	<LOD-4300	Gomez et al., 2007
3	Aminophenazone	Berlin	200	100	Heberer et al., 2002
4	Atenolol	Finland	795	330	Vieno et al., 2007
5	Biosol	USA	250	ND	Yu et al., 2006
6	Biphenylol	USA	900	100	Yu et al., 2006
7	Caffeine	Berlin	230000	180	Heberer et al., 2002
		Spain	52000-192000	1400-44000	Gomez et al., 2007
		USA	2450-4860	3.9-23.1	Spongberg et al., 2008
8	Carbamazepine	Berlin	1780	1630	Heberer et al., 2002
		Finland	350	720	Vieno et al., 2007
		Sweden	1680	1180	Bendz et al., 2005
		Austria	325 – 1850	465 – 1595	Clara et al., 2005
		Canada	356	251	Miao et al., 2005
		Spain	120-310	110-230	Gomez et al., 2007
		USA	24.8-50.9	33.7-111.2	Spongberg et al., 2008
9	Ciprofloxacin	Finland	600	60	Vieno et al., 2007
		Sweden	220	48	Lindberg et al., 2006
		Sweden	90 – 300	<6 -60	Lindberg et al., 2005
		USA	11.4-377.2	8.8-109.9	Spongberg et al., 2008
31	Clarithromycin	USA	< LOQ – 724.2	< LOQ – 610.6	Spongberg et al., 2008
10	Clofibric acid	Berlin	460	480	Heberer et al., 2002
11	Diclofenac	USA	110	90	Yu et al., 2006

		Berlin	302	251	Heberer et al., 2002
		Austria	905-4114	780-1680	Clara et al., 2005
		Spain	200-3600	140-2200	Gomez et al., 2007
		USA	<LOQ-13.9	8.3-177.1	Spongberg et al., 2008
12	Gabapentin	USA	100	ND	Yu et al., 2006
13	Gemfibrozil	USA	410	130	Yu et al., 2006
		USA	181.8-451.3	<LOQ-83.5	Spongberg et al., 2008
14	Ibuprofen	USA	1900	250	Yu et al., 2006
		Spain	34000-168000	240-28000	Gomez et al., 2007
		Austria	1200-2679	ND-2400	Clara et al., 2005
15	Indomethacine	Berlin	800	800	Heberer et al., 2002
16	Ketoprofen	USA	1200	280	Yu et al., 2006
		Berlin	300	230	Heberer et al., 2002
17	Metoprolol	Finland	1060	755	Vieno et al., 2007
		Greece	160	100	Andreozzi et al., 2003
		Italy		10 - 100	Andreozzi et al., 2003
		France		80	Andreozzi et al., 2003
		Sweden		390	Andreozzi et al., 2003
		Sweden		<10 – 310	Bendz et al., 2005
		USA		<1 – 1200	Hugget et al, 2003
18	Naproxen	USA	3200	380	Yu et al., 2006
		Berlin	440	80	Heberer et al., 2002
19	Norfloxacin	Finland	120	ND	Vieno et al., 2007
		Sweden	293	58	Lindberg et al., 2006
		Sweden	66 - 174	<7 – 37	Lindberg et al., 2005
20	Ofloxacin	Finland	100	14	Vieno et al., 2007
		Sweden	<6 - 287	<6 - 52	Lindberg et al., 2005
21	Phenazone	Berlin	920	520	Heberer et al., 2002
22	Phenobarbital	USA	70	ND	Yu et al., 2006
23	Phenytoine	USA	450	250	Yu et al., 2006
		Berlin	50	100	Heberer et al., 2002
24	Primidone	Berlin	1080	390	Heberer et al., 2002
25	Propyphenazone	Berlin	1080	390	Heberer et al., 2002
26	Salicylic acid	Berlin	340	40	Heberer et al., 2002
		USA	433.9 – 8036.1	< LOQ – 25.2	Spongberg et al., 2008
27	Sotalol	Finland	835	280	Vieno et al., 2007
30	Sulfamethoxazole	USA	13.5 – 261	79.4 – 472.4	Spongberg et al., 2008
		Austria	ND-145	ND-91	Clara et al., 2005

28	Triclosan	USA Spain	800 390-4200	250 80-400	Yu et al., 2006 Gomez et al., 2007
29	Valproic acid	USA	140	ND	Yu et al., 2006

ND- not detected, LOD- limit of detection, LOQ: limit of quantification

As shown, the highest concentrations are for caffeine (230000 ng/L) in Berlin, carbamazepine (325-1850 ng/L) in Austria, ibuprofen (34000-168000 ng/L) in Spain, salicylic acid (433.9-8036.1 ng/L) in USA and diclofenac (905-4114 ng/L) in Austria in wastewater influents. Below, in Table 1.3 the removal rate of the pharmaceuticals in different WWTPs is shown.

Table 1.3: Removal rate (%) of pharmaceutical compounds in WWTPs

a/a	Pharmaceutical compound	Removal rate (%)	Reference
1	Acetaminophen	99	Gomez et al., 2007
2	Bezafibrate	(-11)–100 50-83	Lindqvist et al., 2005 Ternes, 1998; Stumpf et al., 1999; Heberer, 2002; Soulet et al., 2002
3	Caffeine	>99.9 85	Heberer and Reddersen, 2001 Gomez et al., 2007
4	Carbamazepine	8 20	Heberer and Reddersen, 2001 Gomez et al., 2007
4	Diclofenac	9 – 60 17 3-75 59	Lindqvist et al., 2005 Heberer and Reddersen, 2001 Ternes, 1998; Stumpf et al., 1999; Heberer, 2002; Soulet et al., 2002 Gomez et al., 2007
5	Ibuprofen	78 – 100 75-90 95 86	Lindqvist et al., 2005 Ternes, 1998; Stumpf et al., 1999; Heberer, 2002; Soulet et al., 2002 Gomez et al., 2007 Jones et al., 2007
6	Ketoprofen	51 – 100 23-78	Lindqvist et al., 2005 Ternes, 1998; Stumpf et al., 1999; Heberer, 2002; Soulet et al., 2002
7	Mefenamic acid	92	Jones et al., 2007
8	Naproxen	55 – 98 66-82	Lindqvist et al., 2005 Ternes, 1998; Stumpf et al., 1999; Heberer, 2002; Soulet et al., 2002
9	Paracetamol	92	Jones et al., 2007
10	Salbutamol	95	Jones et al., 2007
11	Triclosan	88	Gomez et al., 2007

Removal rates are mostly reported as the difference in gram per day per inhabitant between influent and effluent (Kassinos et al., 2010; Castiglioni et al., 2006; Gros et al., 2007; Vieno et al., 2007). The removal rate for acetaminophen, caffeine, mefenamic acid, paracetamol, salbutamol was found to be in certain cases above 90%. Also for bezafibrate, removal rates were between (-11%)-(100%), for ibuprofen 75-100%, ketoprofen 23-100%, for naproxen 55-98% and for triclosan 88%. The fate of the pharmaceutical compounds during treatment along with the various design parameters affecting the capacity of the plants to remove such compounds are further discussed in the following sections.

1.5 Photolysis and advanced oxidation processes for the removal of pharmaceuticals from aqueous matrices

WWTPs are regarded as already mentioned, as one of the most important sources of pharmaceutical residues in the environment (Sim et al., 2010). At present, WWTPs mainly remove the classical contaminants such as solids, nutrients and pathogens, not focused on the elimination of emerging pollutants such as pharmaceuticals (Clara et al., 2005; Nakada et al., 2007; Sim et al., 2010). For this reason, researches for understanding the fate of pharmaceuticals in WWTPs are intensively performed (Clara et al., 2005; Joss et al., 2005; Yu et al., 2006; Gomez et al., 2007; Jones et al., 2007; Sim et al., 2010).

The fate of a certain pharmaceutical compound in a complex system of WWTP depends on various parameters including applied sludge retention time (SRT), hydraulic retention time (HRT), temperature, pH, biomass concentration, compound's polarity, biodegradability and cation-exchange properties, (Radjenovic et al., 2009). During sewage treatment, pharmaceutical residues can be removed from the aqueous phase either through abiotic processes (e.g., sorption, isomerisation/epimerisation, hydrolytic degradation) or by biotic physico and chemical transformation/degradation (Radjenovic et al., 2009) although pharmaceuticals are designed to resist microbial degradations and to be chemically stable (Löffler et al., 2004; Khetan and Collins, 2007; Sammartino et al., 2008; Mompelat et al., 2009).

However, abiotic pharmaceuticals and residues elimination is the most likely reaction occurring in WWTPs with predominantly direct and indirect photodegradation (Löffler et al., 2004; Khetan and Collins, 2007; Nikolaou et al., 2007; Sammartino et al., 2008; Mompelat et al., 2009).

The photodegradation of numerous pharmaceuticals can be direct by solar absorption or indirect through radicals (e.g. HO·) generated by the solar irradiation of photosensitizers like nitrate, humic acids, etc (Buerge et al., 2006; Khetan and Collins, 2007; Nikolaou et al., 2007; Sammartino et al., 2008; Mompelat et al., 2009). Photodegradation depends also on the

intensity of solar irradiation, eutrophic conditions, depth of water, composition of organic matter, latitude and season (Heberer, 2002; Fent et al., 2006; Mompelat et al., 2009).

Hence, two types of photolytic processes occur in aquatic systems: direct and indirect. In direct photolysis, the target contaminant (in this case pharmaceuticals) absorbs a solar photon. In an indirect photolysis mechanism, the target does not need to or is unable to absorb light because another chromophore in the system such as dissolved organic matter acts as a sensitizing species. Direct photolysis of pharmaceuticals is initiated by photon absorption, a fact that is well known to pharmacists who dispense medication in amber bottles and advise patients to stay out of the sun when taking certain medications. The phototoxicity of some drugs has led to an active area of research on this topic that complements the study of the environmental photochemistry of pharmaceuticals. The excited state of a molecule is short-lived and may undergo various physical or chemical relaxation processes. Physical relaxation processes, such as vibrational energy loss, energy transfer to another species, or emission of a photon lead to the regeneration of the parent compound. Only those processes that lead to chemical changes in the parent compound lead to a decrease in the concentration of the species being photolyzed. Such transformations may include fragmentation, isomerization/intramolecular rearrangement, H-abstraction, dimerization/ polymerization, and electron transfer. The fraction of chemical transformation events per photon absorbed is defined as the quantum yield (F) for that process. This value may range from 0 to 1, but values between 0.0001 and 0.1 are common for compounds that are photodegraded on reasonable time scales (half-lives of minutes to days) (Arnold and McNeill, 2007).

All compounds, whether or not absorbing solar photons, are potentially subject to indirect photolysis. In an indirect photochemical mechanism, a sensitizer absorbs light and subsequently reacts directly with the substrate or produces a reactive intermediate that reacts with the substrate. The principal light-absorbing species in indirect photolysis is the dissolved organic matter (DOM) present in natural waters (Arnold and McNeill, 2007).

Photoexcitation of DOM leads to the production of a variety of photochemically produced reactive intermediates (PPRIs) including the reactive oxygen species hydroxyl radicals, singlet oxygen, peroxy radicals, and superoxide. Other PPRIs, such as triplet (excited) DOM and hydrated electrons, are also produced and can react with pharmaceutical pollutants. It should

also be mentioned that while DOM is the main sensitizing species in natural waters, other light-absorbing species might also generate PPRIs, such as nitrate and nitrite that produce hydroxyl radicals in sunlight. As described above, the rate of loss is a product of the light absorption rate and the quantum yield. Compounds that do not absorb solar photons (e.g. ibuprofen, ketoprofen, and cimetidine) will not react via this pathway. Additionally, some compounds have both a small spectral overlap integral and a small quantum yield. In this case, direct photolysis is most certainly unimportant (Arnold and McNeill, 2007). Below in Table 1.4, selected studies on the photolysis of pharmaceuticals are shown.

Table 1.4: Photolysis of pharmaceuticals

a/a	Compound	Initial concentration of pollutant or COD	Light source	Findings	Reference
1	2 samples of unspecified composition	COD = 670-2700 mg/L AOX = 3-5 mg/L	LP UV at 254 nm	Quantitative AOX removal in 240 min. Comparison with other processes, i.e. O_3, UV, UV/O_3, Fe^{2+}/ H_2O_2.	Hofl et al., 1997
2	clofibric acid	5 10^{-8}-1.5 10^{-3} M	LP UV at 254 nm at pH=5	95% drug removal and 10% mineralization respectively after 60 min.	Andreozzi et al., 2003a
3	paracetamol	10^{-5} M	LP UV at 254 nm at pH=5	Complete drug removal and 40% mineralization in 1 and 4 min respectively. Identification of reaction by-products.	Andreozzi et al., 2003b
4	17β-estradiol (E2), estrone (E1)	3-20 mg/L	UV-light and UV–Vis-light direct photolysis	The results suggest that the photolysis of E2 in aqueous solutions occurs under irradiation with UVdisinfection lamp (λ=254 nm, 30 W), while E1 can also undergo photolysis under irradiation with a high-pressure mercury lamp (λ≥365 nm, 125 W).	Liu et al., 2004
5	carbamazepine	0.02 mM	LP UV at 254 nm at pH=5	Complete drug and 35% TOC removal in 4 min. Insignificant degradation with direct photolysis. Humic acids act as scavenger. Intermediates more toxic than carbamazepine.	Vogna et al., 2004a
6	diclofenac	10^{-3} M	LP UV at 254 nm at pH=5-6	95% drug removal and 40% mineralization after 90 min. Elucidation of reaction by-products and pathways.	Vogna et al., 2004b
7	penicillin	COD = 1555 mg/L	LP UV at 254 nm at pH=7	10-20% COD removal after 60 min. Poor improvement in biodegradability.	Arslan-Alaton and Dogruel, 2004
8	mefenamic acid	5μM	Natural sunlight photolysis	Photolysis data taken under natural sunlight in a solution of SRFA suggest that photosensitization by DOM can contribute significantly to the environmental photodegradation of MEF.	Werner et al., 2005
9	metronidazole	1 mg/L	LP UV at 254nm and MP UV at 200-400 nm at pH=6	Degradation followed first-order kinetics and rate increased with increasing H_2O_2 concentration. MP irradiation more effective than LP.	Shemer et al., 2006
10	17β-Ethinylestradiol	10^{-5} mM	LP UV and MP UV	Reduction in estrogenic activity occured faster in laboratory water than in surface water indicating scavenging effects and dependance on water alkalinity. In most cases, complete removal occured at ≤600 mJ/cm^2 fluence.	Linden et al., 2007

11	naproxen iohexol carbamazepine clofibric acid	1-3 μM	UV at 200-300 nm at pH=7	Moderate degradation at 100 mJ/cm^2 fluence and >99% at 600-1700 mJ/cm^2 depending on the drug. Lower degradation with direct photolysis. Rates decreased in surface water compared to laboratory water.	Pereira et al., 2007a
12	naproxen ketoprofen carbamazepine clofibric acid ciprofloxacin iohexol	1-3 μM	UV at 254 nm at pH=7	Complete degradation at 1700 mJ/cm^2 fluence for all drugs. Lower degradation with direct photolysis. Rates decreased in surface water compared to laboratory water.	Pereira et al., 2007b
13	17α-ethinylestradiol 17β-estradiol	5 μM	LP UV and MP UV at pH=7-8	Substrate degradation and estrogenic activity removal followed comparable first order kinetics.	Rosenfeldt et al., 2007
14	tetracycline (TC)	10-40 mg/L	500 W medium mercury lamp	The photolysis rate was found to be dependent on the initial tetracycline concentration and increasing TC concentration from 10 to 40 mg/L led to the decrease of the photolysis rate constant from 0.0045/ min to 0.0014/min. TC photolysis was highly pH-dependent and strongly enhanced at high pH value. Markedly elevated TC photolysis was also observed in the presence of nitrate and dissolved organic matter. Upon irradiation for 300 min, only 15% reduction of total organic carbon (TOC) occurred in spite of quick conversion of 73% of TC, suggesting that a majority of TC transformed into intermediate products without complete mineralization.	Jiao et al., 2008
15	acetaminophen atenolol carbamazepine, ibuprofen, ifenprodil, indomethacin, mefenamic acid propranolol	100 mg/L	Direct sunlight	In the results of batch sunlight photolysis experiments, three out of eight Pharmaceuticals propranolol, indomethacin, and ifenprodildwere relatively easily photodegraded (i.e., half-life < 24 h), whereas the other five pharmaceuticals were relatively stable against sunlight.	Yamamoto et al., 2009
16	diclofenac	6.3×10^{-4} - 5.0×10^{-5} M.	UV-C light at 254 nm	Diclofenac initial concentration plays an important role in its conversion profile. First order kinetics is ruled out under the applied experimental	Rivas et al., 2010

				conditions. The process efficiency is significantly enhanced if oxygen is bubbled instead of air.	
17	meprobamate carbamazepine dilantin atenolol primidone trimethoprim	Not specified	UV/H_2O_2	The removal of these six pharmaceuticals varied between no observed removal and >90%.	Rosario- Ortiz et al., 2010
18	norfloxacin doxycycline mefenamic acid	10x 10^{-5} M	UV-C radiation (254 nm) in the presence and absence of inorganic peroxides (hydrogen peroxide or sodium monopersulfate	Quantum yields in the range $(1.1–4.5)\times10^{-3}$ mol/ einstein indicated the low photo-reactivity of these pharmaceuticals. Inorganic peroxides considerably enhanced the contaminants conversion, although no appreciable mineralization could be obtained.	Rivas et al., 2010
19	propranolol (PRO) metronidazole (MET)	50 and 100 mg/L	UV-254 germicidal lamp (UV-C), UV-365 black light lamp (UV-A).	After 8 h of irradiation, direct UV photolysis promoted substantial pharmaceuticals removal, especially with the use of UV-C radiation (near 50%). However, on average only 12% of the organic matter content was photodegraded. The photo-transformation of both compounds promoted the formation of more biodegradable byproducts.	Dantas et al., 2010
20	sulfamethoxazole trimethoprim	1 mM	Solar simulator with a UV-Suprax optical filter with the light intensity set at 765 W/m^2.	The rate of loss of sulfamethoxazole was enhanced in wastewater effluent due to indirect photolysis reactions, specifically reactions with hydroxyl radicals and triplet excited state effluent organic matter. Photolysis in the presence of natural organic matter, however, did not lead to enhanced degradation of sulfamethoxazole. Trimethoprim was also found to be susceptible to indirect photolysis in wastewater effluents, with hydroxyl radical and triplet excited effluent organic matter being the responsible species.	Ryan et al., 2011

AOX: Adsorbable organic halogen, LP: low pressure mercury vapor germicidal lamp, MP: medium pressure mercury lamp

1.6 Advanced chemical oxidation processes (AOPs)

1.6.1 Photocatalysis

Advanced chemical oxidation processes like photocatalysis have turned out to be a promising tool for water and wastewater treatment (Doll et al., 2005), and have gained considerable attention due to their ability to degrade a wide class of pollutants. The effort and necessity to remove such pollutants stem from the potential of various chemicals or of their mixtures to induce adverse effects to environmental organisms even in very low concentrations during long-term exposure.

Various chalcogenides oxides such as TiO_2, ZnO, ZrO_2, CeO_2, or sulfides such as CdS, ZnS have been used as photocatalysts in different studies (Andreozzi et al., 2000; Nepolian et al., 2002; Gogate et al., 2004). The surface area and the number of active sites offered by the catalyst thus, the nature of the catalyst, crystalline or amorphous, is important for the adsorption of pollutants. They play an important role in the overall rates of degradation, as usually adsorption is the rate-controlling step. It should be noted that the best photocatalytic performances with maximum quantum yields have been always obtained with titania (Abellan et al., 2009). According to Abellan et al. (2009), some authors attribute this property of titania to the slow recombination electron/hole taking place on the surface of P25 and some others attribute its higher activity to its structure formed by a mix of the phases of anatase and rutile; the activity of the latter being greater than the activity of the pure crystalline phases.

TiO_2 photocatalysis is an emerging treatment technology for the destruction of various micropollutants found in effluents with key advantages including no mass transfer limitations (when TiO_2 is in slurry form), operation at ambient conditions and the possible use of solar irradiation. The catalyst itself is inexpensive, commercially available in various crystalline forms and particle characteristics, non-toxic and photocatalytically stable (Doll et al., 2005; Sioi et al., 2006; Belgiorno et al., 2007; Papadam et al., 2007). It is well established that by the irradiation of an aqueous TiO_2 suspension with light energy greater than the band gap energy of the semiconductor (Eg > 3.2 eV) conduction band electrons (e^-) and valence band holes (h^+) are generated (Adewuyi et al., 2005). Part of the photogenerated carriers recombine in the bulk of the semiconductor, while the rest reach the surface, where the holes as well as the electrons act as powerful oxidants and reductants, respectively. The photogenerated electrons react with

the absorbed molecular O_2 on the catalyst sites, reducing it to a superoxide radical anion O_2^-, while the photogenerated holes can oxidize either the organic molecules directly, or the OH^- ions and the H_2O molecules adsorbed at the TiO_2 surface to hydroxyl radicals. These radicals together with other highly oxidant species (e.g. peroxide radicals) are reported to be responsible for the primary oxidizing step in photocatalysis. The HO· formed on the illuminated semiconductor surface are very strong oxidizing agents, with a standard potential of 2.8 V. These can easily attack the adsorbed organic molecules or those located close to the surface of the catalyst, thus leading finally to their complete mineralization (Kositzi et al., 2004). Figure 1.3 represents the principle mechanism of photocatalysis.

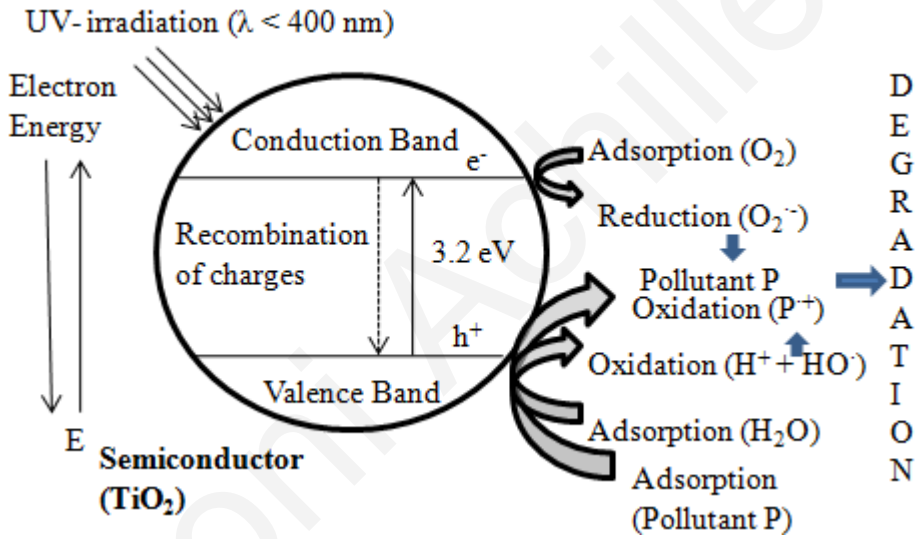

Figure 1.3: Principle mechanism of photocatalysis (Herrmann et al., 2010)

According to Chong et al. (2010), the series of chain oxidative- reductive reactions (Eqs. (1.8) – (1.18) that occur at the photon activated surface has been widely postulated as follows:

Photoexcitation: $TiO_2 + h\nu \rightarrow e^- + h^+$ (1.8)

Charge–carrier trapping of e^-: $e^-_{CB} \rightarrow e^-_{TR}$ (1.9)

Charge–carrier trapping of h^+: $h^+_{VB} \rightarrow h^+_{TR}$ (1.10)

Electron-hole recombination: $e^-_{TR} + h^+_{VB}\ (h^+_{TR}) \rightarrow e^-_{CB}$ + heat (1.11)

Photoexcited e^- scavenging: $(O_2)_{ads} + e^- \rightarrow O_2$ (1.12)

Oxidation of hydroxyls: $OH^- + h^+ \rightarrow HO$ (1.13)

Photodegradation by HO·: $R\text{-}H + HO\cdot \rightarrow R\cdot$ (1.14)

Direct photoholes: $R + h^+ \rightarrow R^{+\cdot} \rightarrow$ Intermediates / Final Degradation Products (1.15)

Protonation of superoxides: $O_2^{-}\cdot + HO\cdot \rightarrow HOO\cdot$ (1.16)

Co- scavenging of e^-: $HOO\cdot + e^- \rightarrow HO_2^-$ (1.17)

Formation of H_2O_2: $HOO^- + H^+ \rightarrow H_2O_2$ (1.18)

Based on the detailed and critical analysis of the existing literature on the photocatalytic oxidation of the contaminants, the important operating parameters, which affect the overall destruction efficiency of the photocatalytic oxidation process, are the following (Gogate et al., 2004; Klavarioti et al., 2009; Malato et al., 2009):

1. *Amount and type of the catalyst*. The use of catalyst concentration only till an optimum value as using excess catalyst reduces the amount of photo-energy being transferred in the medium due to opacity offered by the catalyst particles. The optimum value will strongly be dependent on the type and concentration of the pollutant, as well as the rate of generation of free radicals. Degussa P25 TiO_2 catalyst is the most efficient.
2. *Reactor design.* Usually reactor designs should be such that uniform irradiation of the entire catalyst surface is achieved at the incident light intensity.
3. *Wavelength of the irradiation.* The threshold wavelength corresponds to the band gap energy 3.2 eV and the ideal wavelength is ca. 400 nm. Sunlight may also be used for the excitation of the catalyst.
4. *Initial concentration of the reactant.* For highly concentrated effluents absolutely no destruction may be observed and dilution is essential.

5. *Temperature.* Usually photocatalytic systems are operated at room temperature, but with the release of energy in the destruction process due to recombination of electron – hole pairs, temperature might increase. If the temperature is expected to go beyond 80°C, intermediate cooling is recommended. At temperature above 80°C, the exothermic adsorption of pollutant becomes unfavorable and tends to be the rate limiting step, leading to decreased activity and hence reduction in the reaction rates. In the range of 20-80°C, usually weak dependence of the degradation rates on temperature has been observed.
6. *Radiant flux.* The reaction rate is directly proportional to the intensity of radiation. Usually linear variation is observed at low intensities and beyond a certain magnitude of intensity, the rate of the reaction shows a square root dependence on the intensity. Lower dependency on the intensity of irradiation is usually attributed to increased contribution of the recombination reaction between the generated holes and electrons when their intensity is high. Moreover the angle of incidence of the UV light should always be 90° as maximum rates are observed at this angle of incidence.
7. *Medium pH.* Medium pH has a complex effect on the rates of photocatalytic oxidation and the observed effect is generally dependent on the type of the pollutant as well as the zero point charge (zpc) of the semiconductor used in the oxidation process (more specifically on the electrostatic interaction between the catalyst surface and the pollutant). The adsorption of the pollutant and the rates of degradation will be maximum near zpc of the catalyst. For some of the pollutants which are weakly acidic, the rate of photocatalytic oxidation increases at lower pH due to an increase in the extent of adsorption under acidic conditions. Some of the pollutants, which undergo hydrolysis under alkaline conditions or undergo decomposition over a certain pH range may show an increase in the rate of photocatalytic oxidation with an increase in the pH.
8. *Aeration.* Presence of electron acceptors is recommended so as to prevent the recombination reaction between the generated positive holes and electrons. Generally aeration is used for this purpose as it also provides uniform mixing, suspension of the catalyst in the case of slurry reactors and economical source of oxygen. The concentration of oxygen also affects the reaction rate but it seems that the difference between using air (P_{O2}=0.21 bar) or pure oxygen (P_{O2}=1 bar) is not drastic. The role of oxygen may not only be that of an electron acceptor. Oxygen may be involved in the formation of other oxidative species (superoxide, hydrogen peroxide, hydroxyl radicals)

in the prevention of reduction reactions, in the stabilization of radical intermediates, mineralization and direct photocatalytic reactions.

9. *Effect of ionic species.* Presence of ions may affect the degradation process via adsorption of the contaminants. In general it can be said that CO_3^-, HCO_3^- act as radical scavengers and also affect the adsorption process and Cl^- affect the adsorption step strongly and also adsorb UV light partly.

Table 1.5 provides information on various studies with regard to the treatment of pharmaceuticals in aqueous matrices by heterogeneous photocatalysis.

Table 1.5: Removal of pharmaceuticals in aqueous matrices by heterogeneous photocatalysis

Reference	Target drug/ Initial Concentration	Matrix	AOP features	Scale	Measure of degradability	Summary of results
Abellan et al., 2007	sulfamethoxazole 25-200 mg/L	Distilled water	Suspended Degussa TiO_2/Artificial sunlight at pH=2-11	Bench	Specific drug, TOC, COD BOD_5	Drug removal and mineralization was found to depend on catalyst loading and pH. Comparison of various kinetic models. Determination of by-products and mechanisms. Slight increase in biodegradability was achieved.
Achilleos et al., 2010	diclofenac 5-20 mg/L	Deionized water	Suspended Degussa TiO_2 (50-1600 mg/L), UV-A, 9W lamp	Bench	UV-absorbance, DOC	Reaction rate constants increase with decreasing initial concentration. Since the levels of diclofenac and alike compounds in environmental samples are relatively low, their degradation is likely to occur readily at mild operating conditions.
Augugliaro et al., 2005	lincomycin 10-75 μM	Distilled water	Suspended Degussa TiO_2/Sunlight coupled with nanofiltration	Pilot plant	Specific drug, TOC	Fast first-order drug degradation. Filtration separates catalyst particles and reaction by-products from the permeate.
Baran et al., 2006	sulfacetamide sulfathiazole sulfamethoxazole sulfadiazine 0.1 mM	Distilled water	Suspended TiO_2/UV-365nm	Bench	Specific drug, BOD_5, toxicity to *C.vulgaris*	Complete degradation of all drugs within 180-300 min with first-order kinetics. Sulfamethoxazole was far more reactive than the rest. Intermediates were found to be more biodegradable and less toxic than the parent compounds.
Calza et al., 2004	buspirone 15 mg/L	Distilled water	Suspended Degussa TiO_2/Artificial sunlight	Bench	Specific drug	Complete drug removal after 30 min with first-order kinetics. Determination of by-products and pathways.
Calza et al., 2006	diclofenac 0.76-15 mg/L	Distilled water	Suspended Degussa TiO_2/Artificial sunlight at ambient pH	Bench	Specific drug, TOC, toxicity to *V.fischeri*	A factorial design approach is implemented to optimize conversion regarding catalyst loading and drug concentration. Determination of by-products and pathways. Toxicity increases during early stages and decreases thereafter.

Calza et al., 2008	imipramine 15 mg/L	Deionized water	Suspended Degussa TiO_2/Artificial sunlight combined with Fenton	Bench	Specific substrate, TOC, toxicity to *V.fischeri*	A factorial design approach was implemented to assess the effect of TiO_2, H_2O_2 and Fe^{2+} concentrations on conversion. Determination of by-products and pathways. By-products were found to be as toxic as imipramine and resistant to mineralization.
Chatzitakis et al., 2008	chloramphenicol 10-80 mg/L	Deionized water	Suspended Degussa or anatase TiO_2 or ZnO/UV-(320-400nm) at pH=5	Bench	Absorbance at 276.5nm, TOC, antimicrobial activity to *E.coli*	First-order rate increases with increasing drug concentration and catalyst loading and adding H_2O_2. Degussa TiO_2 and ZnO were found to equally active. Complete elimination of drug activity after 90 min corresponding to 70% mineralization.
Coleman et al., 2000	17β-estradiol 0.05-3 μM	Acetonitrile/water	Immobilized TiO_2/UV-(300-400nm) at pH=1-12	Bench	Specific substrate, TOC	98% degradation after 210 min following Langmuir-Hinshelwood kinetics.
Coleman et al., 2004	17β-estradiol, estrone, 17α-ethylestradiol 10 ug/L	Distilled water	Immobilized TiO_2/UVA	Bench	Yeast-based estrogenicity assay	50% and complete removal of estrogenic activity for all three steroids after 10 and 60 min respectively with first-order kinetics. Photolysis was 2.4-9 times slower than photocatalysis.
Coleman et al., 2005a and 2005b	17α-ethinylestradiol, 17β-estradiol, estriol 0.1-3 μM	Acetonitrile/water	Immobilized Degussa TiO_2/UVA & B at pH=4 and 3 respectively	Bench	Specific substrate	First-order estrogen degradation in the order: 17α-ethinylestradiol > 17β-estradiol > estriol. Photolysis was slower than photocatalysis. Rate decreases with decreasing light intensity and initial concentration. TiO_2 doping with Pt or Ag had no effect on catalyst activity.
Coleman et al., 2007	17α-ethinylestradiol, 17β-estradiol, estriol 0.8 mg/L	Distilled water	Immobilized Degussa TiO_2/Artificial sunlight or UV-350nm	Bench	Specific substrate	Degradation followed first order kinetics for all three estrogens at comparable rates. UVA was more efficient than solar irradiation. The method of catalyst immobilization affected the performance.
Doll and Frimmel, 2004	clofibric acid, carbamazepine, iomeprol, iopromide 0.5-10 mg/L	Distilled water	Suspended Degussa or Hombikat TiO_2/ Artificial sunlight	Bench	Specific substrate, DOC	First-order kinetic rates increase with increasing catalyst loading and decreasing initial concentration. Degussa was generally more active than Hombikat. Determination of by-products and pathways.

			at pH=3.4-6.5			
Doll and Frimmel, 2005a	iomeprol, clofibric acid, carbamazepine ~2 mg/L	Deionized water	Suspended Degussa or Hombikat TiO_2/UV-254nm coupled with microfiltration at pH=6.8	Pilot plant	Specific substrate, DOC	Assessment of long-term stability/activity of catalysts following membrane separation and reuse. Hombikat was more active than Degussa.
Doll and Frimmel, 2005b and 2005c	carbamazepine, clofibric acid, iomeprol 0.5-5.2 mg/L	Spiked lake water	Suspended Degussa or Hombikat TiO_2/Artificial sunlight at pH=6.5	Bench	Specific substrate	First-order rates decreased with increasing concentration of NOM and other xenobiotics. Degussa was more active than Hombikat for carbamazepine and clofibric acid but less for iomeprol. Rate increased with increasing catalyst loading. Determination of by-products and pathways.
Elmolla et al., 2010	amoxicillin 104 mg/L ampicillin 105 mg/L and cloxacillin 103 mg/L	Deionized water	Suspended Degussa TiO_2 (0.5-2 g/L), UVA lamp, 6W	Bench	HPLC-DAD, COD, TOC	No significant degradation occurred by 300 min UVA irradiation per se. pH had a great effect on antibiotic degradation and the highest degradation was achieved at pH 11.
Giraldo et al., 2010	oxolinic acid 20 mg/L	Deionized water	Suspended Degussa TiO_2 (0.2-1.5 g /L)	Bench	DOC, COD, LC-MS	Under the studied conditions, pH 7.5 and 1.0 g/L of TiO_2 favored the efficiency of the process. Adsorption and oxidation by the TiO_2 holes seemed to be the initial step of the process.
Hapeshi et al., 2010	ofloxacin atenolol 5-20 mg/L	Deionized water Groundwater Wastewater	composite 10:100 (w/w) oxidized multi-walled carbon nanotube (MWCNTox): Anatase (10-MWCNTox-TiO_2), UV-C/Vis	Bench	UV-Vis TOC	Optimal conditions for CBZ degradation under near UV-Vis and UV irradiation were obtained using P25 (0.5 g/L), 5 mM of H_2O_2 or 50% of $P(O_2)$, with rate constants ca. 0.3144 /min and 0.2005 /min, respectively.
Hu et al., 2007	sulfamethhoxazole 5-500 μM	Deionized water spiked with NOM	Suspended Degussa or	Bench	Specific drug, DOC	Degussa was more active than pure anatase or rutile. Rate depends on catalyst loading, initial drug concentration, solution pH and the

		and bicarbonates	anatase or rutile TiO_2/UV-(324-400nm) at pH=3-11			water matrix (presence of NOM, bicarbonates, and dissolved gases). Determination of by-products and pathways.
Kaniou et al., 2005	sulfamethazine 10-70 mg/L	Distilled water	Suspended Degussa TiO_2 or ZnO/UV-(350-400nm) at pH=4.8	Bench	Absorbance at 260nm, TOC	First-order rate increased with increasing catalyst loading and was enhanced in the presence of H_2O_2. ZnO was more active than TiO_2 for both drug removal and mineralization.
Klauson et al., 2010	amoxicillin 1-100 mg/L	Deionized water	Slurry TiO_2 artificial UV-light source, Phillips 365-nm low pressure luminescent mercury UV-lamp (15 W), Solar irradiation	Bench	UV-absorbance, COD, UPLC-MS	P25 under artificial light, doped catalysts were close by their efficiency to Degussa catalyst under solar radiation. The PCO of AMOX proceeded with maximum efficiency in neutral solutions. The PCO efficiency increased with growing concentration of AMOX achieving maximum at 50 mg/l and remaining constant with further concentration increase.
Malygina et al., 2005	β-estradiol 0.5 mg/L	Distilled water	Suspended TiO_2/UV-366nm at pH=3-11	Bench	Specific substrate	Both dark adsorption and degradation increased considerable with increasing pH in the range 5-11.
Martinez et al., 2010	carbamazepine, 8 mg/L	Deionized water	P25, nanocrystalline sol-gel TiO_2 (anatase and rutile) (0.1-2 g/L),	Bench	UV-Vis, HPLC-PDA	Photocatalytic reactions approximately followed pseudo-first order kinetics Addition of H_2O_2 at ambient pH=5 and TiO_2 1.0 g/L resulted in complete degradation of amoxicillin, ampicillin and cloxacillin in 30 min.
Mendez-Arriaga et al., 2008	diclofenac, naproxen, ibuprofen 25-200 mg/L	Deionized water	Suspended Degussa TiO_2/Artificial sunlight	Bench	Specific drug, TOC, BOD_5, COD, toxicity to *V.fischeri*	Diclofenac and naproxen were susceptible to photolysis but not ibuprofen. By-products of low biodegradability accompanied diclofenac and naproxen degradation.
Mitamura et al., 2004	unconjugated and	Distilled water	Immobilized	Bench	Specific substrate	Conjugated estrogens degraded much slower (by about an order of

	conjugated estrone and estradiol 1 mM		TiO_2/UVA			magnitude) than their unconjugated counterparts with first order kinetics.
Molinari et al., 2006	furosemide, ranitidine, ofloxacin, phenazone, naproxen, carbamazepine, clofibric acid 5-10 mg/L	Distilled water and surface river water	Suspended Degussa TiO_2/MP UV coupled with nanofiltration at pH=2-12	Bench	Absorbance at 230-280nm	First-order rate depended on solution pH in the range 3-11. Filtration separated catalyst particles but not reaction by-products from the permeate. Comparison of various membranes.
Munoz et al., 2006	α-methyl-phenylglycine 500 mg/L	Distilled water	Suspended Degussa TiO_2/Sunlight	Pilot plant	Specific drug, DOC, COD	Complete drug and 85% COD removal after 1500 min. Life cycle assessment was implemented to assess environmental impact.
Nakashima et al., 2003	17β-estradiol, estrone 250 ug/L	Deionized water and treated effluent from a sewage treatment plant	Immobilized TiO_2/UV-black fluorescent lamp	Bench	Specific substrate	Fast degradation of both estrogens following first-order kinetics. Rate increased with increasing catalyst surface area and temperature.
Nasuhoglu et al., 2010	sulfamethoxazole, 3-12 mg/L	Deionized water	Suspended Degussa TiO_2 (0.4 g/L), Xe-OP lamp (Phillips 1 kW)	Bench	LC-MS, Toxicity	At the used experimental conditions, photocatalytic treatment was proved to be an effective method to achieve mineralization degrees inthevicinity of 55% for waters containing MET and PRO.
Ohko et al., 2002	17β-estradiol 1 μM	Deionized water	Suspended Degussa TiO_2/UV-365nm	Bench	Specific substrate, CO_2 evolution, yeast-based estrogenicity assay	Complete estrogen removal after 30 min with first-order kinetics. Complete mineralization after 180 min. Determination of by-products. Estrogenic activity was lost upon estrogen removal.
Paul et al., 2010	ciprofloxacin, 100 μM	Deionized water	Suspended Degussa TiO_2 (0.5 g/L)	Bench	HPLC-UV/FLD	Considerably higher COD removal was observed during photo-catalysis. Even though with photolysis SMX was removed faster, the presence of TiO_2 leaded to removal of the persistent products formed.
Rafqah et al., 2006	triclosan 15-37 μM	Distilled water and surface river water	Suspended Degussa or	Bench	Specific drug, TOC	Degussa was far more active than pure anatase. Degradation increased with increasing catalyst concentration except at

			anatase TiO_2/UV-(300-450 nm) at pH=5			excessive loadings. Mineralization was much slower than drug degradation. Oxidation in river water was slower than in distilled water due to water matrix. Determination of by-products and pathways.
Reyes et al., 2006	tetracycline 40 mg/L	Deionized water	Suspended Degussa TiO_2/UV > 254 nm or solarium device (300-400 nm) or UV-365 nm	Bench	Specific drug, BOD, TOC, COD, microbiological assay with *S.aureus*	First-order rate depends on the light source in the order: UV (>254 nm)>solar>UV(365 nm). Partial mineralization was accompanied by complete loss of antibacterial activity and increase of biodegradability after 55 min with solar.
Romero et al., 2010	metoprolol (MET) propranolol (PRO) 50 mg/L	Deionized water	Suspended Degussa TiO_2 (50-1500 mg/L), UVA lamp, 9W	Bench	UV-Vis, TOC, COD, BOD_5, Toxicity	Treatment efficiency depended on the operating conditions employed such as the type and concentration of TiO_2, initial substrate concentration, solution pH, water matrix and the presence of extra hydroxyl radical sources.
Sakkas et al., 2007	salbutamol 15 mg/L	Distilled water	Suspended Degussa TiO_2/Artificial sunlight at pH=2.5-9.5	Bench	Specific drug, TOC, toxicity to *V.fischeri*	A factorial design approach was implemented to optimize conversion regarding catalyst loading and pH. Mineralization took 6 times longer than drug removal. Determination of by-products and pathways. Toxicity increased during early stages and decreases thereafter.
Tanizaki et al., 2002	several compounds including 10 endocrine disruptors, 17β-estradiol, estrone, ethinylestradiol 0.1 mg/L	Deionized water	Immobilized nanostructured TiO_2/UVA	Bench	Specific substrate, TOC	First order kinetics for all substrates. Rate depended on the specific compound and, in general, took values between 10^{-1}-10^{-2} 1/min.
Xekoukoulotakis et al., 2010	erythromycin (ERM), 2.5-30 mg/L	Deionized water	Suspended Degussa TiO_2 (0 - 0.5 g/L),	Bench	TOC	UVA-TiO_2 photocatalysis was the most energy efficient process for achieving ciprofloxacin inactivation under laboratory conditions Degussa P25 (75:25, anatase:rutile) was highly active yielding 90% TOC reduction after 90 min of reaction with 10 mg/L ERM and 250 mg/L TiO_2; the second best catalyst consisting of pure anatase (Hombikat UV 100) yielded. Only 65% reduction. TOC removal decreased with decreasing titania loading

						and increasing ERM concentration and solution pH.
Xekoukoulotakis et al., 2010	sulfamethoxazole (SMX), 2.5-30 mg/L	Deionized water	Suspended Degussa TiO_2 100-750 mg/L, UVA lamp, 9W	Bench	TOC	Of the various catalysts tested, Degussa P25 was highly active, i.e. nearly complete SMX degradation and mineralization could be achieved after 30 and 120 min of reaction, respectively at 10 mg/.L SMX and 250 mg/L catalyst concentrations.
Yang et al., 2008	paracetamol 2-10 mM	Deionized water	Suspended Degussa TiO_2/UV-254 nm or UV-365 at pH=3.5-11	Bench	Specific drug, TOC	First order rate under UVC irradiation was much faster than under UVA. Several factors such as initial drug, catalyst and oxygen concentrations, pH and light intensity were tested concerning drug degradation. Identification of by-products.
Yu et al., 2006	triclosan 9 mg/L	Distilled water	Suspended Degussa TiO_2/UV-365 nm	Bench	Specific drug, TOC	Mineralization took 3-4 times longer than drug degradation. Both improved with the addition of H_2O_2. Determination of by-products and pathways.
Yurdakal et al., 2007	gemfibrozil, tamoxifen 2.5-47 mg/L	Deionized water	Suspended Degussa or anatase TiO_2/UV-360 nm at pH=10	Bench	Specific drug, TOC	Gemfibrozil underwent only photocatalytic degradation but not photolytic. Tamoxifen underwent direct photolysis but its metabolites underwent photocatalytic degradation. Degussa is more active than anatase. Mineralization took much longer than drug removal.
Zhang et al., 2007	estrone, 17β-estradiol 0.1-1 ug/L	Deionized water	Suspended Degussa TiO_2/UV-253 nm or UV- (238-579 nm) at pH=2-10	Bench	Specific substrate	Estrogens were equally reactive following first-order kinetics. Reaction at 253 nm was 3 times faster than at 238-579 nm. Degradation increased with increasing catalyst loading and adding H_2O_2 and also depended on pH. Humic substances facilitated degradation due to photosensitization.

1.7 Sonolysis

Of the various AOPs commonly employed in water treatment, ultrasound irradiation has recently gained considerable attention as a means of catalyzing environmentally important reactions and for wastewater treatment (Mahamuni et al., 2009). Ultrasound irradiation or sonolysis is a relatively new process in water treatment and, therefore, has unsurprisingly received less attention than other AOPs.

Sonochemical reactions are induced upon high-intensity acoustic irradiation of liquids at frequencies that produce cavitation (typically in the range 20-1000 kHz). Thus, cavitation serves as a means of concentrating the diffused energy of ultrasound as a hot spot. Pyrolytic reactions inside or near the bubble as well as solution radical chemistry are the two major pathways of sonochemical degradation (Emery et al., 2005). Organics of low solubility and/or high volatility are likely to undergo fast sonochemical degradation as they tend to accumulate inside or around the gas-liquid interface; in this respect, the process may be well suited to tackle pharmaceutical micropollutants. Sonolysis generated by ultrasound waves in liquid media, results in a remarkably suitable medium for high-energy chemistry. Under well-established conditions, these extremes not only promote the oxidative destruction of the target compound via free radical reactions, but also provide an excellent medium for their thermal decomposition in the gas phase (Adewuyi et al., 2001). The production of free radical species by sonolysis extends the goal of the advanced oxidation process beyond aqueous phase oxidative destruction to gaseous decomposition, due to the special effects generated by the formation and collapse of acoustic cavities in sonicated water. When a liquid is exposed to an acoustic field, the pressure waves of the sonic vibrations create a time/frequency dependent acoustic pressure, consisting of alternating compression and rarefaction cycles (Adewuyi et al., 2001). If the applied pressure is equal to the negative pressure developed in the rarefaction cycle of the wave such that the distance between the molecules of the fluid exceeds the critical molecular distance to hold it together, the liquid breaks apart to form cavities made of vapour and gas-filled microbubbles (Adewuyi et al., 2001).

The phenomenon called acoustic cavitation consists of at least three distinct and successive stages: nucleation, bubble growth and under proper conditions implosive collapse (Adewuyi et

al., 2001). The consequences of these extreme conditions are the cleavage of dioxygen and water molecules to produce active species, such as H· and HO· radicals capable of attacking the organic compounds in water (Augugliaro et al., 2006).

$$H_2O_2 \rightarrow H\cdot + HO\cdot \quad (1.19)$$

Hydrogen radicals from the above reaction can also interact with the oxygen present in the system to form peroxide radicals and hydrogen peroxide.

So far four theories have been proposed to explain the sonochemical events (Adewuyi et al., 2001):

- Hot spot theory
- Electrical theory
- Plasma discharge theory
- Supercritical theory

These have led to several modes of reactivity being proposed: pyrolytic decomposition, hydroxyl radical oxidation, plasma chemistry, and supercritical water oxidation. The "hot-spot" theory suggests that a pressure of thousands of atmosphere (up to 1000 atm) is generated and a temperature of about 5000 K results during the violent collapse of the bubble. Both Margulis et al. (1992) and Lepoint et al. (1994) advocate that the extreme conditions associated with fragmentative collapse are due to the intense electrical fields. The "electrical" theory by Margulis suggests that during bubble formation and collapse, enormous electrical field gradients are generated and these are sufficiently high to cause bond breakage and chemical activity (Adewuyi et al., 2001). The "plasma theory" by Lepoint and Mullie also suggests the extreme conditions associated with the fragmentative collapse is due to intense electrical fields and seems not to involve a true implosion. They liken the origin of cavitation chemistry to corona-like discharges caused by a fragmentation process and supported their views by drawing numerous analogies between sonochemistry and corona chemistry and indicating the formation of microplasmas inside the bubbles (Adewuyi et al., 2001). The supercritical theory recently proposed by Hoffmann (Hua et al., 1995), suggests the existence of a layer in the bubble-solution interface where temperature and pressure may be beyond the critical conditions of water (647 K, 22.1 MPa) and which may have physical properties intermediate between those of a gas and a liquid (Hua et al., 1995; Adewuyi et al., 2001). They

showed that supercritical water is obtained during the collapse of cavitation bubbles generated sonolytically. In general, most studies in environmental sonochemistry have adopted the "hot spot" concepts to explain experimental results. This theory considers a sonochemical reaction as a highly heterogeneous reaction in which reactive species and heat are produced from a welldefined microreactor, "the bubble of cavitation".

In aqueous phase sonolysis, there are three potential sites for sonochemical activity (Figure 1.4), namely (Berberidou et al., 2007):

- the gaseous region of the cavitation bubble where volatile and hydrophobic species are easily degraded through pyrolytic reactions as well as reactions involving the participation of hydroxyl radicals with the latter being formed through water sonolysis,
- the bubble-liquid interface where hydroxyl radicals are localized and, therefore, radical reactions predominate although pyrolytic reactions may also, to a lesser extent, occur and
- The liquid bulk where secondary sonochemical activity may take place mainly due to free radicals that have escaped from the interface and migrated to the liquid bulk.

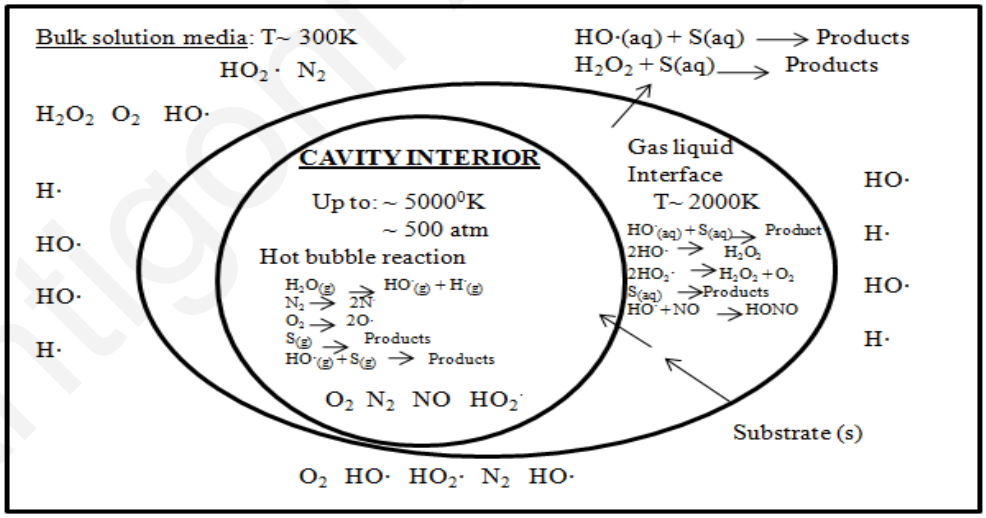

Figure 1.4: Reaction zones in the cavitation process (Adewuyi et al., 2001)

Reactions involving free radicals can occur within the collapsing bubble, at the interface of the bubble, and in the surrounding liquid. Within the center of the bubble, harsh conditions generated on bubble collapse cause bond breakage and/or the dissociation of the water and

other vapors and gases, leading to the formation of free radicals or the formation of excited states. Solvent and/or substrates suffer homolytic bond breakage to produce reactive species. The high temperatures and pressures created during cavitation provide the activation energy required for the bond cleavage. The radicals generated either react with each other to form new molecules and radicals or diffuse into the bulk liquid to serve as oxidants. The second reaction site is the liquid shell immediately surrounding the imploding cavity, which has been estimated to heat up to approximately 2000 K during cavity implosion. In this solvent layer surrounding the hot bubble, both combustion and free-radical reactions (involving HO· derived from the decomposition of H_2O) occur. Reactions here are comparable to pyrolysis reactions. Pyrolysis (i.e., combustion) in the interfacial region is predominant at high solute concentrations, while at low solute concentrations, free-radical reactions are likely to predominate. At this interface between the bubble and bulk liquid, surface-active reagents also accumulate and species produced in the bubble first react with chemicals in the bulk liquid. It has been shown that the majority of degradation takes place in the bubble-bulk interface region. The liquid reaction zone was estimated to extend 200 nm from the bubble surface and had a lifetime of < 2μs. In the bulk liquid, no primary sonochemical activity takes place although subsequent reactions with ultrasonically generated intermediates may occur. A small number of free radicals produced in the cavities or at the interface may move into the bulkliquid phase and react with the substrate present therein in secondary reactions to form new products. Depending on their physical properties and concentrations, molecules present in the medium will be "burned" in close to the bubble or will undergo radical reactions

Several factors may affect the process efficiency in a complex way. The most important ones are (Klavarioti et al., 2008):

1. *The frequency and intensity* of ultrasound
2. *Reactor geometry*
3. *The physicochemical properties of the liquid medium* (vapour pressure, surface tension, viscosity, presence of impurities/gases) also crucially affect the performance of the sonochemical reactors. The initial size of the nuclei generated, cavitations inception and number of cavities produced depends mainly on these liquid properties.
4. *Temperature*. The rate of destruction is inversely proportional to the operating temperature, which also affects the vapour pressure of the medium, and hence lower temperatures will be preferred (Thompson and Doraiswamn, 2009).

5. Aeration and addition of catalyst such as TiO_2, $NiSO_4$, CCl_4, Fe^{2+}/Fe^{3+}, $CuSO_4$ and also salts such as NaCl, significantly enhances the extent of degradation.
6. *The presence of gases* (oxygen, ozone), or gaseous mixtures such as Ar/O_3 mixture also increases the efficiency of acoustic cavitation in some cases. The presence of dissolved gases or solids usually improves performance as they serve as extra nucleation centers.
7. *Type and nature of contaminant.*

1.8 Sonophotocatalysis

Although photocatalysis and sonolysis have been employed individually for the degradation of several organic species in water, their combined use (i.e. sonophotocatalysis) has received appreciably less attention. Both processes predominantly involve the formation of free radicals and other reactive moieties, which consequently react with and destroy the pollutant species (Silva et al., 2007). Process integration may be favorable in eliminating the disadvantages associated with each individual process, thus increasing degradation rates. For instance, in heterogeneous catalytic systems, the use of ultrasound creates conditions of increased turbulence in the liquid, thus decreasing mass transfer limitations and increasing the surface area available due to catalyst fragmentation and de-agglomeration.

The following benefits are associated with the sonophotocatalytic process (Collin et al., 2009):

- Pore trappings from loading or deposition of titania onto an opaque substrate (catalyst support) may no longer reduce the efficiency of the supported photocatalyst. This is because ultrasound irradiation can be used as an irradiation source to induce TiO_2 particles to perform sonocatalytic activity (even if UV radiation is blocked or is not present during the degradation process)
- The reactor can be operated at high catalyst slurry concentration, maximizing the number of catalytically active sites per unit volume of reactor, since, UV light shielding by the slurry can be overcome by sonication acting on the entire volume.
- Both UV intensity and ultrasonic energy can be adjusted independently with ease, to optimize.
- The synergistic effect of UV and ultrasonic irradiation will enable a higher local concentration of hydroxyl radicals to be generated, further complementing the adsorption properties of selected catalyst support such as activated carbon. This synergy will assist the degradation and mineralization of the generated intermediate by-products.
- Sonication, influences favorably both the oxidation and reduction reactions process of the targeted pollutant. However, some pollutants may exhibit temperature dependence for an efficient degradation process.

- Sonication increases turbulence in the liquid, thus decreasing mass transfer limitations and increasing the catalytically active surface area due to particle fragmentation and deagglomeration.
- The frequency of ultrasound irradiation may influence the degradation efficiency of the pollutant molecules. This may be due to the fact that sonochemical reactions are driven by secondary radical reactions in the liquid bulk, which are less efficient. However, this factor may be pollutant specific.
- Various research teams investigating sonophotocatalysis reaction using different model pollutants and parameters reported that sonophotocatalysis was more effective than sequential combination of sonolysis and photocatalysis and in most cases, even more effective than the additive effects of sonolysis and photocatalysis. Photocatalysis combined with high frequency sonolysis resulted in an overall pollutant degradation rate that was equal to the sum of the individual rates for photocatalysis and sonolysis. However, low frequency sonolysis in combination with photocatalysis resulted in a stronger synergistic effect, no effect or sometimes demonstrating dependence on the level of ultrasound power.

In Table 1.6, studies utilizing sonophotocatalysis/sonocatalysis/sonolysis for the degradation of various pollutants by advanced oxidation are shown.

Table 1.6: Studies utilizing sonophotocatalysis/sonocatalysis/sonolysis for the degradation of various pollutants

a/a	Contaminants degraded	Initial Concentration	Treatment scheme	Comments	Reference
1	1,4-dioxane	100 mg/L	Horn-type Sonicator (f = 20 kHz, i = 600 W) Fe0, Fe^{2+} and $S_2O_2^{-8}$ were used as oxidants at 0.5 mg/L each. HCO^{-3} was used as a radical scavenger	Degradation kinetics established that there were 3 steps involved: initiation, acceleration and stabilization. Sonolysis generates HO· in the acceleration step but adding the oxidants made HO· the main degradation factor at the initiation step and increased the pollutant degradation efficiency.	Son et al., 2006
2	1,4-dioxane	50 mg/L	Anatase TiO_2 and HF-treated TiO_2 (200 mg/L), UV-A, Hg–Xe-lamp, (365 nm), Horn-type sonicator, (f = 20 kHz, i = 50W)	SPC process demonstrated synergistic effect in the degradation process. Treating TiO_2 with hydrofluoric acid solution improved the absorption capabilities of the TiO_2 in adsorbing the target pollutant.	Nakajima et al., 2004
3	17α-estradiol 17β-estradiol estrone estriol equilin 17α-dihydroequilin 17α-ethinyl estradiol norgestrel.	10 μg/L	0.6, 2 and 4 kW ultrasound sources, 0.6 kW sonication unit, probe diameter of 4.5 cm, 20 kHz.	The sonolysis process produced 80–90% destruction of individual estrogens at initial concentration of 10 μg/L within 40–60 min of contact time.	Suri et al., 2007
4	2,4,6- trichlorophenol	100 mg/L	(Anatase) TiO_2 (0.1 g), UV (15 W), Horn-type sonicator (f = 22 kHz, i = 400 W), ultrasonic bath (f = 22 kHz, i = 120 W) air	Sonication by bath type sonicator was more efficient as compared to a horn-type due to the localized cavitation produced by the horn-type sonicators. Lower sonication intensity and higher solution temperature enhanced degradation of targeted pollutant.	Shirgaonkar et al., 1998
5	2-chlorophenol	Varied $(1\text{-}7)*10^{-4}$ M	(Anatase–Aldrich, Degussa P25, Alfa 1, Alfa 2) TiO_2 (0.1 g/L), UV-A, Iron alongenide lamp, (250 W, 315–400 nm), Horn-type sonicator (f = 20 kHz, i = 20 W), Ar, O_2 or O_2/O_3	P25 was found to be the most effective catalyst in the degradation of 2-chlorophenol. Gas mixtures (Ar–O_2) gave the maximum reaction rate.	Ragaini et al., 2001
6	2-chlorophenol,	$5*10^{-4}$ M,	(Degussa P25) TiO_2 (0.1 g/L), UV-A, Iron	Sonication promoted the rate of photocatalytic degradation by promoting the	Mrowetz et al.,

	acid orange 8 and acid red 1	2–7*10^{-5} M	alongenide lamp, (250 W, 315–400 nm), Horntype sonicator (f = 20 kHz, i = 15W)	deaggregation of the photocatalyst and by inducing the desorption of organic substrates as well as the degradation of the intermediates from the photocatalyst surface.	2003
7	Acid orange 7	1.43*10^{-4} M	He–Ne laser, (632nm, 100 mW/mm^2), 2 transducer-type sonicator (f = 20 kHz and 1 MHz, i = 40W)	Combining visible light and sonication provided the synergistic degradation effect which can be explained as the effect to the reduction of the band gap energy of the dye (from absorption of photon energy of light), induced by high temperature and high pressure via the bubble collapse under the sonication process.	Ma et al., 2006
8	Acid orange 8	4*10^{-5} M	(Degussa P25) TiO_2 and ZnO (0.1 g/L), UV-A, Iron halogenide lamp, (315–400 nm, 250 W), Horn-type Sonicator (f = 20 kHz, i = 20W)	Sonication of the aqueous system produced H_2O_2, which in turn generated (HO·) during SPC reaction, thus enhancing the degradation process via a synergistic effect.	Selli et al., 2002
9	Acid red 88	0.025–0.09mM	16-64 $mWml^{-1}$, 1g.L^{-1} catalyst loading TiO_2,	The degradation by sonolysis and PC followed first-order like kinetics with respect to the concentration of AR88. The SPC degradation rates using TiO_2 or Fe^{3+} were found to be higher than that observed with sonolysis or PC. The synergy index calculated for TiO_2 SPC was 1.3, suggesting that the combination of sonolysis and TiO_2 PC resulted in a small synergetic effect. Also, the SPC in the presence of Fe^{3+} was synergistic with a synergy index of 2.3.	Madhavan et al., 2010
10	alazine gesaprim commercial herbicides	Atrazine content of 1.93*10^{-4} M present in the gesaprim and atrazine alachlor content of 5.7*10^{-5} M and 1.46*10^{-4}M present in the alazine, respectively	(Degussa P25) TiO_2 (200 mg/L), UV-A (15 W, 352 nm), Horn-type sonicator (f = 20 kHz, i = 500 W)	Using SPC, 90% of the active component in the gesaprim was degraded while those in alazine were completely degraded. 80% of COD were abated for both herbicides with SPC at 150 min of irradiation time.	Bahena et al., 2008

11	arsenic(III)	0.0013- 0.0268 mM	Branson Digital Sonifier-450, tip diameter) 19 mm or 10 mm, USA), constant temperature at 20 °C. Sonication at 20 kHz was carried out with a Branson Digital Sonifier, acoustic power range of 34-36 W.	Pulsed sonication showed a profound effect on the oxidation of As(III) to As(V) in comparison to the continuous mode of operation, that consequently reduced the reaction time and energy requirement for the process. Increasing acoustic amplitude led to an enhanced rate of oxidation of As(III).	Neppolian et al., 2009
12	bioxalate	0.9 mM	The reactor employs a bottom-mounted 358 kHz transducer operated between 0 and 100 W.	The degradation rate of bioxalate exposed to "sonozone" (i.e., simultaneous ultrasonication and ozonolysis) was found to be 16-times faster than predicted by the linear addition of ozonolysis and ultrasonic irradiation rates.	Vesitis et al., 2010
13	$C_9H_8O_2$ p-$C_9H_8O_3$ o-$C_9H_8O_3$ $C_9H_8O_4$ $C_{10}H_{10}O_4$ $C_9H_{10}O_5$ $C_8H_8O_4$ $C_7H_6O_5.H_2O$ $C_7H_6O_3$ $C_6H_6O_2$ $C_6H_6O_2$ $C_9H_{10}O_4$ $C_7H_6O_4$	50 mg/L each	(Degussa P25) TiO_2 (0.75 g/L), UV-A (9W 350– 400 nm, 250 W and 400 W 366 nm), Horn-type sonicator (f = 80 kHz, i = 120 W), H_2O_2 (0.118 mol/L)	Complete mineralization and toxic reduction of pollutants were achieved after SPC treatment at 400W UV-A with H_2O_2 for 120 min. No change in catalyst composition and morphology were observed but surface area increased due to sonication deaggregating properties.	Silva et al., 2007
14	chitosan	5g/L	Ultrasound irradiation (24 kHz) was provided by a sonicator, while an ultraviolet source of 16W was used for UV irradiation, ultrasound power 30–90 W,	The extent of sonolytic degradation increased with increasing ultrasound power (30–90 W), while the presence of TiO_2 in the dark generally had little effect on degradation. On the other hand, TiO_2 SPC, led to complete chitosan degradation in 60 min with increasing catalyst loading. TiO_2 SPC was always faster than the respective individual processes due to the enhanced formation of reactive radicals as well as the possible ultrasound-induced increase of the active surface area of the catalyst.	Taghizadeh et al., 2011
15	ciprofloxacin	15 mg/L	544-1081 KHz, input power 200W/L	For this experimental setup, 544 kHz proved to be the most favorable working frequency. An increasing bulk temperature resulted in a faster decline in concentration.	De Bel et al., 2011
16	congo red	10 mg/L	(Nanometer rutile powder) TiO_2 (1.0–1.5 g/L), Transducer-type sonicator (f = 40 kHz, i = 50	Sonocatalysis degradation was performed successfully and followed pseudo first-order kinetics. The sonocatalyst degradation exhibited pH and temperature	Wang et al., 2007

			W), pH 3.0–5.0	dependence. However, these effects may be pollutant specific.	
17	congo red, methyl orange	Unknown	(Anatase–Aldrich, Degussa P25) TiO_2 (0.3–1 g), UV-A (4W, 300–400 nm), ultrasonic bath (f = 47 kHz, i = 81 W), Ar, N_2 or air ascorbic acid (hole scavenger) pH (6.4 for congo red, 6.2 for methyl orange)	The positive effect ultrasound from SPC does not only occur on oxidation reactions but also on reduction reactions.	Perez et al., 2007
18	diclofenac	50-100 mg/L	Irradiation at 24 kHz, processor power 400 W, ultrasonic irradiation at 216 kHz and 617 kHz in ultrasound reactor URS 1000. Processor power of generator from 30-120 W	Degradation of diclofenac was directly related to the formation of hydrogen peroxide. The highest decrease of diclofenac concentration was achieved at 617 kHz. Minor differences between the decomposition rates at 216 and 617 kHz were observed more than 90% of the initial amount of diclofenac in 60 min.	Hartmann et al., 2008
19	diclofenac	4, 40 and 80 mg/L	ultrasonic transducer 20 kHz converter titanium horn tip of 1.3 cm diameter, power densities of 100, 200 and 400 W/L	Higher US density results in higher supply energy that leads to a more intense cavitation bubbles' formation.	Naddeo et al., 2009
20	diclofenac	2.5-80 mg/L	20 kHz, power density 25–100 W/L, electric power output up to 750 W,	Operating conditions, such as applied ultrasound power, solution pH, contact time, substrate concentration, liquid bulk temperature and the presence of dissolved gases can all affect treatment performance in a positive or adverse side.	Naddeo et al., 2010
21	diclofenac (DCF)	15, 30,70 and 130 μM	577, 861 and 1145 kHz, 120 W	The study has shown that anti-inflammatory drugs such as DCF is eliminated in water by high frequency ultrasound and the efficiency of elimination is considerably improved by the Fe species.	Guyer et al., 2011
22	diclofenac (DCF)	0.01–0.12 mM	Ultrasound frequency of 213 kHz in a continuous wave mode and the power delivered was 55 mWm/L, TiO_2 1g/L	The degradation of DCF using a sonophotocatalytic process showed a slight synergy effect when TiO_2 was present as a photocatalyst under UV light irradiation. In the presence of FeZnO, degradation shows an additive effect. However, the mineralization process during the combined process showed a detrimental effect.	Madhavan et al., 2010
23	diclofenac (DCF), amoxicillin (AMX), carbamazepine (CBZ)) in single solutions and also in three mixtures	2.5-10 mg/L	power density (25–100W/L), initial solution pH (3–11),	It was found that the pharmaceuticals conversion was enhanced at increased applied power densities, acidic conditions and in the presence of dissolved air. The reaction rate increased with increasing initial concentration of single pharmaceuticals but it remained constant in the mixtures, indicating different kinetic regimes (i.e. first and zero order respectively).	Naddeo et al., 2009

	spiked in urban wastewater effluent.				
24	distilled water	-	TiO_2 (5 mg/ml), Xe (500 W) Horn-type sonicator (f = 200 kHz, i = 200 W), Ar	Liquid water was effectively decomposed to H_2 and O_2 using SPC, which was not possible by using photocatalysis or sonolysis independently.	Harada et al., 2001
25	DMPO methanol	8 mM, 4% v/v	Au/TiO_2 dosage 0.3 g/L, 0.5 and 1.0 g/L, 140 kHz transducer, 50 W, the average power intensity of ultrasound 0.045 W/mL	The high sonocatalytic activity of Au/TiO_2 can be attributed to its high activity for the thermal cleavage of water and the thermal reforming of methanol.	Wang et al., 2010
26	ibuprofen (IBP)	2, 5, 10 and 21 mg/L	Ultrasound frequency 300 kHz, power output 80W	IBP destruction by sonolysis used 300 kHz and 80 W of applied power leading to 98% destruction in 30 min. pH values above its pKa, reduces the degradation rate of IBP, compared to results obtained in acidic media where the most favorable condition for the degradation was observed. Optimal conditions to increase the degradation rate were found under air and oxygen. IBP was completely eliminated when only 8% of DOC was left after 120 min of treatment.	Mendez- Arriaga et al., 2008
27	laurylpyridinium chloride (LPC)	0.1–0.6 mM	Ultrasound frequency of 355 kHz in continuous wave mode, Power output 30 W	The initial pathway for the decomposition of the cationic surfactant LPC occurred primarily by pyrolytic decomposition of the surfactant molecules adsorbed at the surface of cavitating bubbles. It was also established that further complex processes involving oxidation of intermediates leaded to low molecular weight water soluble species that are difficult to mineralize, indicating that sonolysis alone was not an efficient technique for the completed degradation of LPC.	Singla et al., 2011
28	malachite green	2.5–12.5 mg/L	TiO_2 (0.1–0.5 g/L), UV-A (9 W, 320–400 nm), Horn-type sonicator (f = 80 kHz, i = 75–135 W), (Ar, Air, O_2, He) pH (5.5)	Sonolysis under Ar was highly effective compared to other types of gases, however, SPC was still the most effective due to enhanced free radical generation and increase of catalyst active surface area induced by sonication.	Berberidou et al., 2007
29	methyl orange	32 mg/L	(Degussa P25, Yili TiO_2, Ag/TiO_2) TiO_2 (36 mg/ L), Xenon lamp, (800 W, 688–599 nm), Transducer-type sonicator (f = 40 kHz, i = 180W)	Synergistic effect between sonolysis and photocatalysis were demonstrated in the complete decomposition of methyl orange. The degradation ratio of methyl orange was proportional to the increased in sonication energy.	Wang et al., 2008
30	methyl orange	10 mg/L	(Rutile/Anatase) TiO_2 (250–1250 mg/l) Horntype sonicator (f = 40 kHz, i = 50 W) pH	In comparing the effectiveness of rutile and anatase TiO_2 in a sonocatalysis process, rutile TiO_2 demonstrated better degradation rate than anatase TiO_2.	Wang et al., 2005 Collin et al., 2009

			3.0	Furthermore, the catalytic activity of reused rutile TiO_2 catalyst was higher than that of the new rutile TiO_2 catalyst.	
31	methyl tert-butyl ether	$1*10^{-3}$ M	(Degussa P25) TiO_2 (0.1 g/L), UV-A, Iron alongenide lamp, (250 W, 315–400 nm), Horntype sonicator (f = 20 kHz, i = 22.8 W), $Ar–O_2$ mixture	Photocatalysis was found to be more effective than sonolysis but SPC gave the best degradation rate. A higher degradation rate was obtained under ultrasound in the absence of stirring, thus proving that stirring may reduce the formation of cavitation bubbles. The optimum operation condition in regards to energy consumption was obtained with SPC under intermittent stirring.	Selli et al., 2005
32	naphthol blue black	50 μM	(Degussa P25) TiO_2 (1 g/L), Transducer-type Sonicator, (f = 640 kHz, i = 240 W)	Sonolysis was determined to increase the degradation rate of the targeted pollutant and photocatalysis was instrumental in promoting mineralization.	Stock et al., 2000
33	nitrobenzene	50 μ/L	Ultrasonic power input and frequency of A, B, or C field, 300 W and 28 kHz, respectively	Ultrasound with dual fields can improve the degradation efficiency of nitrobenzene compared to that of single field, and the improvement phenomenon is even more pronounced in the orthogonal dual-field system.	Zhao et al., 2009
34	oxalic acid	0.8 M	(Rutile-type) TiO_2 (0.1 g/L), UV-A, Xe-lamp, (500 W, 315–400 nm), Transducer-type sonicator (f = 200 kHz, i = 200 W), Ar, Ar/O_2, air	The production of CO_2 in SPC was double than the sum of yields of photocatalysis and sonolysis in an Ar atmosphere. H_2O_2 evolved during sonication aided the synergistic effect.	Harada et al., 2006
35	oxalic acid	0.8 mol/L	Sonolysis of oxalic acid solution was carried out under photoirradiation in an Ar atmosphere.Ultrasonic generator: Kaijo TA-4021-4611, 200 kHz, 200 W). For photosonolysis: 500 W Xe lamp,	The degradation of oxalic acid was promoted by active species from H_2O_2 which was produced by sonolysis of water.	Tanaka et al., 2010
36	paracetamol, levodopa	25, 50, 100 and 150 mg/L	574, 860 and 1134 kHz of ultrasonic frequency with horn-type sonicator and actual power values of 9, 17, 22 and 32W at 20^0C	The sonochemical degradation of both products follows a pseudo-first-order reaction kinetics. Complete removal of pharmaceuticals was achieved in some cases but some dissolved organic carbon remains in solution showing that long lived intermediates were recalcitrant to ultrasound irradiation. Pollutants conversion and COD removal were found to decrease with increasing the initial solute concentration and decreasing power. The best results were obtained with	Isariebel et al., 2009

				574 kHz frequency.	
37	phenol	0.5–5 mmol/ dm^3	TiO_2/Activated Carbon sol gel catalyst (3–4 g/dm^3), Horn-type sonicator (f = 20 kHz, i = 75 W)	Under sonication, the amount of catalyst was proportionate to the degradation rate of the phenol.	Kubo et al., 2007
38	phenol	1 mol/m^3	Anatase) TiO_2 (0–10 g), Horn-type sonicator (f = 20 kHz, i = 50 W), air	Degradation rate of the targeted pollutant was proportionate to the amount of TiO_2 and dissolved O_2.	Kubo et al., 2005
39	phenyltrinuoro–methylketone	160 μmol/L	(Degussa P25, 3.5 g/L) TiO_2 and Synthesized TiO_2 (14 g/L), high pressure mercury lamp, (>290 nm, 125W), Horn-type sonicator (f = 30 kHz) and Transducer-type sonicator (f = 515 kHz)	Increasing ultrasound irradiation frequency (30 to 515 kHz) had a profound effect of the degradation of the targeted pollutant, which followed the 1st order removal rate. Cavitation can cause some recalcitrant species, CF_3 to degrade.	Theron et al., 1999
40	propyzamide	30 μmol/ dm^3	(Anatase) TiO_2 (0–250 mg), high pressure mercury lamp, (100 W), Transducer-type sonicator, (f = 200 kHz, i = 200 W), He	SPC process resulted in the complete mineralization of the propyzamide whereas the photocatalysis process required higher temperature and pH to effectively degrade propyzamide while producing intermediates.	Yano et al., 2005
41	reactive black 5	20–120 mg/L	(Anatase–Aldrich, Hombikat UV-100, Degussa P25, Tronox AK1 Millennium PC 500) TiO_2 (0.05–1 g/L), UV-A (9 W, 350–400 nm), Horntype sonicator (f = 80 kHz, i = 135 W), H_2O_2 (0.01 M) pH (2.6–9)	Addition of H_2O_2 hindered degradation due to scavenging of photogenerated holes and HOº.Complete decolorization was achieved after SPC treatment of 60 mg/L dye, 0.25 mg/L catalyst, ambient pH 5.8 with O_2 sparging.	Kritikos et al., 2007
42	reactive Red dye 198	Unknown	Degussa P25, Hombikat UV-100, ZnO, irradiations (50 W, halogen lamps), Ultrasonic bath (f= 47 kHz, i = 130 W), O_2, pH(varied by adding NaOH or HCl)	Cavitations caused H_2O_2 to split, producing oxidative species ($^1O_2$, O_2^-); inducing faster oxidation of the targeted pollutant and intermediates as well as deaggregating the photocatalyst particles producing synergistic effect.	Kaur et al., 2007
43	salicylic acid	276 mg/L	(Anatase–Aldrich, Degussa P25, Hombikat	SPC had a pronounced effect on the pollutant degradation rate and efficiency due	Davydov et al.,

			UV-100, Ishihara ST-21) TiO_2 (0.25 g/L) UV-A (4 W, 320nm), Horn-type sonicator (f = 20 kHz, i = 100–110 W), O_2 (500 cm^3/min)	to aggregate breakage and photocatalytic usage of radicals formed by the sonication process. SPC seemed preferential towards smaller sized catalyst particle.	2001
44	sulphur	0–2 g	(Anatase–Aldrich, Degussa P25) TiO_2 (0.56 g/L), UV-A (4, 6, 8 W, 300–400 nm), Horn-type sonicator(f = 30 kHz, i = 81 W), air	Zero-order degradation rate of sulphur using SPC was reached after 150 min and was 20 times higher than sonolysis alone. P25 was determined to be more effective than Anatase.	Mendez et al., 2007
45	ten dihydropyrimidinones	0.23 mM	Horn-type sonication at 24 kHz, 460 W/cm^2	Complete conversion at 70°C in the presence of $K_2S_2O_8$ within 5-27 min depending on the substrate.	Memarian and Farhadi, 2008
46	trichloroethylene (TCE), carbon tetrachloride (CT)	1, 5, 10 mg/L	Sonication 20 kHz, 20% amplitude, 54 W	Initial concentration of TCE and CT were decreased the degradation rate for TCE increased, while that of CT was not affected. The enhancement of TCE degradation is attributed to both the increase of hydroxyl radical concentration by scavenging of CT for hydrogen atoms and the generation of chlorine-containing radicals and HClO from pyrolysis of CT during sonolysis of CT.	Lee et al., 2010
47	triclosan	5 μg/L	Horn-type sonication at 80 kHz, 135 W, pH=7-8	First-order rate was affected strongly by the water matrix in the order: seawater >3.5% NaCl in water>urban runoff>deionised water>wastewater. In all samples but wastewater, complete removal after 120 min.	Sanchez-Prado et al., 2008
48	triphenylphosphine oxide	10-350 mg/L	Horn-type sonication at 20 kHz, 125-250 W, pH=7	First-order rate increases with increasing power and decreasing volume. Conversion decreases at increased initial concentrations and temperatures. Water matrix (H_2O_2, butanol, Fe^{2+}) affects performance. By-products were more toxic than the drug.	Emery et al., 2005

1.9 Monitoring of the treatment efficiency of various processes with regard to organic pollutants' removal

To monitor the treatment efficiency several equipment such as Total Organic Carbon analyzer, UV-Vis spectrometer, liquid and gas chromatography are used. More information on each one of them is provided in the following paragraphs.

1.9.1 Total Organic Carbon (TOC) analyzer

The TOC-VCPH/TOC-VCPN instrument measures the amount of total carbon (TC), inorganic carbon (IC) and total organic carbon (TOC) in water. "Oxidative combustion-infrared analysis" is a widely used TOC measurement method that has been adopted by international standards. Moreover, when the ASI-V Autosampler is used in combination with the main unit, a fully automatic system is created, allowing automatic analysis of multiple samples. Either standard or high sensitivity catalyst can be used for TOC analysis.

The furnace temperature is set to 680 °C for TOC analysis. The detection rate for IC decreases with increasing concentration. As a result, the Non Purgeable Organic Carbon (NPOC) method is used instead of the TC-IC method when analyzing samples that contain IC concentrations in excess of 5 mg/L. TOC/TN catalyst is used for TN analysis and TOC/TN simultaneous analysis. The detection rate is low for the IC component when it exceeds 10 mg/L; as a result, TOC in samples containing more than 10 mg/L IC cannot be measured using the TC-IC method and should be measured using the NPOC method. The furnace temperature is set to 720 °C for TOC/TN and TN analysis. Preparation of acid used for IC removal in NPOC analysis or for IC analysis with the N Type instrument. A CO_2 absorber is used to remove CO_2 from the carrier gas that purges the optical system of the detector.

1.9.2 UV-Visible spectrophotometer (UV-Vis)

UV/Vis spectroscopy is routinely used in the quantitative determination of solutions of transition metal ions, highly conjugated organic compounds, and biological macromolecules.

Organic compounds such as pharmaceuticals, especially those with a high degree of conjugation, also absorb light in the UV or visible regions of the electromagnetic spectrum.

The solvents for these determinations are often water for water-soluble compounds, or ethanol for organic-soluble compounds. (Organic solvents may have significant UV absorption; not all solvents are suitable for use in UV spectroscopy. Ethanol absorbs very weakly at most wavelengths.) Solvent polarity and pH can affect the absorption spectrum of an organic compound. While charge transfer complexes also give rise to colours, the colours are often too intense to be used for quantitative measurement.

The Beer Lambert- Law states that the absorbance of a solution is directly proportional to the concentration of the absorbing species in the solution and the path length. Thus, for a fixed path length, UV/Vis spectroscopy can be used to determine the concentration of the absorber in a solution. A UV/Vis spectrophotometer may be used as a detector for HPLC. The presence of an analyte gives a response assumed to be proportional to the concentration. For accurate results, the instrument's response to the analyte in the unknown should be compared with the response to a standard; this is very similar to the use of calibration curves.

The wavelengths of absorption peaks can be correlated with the types of bonds in a given molecule and are valuable in determining the functional groups within a molecule. The spectrum alone is not, however, a specific test for any given sample. The nature of the solvent, the pH of the solution, temperature, high electrolyte concentrations, and the presence of interfering substances can influence the absorption spectrum. Experimental variations such as the slit width (effective bandwidth) of the spectrophotometer will also alter the spectrum. To apply UV/Vis spectroscopy to analysis, these variables must be controlled or accounted for in order to identify the substances present.

1.9.3 Chromatographic separation, quantification and elucidation

Nowadays, gas and liquid chromatography (GC and LC) in combination with modern extraction, derivatization, and clean-up methods provide the opportunity to quantify many pharmaceutical compounds and metabolites down to ng/L levels. Capillary electrophoresis (CE) has also been used for analysis of pharmaceuticals. It is less complex and less expensive than GC and LC, but less sensitive than GC and LC, with detection limits in the μg/L range. Therefore CE methods are more appropriate for analysis of wastewater samples rather than surface water samples. In a continuous effort to optimize analytical techniques, several advances have recently been made in equipment and in sample preparation, derivatization, and

clean-up procedures (Stolker et al., 2004; Himmelsbach et al., 2006; Perez et al., 2007; Kostopoulou et al., 2008; Kassinos et al., 2011). To confront such analytical problems in both GC and LC analytical procedures, a clean-up step is considered necessary and added before analysis of the final extract.

Both GC and LC are applicable to the analysis of pharmaceuticals in environmental samples. GC is preferable for the analysis of non-polar and volatile compounds, but it can be applied for the analysis of low concentrations of pharmaceuticals by addition of a derivatization step. This step is very important and many optimization efforts have been made, because it can affect the accuracy of the method, because of the losses of analytes that can occur.

The advantages of GC include very high selectivity and resolution, good accuracy and precision, wide dynamic range, and high sensitivity (Hada et al., 2000, Cochran et al., 2002, Kassinos et al., 2011). Recently, GC×GC has been introduced in environmental analysis, providing even better separation and identification of the analytes in complex environmental samples (Hyotylainen et al., 2002; Kassinos et al., 2011).

LC is the preferred technique for separation of polar organic pollutants, and has the advantage of shorter analysis time, necessary for monitoring studies. The main drawback of HPLC analysis of pharmaceuticals in environmental samples is matrix effects (the ion-suppression phenomenon) which can reduce the sensitivity, linearity, accuracy, and precision of the method. For the detection of the analytes, tandem MS-MS is increasingly being used, replacing other detectors, in combination with LC (fluorescence, UV, PAD) and GC(FID, ECD) (Fatta et al., 2007; Petrovic et al., 2007; Kassinos et al., 2011).

The accurate quantification of pharmaceuticals, especially in environmental samples can be an analytical challenge, because of the complexity of the matrix and their low levels of occurrence. Several years ago, appropriate analytical techniques did not exist. Depending on the objective of a particular analysis, analytical methods can generally be classified into categories of methods (i.e. screening, quantitative, confirmatory and elucidation) (Sancho et al., 2006; Kosjek et al., 2007).

Elucidation methods are crucial in identifying pharmaceutical biodegradation products and should discover the identity of a suspected or unknown analyte that was previously detected by a screening method but not confirmed afterwards. Screening for unknown non-polar and thermally stable contaminants can be performed by GC-MS. Identification of the unknown compounds is then based on comparing their mass spectra with special mass spectral libraries (e.g. NIST), together with interpreting very abundant fragment-ion patterns obtained by electron ionization (EI)-MS (Bobeldjik et al., 2001; Zwiener et al., 2002; Pozo et al., 2006; Kosjek et al., 2007a; Kosjek et al., 2007b). However, single MS coupling will not give sufficient information to confirm the chemical structure of an unknown, even though the resolved chemical structure is in agreement with the library report. Also, comparison with authentic standard compounds is possible, but they are rarely commercially available.

The overall trend in chromatographic analysis of environmental samples involves employment of fast-LC methods using short, narrow bore columns, high mobile phase flow-rates and ultra high pressures. Shortening the analytical run times is an important step towards high sample throughput often required in laboratories conducting monitoring studies (Petrovic et al., 2010). In MS, two common strategies are applied, depending on the instrumentation used (Kosjek et al., 2007):

- one relies on MS measurement of accurate molecular mass, and subsequently, the determination of empirical formula using orthogonal acceleration time-of-flight (oaToF) instruments; and,
- the other involves structural elucidation on the basis of structural information gained in MS (MS^2) experiments that can be accomplished either by coupling mass analyzers in series (triple quadrupole (QqQ)) or by using a single ion-trap (IT) analyzer (Petrovic et al., 2007; Kosjek et al., 2007).

One of the options, increasingly being used in environmental analysis, is ultra-high performance liquid chromatography (UHPLC) that uses columns packed with sub-2μm particles, which enable elution of sample components in much narrower, more concentrated bands, resulting in better chromatographic resolution and increased peak capacity (Petrovic et al., 2010).

Another approach recently used to confirm positive findings involves the application of hybrid instruments such as quadrupole linear ion trap (QqLIT) that permits performing a sensitive quantitative analysis combined with an unequivocal identification and confirmation of target compounds (Petrovic et al., 2010). This is due to application of the Information Dependent Acquisition (IDA) function, with selected reaction monitoring (SRM) being the survey scan and an enhanced product ion (EPI) scan of each specific analyte, recorded at three different collision energies, as the dependent scan. Spectra achieved were afterwards compared with MS/MS library data, based on EPI spectra at the three collision energies used (Petrovic et al., 2010). The significance of including an IDA experiment is to avoid the reporting of false positive findings in the situations where: (i) due to poor fragmentation of the target compound or low intensity of the fragments, only one SRM transition is available; (ii) when the identification of target compounds is hampered by monitoring non-selective transitions, such as loss of water, carbon dioxide and hydrochloric acid; and (iii) when compounds are found at low levels and therefore, transitions are recorded at low intensity (Petrovic et al., 2010). Therefore, using both SRM and IDA mode, analyte identification and confirmation fulfill the stringent criteria set by the EU regulations (EU Commission Decision 2002/657/EC), obtaining more than enough IPs to ensure an accurate identification of target compounds in the samples (Petrovic et al., 2010).

In several studies (Marin et al., 2006; Petrovic et al., 2006; Pozo et al., 2006; Fernandez et al., 2008; Petrovic et al., 2010) hybrid quadrupole-time-offlight (QqTOF) instruments were used to confirm the identity of compounds identified by triple quadrupole (QqQ). An unequivocal identification of target compounds was based on accurate mass measurements of the molecular ions in TOF mode, and of the product ions obtained in QqTOF mode, by performing collision induced dissociation (CID). However, direct confirmation with a TOF instrument is only feasible for those compounds showing sufficient sensitivity, isotopic pattern, or easy in-source fragmentation (Petrovic et al., 2010). The main field of application is the identification of unknowns and elucidation of structures proposed for transformation products, where the amount of information obtained allows secure identification of the identity of compounds (Petrovic et al., 2007). Because of its unique characteristic of generating full scan product ion spectra with exact masses is the elimination of of false positives and avoiding interpretation ambiguities (Petrovic et al., 2007). The increased specificity provided by the high resolution QqTOF may provide S/N (signal-to-noise ratio) benefit in some analytical applications and

enable rather sensitive quantitative determination as reported by Stolker et al. (2004) and Petrovic et al. (2007), (MDL of 1-100 ng/L for selected analgesics, antibiotics lipid regulators, b-blockers and antiepileptics after SPE preconcentration of 100 ml of surface, drinking and groundwater).

In the identification of TPs with mass spectrometric techniques, the first step is usually the acquisition of MS^2 (and of higher order if working with IT-MS) spectra of the unchanged parent compound in order to elucidate the fragmentation pathway of the molecule. Comparison of the $MS^{2/n}$ fragment ions of the parent compound with those obtained from the TP provides valuable clues in determining the structure, for example, which parts of the molecule undergo modification in the degradation of the parent compound and which parts remain unchanged.

Accurate mass measurements provide additional evidence for postulated structures of the TPs by confirming proposed elemental compositions. Several studies describe the identification of TPs combining MS^n experiments (LC-QqLIT-MS and LC-IT-MS) with accurate mass measurements (LC-QqTOF-MS) (Eichhorn et al., 2005; Perez et al., 2006; Perez et al., 2007; Perez et al., 2008; Radjenovic et al., 2008; Petrovic et al., 2010).

A survey of the most representative recent multi-residue LC-MS/MS methods developed for the determination of regularly used pharmaceuticals in aqueous environmental matrices is given in Table 1.7. Table 1.8 shows a summary of photocatalytic and photochemical studies, analytical methods, reaction pathways and major TPs of selected pharmaceutical compounds.

Table 1.7: Most representative multiresidue LC/MS/MS methods for the quantitative determination of pharmaceuticals in aqueous samples

a/a	Reference	Pharmaceutical Compound	Matrix	MS system	Limit of quantitation (ng/L)
1	Castiglioni et al., 2005	30 compounds Antibiotics anti-inflammatory anticancer bronchodilator cardiovascular gastrointestinal drugs diuretics, estrogens and lipid regulators	Urban wastewater	QqQ (ESI)	0.1–5.2
2	Gomez et al., 2006	16 compounds Antibiotics b-blockers psychiatric drugs and anti-inflammatory	Hospital effluent wastewaters	QqQ (ESI)	4–47 (LOD)
3	Petrovic et al., 2006	28 compounds anti-inflammatories lipid regulators anti-ulcer agents anti-histaminics antibiotics and b-blockers	Urban and industrial wastewater	QqTOF (ESI)	15-500 (LOD)
4	Gros et al., 2006	28 compounds anti-inflammatories lipid regulators anti-ulcer agents anti-histaminics antibiotics and b-blockers	River and wastewater	QqQ (ESI)	River water 0.5–47 (LOD) and wastewater 1–60 (LOD)
5	Class et al., 2005	16 compounds Illicit drugs and their	Wastewater	QqQ (ESI)	0.63–8.7 (influent) and 0.48–3.2 (effluent)

		metabolites			
6	Hummel et al., 2006	20 compounds Psychoactive drugs and their metabolites	Surface and wastewater	QqQ (ESI)	10–100 (influent), 5–50 (effluent) and 1–10 (river water)
7	Hao et al., 2006	27 compounds antibiotics carbamazepine lipid regulators and antiinflammatories	Surface water	Qq-LIT	0.3–60
8	Calamari et al., 2003	23 compounds (A) b-agonist and antagonist anti-ulcer agent antibiotics lipid regulator and psychiatric drugs, (B) Antibiotics, anti-inflammatories and others and (C) Amoxycillin and omeprazole	River water	QqQ (ESI)	0.3–10
9	Quintana et al., 2004	12 compounds anti-inflammatories lipid regulators and triclosan	Surface and wastewater	QqQ (ESI)	0.3–5.6
10	Hilton et al., 2003	13 compounds Antibiotics Lipid regulator Analgesic/antiinflammatories b-blocker	River water	QqQ (ESI)	10–50 (LOD)

		anti-cancer and antidepressant			
11	Stolker et al., 2003	13 compounds analgesic/antiinflamamtory b-blocker lipid regulators antibiotics and antiepileptic	Surface water	QqQ (ESI) and QqTOF (ESI)	5–25
12	Vanderford et al., 2003	28 compounds Neutral and acidic pharmaceuticals and EDC and PCP	Surface and wastewater	QqQ (ESI/APCI)	1.0 (LOD)
13	Sacher et al., 2001	60 compounds analgesic b-blocker broncholytics secretolytics antineoplastics and lipid regulators	Ground water	QqQ (ESI)	7.9–44 (LOD)
14	Roberts et al., 2006	11 compounds OSPAR priority pharmaceuticals	Surface and wastewater	IT (ESI)	1–20 (LOD)
15	Petrovic et al., 2005	Neutral drugs (phenazone, pentoxifyline, carbamazepine)	Wastewater	Triple quadrupole ESI	0.5–1 μg/L (influent) 0.1–0.25 μg/L (effluent)
16	Petrovic et al., 2005	Oxytetracyclines	Soil interstitial water	Triple quadrupole ESI	0.1–0.25 mg/L
17	Petrovic et al., 2005	Sulphonamides	Wastewater effluent surface waters	Triple quadrupole ESI	200–370 (LOD) 600–10200 (LOQ)
18	Petrovic et al., 2005	Tetracyclines	Ground waters	Ion trap MS ESI	200–380
19	Petrovic et al.,2005	Erythromycin, roxythromycin, tylosin	Natural and Wastewater	Ion trap ESI	30–70

20	Grujic et al., 2009	Pharmaceuticals 19 compounds	Surface and ground water	LC–IT-MS (IT)	0.15-12.46
21	Kasprzyk-Hordern et al., 2007	28 basic/neutral pharmaceuticals	Surface water	UHPLC–MS/MS (QqQ)	0.3-50
22	Gros et al., 2009	Pharmaceuticals 73 compounds	Surface water, wastewater (effluent, influent)	LC–MS (QqLIT)	0.1-55

LOD: limit of detection, LOQ: limit of quantification

Table 1.8: Photochemical and photocatalytic studies, analytical methods, reaction pathways and major TPs of selected pharmaceutical compounds

a/a	References	Pharmaceutical compounds	Process	Water matrix	Identification methods	Reaction pathways	Major TPs identified
1	Vogna et al., 2002 Andreozzi et al., 2003 Zhang et al., 2008 Yang et al., 2008	Paracetamol	H_2O_2/UV (λ=254 nm) H_2O_2/UV (λ=254 nm) TiO_2/Simulated sunlight (λ> 365 nm) TiO_2 /UV (UVA and UVC)	Distilled water Distilled water Distilled water Milli-Q water	GC/EI-MS (IT) GC/MS (IT) GC-EI-MS (Q) GC-EI-MS (Q)	Hydroxylation Hydroxylation- addition mechanism Detachment of the acetamide group Oxidation	Acetamide (2-hydroxy-4-(N-acetyl)-aminophenol and 3-hydroxy-4-(N-acetyl)-aminophenol) Hydroxy-nitrogenous TPs Hydroquinone, 1,4-benzoquinone Hydroxy/keto dicarboxylic acids
2	Vogna et al., 2004	Diclofenac	H_2O_2/UV (λ=254 nm)	Distilled water	GC-EI-MS (IT)^{1}H-^{13}C-NMR authentic standards	Hydroxylation Dechlorination Cleavage of C-N bond	Hydroxy-derivatives2-(2-(2-chloro-6-hydroxyphenylamino)phenyl)acetic acid C-N cleavage products (i.e. 2,5-dihydroxyphenylacetic acid, 2,6-dichloroaniline, 2-hydroxyphenylacetic acid
3	Vogna et al., 2004	Carbamazepine	H_2O_2 /UV (λ=254 nm)	Distilled water	GC-EI-MS (IT)	Opening of the dibenzoxazepine moiety and cleavage of the C-N bond Decarboxylation	2-aminobenzoic, 2-hydroxybenzoic acid, 2-hydroxyphenol Aliphatic acids
4	Doll and Frimmel 2005	Carbamazepine	TiO_2/Simulated sunlight	Milli-Q water	LC-ESI-MS/MS (QqQ)	Hydroxylation Oxygenation Ring contraction and subsequent loss of the carboxaldehyde and the –$CONH_2$ groups	Hydroxy and dihydroxy- carbamazepine 10,11-Dihydrocarbamazepine-10,11-epoxide, Acridine, acridine-9- carboxaldehyde, hydroxyacridine- 9- carboxaldehyde, hydroxyacridine-9-carboxyalcohol
5	Perez-Estrada et al., 2005	Diclofenac	Photo-Fenton Solar light	Deminaralized water	GC-ESI-MS (Q) GC-PCI-MS (Q) LC-ESI-MS (ToF)	Hydroxylation-OH group oxidation Dechlorination Cyclization-dehydration Decarboxylation-aliphatic chain oxidation Cleavage of C-N bond Opening of the non-chlorinated ring	Hydroxy and quinine imine derivatives Hydroxy-dechlorinated quinine imine derivatives 1-(2,6-dichlorophenyl)-5-hydroxyindolin-2-one Decarboxylated, alkyl-oxidized derivatives (i.e. (E)-6-(2,6-dichlorophenyllimino)- 3-oxocyclohexa-1,4-dienecarbaldehyde, 2-(2,6-dichlorophenylamino) benzaldehyde) C-N cleavage products (i.e. 4-amino-3,5-dichlorophenol, 2,6-dichloroaniline, N-(2,6-dichlorophenyl) acetamide Small organic acids (acetic, maaleic, oxalic, formic)
6	Calza et al., 2006	Diclofenac	TiO_2/Simulated sunlight	Milli-Q water	LC-ESI-MSn(IT)	Hydroxylation-OH group oxidation Decarboxylation-aliphatic chain oxidation Cleavage of C-N bond Opening of the aromatic ring	Hydroxy, bihydroxy and quinine imine derivatives Decarboxylated and oxidized derivatives Chloro or hydroxyl-phenol derivatives Carboxylic acids (formic acid)
7	Mendez-Arriaga	Ibuprofen	TiO_2/Simulated	Milli-Q water	LC-ESI-MS(ToF)	Hydroxylation in the isobutyl	Hydroxy derivatives

	et al., 2008		sunlight			chain or/and on the propanoic moiety Demethylation or decarboxylation	Propionic acid, formic acid and hydroxypropionic acid or sodium salts
8	Trovo et al., 2009	Sulfamethoxazole	Photolysis/ Simulated sunlight	Distilled water Seawater	LC-ESI-ToF-MS	Hydroxylation Cleavage of the bond between the aminophenylsulfone and the methylisoxazoleamine moieties Cleavage of C-N bond Opening of the aromatic ring	Mono- and di-hydroxyl derivatives of sulfamethoxazole Hydroxyl derivative of the sulfanilic acid, 4-(hydroxyamino)benzenesulfonic acid 5-methylisoxazol-3-amine
9	Yang et al., 2010	Sulfachlorpyridazine Sulfapyridine Sulfisoxazole	TiO_2/UV light	Milli-Q water	HPLC/MS/MS	Cracking of the S-N bond decontamination of the nitrogen atom	Sulfapyridine, sulfisoxazole, monohydroxylated intermediates 6-chloropyridazin-3-amine, 6-aminopyridazin-3-ol, monohydroxylated intermediates, 3,4-dimethylisoxazol-5-amine, 3,4-dimethylisoxazol-5-ol
10	Sirtori et al., 2011	Nalidixic acid	Solar/ Photo-Fenton process	Demineralised water Saline water Simulated industrial effluent real industrial effluent	LC-ESI-ToF-MS	Hydroxylation Loss of a neutral molecule of H_2O Loss of carboxylic acid, alcohol functional groups Loss of C_2H_4 and C_2H_2O Electrophilic attack Oxidation and loss of ethyl chain and reduction of the carboxyl group	Aldehyde and carboxylic acid functionalities Chlorinated intermediates Methyl pyridine ring remained unchanged, reactions in the 1-ethyl-1,4,5,6-tetrahydro-4-oxopyridine-3-carboxylic acid moiety

CHAPTER 2

DESCRIPTION OF THE EXPERIMENTAL WORK

2.1 Objectives of the research work

The objective of this work was to study the conversion/mineralization of Diclofenac (DCF), Ibuprofen (IBP) and Carbamazepine (CBZ), in ultrapure water, urban wastewater and groundwater by means of photocatalysis using UV-A and simulated solar irradiation, sonolysis and sonophotocatalysis, in respect to the operating conditions.

More specifically the methodology followed included the following:

- The influence of the various parameters on the conversion/mineralization of the three active pharmaceutical ingredients (APIs) was assessed through UV absorption and dissolved organic carbon (DOC) measurements.
- Preliminary experiments were conducted to evaluate (i) the extent of the pharmaceutical adsorption onto the catalyst surface (Degussa P25) in the dark and (ii) the photolytic degradation in the absence of catalyst.
- Screening experiments were performed to assess the catalytic activity of seven semiconductors, namely Degussa P25, Tronox T-R, Hombikat UV-100, Tronox T-R HP2, Tronox A-K-1, Aldrich Anatase and Aldrich Rutile in respect to the degradation/mineralization of the APIs.
- In order to study the effect of the catalyst's loading on the degradation of the APIs, experiments were conducted, using Degussa P25, in the range of 50-800 mg/L.
- The influence of the initial concentration of the APIs on the kinetic rate was also examined. The concentration of the APIs varied from 5 to 20 mg/L.
- The amphoteric behavior of most semiconductor oxides affects the surface charge of the photocatalyst. Therefore, the dependence of degradation efficiency for DCF, IBP and CBZ on initial pH was investigated. Experiments were performed at acidic, near-neutral and alkaline conditions under the optimum conditions for each API.
- Experiments were performed with the addition of an electron acceptor, i.e., hydrogen peroxide (H_2O_2), which usually enhances the photodegradation of the substance in question due to the fact that these kinds of substances capture the photogenerated

electrons more effectively than dissolved oxygen, leading to a reduction of the electron hole recombination. The effect of the oxidant concentration on the APIs degradation during solar and UV-A photocatalysis was studied in the range of 0.07-1.4 mM.

- In order to evaluate the effect of water matrix on mineralization, effluent of a local urban wastewater treatment plant (WWTPEf) and groundwater (GW) samples were spiked with 10 mg/L of DCF, IBP and CBZ, added varying loadings of Degussa P25 in the range 500-3000 mg/L. Also, the effect of H_2O_2 addition was investigated at the optimum catalyst loading.
- The conversion of DCF, IBP and CBZ in single-compound solutions in ultrapure water by means of sonolysis was studied in respect to the effect of key operating conditions such as power density, addition of electron acceptor, effect of drug initial concentration, effect of gas sparging and the water matrix on the kinetics of pharmaceuticals reduction and mineralization.
- Combined photocatalytic/sonolytic tests were carried out taking into account the respective experimental conditions optimized from the photocatalytic experiments on the conversion of pharmaceuticals spiked into ultrapure water.
- In order to evaluate the toxicity of the treated solutions one bioassay was carried out such as *Daphnia magna*.
- To understand the reaction kinetics of the conversion of DCF, IBP and CBZ, a kinetic model was applied to the optimum conditions for all the processes.

The aforementioned activities are summarized schematically in Figure 2.1.

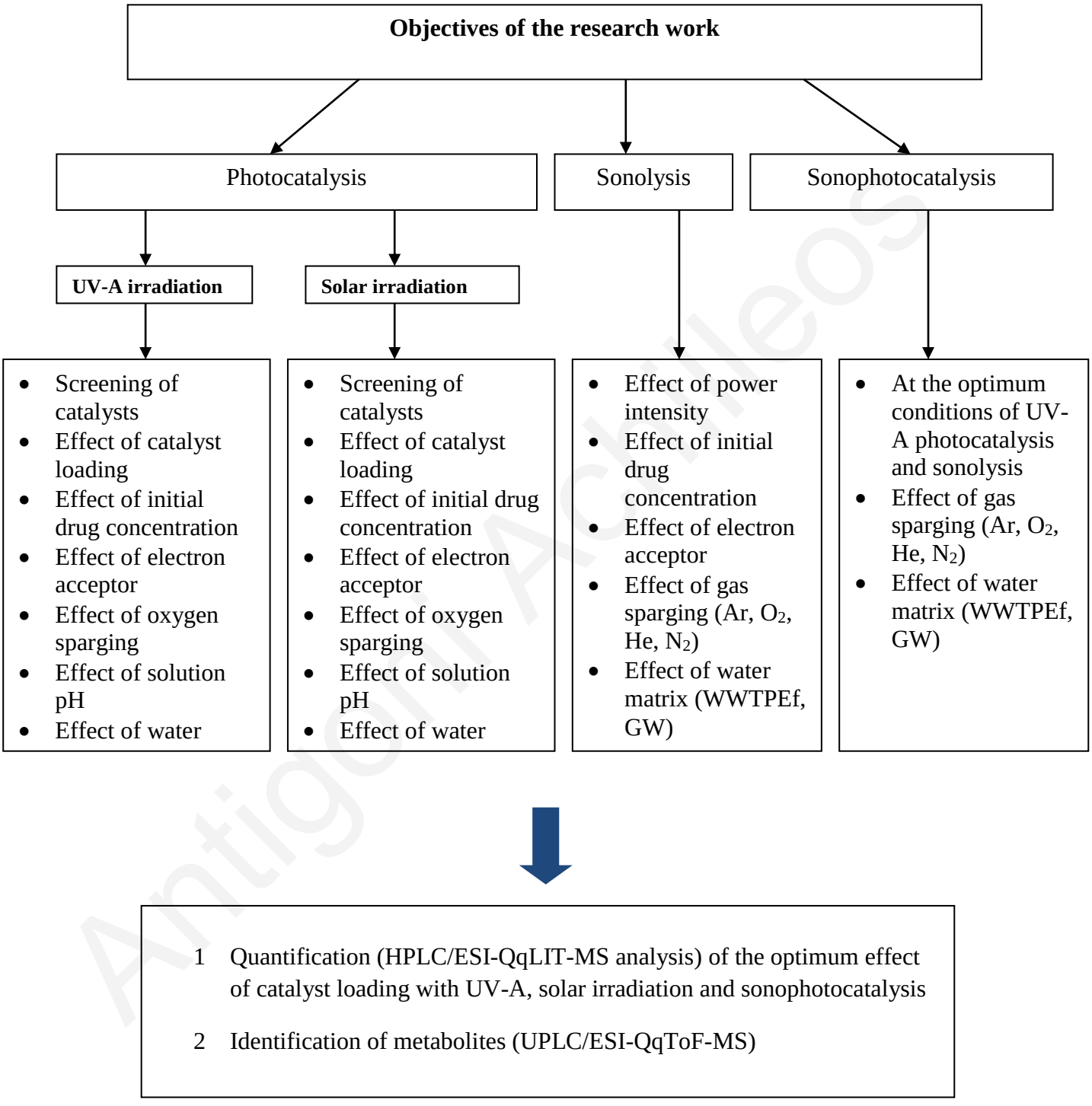

Figure 2.1: Objectives of the research work

2.2 Pharmaceutical substances investigated

DCF and IBP are non-steroidal anti-inflammatory drugs (NSAIDs) and a special group of pharmaceuticals that are often found in waters and wastewaters being one of the most widely available drug classes. The main common characteristic in the NSAID group is the carboxylic acid moiety that provides their acidic properties (Arriaga et al., 2008).

The name of DCF is derived from its chemical name: 2-(2,6-dichloranilino) phenylacetic acid. DCF is one of the pharmaceutically active compounds most frequently detected in the water-cycle. It is considerably stable under normal environmental conditions and the most probable decomposition pathway for its onsite elimination is photodecomposition (Perez- Estrada et al., 2005). DCF can be applied orally, as gel, or as liposome system for dermal application. Therefore personal hygiene leads to considerably high concentrations of DCF in wastewater (Hartmann et al., 2007). 15% is excreted unchanged after human consumption (Landsdorp et al., 1990; Rizzo et al., 2009). Approximately 65% of DCF is eliminated as the glucuronide and the sulphate conjugates of the hydroxylated metabolites in the urine and approximately 35% via the bile to the feces as conjugates of diclofenac plus metabolites (Khetan et al., 2007).

IBP is known to have an antiplatelet effect, though it is relatively mild and short-lived when compared with that of aspirin or other better-known antiplatelet drugs. Ibuprofen is a core medicine in the World Health Organization's "Essential Drugs List", which is a list of minimum medical needs for a basic health care system. The name of IBP is derived from its chemical name: (RS)-2-(4-(2-methylpropyl) phenyl) propanoic acid. Both DCF and IBP are prescribed for skeletal-muscle pain and inflammatory rheumatic disorders and also used for analgesic and antipyretic purposes (Kanabar et al., 2007). Unfortunately the extensive use of IBP has enclosed a secondary effect: IBP has been detected in water and its ecotoxicological impact on the microbiological systems can provoke irreversible harmful effects on bio receptors (Fabiola et al., 2009). IBP is negatively charged at neutral pH because their carboxylic moieties are deprotonated. Approximately 15% of IBP is excreted unchanged or as its glucuronide. The remaining percentage is allocated to further metabolites such as hydroxyl-IBP, carboxy-IBP, carboxy-hydratropic acid, and their respective conjugates, portions of which are also excreted (Khetan et al., 2007).

CBZ is also a worldwide used antiepileptic drug, prescribed for medical conditions such as chronic pain, treatment of epilepsy as well as for various psychotherapy applications (Miao et al., 2005). It is mainly metabolized into the active compound carbamazepine-10, 11-epoxide and further into other inactive compounds, principally glucuronides. Approximately 3% is excreted unchanged in urine, and is not significantly removed (less than 10%) during sewage treatment, resulting in the contamination of the receiving waters (Ternes et al., 1998; Andreozzi et al., 2002; Heberer et al., 2002; Jones et al., 2002; Jos et al., 2003). Studies in Europe and North America have shown that CBZ is one of the most frequently detected pharmaceuticals along with its metabolites in μg/L levels in surface water, drinking water and in WWTPs effluents (Miao et al., 2005).

The chemical structures and the properties of the above pharmaceuticals are shown below (Schematic 2.1 and Table 2.1).

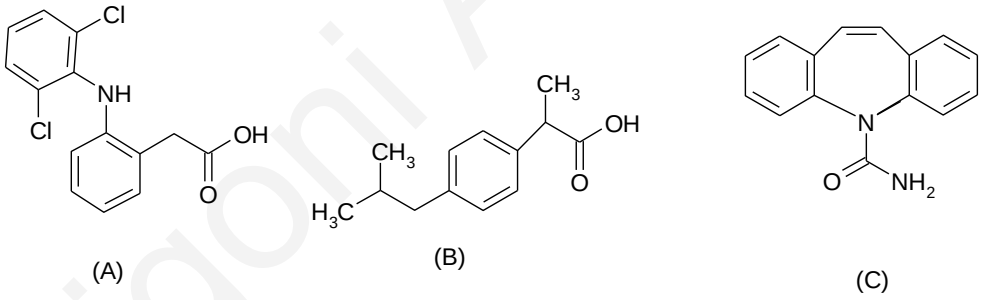

Schematic 2.1: Chemical structures: (A) DCF, (B) IBP (C) CBZ

Table 2.1: Properties of DCF, IBP and CBZ

Property	**Compound**		
	Diclofenac (DCF)	**Ibuprofen (IBP)**	**Carbamazepine (CBZ)**
Therapeutic group	NSAIDs	NSAIDs	Antiepileptic
Molecular formula	$C_{14}H_{11}Cl_2NO_2$	$C_{13}H_{18}O_2$	$C_{15}H_{12}N_2O$
Molecular weight	296.2	206.3	236.3
CAS No.	15307-86-5	15687-27-1	298-46-4
Solubility in water[d] (mg/ml)	50	0.021(25°C)	0.015 (25°C)
pKa	(4 - 4.2)[a, d]	(4.9 - 5.7)[b,d]	(13.9)[c ,d], (2.3)[e]
loqKow[d]	4.5 – 4.8	3.5 – 4.5	2.3 – 2.5

[a] Conors et al., 1986; [b]Arriaga et al., 2009; [c] Jones et al., 2002; [d] Carballa et al., 2005, [e] Nghiem et al., 2005

2.3 Reagents and Materials

IBP of purity 99% was purchased from Dr. Ehrenstorfer GmbH Germany and DCF, CBZ of purity 99% were purchased from Sigma Aldrich and used as received. Hydrogen peroxide (35% w/w solution) was supplied by Merck. Milli-Q water system (Millipore, USA) was used for the preparation of model solutions.

For the HPLC/ESI-QqLIT-MS analysis CBZ was obtained from Sigma Aldrich (Munich, Germany). IBP (> 98%) was obtained from Wellington Laboratories Inc, Canada. Acetonitrile, methanol and water used for the LC-MS analysis were Chromasolv LC grade solvents provided by Sigma Aldrich's Riedel de Häen (Steinheim, Germany). Formic acid (ACS grade) was obtained from Merck (Darmstadt, Germany).

Six commercially available TiO_2 samples were employed in the present study whose main properties are summarized in Table 2.2, for slurry photocatalytic experiments. All gases (Ar, N_2, O_2, Air), used for sparging were purchased from Linde Gas.

Table 2.2: TiO_2 catalysts used in this study. A: anatase; R: rutile; ND: not determined

Catalyst	Crystal form	BET area, m^2/g	Particle size, nm	Supplier
Degussa P25	75% A:25% R	50	21	Degussa AG
Hombicat UV100	100% A	>250	5	Sachleben Chemie GmbH
Aldrich	100% A	190-290	15	Aldrich
Tronox AK-1	100% A	90	20	Kerr-McGee Chemicals LLC
Tronox TRHP-2	100% R	7	ND	Kerr-McGee Chemicals LLC
Tronox TR	100% R	5.5	300	Kerr-McGee Chemicals LLC

2.4 Photocatalytic experimental process

Photocatalytic experiments were carried out as follows: 350 mL of an aqueous drug solution was loaded with the appropriate amount of TiO_2 (in the range 50 to 800 mg/L) and the resulting mixture was added in the photochemical reactor (Figure 2.2), (ACE Glass Incorporated).

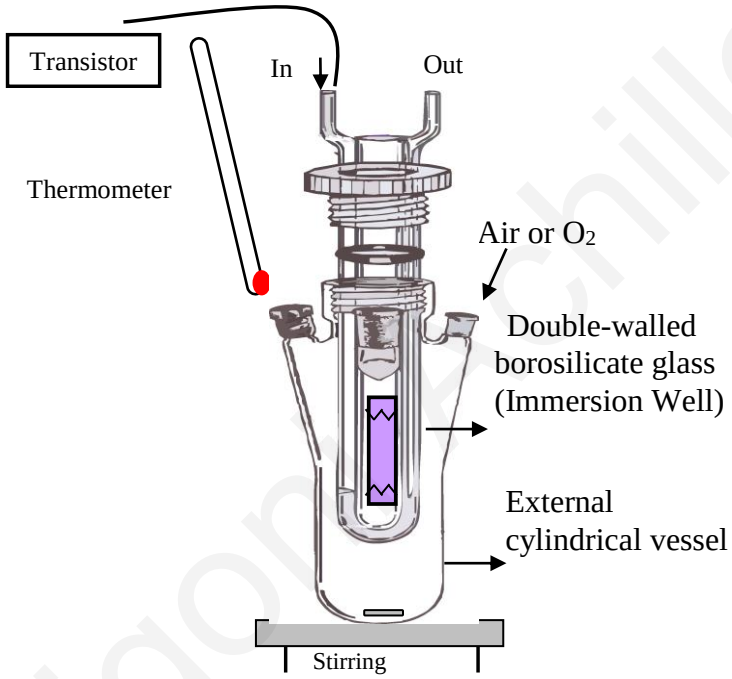

Figure 2.2: Photochemical reactor Ace glass

The suspension was magnetically stirred for 30 min in the dark to ensure complete equilibration of adsorption/desorption of the drugs on the catalyst surface. After that period the solution was irradiated by a 9 W UV-A lamp, 3.16 W/m^2 (Radium Ralutec lamp, 9 W/78, 350-400 nm). The photon flux of the lamp was frequently determined actinometrically using the potassium ferrioxalate method and it was found 3.37 x10^{-6} einstein/s (Kuhn et al., 2004). Experiments were conducted in an immersion well, batch type, laboratory scale photoreactor. It is a three- compartment apparatus and consists of an inner, double- walled, borosilicate glass housing tha lamp and an external cylindrical reaction vessel joined together with an

internally threaded connection with the aid of a nylon bushing connector and an O-ring. The reaction mixture was placed in the external cylindrical reaction vessel and the inner double-walled borosilicate glass was immersed inside the reaction mixture. The lamp was placed inside the inner borosilicate glass and was effective cooled by a water circulation stream through the double-walled compartment, acting as a cooling water jacket. During photocatalytic experiments the temperature was maintained constant at 25±2°C. The external reaction vessel was covered with aluminium foil to reflect irradiation exerting the outer wall of the reaction vessel. This reaction geometry is ideal for full exploitation of UV-A irradiation emitted from the lamp (Chatzisymeon et al., 2008).

For runs conducted under artificial sunlight conditions, solar irradiation was provided by a Phillips xenon lamp (Xe-OP) of 1000 W nominal power in a Newport (91113) solar simulator (Figure 2.3). Reactions were conducted in a glass vessel illuminated from the top (at a distance of 8 cm).

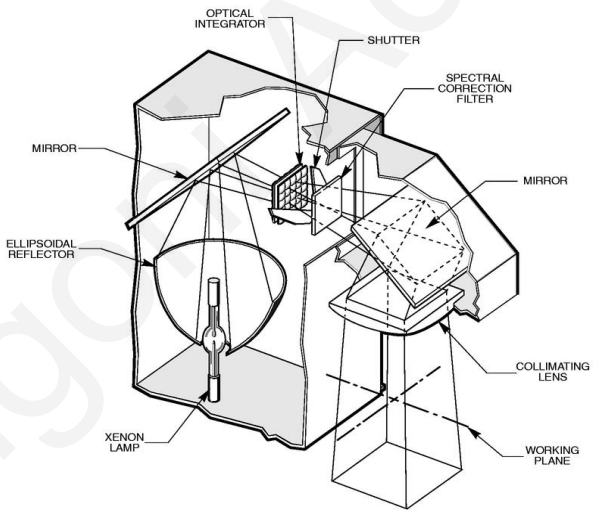

Figure 2.3: Solar simulator

An average irradiation intensity of 272.3 W/m^2 was maintained throughout the experiments and was measured by a radiometer (Newport model 70260). Periodically, samples were taken off from the reactor and were filtered with 0.22 μm filters to remove catalyst particles.

A similar procedure with 0 - 3000 mg/L TiO_2 loading was followed with real wastewater samples collected from a local urban wastewater treatment plant (WWTPEf), which applies

conventional activated sludge treatment train. The sample was collected after the tertiary treatment step which includes sand filtration and disinfection (chlorination). Groundwater (GW) was collected from a pumping well by the Geological survey department of Cyprus.

The physico-chemical characterization of the wastewater samples and groundwater is summarized in Tables 2.3 and 2.4, respectively.

Table 2.3: Wastewater characterization before pharmaceuticals spiking

Parameter	Unit	Value*
Temperature	°C	19.7
Conductivity	μS/cm	1424
DO	mg/L	4
pH	--	8.22
Turbidity	NTU	1.9
TOC	mg/L	11
SST	mg/L	4.6
COD	mg/L	6
Total-N	mg/L	3.7
Total-P	mg/L	2.96
Chlorides	mg/L	196
NH_4-N	mg/L	0.16

*average of three sampling analyses

Table 2.4: Groundwater characterizations before pharmaceuticals spiking

Parameter	Unit	Value*
Sample depth	M	207
Water level	M	181
Total hardness	mg/L	180
Sulphates	mg/L	1.25
Chlorides	mg/L	50
Boron	mg/L	0.1

*average of three sampling analyses

It must be mentioned that the analysis for the groundwater characterization before pharmaceuticals spiking was given by the geological survey department of Cyprus. Also some of the wastewater characterization analysis was given by the WWTPs laboratory.

2.5 Sonochemical experimental process

For the implementation of the experiments related to the application of sonolysis a digital sonifier has been used (Figure 2.4).

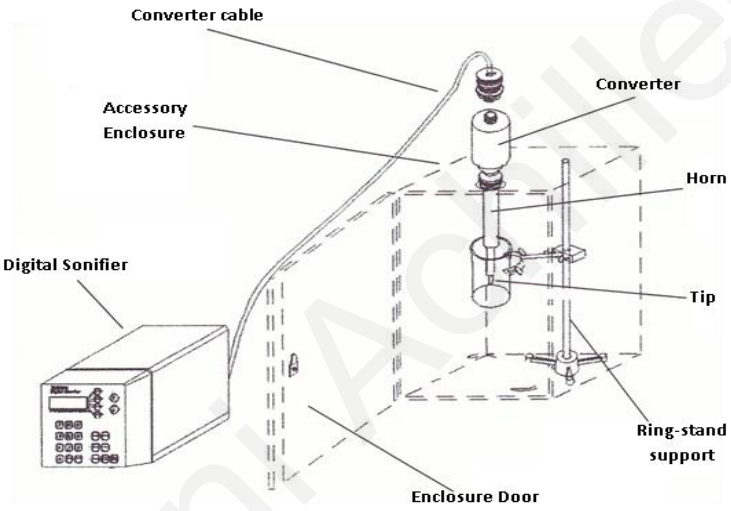

Figure 2.4: Schematic of the sonochemical experimental setup

The system consists of three core elements: the power supply, the converter and horn. The ultrasonic vibration transmitted through the horn can also be applied directly to a solid workpiece. The sonochemical experiments were carried out using a digital Sonifier 450 Branson device equipped with a titanium horn tip of 1.9 cm in diameter. Its maximum available output power is up to 400 Watts, while the operating frequency was 20 kHz. In a typical run, 350 mL of an aqueous pharmaceutical solution were loaded in a cylindrical water-jacketed vessel for temperature control and the horn was immersed at 2/3 of its height inside the liquid. As the load or pressure on the horn face increases, the power supply develops more power to maintain the amplitude for any given output control setting.

2.6 Sonophotocatalytic experimental process

For the sonophotocatalytic experiments, the reactions were carried out in a cylindrical Pyrex glass vessel (Figure 2.5). A titanium-made probe immersed in the liquid from the open to the atmosphere top of the vessel was used to deliver the ultrasound energy in the reaction mixture. The bottom of the vessel was fitted with a glass cylindrical tube housing the light source (9 W/78, UV-A). The vessel was fed with a 350 ml drug aqueous solution.

The reaction temperature in the case of sonophotocatalysis varied between 25 and 30°C. This experimental setup was suitable to study the effects of the individual or combined use of ultrasound and light avoiding any modifications in the reactor geometry. Sonophotocatalytic experiments were carried out as follows: 350 mL of an aqueous drug solution was loaded with the appropriate amount of TiO_2 (500 mg/L for DCF and IBP and 100 mg/L for CBZ) and the resulting mixture was added in the sonophotochemical reactor (Figure 2.5). The suspension was magnetically stirred for 30 min in the dark to ensure complete equilibration of adsorption/desorption of the drugs on the catalyst surface. After that period the solution was irradiated by a 9 W UV-A lamp, 3.16 W/m^2 (Radium Ralutec lamp, 9 W/78, 350-400 nm) and ultrasound was applied.

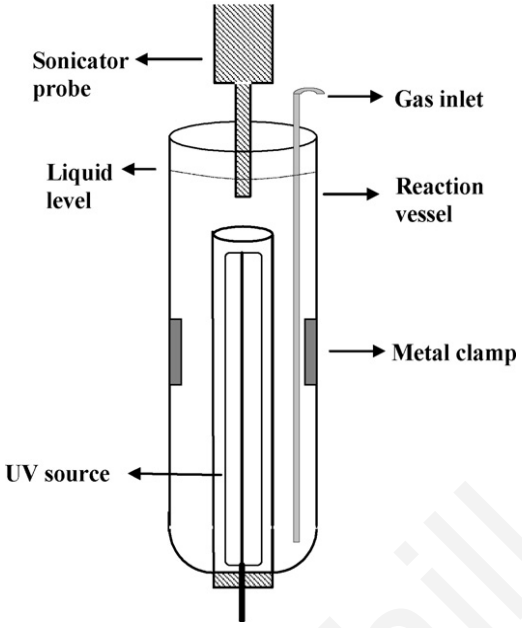

Figure 2.5: Schematic of the sonophotocatalytic experimental setup

2.7 Total Organic Carbon (TOC) analysis

In order to determine the extent of mineralization, dissolved organic carbon (DOC) was measured by a TOC analyzer, (TOC-VCPH/CPN Shimadzu with autosampler ASI-V). Potassium hydrogen phthalate (KHP) standards were used for the calibration curves. All experiments were performed at least twice. Errors for TC and IC analyses are additive. For samples that have comparatively large IC concentrations relative to TOC concentrations, the TOC analysis error is large if it is determined by the difference between TC and IC results. Samples of this type include samples from water treatment facilities or from the natural environment, such as rivers, lakes, swamps, oceans and groundwater.

Using the difference between TC and IC to determine TOC is not appropriate for purified water or ultra-pure water samples. The CO_2 in air dissolves in the sample and is measured as IC, causing the concentration to vary.

In such cases, the sample is pretreated with aeration or sparging before analysis to remove the IC. The sample is then subjected to TC analysis, immediately followed by TOC analysis using the NPOC method.

When analysis is started, acid is drawn from the acid bottle into the syringe, and the set amount of acid is added from the sample needle into each of the vials that have been designated for acid addition (2M hydrochloric acid). The acid addition ratio (ratio of acid with respect to sample) should be set to about 2-5%. However, a setting of about 0.5% is used for purified water analysis.

The hydrochloric acid concentration or amount added should be adjusted in accordance with the sample pH or buffering strength to bring the sample pH to 2-3. The pH need not be checked each time if the same type of sample is routinely measured (PC-Controlled Total Organic Carbon Analyzer, TOC-VCPH/CPN and TOC-Control V Software User Manual, Shimadzu Corporation analytical & measuring instruments division Kyoto, Japan).

2.8 UV-Visible spectrophotometer (UV-Vis) measurements

Changes in the concentration of the pharmaceuticals were monitored using a UV-Vis Jasco V-530 spectrophotometer. The absorbance was measured at the wavelength that corresponds to the maximum of absorbance in the visible region for each one of the compounds: 276 nm (UV_{276}) for DCF, 220 nm (UV_{220}) for IBP and 284 nm (UV_{284}) for CBZ.

Conversion herein, refers to the degradation of the parent compound, but also to that of the DCF, IBP or CBZ oxidation intermediate products, which contribute to the absorption at the characteristic wavelength of the parent compound (276, 220 or 284 nm), calculated by the decrease of UV absorption at 276, 220 or 284 nm (Figure 2.6).

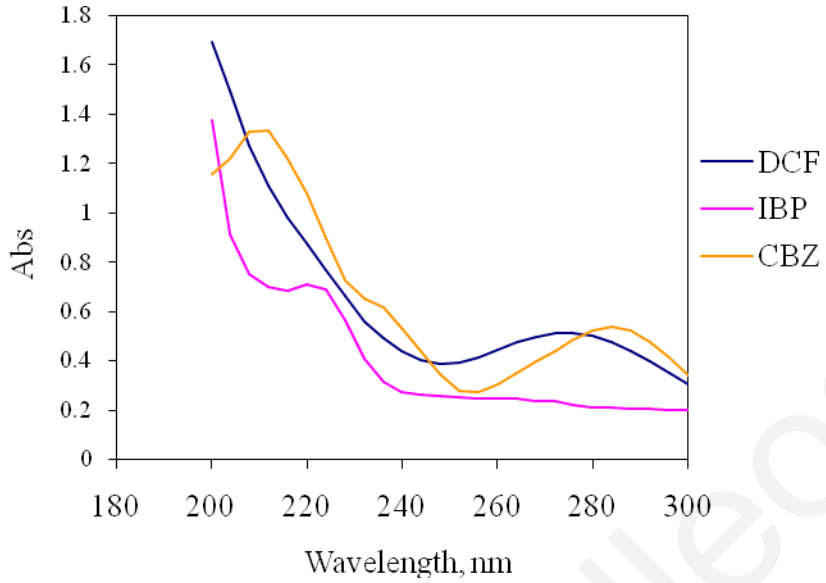

Figure 2.6: Maximum absorbance of 10 mg/L DCF, IBP and CBZ

The linearity between absorbance and concentration was tested using solutions at various concentrations of either substrate in the range 0-20 mg/L and the response was found to be linear over the whole range of concentrations under consideration.

2.9 Chemical actinometry

The photon flux of the lamp was determined actinometrically using the potassium ferrioxalate method.

The experiment was carried out under red safe light. Green crystals of $K_3Fe(C_2O_4)_3.H_2O$ were prepared by mixing 3 volumes 1.5 M $K_2C_2O_4$ (Riedel de Haen, 99%) with 1 volume 1 M $FeCl_3$ (Riedel de Haen, 99%) solution, recrystallized three times from warm water, dried at 45 ºC and kept in the dark. 0.006 M solution (≥405nm) was used for actinometry and was prepared by dissolving 2.947 g of the crystals in 100 ml 1 N H_2SO_4 and dilution with distilled water to 1 L. 350 ml (V_1) solution were irradiated using UV-A irradiation provided by a 9 W lamp (Radium Ralutec, 9W/78, 350-400 nm) under efficient stirring. One ml (V_2) of the irradiated solution was provided into a 10 ml (V_3) volumetric flask containing a mixture of 4 ml 0.1% 1,10- phenanthroline solution (Fluka, 99%, store in dark) and 0.5 ml buffer (stock solution: 82 g NaOAc (Himedia, 99%), 10 ml conc. H_2SO_4, diluted to 1 L with distilled water)

which was then diluted to the mark with distilled water. A reference was prepared in the same way except that it had not been irradiated. Both solutions were kept in dark (about an hour) until full colour development was achieved and the absorbance of the first minus that of the second sample was measured at 510 nm. A_{510} was kept within the range 0.4-1.8 as required. The evaluation of the photon flow Φ_p was given below:

$$\Phi_p = \frac{\Delta A.V_1 10^{-3}.V_3}{\Phi_\lambda.\varepsilon_{510}.V_2.t} \text{ (einstein/s)} \quad (1.20)$$

where: t is in seconds, Φ_λ at room temperature equals 1.20-1.26 (0.006 M) for the wavelength range 254-366 nm, and ε= 11100/dm^3·mol.cm.

2.10 HPLC/ESI-QqLIT-MS analysis

The irradiated solution (10 mL) was extracted by means of solid phase extraction (SPE). Cartridges Oasis HLB (hydrophilic–lipophilic balance) (6 mL, 200 mg) were placed in a filtration apparatus (Supelco, Bellefonte, PA) and washed with 5 mL of methanol and 5 mL of deionized water. Then, the irradiated solution was extracted at a flow rate of 10 mL/min.

The compounds trapped in the cartridges were collected by using 2x3 mL of methanol as eluting solvent. The SPE extract was concentrated by solvent evaporation with a gentle stream of nitrogen and reconstituted to a final volume of 200 uL in water/methanol (95:5, v: v) prior to analysis into UPLC QqTOF/MS instrument.

The quantitative analysis of CBZ, IBP and DCF and the semi-quantitative determination of its transformation products was performed using Symbiosis Pico™ (SP104.002, Spark, Holland), equipped with an autosampler and connected in series with a 4000 QTRAP Hybrid Triple Quadrupole - Linear Ion Trap mass spectrometer equipped with a Turbo Ion Spray source (Applied Biosystems-Sciex, Foster City, CA, USA). Chromatographic separation was achieved with a Purospher Star RP-18 endcap-ped column (125mm x 2.0mm, particle size 5 mm) preceded by a C18 guard column (4 mm x 4 mm, particle size 5 mm), both supplied by Merck (Darmstadt, Germany).

The mobile phases were (A) acetonitrile and (B) HPLC grade water with 0.1% formic acid. For IBP the mobile phases were (A) acetonitrile and (B) HPLC grade water. The gradient was as follows: isocratic for 5 min at 5 % eluent A, linear increase to 95 % A within 10 min, hold for 2 min, return to initial conditions in 2 min, equilibration for 3 min. The flow rate was 300 µL/min and the injection volume was 20 µL.

For the analysis, the Turbo Ion Spray source was operated in the positive ion mode using the following settings for the ion source and mass spectrometer: curtain gas 30 psi, spraying gas 50 psi, drying gas 50 psi, drying gas temperature of 700 °C and ion spray voltage of 5500 V.

The transitions for multiple reaction monitoring (q1: quantifier ion, q2: qualifier ion), declustering potential (DP), collision energy (CE), and collision cell exit potential (CXP) were as follows: for CBZ: q1 *m/z* 237→194 (DP 76 V, CE 29 eV, CXP 19 V); for 2-OH-CBZ: q1 *m/z* 253→210 (56 V, 23 eV, 8 V) and q2 *m/z* 253→167 (56 V, 53 eV, 8 V); for 3-OH-CBZ: q1 *m/z* 253→210 (61 V, 25 eV, 12 V) and q2 *m/z* 370→266 (61 V, 51 eV, 8 V).

For IBP the transitions for multiple reactions monitoring, declustering potential (DP), collision energy (CE), and collision cell exit potential (CXP) were as follows: m/z 205→161, DP -45 V, CE –10 eV, CXP -7 V. For DCF were: q1 m/z 294→250 (DP 40 V, CE 16 eV, CXP 1 V) and q2 m/z 294→214 (40 V, 30 eV, 15 V).

2.11 Identification and quantitation of transformations products by UPLC/ESI-QqToF-MS

Accurate mass measurements of CBZ and its transformation products formed in time-course degradation experiments were carried out in full-scan and product ion scan mode using a Micromass QqToF-system interfaced with a Waters ACQUITY UPLC system (Micromass, Manchester, UK). Samples from the degradation experiments were separated on a Waters ACQUITY BEH C18 column (50 × 2.1 mm, 1.7 µm particle size) equipped with precolumn (5 × 2.1 mm) of the same packing material. The mobile phases were (A) formic acid 0.05% in water and (B) acetonitrile/methanol, 2/1. After 1 min isocratic conditions at 90 % A, the

portion of A was linearly decreased to 5 % within 7 min. This condition was held for 1 min and then the initial mobile phase composition was restored within 1 min and maintained for column regeneration for another 2 min. The flow rate was 300 μL/min. The injection volume was 5 μL. The MS analysis was performed with electrospray ionization (ESI) interface in the positive ion mode applying a capillary voltage of +3500 V. The nebulizer gas flow was set to 50 L/h and the drying gas flow to 600 L/h with a temperature of 350 °C. The ToF analyzer was operated at a resolution of 5000 (FWHM) and ESI mass spectra were recorded in 1-s intervals with automatic switching of the dual-sprayer every 10 s for infusion of the internal calibrant for a duration of 1 s. Tyrosine-valine-tyrosine served as internal lock mass with [M+H]+= m/z 380.2185. All MS data acquisition and processing was done using the software package MassLynx V4.1.

For IBP the mobile phases were (A) ammonium acetate buffer, pH 6.8, and (B) acetonitrile/methanol, 1/1. After 1 min isocratic conditions at 90 % A, the portion of A was linearly decreased to 5 % within 6 min. This condition was held for 1 min and then the initial mobile phase composition was restored within 1 min and maintained for column regeneration for another 2 min. The MS analysis was performed with electrospray ionization (ESI) interface in the negative ion mode applying a capillary voltage of -2800 V and the cone voltages ranging from 10 to 40 V. The nebulizer gas flow was set to 500 L/h at a temperature of 300°C. The drying gas flow was 50 L/h, and the source temperature 120°C. For MS experiments, the instrument operated in the wide pass quadrupole mode with ToF data collected between *m/z* 70 and 400. Val-Tyr-Val served as internal lock mass with $[M-H]^-$= *m/z* 378.2029.

2.12 Toxicity assessment experiments

DCF, IBP and CBZ solutions in ultrapure water were assessed with respect to their ecotoxicity to freshwater species *Daphnia magna* prior to and after photocatalytic treatment. The tests were performed using the Daphtoxkit F^{TH} magna. Ephippia were activated by rinsing in tap water and were then hatched for 72-90 h in standard freshwater (prepared using $NaHCO_3$, $CaCl_2$, $MgSO_4$ and KCl) suitable for Daphnia at 20-22ºC under continuous illumination of 6000 lux. Dissolved oxygen (DO) was measured and it was always at acceptable levels, while

pH was adjusted to 7±0.5 adding the appropriate amount of 1N NaOH. A multiparameter equipment, was used for measuring DO, temperature, pH, (WTW InoLab Multilevel 3).

Two hours prior to testing, the neonates were fed using a dilution of *Spirulina* microalgae in order to reduce mortality caused by starvation, which can bias the test results. During the subsequent 48 h test exposure the organisms were not fed. One hundred and twenty neonates were used to perform the tests. Five daphnids were tested in quadruplicate in specific test plates covered and incubated at 20ºC, in the dark. Five different concentrations of testing solutions from 10% to 100% were prepared adding standard freshwater and a control using only freshwater was also tested. The multi well plates were covered and incubated at 20^0C, in the dark. After 24 and 48 h of incubation the number of dead and immobilized neonates was calculated. Tests in which mortality greater than 10% was observed were rejected and not used for statistical analysis. Each sample was run in duplicate and mean values are quoted as results with standard deviation never exceeding 1.1%.

CHAPTER 3

RESULTS AND DISCUSSION

3.1 Consumption of pharmaceuticals and Predicted Environmental Concentrations (PEC) in Cyprus

Collection and elaboration of data regarding the pharmaceutical products' consumption in the Cyprus market, including hospitals and pharmacies were carried out. The volumes of sales of the commercial pharmaceuticals and the active pharmaceutical ingredients (APIs) sold by the public hospitals and private pharmacies were determined. These are provided in Tables 3.1-3.2. This information was gathered in collaboration with the Pharmaceutical Services of the Ministry of Health of Cyprus.

Table 3.1: The most commonly prescribed APIs by public hospitals for 2005 (Pharem, 2008)

a/a	Active ingredient	Tonnes	Commercial name	Drug application
1	Amoxicillin	1.220	Amoxil, Noprilam	Antibiotic
2	Acetylsalicylic acid	0.674	Aspirin	NSAIDs
3	Allopurinol	0.641	Alopron, Zyloric Tabs	Antigout
4	Diclofenac	0.322	Diclofenac	NSAIDs
5	Atenonol	0.238	Atelol, Tredol	Beta- blocker
6	Furosemide	0.201	Furosemide	Diuretic
8	Paracetamol	0.192	Panadol	NSAIDs
8	Dipyridamole	0.189	Dipyridamole	Anticoagulant
9	Fusidate	0.00061	Fucicort cream, Fucidin cream	Antibiotic
10	Mefenamic acid	0.00016	Postan	NSAIDs

NSAIDs : Non-steroid anti-inflammatory drugs

Table 3.2: The most commonly sold APIs by private pharmacies for 2005 (Pharem, 2008)

a/a	Active ingredient	Tonnes	Commercial name	Drug application
1	Amoxicillin	0.150	Amoxil, Amoxapen, Edamox, Duramox	Antibiotic
2	Paracetamol	0.134	Calpol infant susp, Panadol, Solpadeine, Uniflu	NSAIDs
3	Erythromycin	0.049	Ermycin, Erythran Tabs	Antibiotic
4	Ibuprofen	0.038	Brufen tabs, Perofen Tabs	NSAIDs
5	Acetylsalicylic acid	0.028	Aspirin, Aspro clear, Nu-seals tabs	NSAIDs
6	Cefalexin	0.026	Cefaxin Caps, Cefrax Caps	antibiotic

7	Ceftriaxone	0.017	Ceftrix caps	antibiotic
8	Cefaclor	0.014	Ceclor Tabs, Medoclor	antibiotic
9	Mefenamic acid	0.0096	Postan	NSAIDs
10	Diclofenac sodium	0.0043	Voltaren Tabs, Almiral, Allvoran	Antibacterial

Table 3.3 shows the quantities and the excretion rates of the ten APIs with the highest consumption volumes in Cyprus, both in the public and private sector according to literature.

Table 3.3: Total quantities and excretion rates of the top ten active ingredients in Cyprus (Pharem, 2008)

a/a	Active ingredients	Tonnes	Excretion in urine unchanged (%)	Reference for the excretion data
1	Amoxicillin	1.370	60	Martindale, 1993
2	Acetylsalicylic acid	0.702	10	Moffat et al., 1986
3	Allopurinol	0.641	10	Moffat et al., 1986
4	Diclofenac	0.326	20	Moffat et al., 1986
5	Paracetamol	0.326	4	Huschek et al., 2004
6	Atenonol	0.238	90	Dollery, 1991
7	Furosemide	0.201	60	Moffat et al., 1986
8	Dipyridamole	0.189	5	Moffat et al., 1986
9	Erythromycin	0.049	5	Martindale, 1993
10	Ibuprofen	0.038	< 0.2	Moffat et al., 1986

Many pharmaceuticals are excreted mainly as metabolites or in unchanged form. However, conjugates formed with glucuronic acid or sulfate within drug metabolising pathways in the human body are likely to be cleaved during sewage treatment to yield the non-metabolised pharmaceuticals and therefore may increase their relevan environmental concentrations. The unchanged excretion rate in urine is the most important factor for calculating the predicted concentration of pharmaceutical in sewers. The volumes calculated and the excretion rates in WWTPs determined in the tables above have been taken into account for the calculations concerning predicted environmental concentrations of the pharmaceuticals.

For the purposes of PEC calculations and according to Equation (1.7), AWW is considered to be 250 L/cap/d for WWTP I, 160 L/cap/d for WWTP II and 150 L/cap/d for WWTP III. The population was 196553, 115268 and 66364 respectively (Statistical Service of Cyprus, 2005).

The F_{APIs} calculated from the elaboration of the data collected from the Pharmaceutical Services are presented in Table 3.4. It is noted that the total quantity of the API was multiplied by the population served within each treatment plant and divided by the total population of the country. The population served by the WWTPs I, II and III is 70000, 43000 and 27661 respectively.

Table 3.5 shows the values for PECs for each treatment plant.

Table 3.4: Consumption of APIs per area (for 2005)

a/a	Active Ingredient	F_{API} Limassol (kg/a)	F_{API} Larnaca (kg/a)	F_{API} Paphos (kg/a)
1	Amoxicillin	413.11208	242.26852	139.48284
2	Acetylsalicylic acid	211.68225	124.14051	71.47223
3	Allopurinol	193.16060	113.27853	65.21859
4	Diclofenac sodium	98.30258	57.64930	33.19081
5	Paracetamol	98.30258	57.64930	33.19081
6	Atenolol	71.76692	42.08752	24.23133
7	Furosemide	60.60988	35.54450	20.46427
8	Dipyridamole	56.99138	33.42244	19.24252
9	Erythromycin	14.77554	8.66508	4.98880
10	Ibuprofen	11.45858	6.71986	3.86887

Table 3.5: PEC values of pharmaceutical compounds in WWTPs of Cyprus

Pharmaceutical compound	WWTP I (μg/L)	WWTP II (μg/L)	WWTP III (μg/L)
Amoxicillin	23.033	13.820	21.594
Acetylsalicylic acid	1.967	1.180	1.844
Allopurinol	1.795	1.077	1.683
Diclofenac	1.827	1.096	1.713
Paracetamol	0.365	0.219	0.343
Atenolol	6.002	3.601	5.627
Furosemide	3.379	2.028	3.168
Dipyridamole	0.265	0.159	0.248
Erythromycin	0.069	0.041	0.064
Ibuprofen	0.002	0.001	0.002

We can see from the above calculations the highest PECs were found for WWTP I and the lowest values for WWTP II.

There are several factors that can affect the actual concentrations of the APIs in the raw sewage. The methodology followed in this thesis includes a number of assumptions that could

lead in concentrations different that the actual ones. The major finding is that the quantities of drugs consumed by hospitals very high and according to the Pharmaceutical Services, until 2005, the situation was partly and not fully uncontrolled and monitored. Although CBZ was not found among the top ten pharmaceutical compounds in this investigation it was chosen for this thesis to be investigated because high concentrations of CBZ have been indeed found in the effluents of WWTPs in Cyprus (Fatta-Kassinos et al., 2010).

The numbers of PECs should only be used as rough estimates and should always be followed by measured environmental concentrations (MECs). Below, in Table 3.6, the detected levels of pharmaceutical compounds in wastewater samples are shown. Samples were collected from the inlet, after the secondary treatment step and finally from the outlet. 24 h composite samples were collected using time-proportional automatic sampler. Results are expressed in μg/L. For some of the compounds high concentrations were obtained for the final effluents (e.g. ofloxacin: 4.82 μg/L, DCF: 5.51 μg/L, CBZ: 27.27 μg/L). Concerning the elimination potential what was derived from the investigation is that the biological (secondary step) and the sand-filtration (tertiary step) do not have the same impact on the removal percentage since the majority of the compounds are removed during secondary treatment. The quantification of the pharmaceuticals does not constitute part of this thesis and was accomplished by GAIA group and CSIC, Spain through project Pharem-Development and application of innovative advance oxidation processes for the removal of active organic compounds in urban wastewaters and monitoring of toxicity (ΑΕΙΦΟ/0506/16, 2007-2009).

The comparison indicated that PECs substantially differ from MECs, particularly when there were not enough data to estimate the environmental fate of the molecule. Predictive models might therefore be useful for studying pharmaceuticals in the environment, when adequate experimental data is available on the environmental fate of the compounds.

Table 3.6: Detected levels (μg/L) of pharmaceutical compounds in wastewater samples (non published data, ©GAIA-Laboratory of Environmental Engineering, UCY in collaboration with CSIC Spain)

WWTP	**I**			**II**			**III**		
Pharmaceutical compounds	**A**	**B**	**C**	**A**	**B**	**C**	**A**	**B**	**C**
Ketoprofen	0.34	bld	bld	bld	bld	bld	1.75	0.27	bld
Naproxen	bld	bld	bld	bld	bld	bld	0.21	0.03	bld
Ibuprofen	**1.43**	**0.52**	**bld**	**1.31**	**0.28**	**0.28**	**2.20**	**4.34**	**3.46**
Indomethacine	bld	bld	bld	bld	bld	bld	bld	bld	bld
Diclofenac	**0.61**	**2.11**	**0.68**	**2.43**	**15.41**	**5.51**	**0.73**	**2.99**	**0.12**
Mefenamic acid	bld	bld	bld	bld	bld	bld	bld	bld	bld
Acetaminophen	309.29	0.11	0.07	77.56	0.11	0.07	405.37	0.05	0.10
Propyphenazone	bld	0.04	0.03	bld	bld	bld	bld	bld	bld
Clofibric acid	bld	bld	bld	0	0	0	bld	bld	bld
Gemfibrozil	bld	0	bld	0	0	0	bld	bld	bld
Bezafibrate	0.51	0.14	0.05	0.73	0.29	0.22	0.99	0.14	0.11
Pravastatin	bld	bld	bld	bld	bld	bld	bld	bld	bld
Mevastatin	bld	bld	bld	bld	bld	bld	bld	bld	bld
Carbamazepine	**0.76**	**0.84**	**0.57**	**14.45**	**24.54**	**27.27**	**2.61**	**1.49**	**1.38**
Fluoxetine	bld	bld	bld	bld	bld	bld	bld	bld	bld
Paroxetine	bld	bld	bld	bld	bld	bld	bld	bld	bld
Lansoprazole	bld	bld	bld	bld	bld	bld	bld	bld	bld
Loratadine	bld	bld	bld	bld	bld	bld	bld	bld	bld
Famotidine	1.00	0.59	bld	2.78	5.06	bld	1.30	0.38	bld
Ranitidine	0.07	0.08	bld	0.14	0.47	bld	0.43	0.31	bld
Erythromycin	0.38	0.20	0.03	0.28	0.25	0.40	0.70	0.42	bld
Azythromycin	1.15	1.60	0.18	0.66	0.30	0.20	1.68	0.53	0.03
Sulfamethoxazole	1.07	0.19	0.01	1.51	0.78	0.46	5.41	0.64	0.03
Trimethoprim	0.05	bld	bld	0.14	0.09	blq	0.35	0.06	bld
Ofloxacin	22.62	3.02	1.29	34.74	5.93	4.82	59.38	3.33	1.90
Atenolol	3.29	0.12	0.13	3.15	0.89	0.73	5.81	0.92	0.94

Sotalol	2.81	0.10	0.11	2.70	0.76	0.62	4.97	0.79	0.81
Metoprolol	1.30	0.98	0.57	2.09	1.23	9.59	1.49	1.31	0.69
Propranolol	0.27	0.49	blq	0.41	0.59	0.28	0.23	0.44	blq

bld: below limit of detection, blq: below limit of quantitation, A: inlet, B: after secondary treatment, C: outlet

3.2 Photocatalytic degradation of the pharmaceuticals under UV-A irradiation

Preliminary experiments were conducted to assess the extent of drugs (i) adsorption onto the catalyst surface (Degussa P25) in the dark and (ii) photolytic degradation in the absence of catalyst.

Some important explanations that refer to the entire set of experiments presented in this thesis are the following:

It should be noticed that the range of DCF, IBP and CBZ concentrations employed is substantially higher than that typically found in environmental samples which is at the μg/L level (Klavarioti et al., 2008; Rizzo et al., 2009). This was done though to allow (i) the assessment of treatment efficiency within a measurable time scale, and (ii) the accurate determination of residual concentrations with the analytical techniques employed in this work. The concentrations for the CBZ used in the study were up to 10 mg/L since the maximum solubility of CBZ was 15 mg/L while those for DCF and IBP were 50 mg/ml and 0.021 mg/ml respectively (Table 2.1).

It is important to note that conversion herein, refers to the degradation of the parent compound, but also to that of the DCF, IBP or CBZ oxidation intermediate products, which contribute to the absorption at the characteristic wavelength of the parent compound (276, 220 or 284 nm), calculated by the decrease of UV absorption at 276, 220 or 284 nm.

Each sample was run in duplicate or triplicate and mean values are quoted as results with standard deviation never exceeding 1.1%.

3.2.1 Dark experiments

Preliminary experiments under dark were performed to study the adsorption capacity of the catalyst at various catalyst loadings. Dark adsorption was complete within 30 min and, therefore, before the irradiation, the suspension was stirred in the dark for 30 min to reach the adsorption/desorption equilibrium. Dark experiments were performed also for 24h but with no

significant adsorption for any of the substances. Below, in Figures 3.1 A, B and C the adsorption of DCF, IBP and CBZ is shown at concentration levels between 5-20 mg/L.

In Figure 3.1 A we can see that for 5 mg/L DCF the maximum adsorption was 9.8% with 250 mg/L catalyst loading, for 5 mg/L IBP was 3.5% for 500 mg/L catalyst loading and for 5 mg/L CBZ was 9.3% for 500 mg/L catalyst loading. In Figure 3.1 B the maximum adsorption onto the catalyst surface was 8.8% for 10 mg/L DCF with 500 mg/L catalyst loading, 8.5% for 10 mg/L IBP with 800 mg/L catalyst loading and 10.4% for 10 mg/L CBZ with 250 mg/L catalyst loading, based on UV absorbance measurements, respectively. This low adsorption is in agreement with the findings of the relevant recent adsorption studies performed by Mendez-Arriaga et al. (2008) and Rizzo et al. (2009). As seen in Figure 3.1 C, the maximum adsorption onto the catalyst surface was 8.8% for 20 mg/L DCF with 1000 mg/L catalyst loading, 8.3% for 20 mg/L IBP with 250 mg/L catalyst loading, based on UV absorbance measurements, respectively.

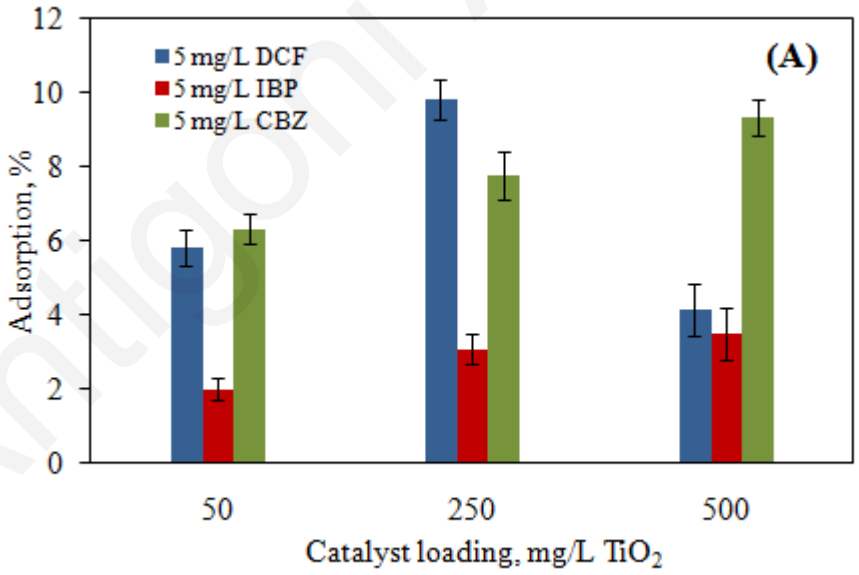

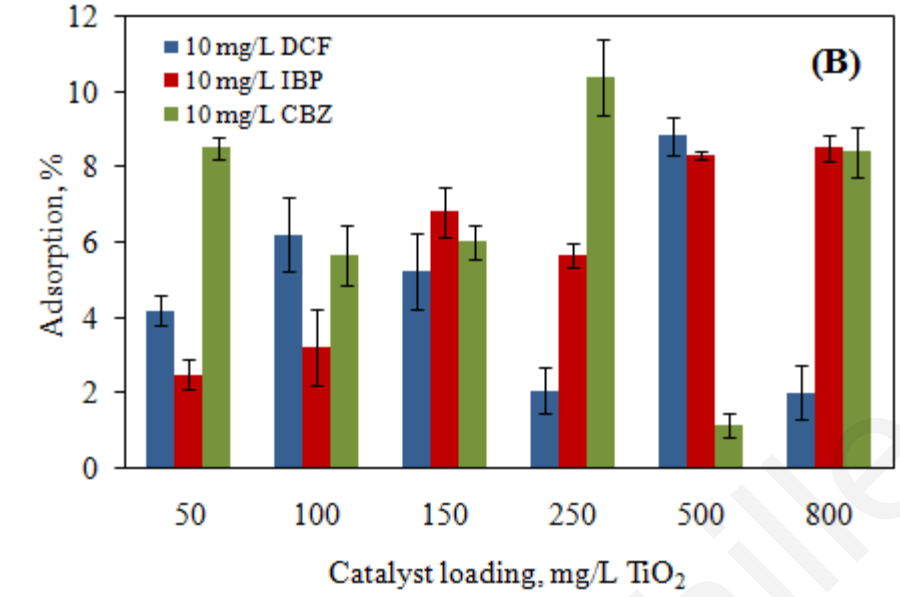

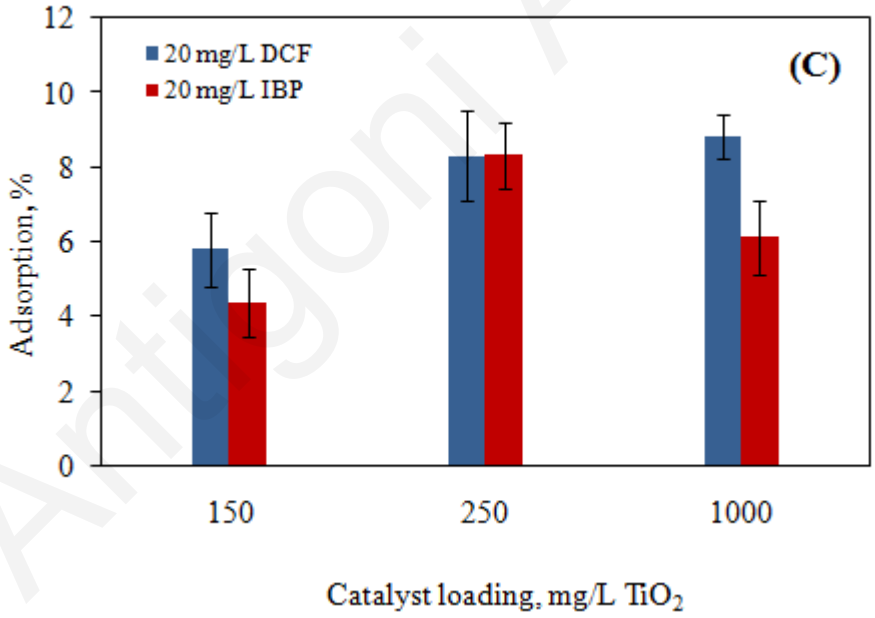

Figure 3.1: Adsorption of (A) of 5mg/L DCF, IBP and CBZ, (B) 10 mg/L DCF, IBP and CBZ, (C) 20 mg/L DCF and IBP after 30 min under dark conditions at various catalyst loadings

3.2.2 Photolysis of DCF, IBP and CBZ

Photolysis experiments were performed in order to determine the contribution of this effect to the entire process. Photolysis was performed for each compound at inherent pH in ultrapure water. Samples were exposed to direct UV-A radiation and continuously stirred during the photolysis experiments. The conversion for 5, 10, 20 mg/L DCF after 120 min of irradiation was 27, 11 and 10% (Figure 3.2 A). In Figure 3.2B the conversion for 5, 10, 20 mg/L IBP was after 120 min of irradiation 15, 12 and 15%. In Figure 3.2C the conversion for 5, 10 mg/L CBZ was after 120 min of irradiation 20 and 7%.

Results from these experiments prove that both chemical adsorption and photolysis for the DCF, IBP and for CBZ after 120 min were not very significant. Moreover, DOC measurements did not show any significant removal (~ 2%) for any of the substances (Figures 3.3 A, B and C).

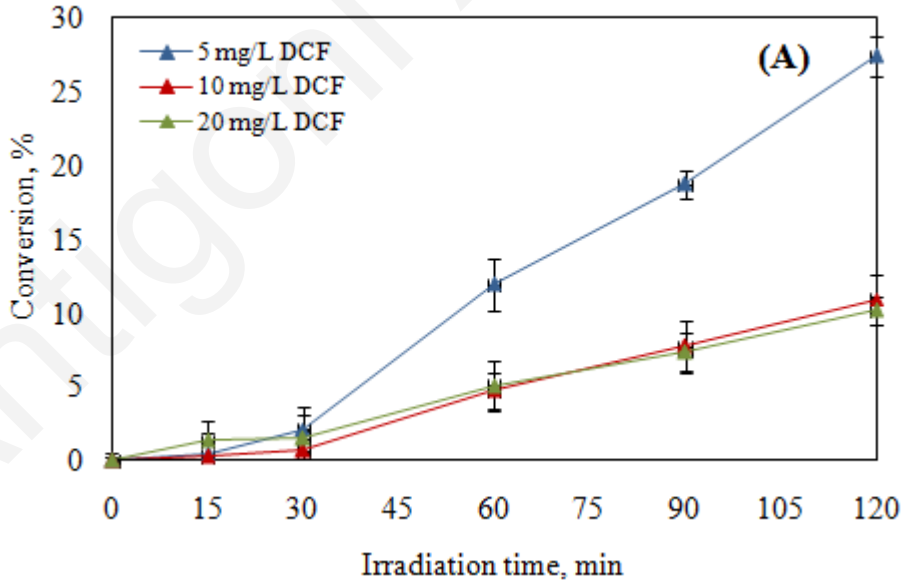

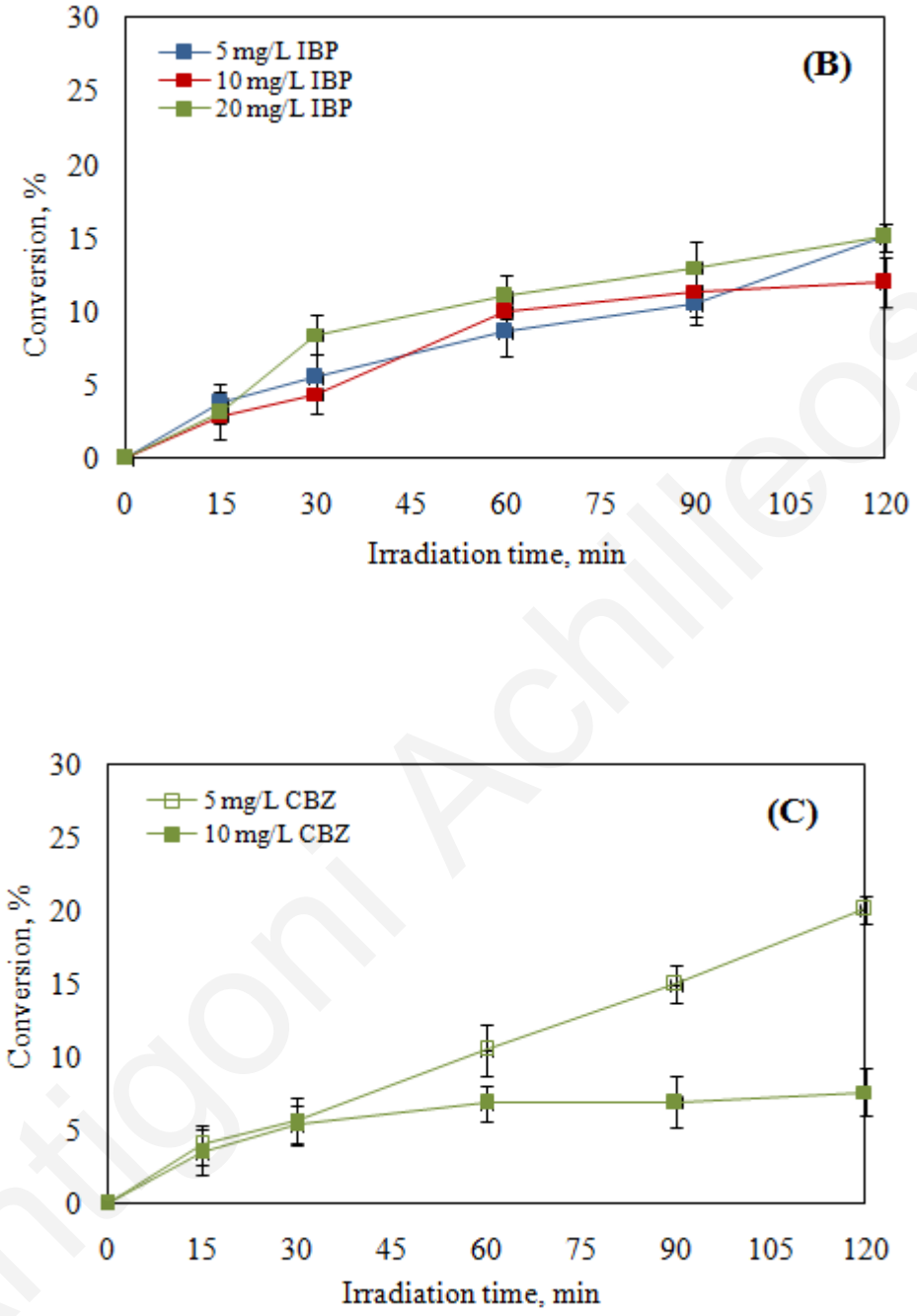

Figure 3.2: Conversion of (A) 5-20 mg/L DCF, (B) 5-20 mg/L IBP, (C) 5 and 10 mg/L CBZ after 120 min of photolysis

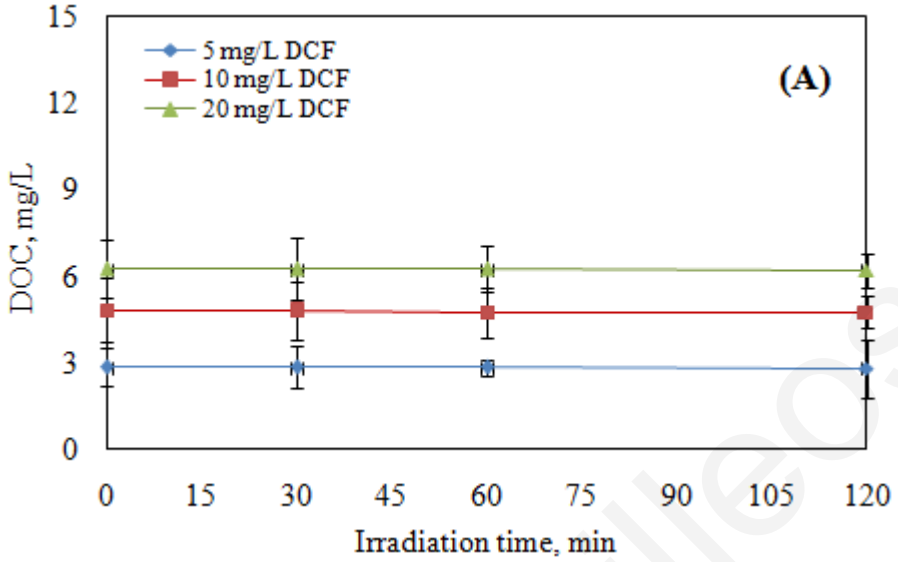

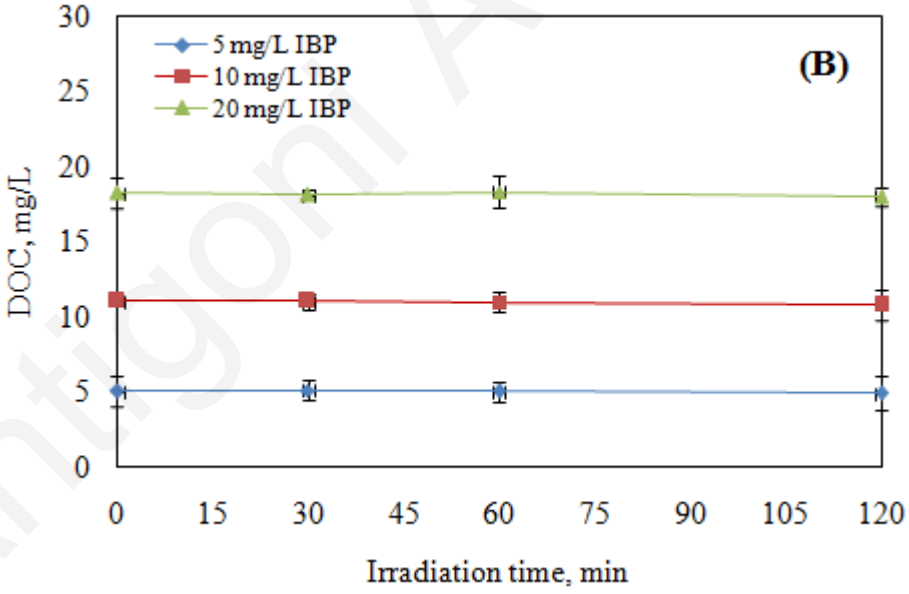

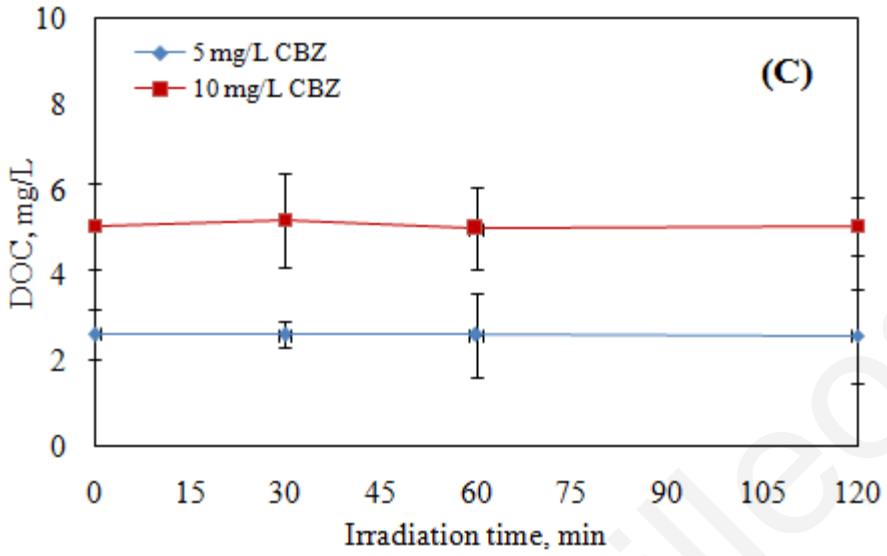

Figure 3.3: DOC values for (A) 5-20 mg/L DCF, (B) 5-20 mg/L IBP, (C) 5 and 10 mg/L CBZ after 120 min of photolysis

3.2.3 Screening of catalysts

To assess the relative catalytic activity of various titania samples, screening experiments were performed with 10 mg/L initial drug concentration and 250 mg/L catalyst loading under UV-A irradiation and ambient solution pH. Figures 3.4 A, B and C clearly show that Degussa P25 exhibits higher photoactivity than all other samples employed in this study. This is believed to be due to the slow recombination of the e^-/h^+ pair taking place on the surface of Degussa P25, different from other photocatalysts. Its higher activity may also be attributed to its structure containing both anatase and rutile, being the activity of the mixed phase greater than the activities of the pure crystalline phases (Bickley et al., 1991; Martin et al., 1994; Emilio et al., 2006; Xekoukoulotakis et al., 2010). Figure 3.4 A also shows that pure anatase TiO_2 is more active than pure rutile for the drugs oxidation.

The photoreactivity of Hombikat is due to a fast interfacial electron-transfer rate (Doll et al., 2004). Assuming that the adsorption/desorption of the pharmaceutical or diagnostic agent is slow in comparison to the formation of electron/hole pairs, P25 will be the better photocatalyst because it has longer lifetimes for electron/hole pairs (Doll et al., 2004). Higher efficiency for

Hombikat is accompanied with relatively fast adsorption/desorption and recombination of electron and hole is prevented by reaction of electron and hole is prevented by eraction of electrons with suitable electron acceptors or by reactions of the holes with adsorbed pollutants (Doll et al., 2004).

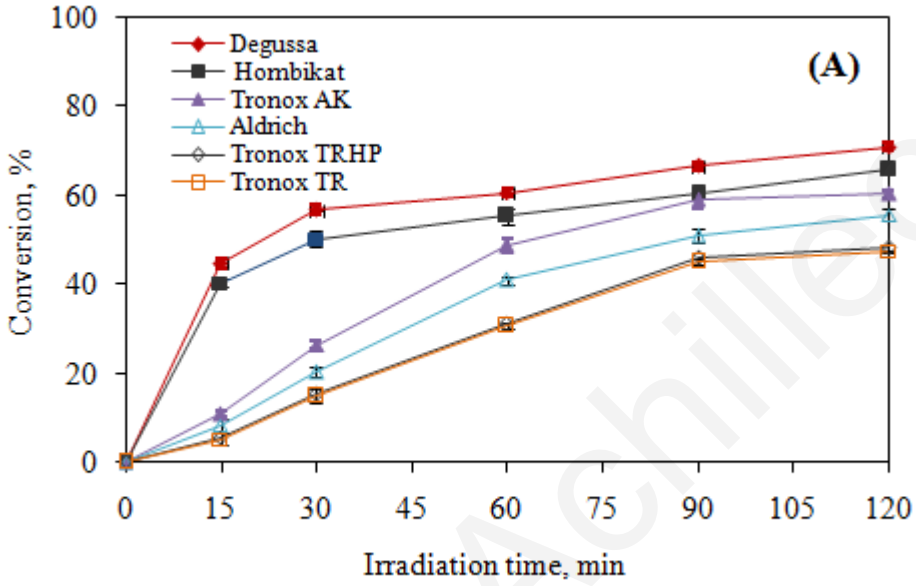

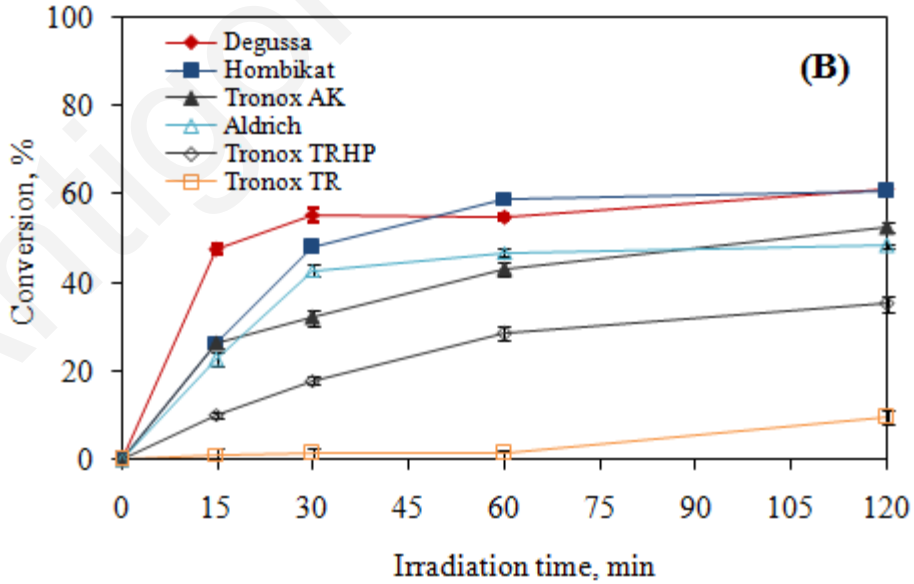

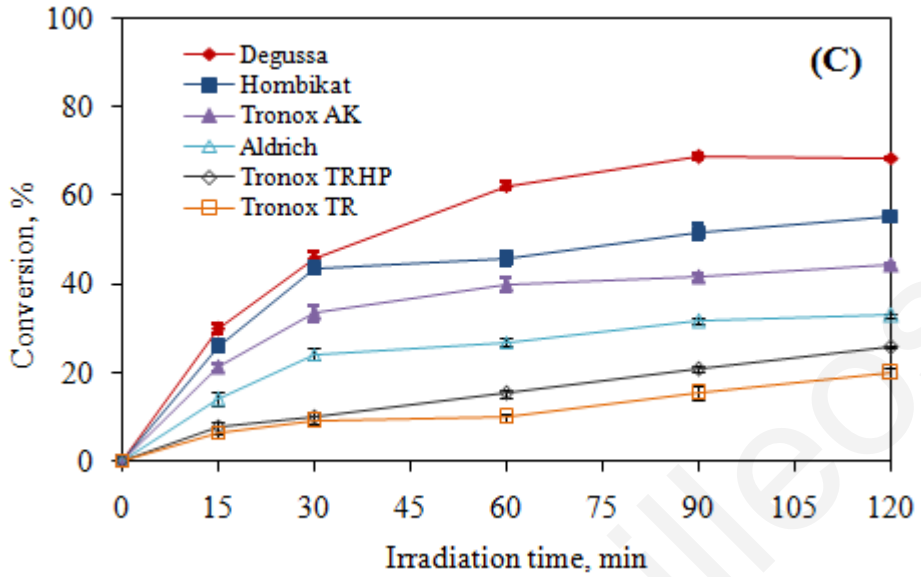

Figure 3.4: Screening of the catalyst activity during the conversion of 10 mg/L (A) DCF, (B) IBP and (C) CBZ

This behavior is attributed to the different position of the conduction band, the higher aptitude of anatase to photoadsorb oxygen and the lower relative electron/hole recombination rate in anatase. With regard to these findings, subsequent runs were done with Degussa P25. The conversion efficiency for DCF after 120 min of illumination was 71, 66, 60, 56, 48 and 47.5% respectively decreases in the order Degussa P25 > Hombikat UV-100 > Tronox A-K-1> Aldrich Anatase > Tronox TR-HP-2> Tronox T-R. For IBP the degradation efficiency after 120 min of illumination being 61, 60.6, 53, 48, 35 and 10% respectively. For CBZ, the degradation efficiency after 120 min of illumination was 68, 55, 44, 33, 26 and 20% respectively.

These findings are in agreement with the relevant studies performed by Pekakis et al. (2006), Herrmann et al. (2007), Kritikos et al. (2007), Chatzisymeon et al. (2008), Hapeshi et al. (2010) and Xekoukoulotakis et al. (2010).

3.2.4 Effect of catalyst loading

In order to study the effect of the catalyst initial concentration on the degradation of 5-20 mg/L DCF, IBP and CBZ, experiments were conducted, using Degussa P25, in the range of 50-800 mg/L for the UV-A experiments in ultrapure water. Figures 3.5 A-C show the effect of the catalyst loading on 5-20 mg/L DCF, IBP and 5-10 mg/L CBZ conversion.

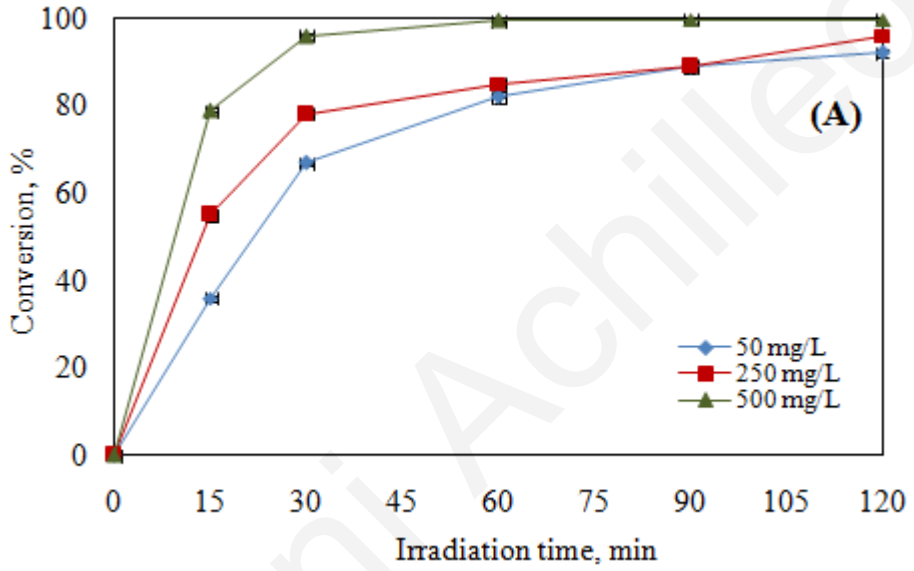

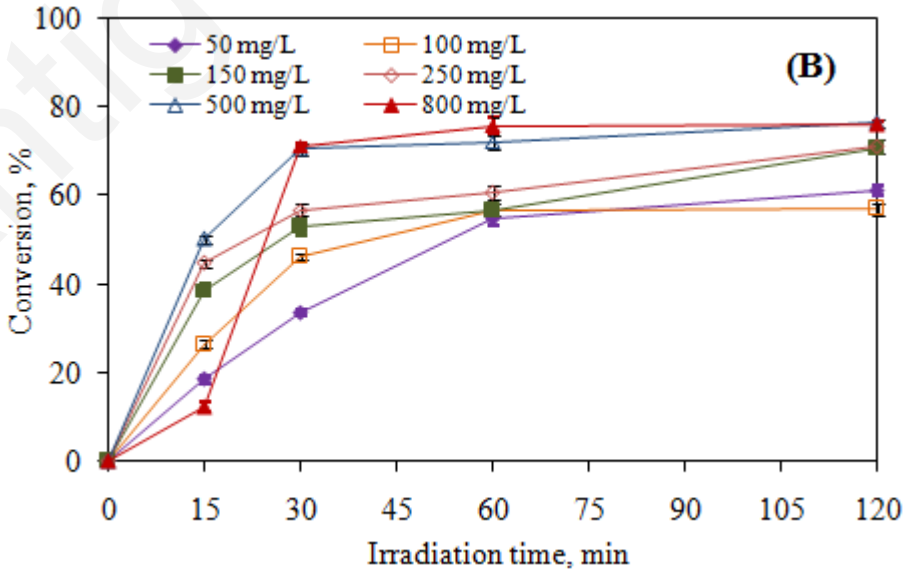

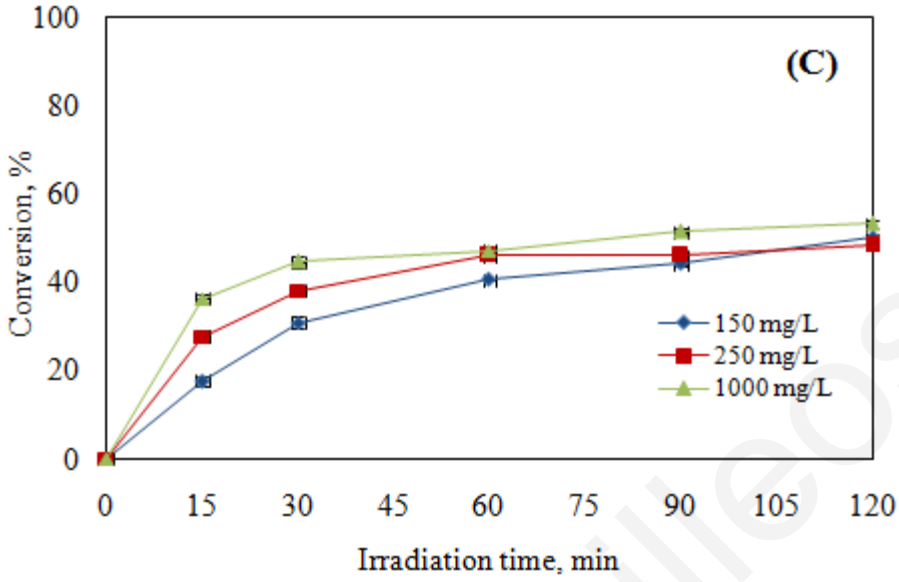

Figure 3.5: Effect of Degussa P25 loading on the conversion of (A) 5 mg/L DCF, (B) 10 mg/L DCF and (C) 20 mg/L DCF under UV-A irradiation in ultrapure water

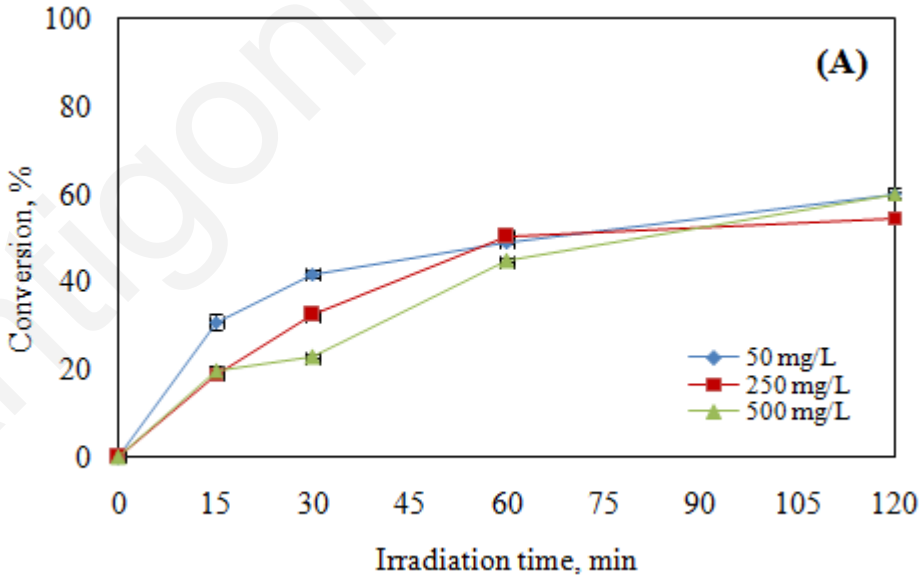

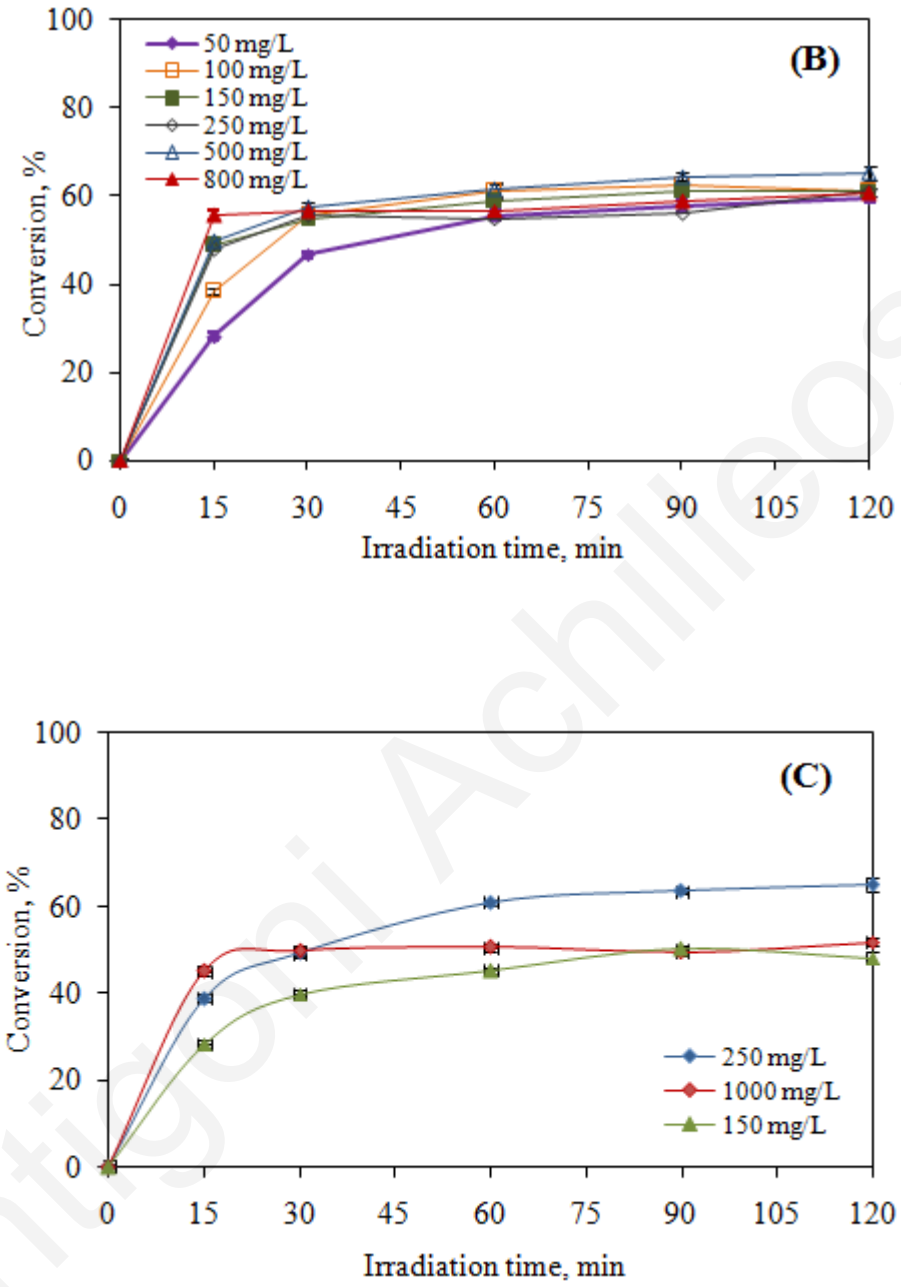

Figure 3.6: Effect of Degussa P25 loading on the conversion of (A) 5 mg/L IBP, (B) 10 mg/L IBP and (C) 20 mg/L IBP under UV-A irradiation in ultrapure water

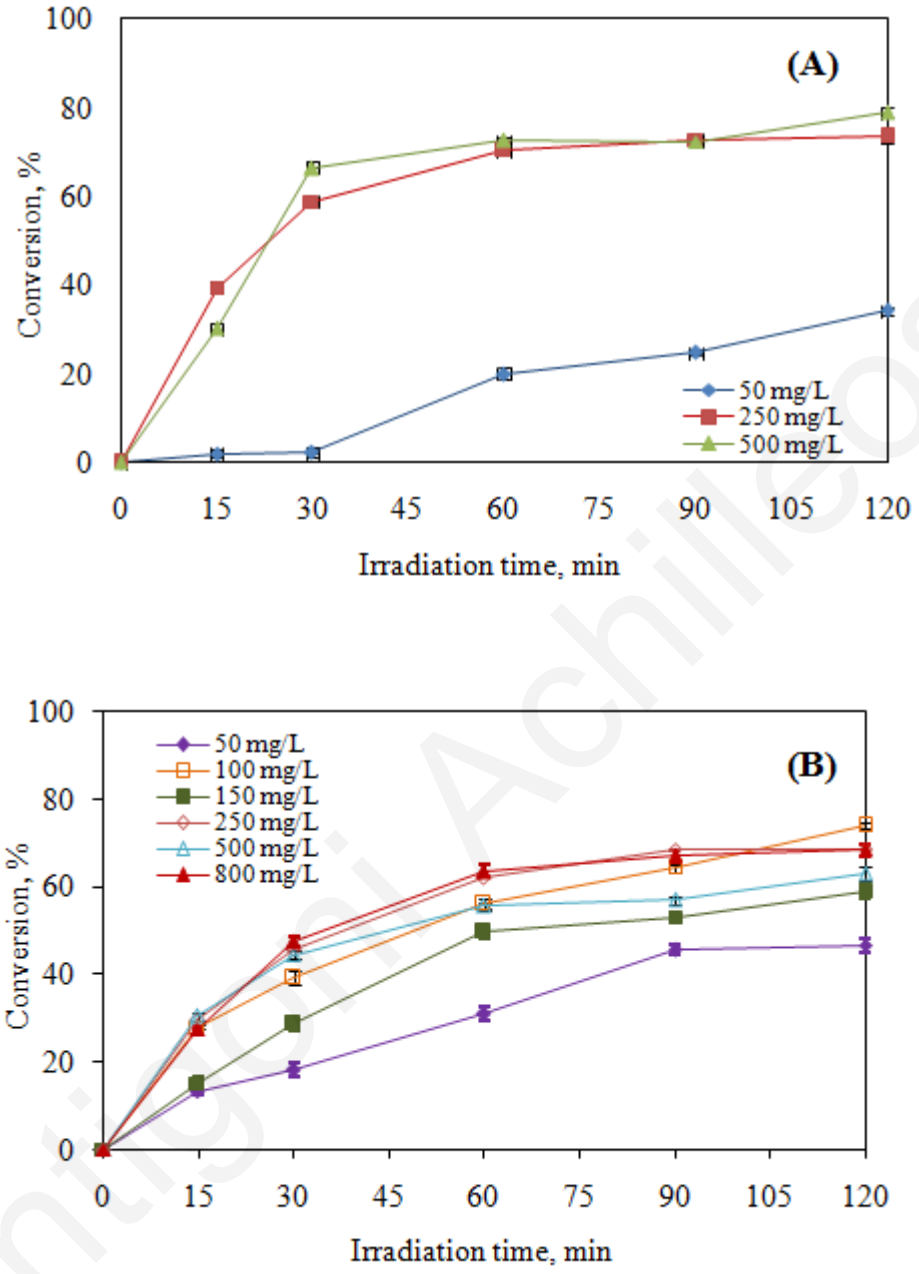

Figure 3.7: Effect of Degussa P25 loading on the conversion of (A) 5 mg/L CBZ and (B) 10 mg/L CBZ under UV-A irradiation in ultrapure water

TiO_2 loading in slurry processes is a significant factor that can affect performance. As seen, the final (i.e. after 120 min) conversion is common at about 80% in terms of absorbance regardless the catalyst loading employed for DCF. DOC removal was 58%. Regarding IBP conversion, the catalyst loading appears to affect the early stages of the reaction (i.e. 15-30

min), after which the reaction reaches a plateau; the final (i.e. 120 min) conversion is 62±3% regardless the catalyst loading used. After 120 min of reaction at 500 mg/L Degussa P25, a 65% IBP conversion was accompanied by 46% DOC removal. After 120 min of reaction a 60% (50 and 500 mg/L TiO_2) and 40% conversion (250 mg/L TiO_2) was achieved of IBP 5mg/L. DOC removal was 40% after 120 min of reaction at 500 mg/L Degussa P25. For IBP 20 mg/L a 65% conversion was achieved with 250 mg/L catalyst. DOC removal for IBP 20 mg/L was 44% after 120 min of reaction with 250 mg/L Degussa P25.

After 120 min of reaction a 34, 74, 79% of 5 mg/L CBZ (Figure 3.7 A) conversion was achieved accompanied by 23, 35, 42% DOC removal with 50, 250, 500 mg/L catalyst loading. CBZ 10 mg/L degradation appears to be more sensitive in changes in the catalyst loading; after 120 min of reaction at 100 mg/L Degussa P25 compared to the other two pharmaceuticals, a 74% CBZ conversion was achieved by 40% DOC removal.

3.2.5 Effect of the initial concentration of the pharmaceuticals

The influence of the initial concentration of the pharmaceutical on the kinetics was also examined in the range 5-20 mg/L at 250 mg/L catalyst loading and the results are shown in Figures 3.8 A, B and C.

Conversion expectedly decreases with increasing initial concentration, i.e. at 60 min it becomes 99.5, 61 and 46% at 5, 10 and 20 mg/L DCF initial concentration respectively. Nonetheless, process efficiency, in terms of mass of DCF destroyed, is enhanced at increased concentrations, i.e. at 60 min it takes values of 5, 6.1 and 9.2 mg/L respectively.

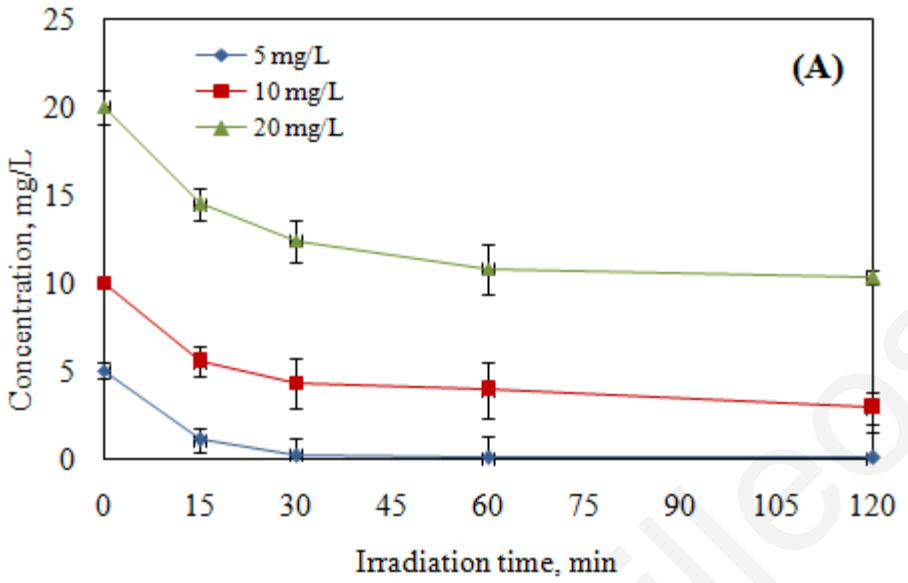

For IBP conversion expectedly decreases with increasing initial concentration, i.e. at 60 min it becomes 80, 70 and 65% at 5, 10 and 20 mg/L IBP initial concentration respectively.

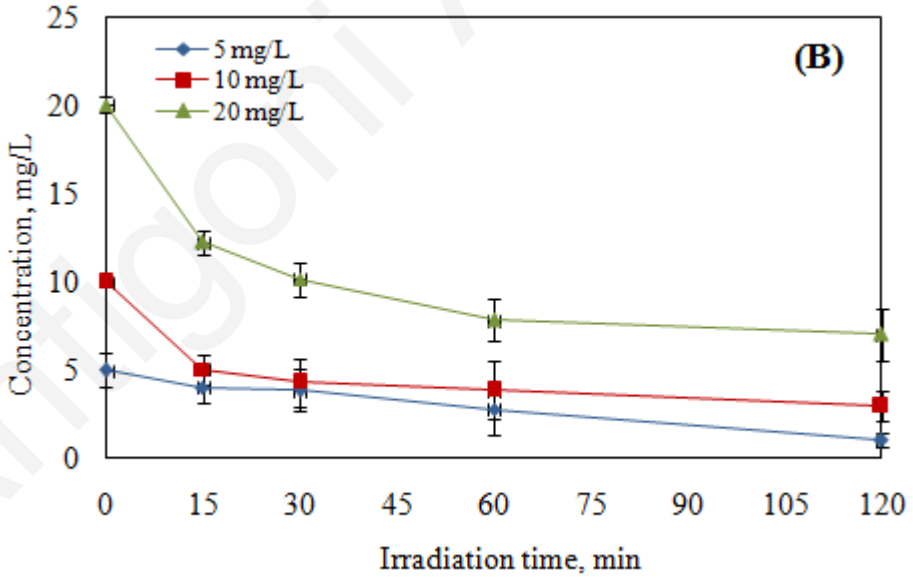

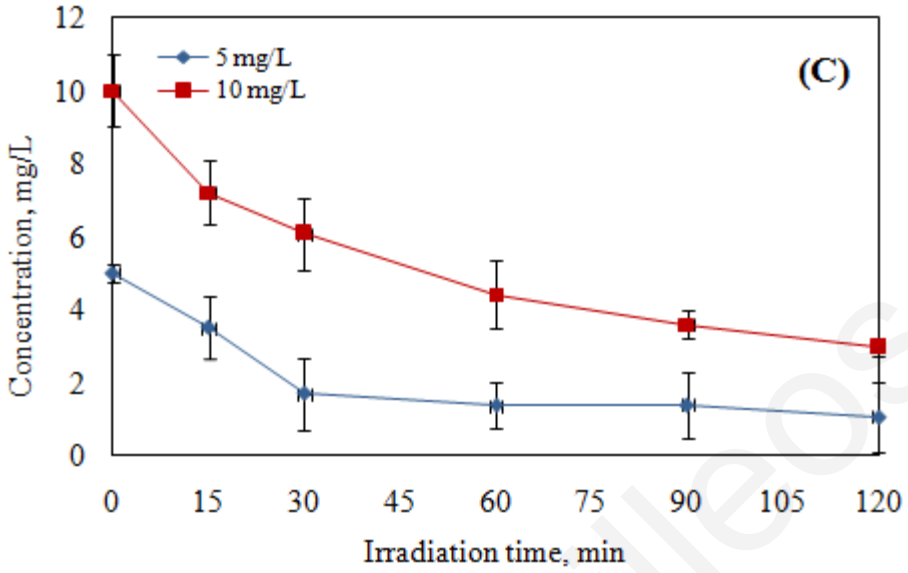

Figure 3.8: Effect of initial concentration, UV-A irradiation with 250 mg/L TiO_2 on (A) 5-20 mg/L DCF, (B) 5-20 mg/L IBP and (C) 5 and 10 mg/L CBZ

Conversion for CBZ becomes 79 and 70% at 5, 10 mg/L CBZ initial concentration respectively. Two factors may delay the conversion of these drugs at higher concentrations. At first, increased concentration of the drug could occupy more active sites of TiO_2, which inhibits generation of the oxidants and secondly, a higher amount of drug absorbs more photons, subsequently decreasing the photons which are available to activate TiO_2 (Yang et al., 2008).

3.2.6 Additional oxidant as promoter of DCF, IBP and CBZ conversion

The effect of adding H_2O_2, in the range 0.07-1.4 mM, on drug mineralization was tested during the photocatalytic degradation of 10 mg/L DCF, IBP and CBZ under UV-A irradiation and the results are shown in Figures 3.9 A-C. H_2O_2 was added at a concentration of (i) 0.07-1.4 mM in the dark and without TiO_2, (ii) 0.07-1.4 mM and the resulting solution was irradiated without TiO_2, (iii) 0.07-1.4 mM and the resulting solution was irradiated in the presence of 500 mg/L TiO_2 for DCF and IBP and 100 mg/L TiO_2 for CBZ. The addition of H_2O_2 in the dark and photolysis did not show any significant removal (data not shown), thus showing that DCF, IBP and CBZ is quite stable under bleaching conditions and photolysis. Photo-bleaching cannot be considered as feasible in the experiments since H_2O_2 does not

absorb at the spectrum of the lamp used (Anipsitakis and Dionysiou, 2004). On the other hand, when the solution was irradiated in the presence of 0.07-1.4 mM H_2O_2 without TiO_2, 7.5, 13 and 16% occurred after 120 min with the presence of 0.07-1.4 mM H_2O_2 according to absorbance measurements. DOC removal was 2.3, 4 and 7.5% after 120 min with the presence of 0.07-1.4 mM H_2O_2. For instance, DOC increased from 45.5 (without oxidant) to 66% after 120 min of reaction for DCF with the presence of 0.14 mM H_2O_2. This can be attributed to the photochemical cleavage of hydrogen peroxide to yield hydroxyl radicals.

The beneficial role of H_2O_2 can be attributed to its reaction with electrons, which (i) yields extra hydroxyl radicals, and (ii) prevents holes from recombining with electrons, a major cause for reduced photocatalytic activity (Arriaga et al., 2009) as follows:

$$H_2O_2 + O_2^{\cdot-} \rightarrow HO^{\cdot} + OH^- + O_2 \quad (3.1)$$

$$H_2O_2 + e_{cb}^- \rightarrow HO^{\cdot} + OH^- \quad (3.2)$$

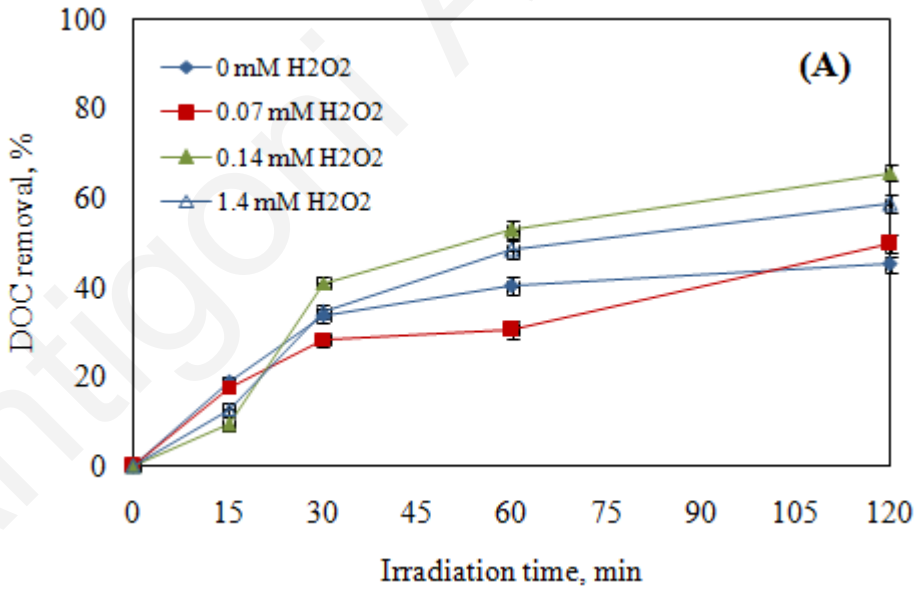

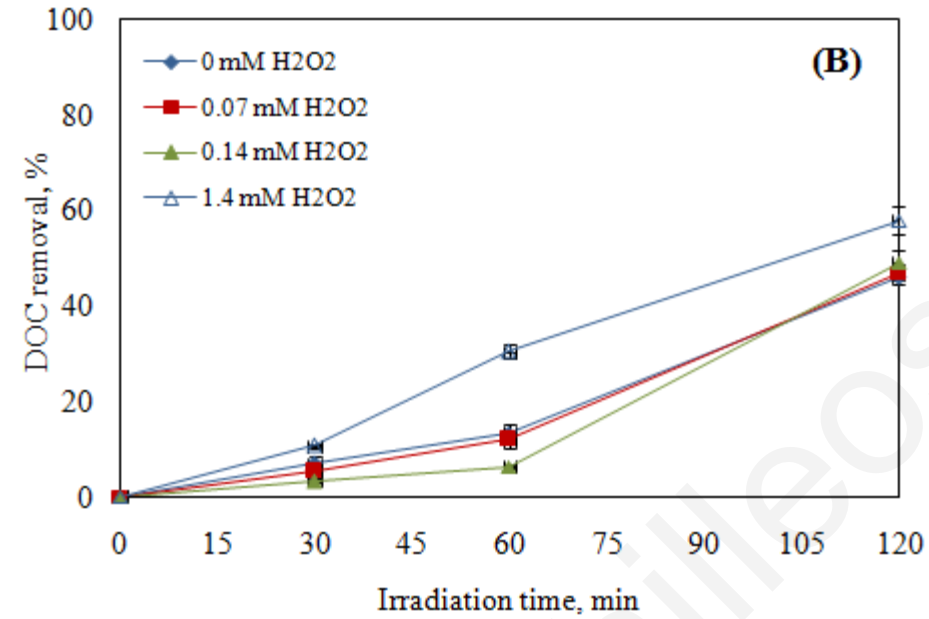

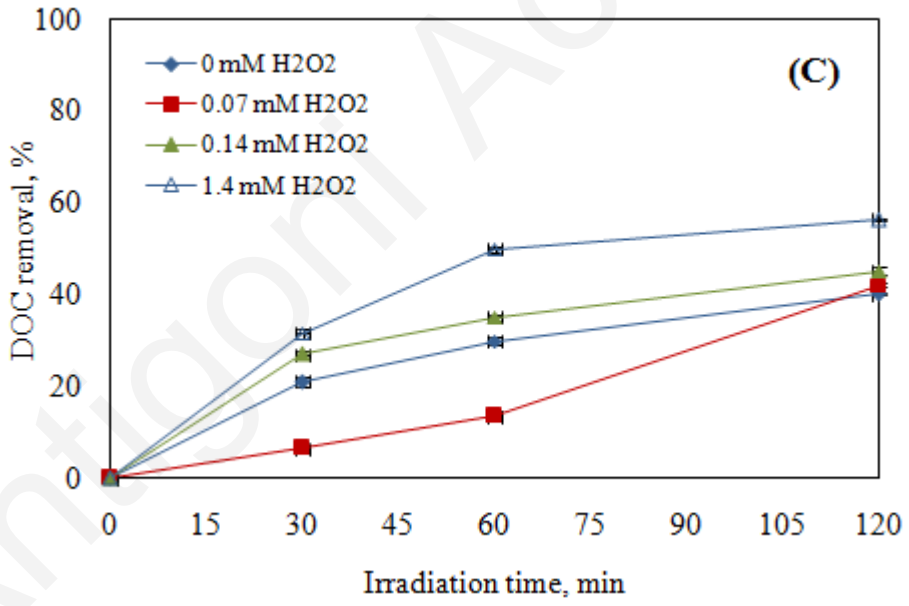

Figure 3.9: Effect of H_2O_2 addition on mineralization during the UV-A degradation of 10 mg/L (A) DCF, 500 mg/L TiO_2 (B) IBP, 500 mg/L TiO_2 and (C) CBZ, 100 mg/L Degussa P25 in ultrapure water

In Figures 3.9 B and C, DOC removal increased from 46 (without oxidant) to 58% and from 40 (without oxidant) to 56% after 120 min of reaction in the presence of 1.4 mM H_2O_2 for IBP and CBZ, respectively.

Hapeshi et al. (2010) investigated the effect of adding H_2O_2 on mineralization during the photocatalytic oxidation of 10 mg/L atenolol and ofloxacin with 250 mg/L TiO_2 with 9W UV-A lamp. DOC reduction after 120 min at 0.07 mM H_2O_2 was 79% and 60% for ofloxacin and atenolol, respectively while the respective values in the absence of H_2O_2 were 69% and 57%. Chatzisymeon et al. (2008) also investigated the addition of H_2O_2 and proved that when the oxidant concentration was increased from 0.1 to 0.15 g/L, COD reduction was 18, 34 and 47% respectively.

3.2.7 Influence of pH on the conversion of DCF, IBP and CBZ

In heterogeneous photocatalytic water system, pH is one of the most important operating parameters that affect the charge on the catalyst particles, size of catalyst aggregates and the positions of conductance and valence bands (Chong et al., 2010). All the experiments described so far were executed at solution's ambient pH; this was 5.5 for 10 mg/L DCF, IBP and 5.9 for 10 mg/L CBZ, respectively. A set of experiments was conducted adjusting the initial solution pH to 3 and 10 with the addition of the appropriate amount of HCl and NaOH, respectively. The pH at which the surface of an oxide is uncharged is defined as the Zero Point Charge (pHzpc), which for TiO_2 depends on the production method ($4.5 < pHzpc < 7$). Above and below this value, the catalyst is negatively or positively charged according to (Rincon et al., 2004; Malato et al., 2009): Below in Schematics 3.1-3.3 the dissociation of DCF, IBP and CBZ is shown in water.

At pH<PZC: $TiOH + H^+ \leftrightarrow TiOH_2^+$ (3.3)

At pH>PZC: $TiOH + OH^- \leftrightarrow TiO^- + H_2O$ (3.4)

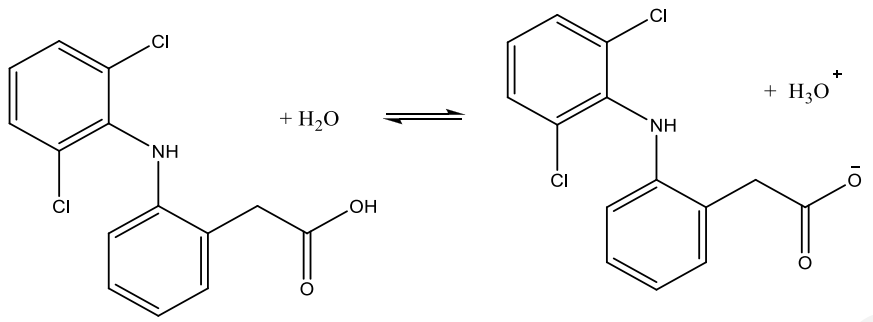

Schematic 3.1: DCF dissociation in water

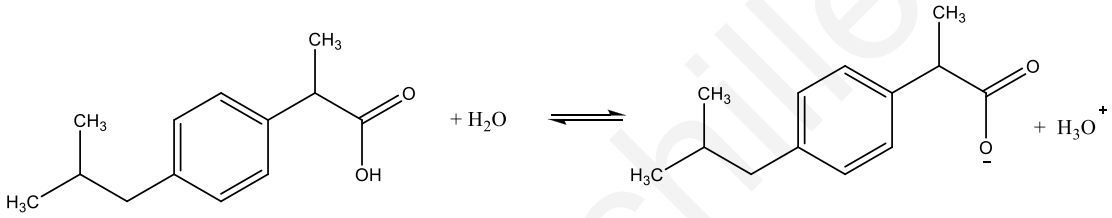

Schematic 3.2: IBP dissociation in water

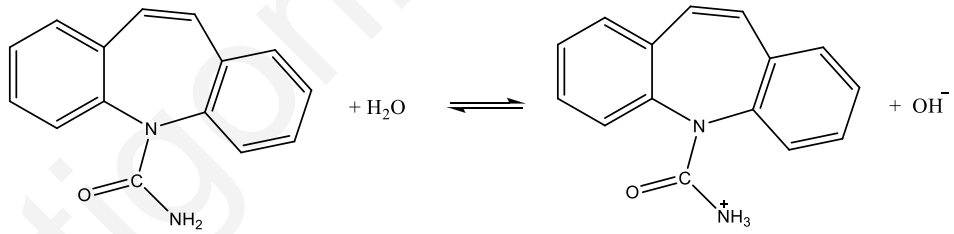

Schematic 3.3: CBZ dissociation in water

When operating at pH<PZC (TiO_2), the surface charge for the catalyst becomes positively charged and gradually exerts an electrostatic attraction force towards the negatively charged compounds. Such polar attractions between TiO_2 and charged anionic organic compounds can intensify the adsorption onto the photon activated TiO_2 surface for subsequent photocatalytic reactions (Chong et al., 2010). At pH>PZC (TiO_2), the catalyst surface will be negatively charged and repulse the anionic compounds in water.

At pH values greater than 4-4.2 (which corresponds to the pka value of DCF) DCF predominantly exists in its ionic form, while at lower values, it is principally found in its molecular form. As clearly seen in Figure 3.10A, DCF conversion increased with the reduction of solution pH. After 120 min of irradiation DOC removal for DCF was 58% (at pH 3) while at natural pH was 55%. That's because the surface charge of the catalyst is attracted towards the negatively charged DCF adsorption on catalyst surface was increased and due to that conversion increased.

For IBP, pH is dependent charge state of ibuprofen (neutral when pH < pKa (≈4.6) and anionic when pH > pKa), (Boggara et al., 2010). That means that at pH 10 the catalyst surface will be negatively charged and repulse the anionic compounds in water, the adsorption is lower and due to that the conversion is low.

The extent of DOC removal decreased in both acidic and alkaline conditions compared to experiments at ambient pH and this was more pronounced at alkaline conditions; for instance, the extent of IBP mineralization after 120 min of reaction at the experimental conditions of Figure 3.10 B was 9 and 21% at pH 10 and 3, respectively.

DOC removal for CBZ was 48% (at pH 3) while at natural pH was 30% (Figure 3.10 C). In the particular case of CBZ, it has a pKa of 13.9 (Jones et al., 2002) related to the deprotonation of the NH_2 group and a pKa of 2.3 (Nghiem et al., 2005) related to the protonation of the amino groups. This means that at environmentally relevant pH, carbamazepine should be present in its neutral form (Calisto et al., 2011).
However, at the tested pH 3, a protonated form of CBZ could exist in equilibrium with the neutral form at a concentration high enough to interfere with the photodegradation rate. Nevertheless, taking into account the observed pH dependence, the existence of a protonated form of carbamazepine at very low pH might not be enough to explain the obtained results, suggesting that a different pH dependence source should be operating (Calisto et al., 2011).

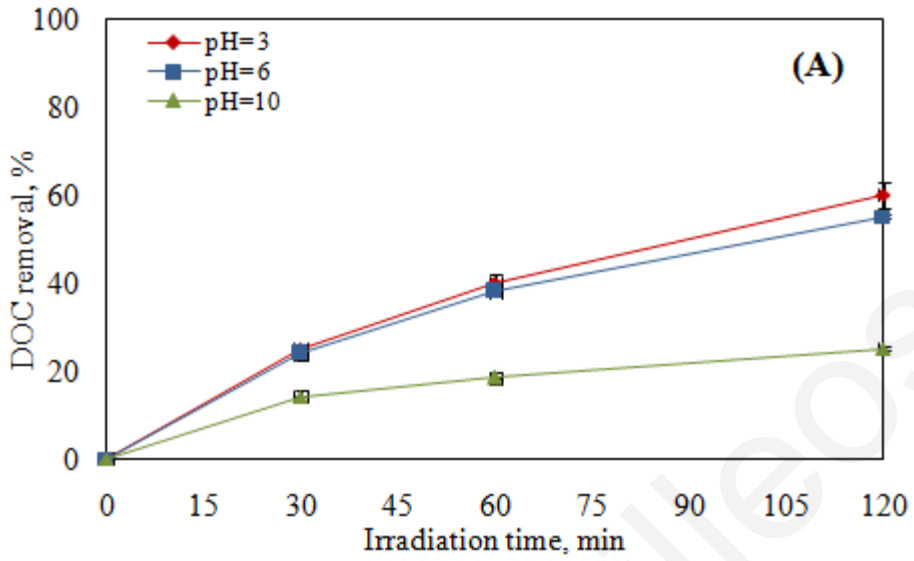

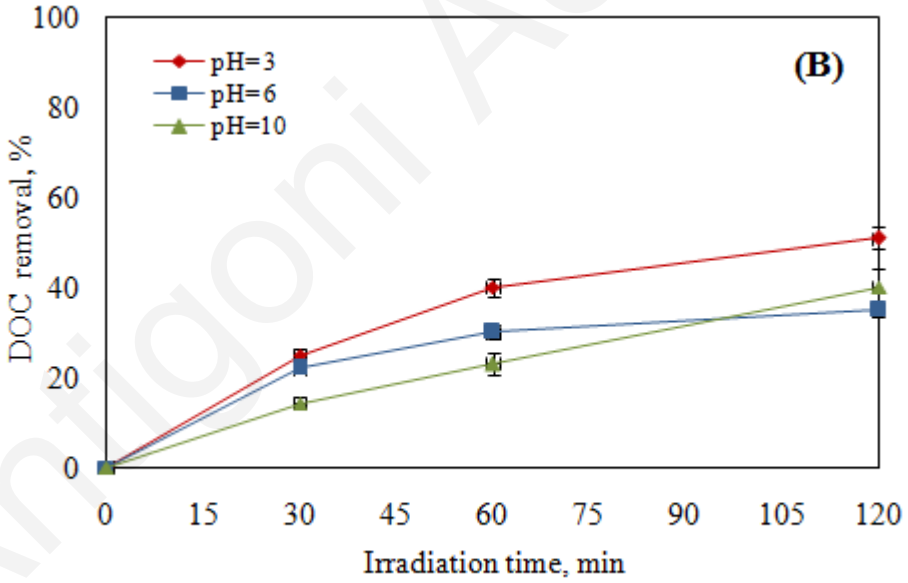

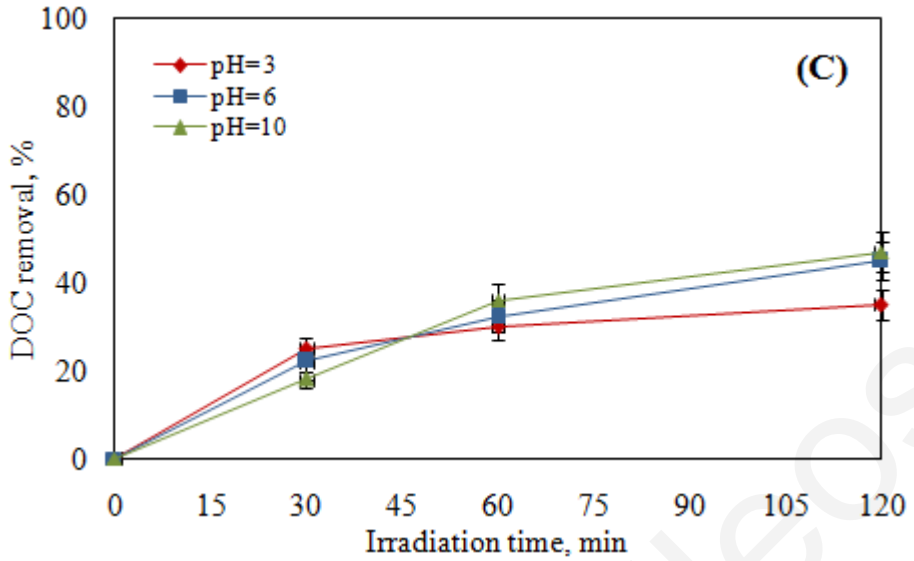

Figure 3.10: DOC removal %, pH=3-10, UV-A irradiation of 10 mg/L (A) DCF, 500 mg/L TiO_2, (B) IBP, 500 mg/L TiO_2 and (C) CBZ, 100 mg/L TiO_2

The solution pH is a complex factor that can affect photocatalytic reactions in many ways, i.e. in relation to (i) the ionization state of titania surface (i.e. negative at pH greater than about 6 and positive below this value), as well as the organic compounds present in the reaction mixture, (ii) the relative contribution of holes and hydroxyl radicals in degrading organic species; the former are believed to dominate at acidic environments, while the latter at neutral or high pH levels, and (iii) the fact that titania particles may agglomerate under highly acidic conditions, thus reducing the surface area available for photochemical reactions.

3.2.8 Influence of oxygen sparging

In general, the presence of O_2 is considered as a prerequisite for efficient TiO_2-photocatalyzed oxidation of organic pollutants in wet systems (Wang et al., 2006). As can be seen in Figures 3.11 A-C, after 120 min, the DCF conversion was 89 (with oxygen) and 76% without oxygen, while the conversion of IBP and CBZ was 83 and 92% (with oxygen) and 65, 74% without oxygen respectively; i.e., conversion increases with the influence of oxygen. Figures 3.12 A, B and C show the percentage of DOC removal. DOC removal for DCF 10 mg/L (Figure 3.12 A) was 58% without the presence of oxygen and 66% with oxygen. DOC removal for 10 mg/L IBP and CBZ (Figures 3.12 B and C) was 35 and 46% without the presence of oxygen and 38, 66% with the presence of oxygen.

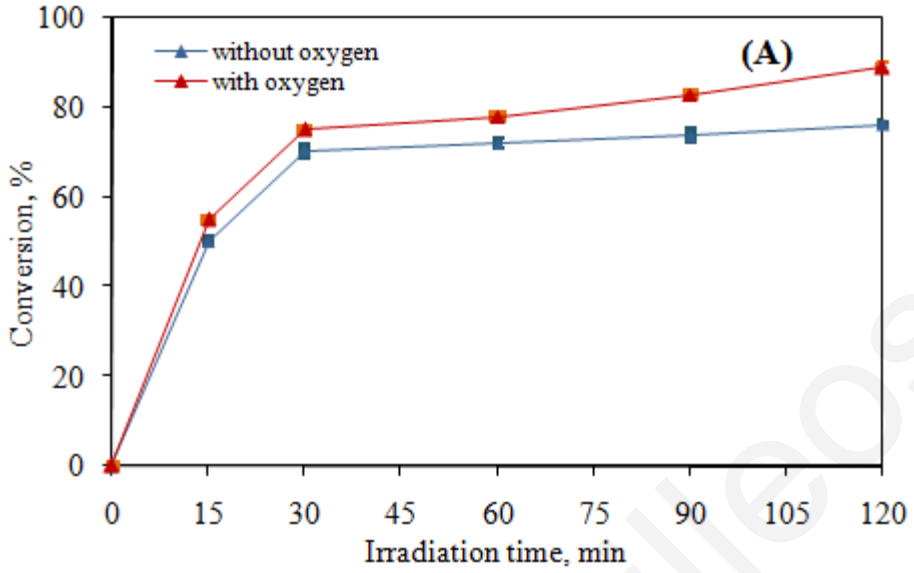

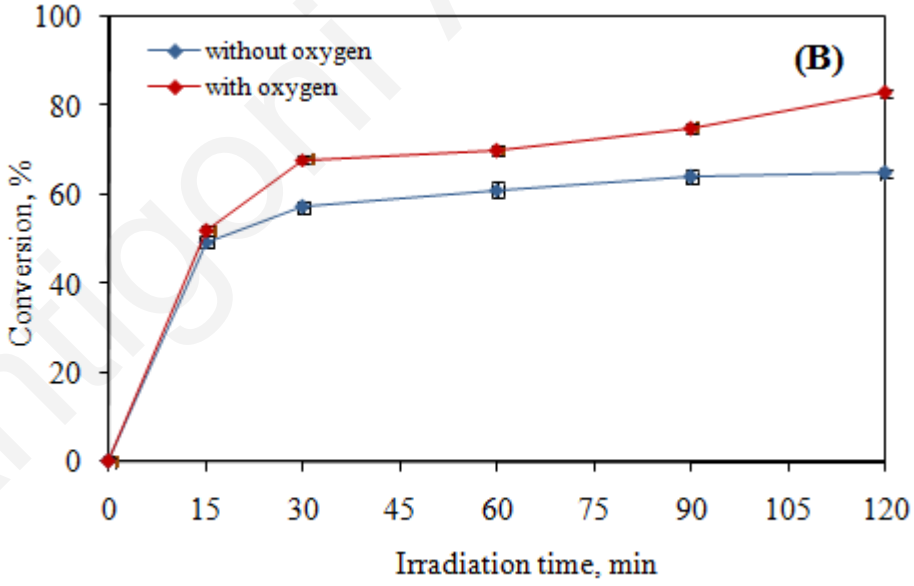

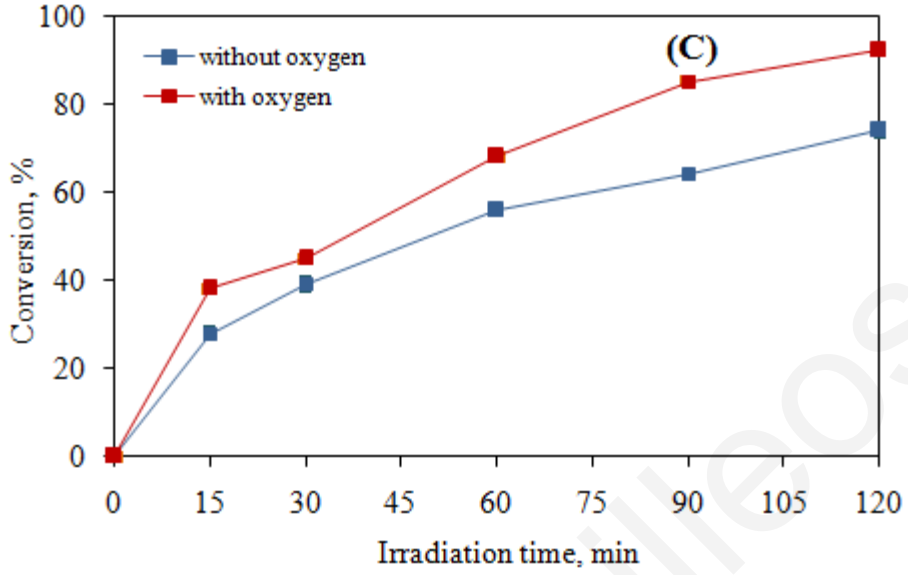

Figure 3.11: Influence of oxygen sparging, 10 mg/L (A) DCF, (B) IBP and (C) CBZ

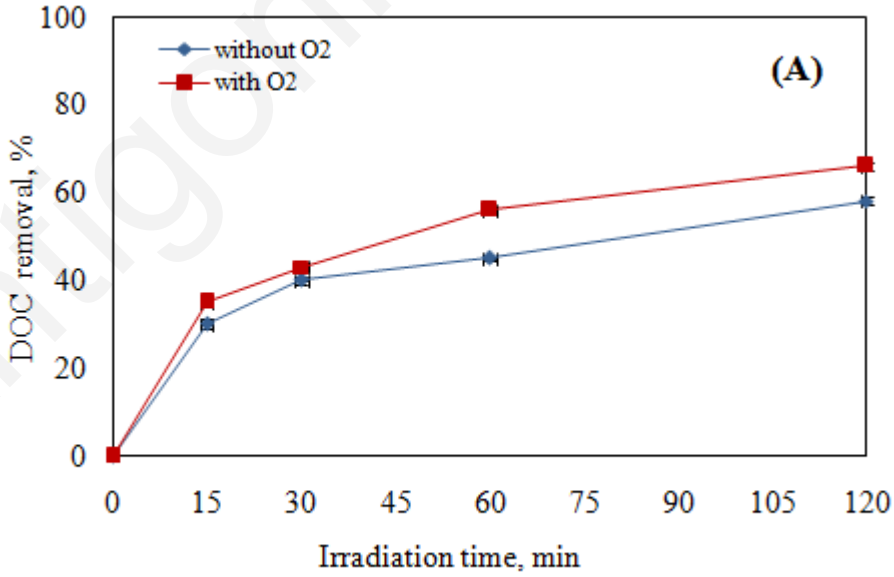

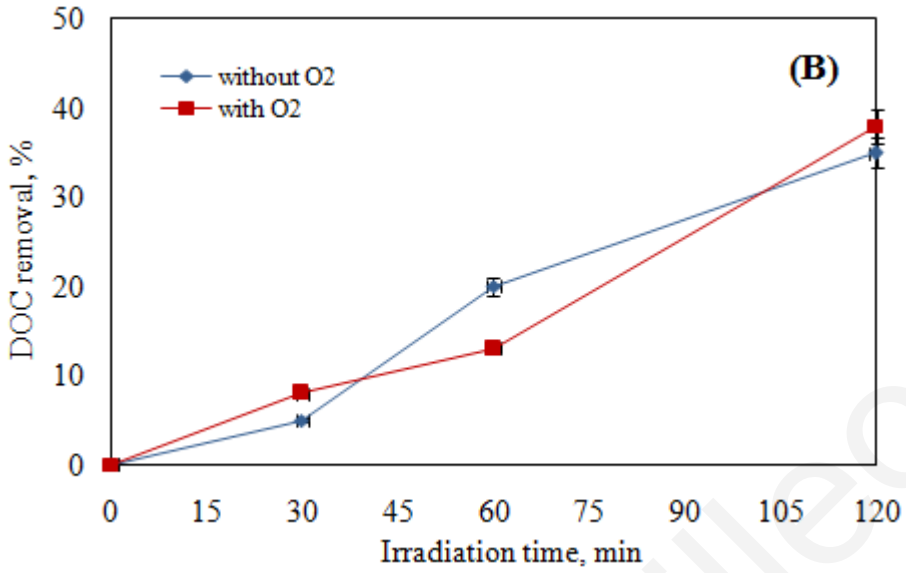

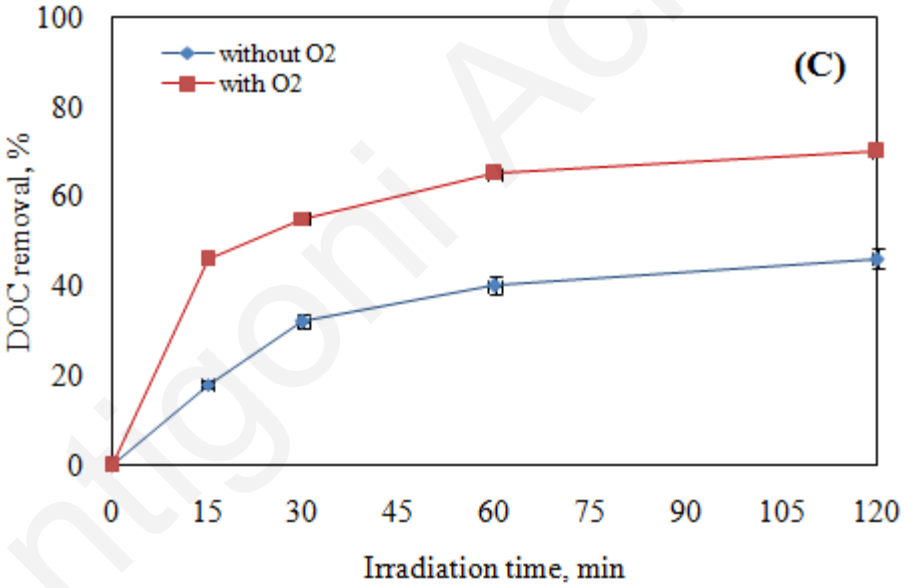

Figure 3.12: DOC removal, influence of oxygen sparging, 10 mg/L (A) DCF, (B) IBP and (C) CBZ

3.2.9 Effect of water matrix

All runs described so far were carried out in ultrapure water. In order to evaluate the effect of water matrix on mineralization, WWTPEf and GW samples were spiked with 10 mg/L of DCF, IBP and CBZ, added with varying loadings of Degussa P25 in the range 500-3000 mg/L

and subjected to UV-A irradiation; results are shown in Figures 3.13 A and B.

As clearly seen, mineralization increased with increasing catalyst loading and under UV-A irradiation. More importantly though, the matrix appears to have a detrimental effect on mineralization and this can be explained in terms of: (i) increased initial carbon concentration; the WWTPEf and GW sample already have 11 and 2 mg/L of DOC which accounts for about 150% of the organic carbon contained in 10 mg/L substrate, conversion decreases with increasing initial concentration, (ii) the presence of species like chlorides and carbonates/bicarbonates that may act as scavengers of hydroxyl radicals and other reactive moieties, and (iii) the increased solution pH (the wastewater sample is alkaline) which, affects adversely mineralization. Experiments were also carried out in the presence of 0.07-3 mM H_2O_2. The addition of H_2O_2 did not practically improve the reduction of DOC (i.e. only about 3% greater than without peroxide), thus indicating the stability of the wastewater matrix.

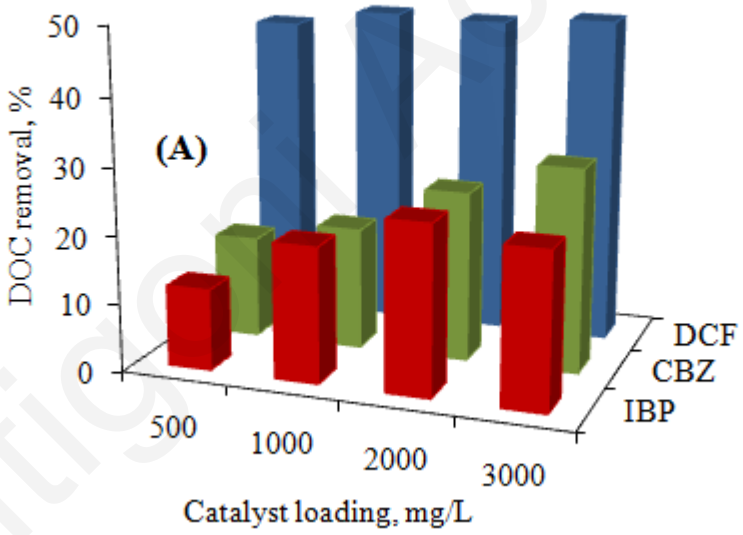

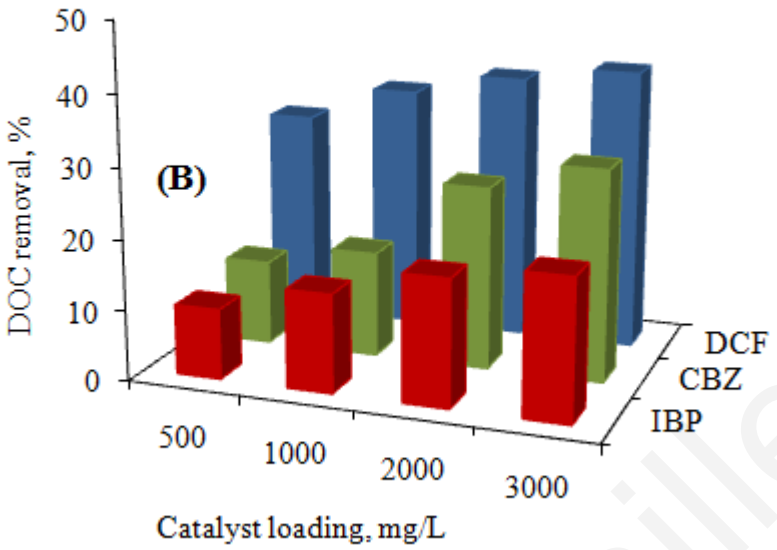

Figure 3.13: DOC removal, % effect of water matrix spiked with 10 mg/L DCF, IBP, CBZ (A) WWTPEf and (B) GW under UV-A irradiation

Conversion and DOC removal after 120 min of irradiation is shown below in Table 3.7.

Table 3.7: Conversion and DOC removal in water matrix spiked with pharmaceutical compounds

Pharmaceutical, catalyst loading	**WWTPEf**	**GW**
Conversion, %		
DCF 10 mg/L, 3000 mg/L TiO_2	47%	42%
IBP 10 mg/L, 2000[a] and 3000[b] mg/L TiO_2	34%	46%
CBZ 10 mg/L, 3000 mg/L TiO_2	38%	55%
DOC removal, %		
DCF 10 mg/L, 3000 mg/L TiO_2	48	20
IBP 10 mg/L, 2000[a] and 3000[b] mg/L TiO_2	25	30
CBZ 10 mg/L, 3000 mg/L TiO_2	30	40

[a]: optimum catalyst loading for WWTPEf, [b]: optimum catalyst loading for GW

In the WWTPEf sample after 120 min DOC removal was 48, 25 and 30% respectively for 10 mg/L DCF, IBP and CBZ with 3000 mg/L, 2000 mg/L and 3000 mg/L catalyst loading. In GW sample after 120 min DOC removal was 20, 30 and 40% respectively for 10 mg/L DCF, IBP and CBZ with 3000 mg/L catalyst loading. In spiked wastewater sample, interferences of

other oxidizable compounds and radicals scavengers can occur which might influence negatively the entire process.

3.2.10 Photocatalyst reuse

The possibility of catalyst reuse has received considerable attention since it can contribute significantly to lowering the operational costs of the process, which is an important parameter in the applicability of photocatalysis as a method for wastewater purification (Pekakis et al., 2006). In order to evaluate the reused photocatalyst efficiency, a series of experiments were performed at the optimum catalyst loading of 500 mg/L TiO_2 for 10 mg/L DCF. The catalyst after each run was washed with milli-Q water and let to dry in the dark. At the conditions tested photocatalytic efficiency remained sufficiently high after the fourth run although the photocatalytic efficiency is marginally decreased on repeated use according to some other studies (Dominguez et al., 1998). In general, when catalyst deactivation takes place this could be explained as follows: upon irradiation, anatase TiO_2 is partly transformed to its rutile counterpart (Pekakis et al., 2006). Rutile is less active than anatase and this could explain the decreased catalytic activity after repeated use. Also, another reason for catalyst deactivation might be the poisoning of catalyst by the effect of intermediates containing N or S adsorbed on the catalyst surface. In Figure 3.14, the effect of TiO_2 reuse on DCF 10 mg/L spiked in Milli-Q water is shown.

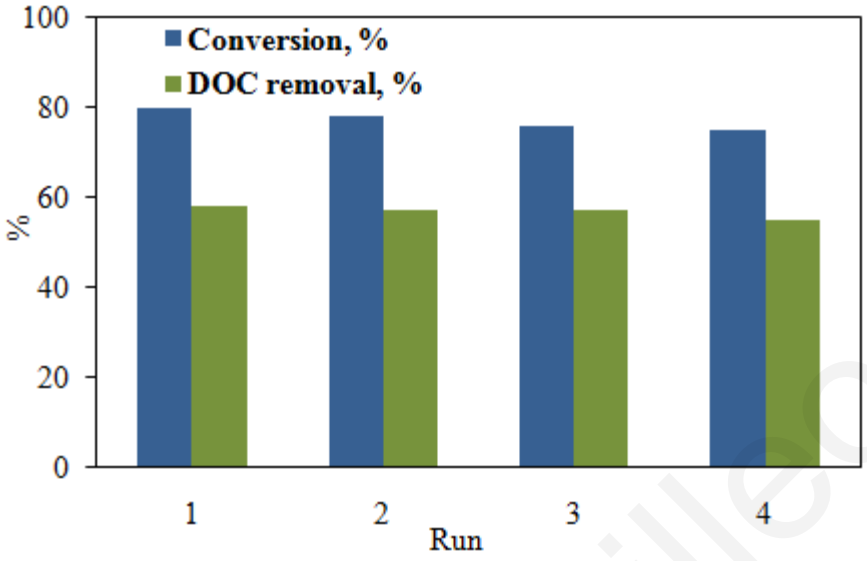

Figure 3.14: Effect of TiO_2 reuse at DCF 10 mg/L and 500 mg/L TiO_2 on conversion and DOC removal

3.3 Photocatalytic degradation of the pharmaceuticals under solar irradiation

The aim of this part of the work was to study the degradation of DCF, IBP and CBZ in single-compound solutions in ultrapure water by means of solar irradiation, concerning the effect of optimum operating conditions such as screening of catalyst, addition of electron acceptor, effect of drug initial concentration, effect of gas sparging, effect of solution pH and the water matrix on the kinetics of pharmaceuticals reduction and mineralization.

3.3.1 Dark experiments

Preliminary experiments were conducted to assess the extent of drug adsorption onto the catalyst surface (Degussa P25) in the dark. Dark adsorption was completed within 30 min and therefore, before the irradiation, the suspension was stirred in the dark for 30 min to reach the adsorption/desorption equilibrium. The results are shown in section 3.2.1.

3.3.2 Photolysis of DCF, IBP and CBZ

Previous to the photocatalytic treatments, photolysis experiments were performed in order to determine the contribution of this effect. Photolysis was performed for each compound at natural pH in ultrapure water. Samples were exposed to direct solar radiation and continuously stirred during the photolysis experiments. Photolysis experiments started with a concentration at 5, 10 and 20 mg/L of each compound. As can be seen in Figures 3.15 A, data for the conversion of 5-20 mg/L DCF, after 120 min of irradiation are shown. The conversion efficiency was 27.4, 11, and 10.2% for 5, 10 and 20 mg/L DCF. In Figure 3.15 B data for the conversion of 5-20 mg/L IBP after 120 min of irradiation are shown. The conversion efficiency was 6,4 and 3.5% for 5, 10, 20 mg/L IBP. In Figure 3.15 C data for the conversion of 5 and 10 mg/L CBZ after 120 min of irradiation are shown. The conversion efficiency was 4.5 and 7% for 5 and 10 mg/L CBZ. DOC removal was maximum at ~1.4% and is shown in Figure 3.16.

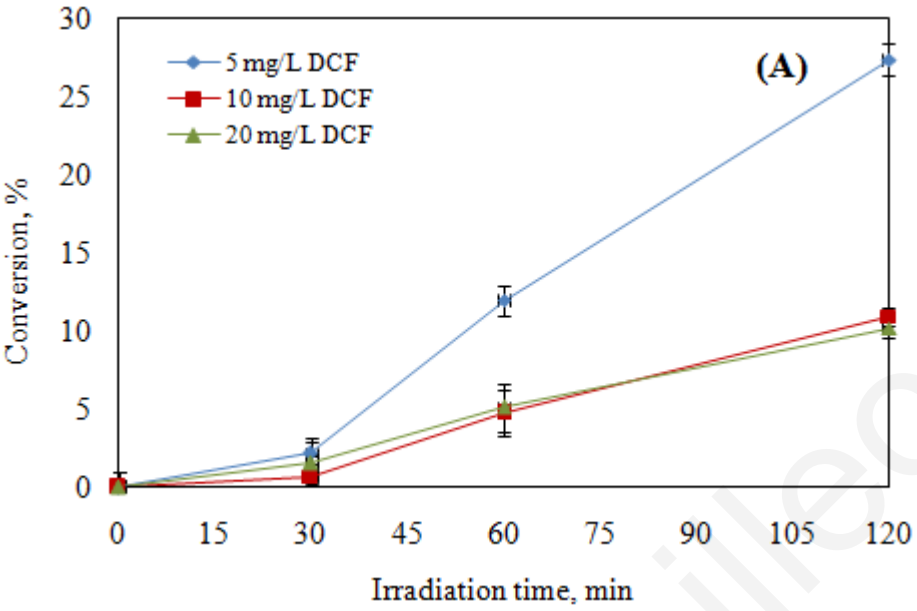

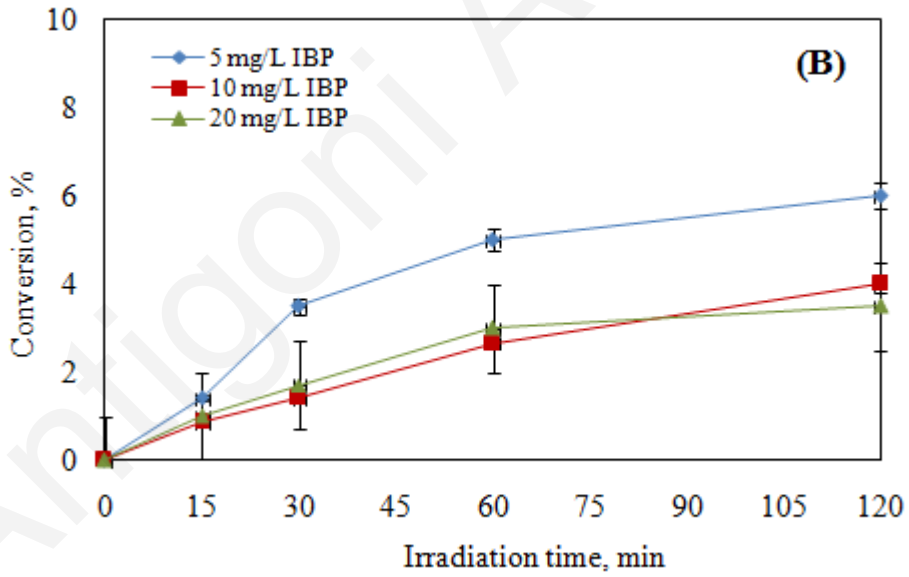

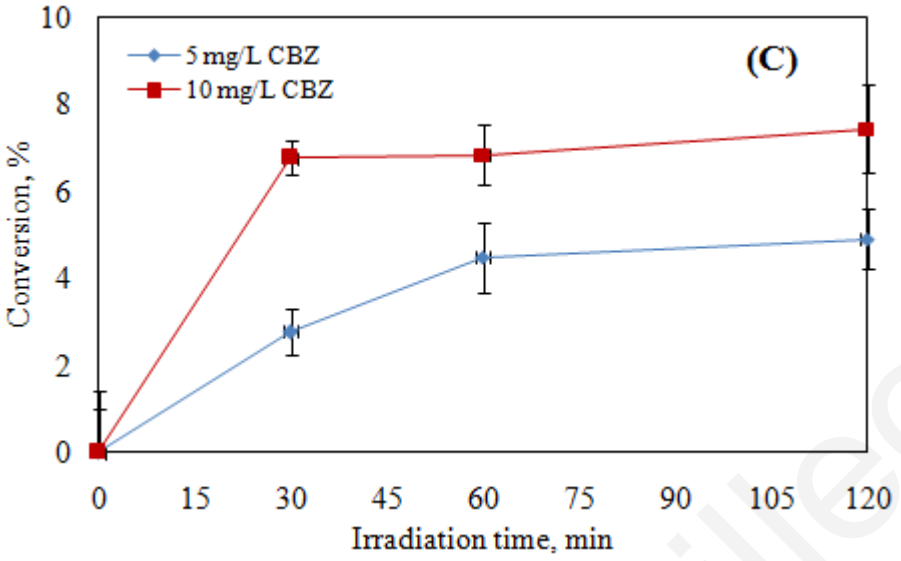

Figure 3.15: Photolysis of (A) 5-20 mg/L DCF, (B) 5-20 mg/L IBP and (C) 5-10 mg/L CBZ under solar irradiation

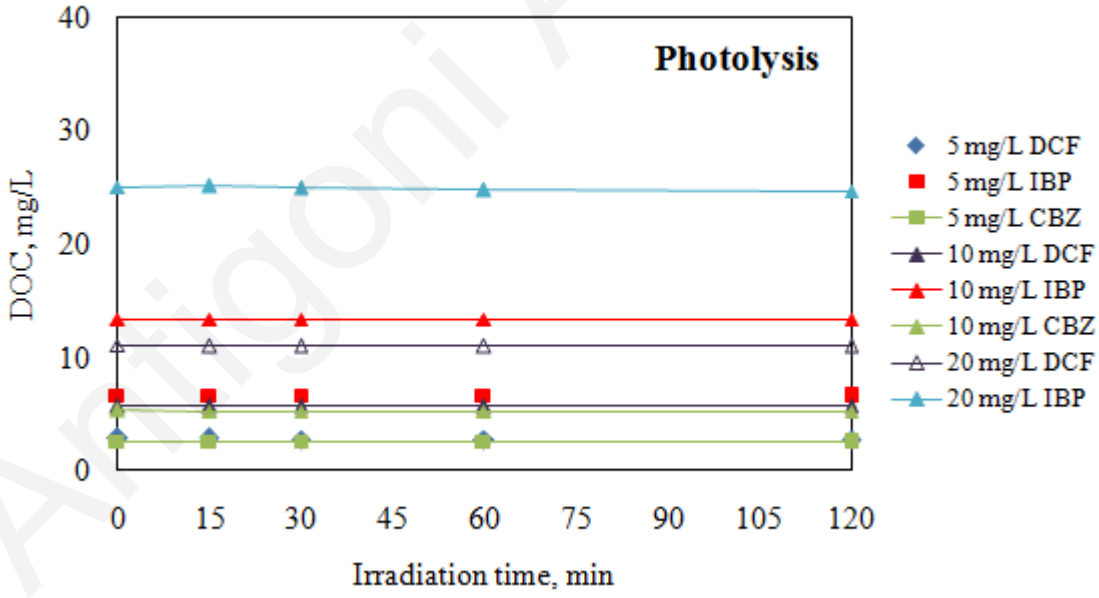

Figure 3.16: DOC values for 5-20 mg/L of DCF, IBP and CBZ after 120 min of photolysis

3.3.3 Screening of catalysts

To assess the relative catalytic activity of various titania samples, screening experiments were performed with 10 mg/L initial drug concentration and 250 mg/L catalyst loading under solar irradiation. As it was mentioned before Degussa P25 exhibits higher photoactivity compared to all other samples employed in this study. The conversion efficiency for DCF after 120 min of illumination was 69% (Figure 3.17 A). For IBP, the conversion efficiency after 120 min of illumination was 55% and for CBZ the conversion efficiency after 120 min of illumination was 60%, respectively (Figures 3.17 B and C).

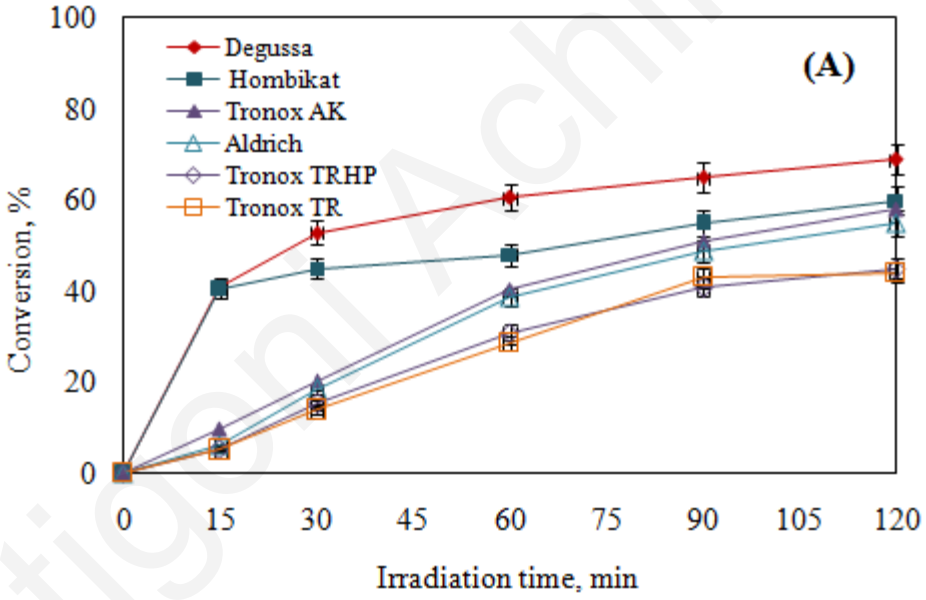

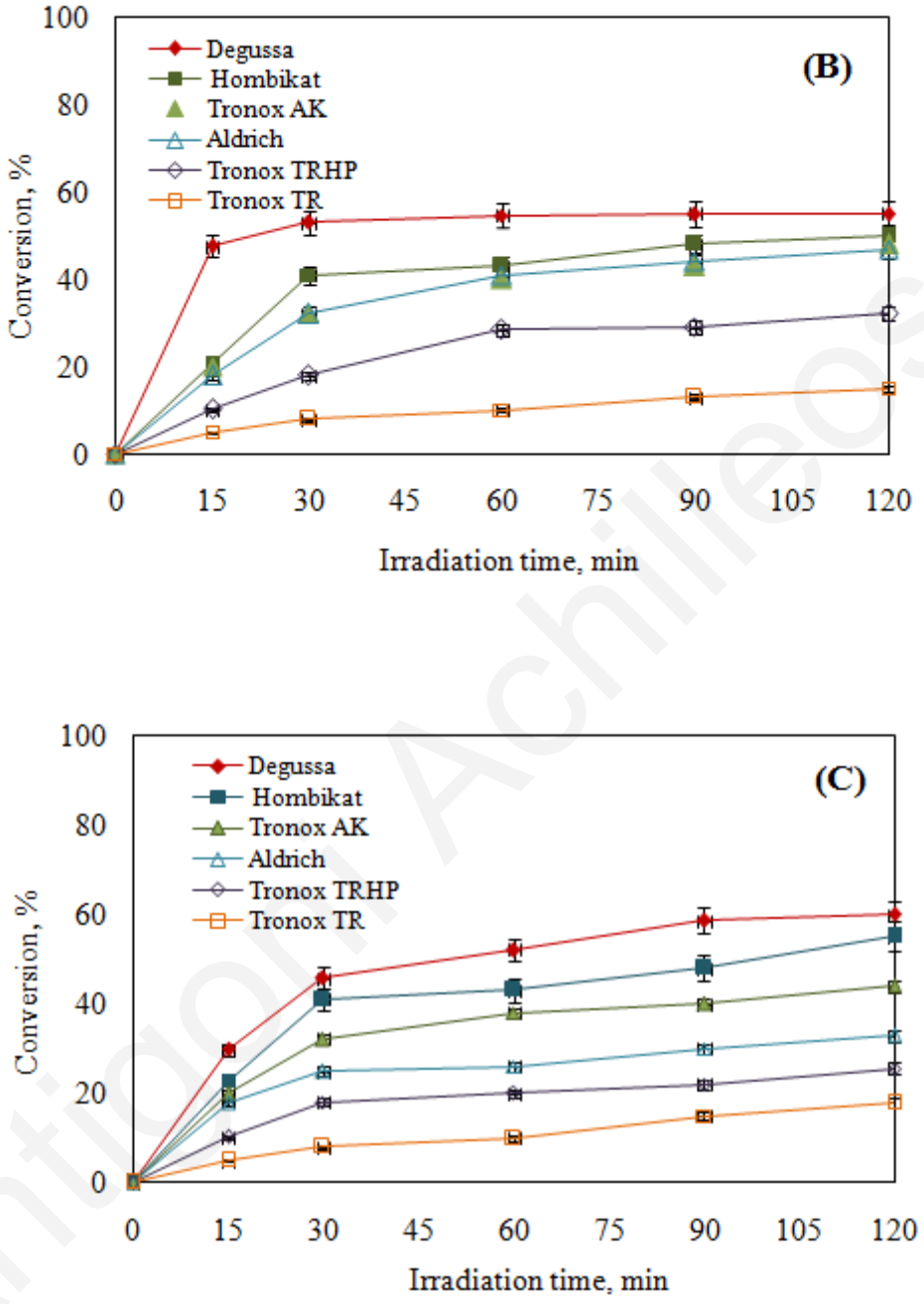

Figure 3.17: Screening of the catalyst activity during the conversion of 10 mg/L (A) DCF, (B) IBP and (C) CBZ under solar irradiation

3.3.4 Effect of catalyst loading

In order to study the effect of the catalyst initial concentration on the degradation of 10 mg/L DCF, IBP and CBZ, experiments were conducted using Degussa P25, in the range of 50-800 mg/L for the solar experiments in ultrapure water. TiO_2 loading in slurry processes is a significant factor that can affect performance. Figures 3.18 A, B and C shows the effect of catalyst loading on 10 mg/L DCF, IBP and CBZ conversion. After 120 min conversion was 90, 59 and 69% in terms of absorbance for 10 mg/L DCF, IBP and CBZ for 500 mg/L, 500 mg/L and 100 mg/L catalyst loading. DOC removal was about 55, 40 and 45% for 10 mg/L DCF, IBP and CBZ.

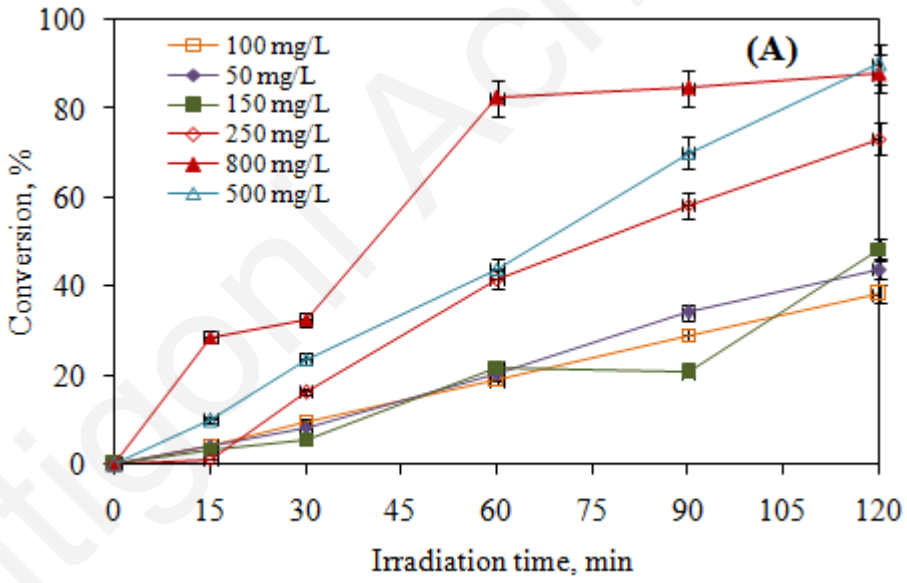

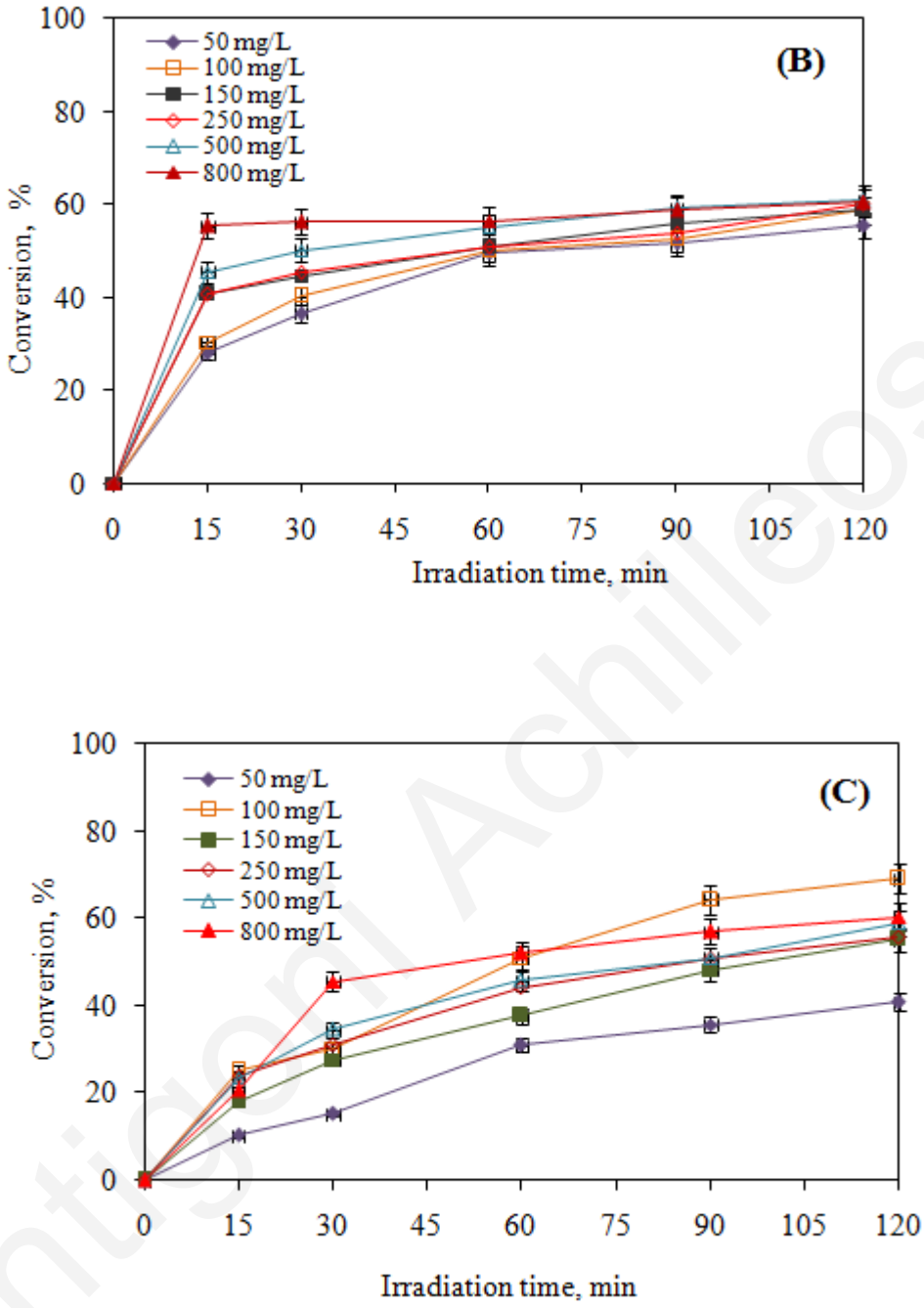

Figure 3.18: Effect of Degussa P25 loading on the conversion of 10 mg/L (A) DCF, (B) IBP and (C) CBZ

Below in Figure 3.19 DOC removal (%) is shown for the optimum catalyst loading for 10 mg/L DCF, IBP and CBZ.

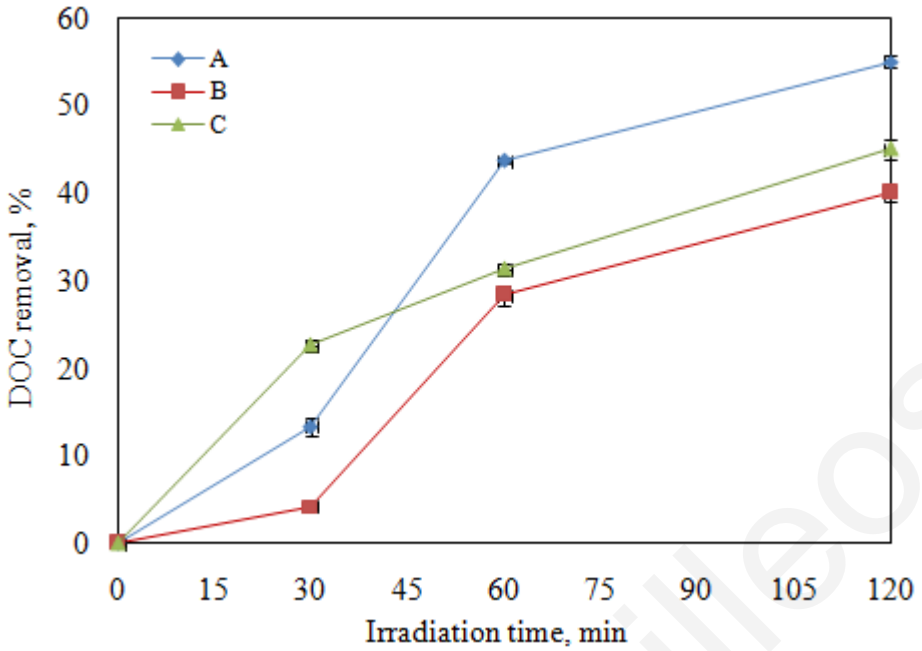

Figure 3.19: DOC removal (%), on optimum catalyst loading on 10 mg/L (A) DCF, (B) IBP and (C) CBZ

3.3.5 Additional oxidant as promoter of DCF, IBP and CBZ conversion

The effect of adding H_2O_2, in the range 0.07-1.4 mM on drug mineralization was tested during the photocatalytic degradation of 10 mg/L DCF, IBP or CBZ under solar irradiation. The addition of H_2O_2 in the water solution of TiO_2 can increase the degradation rate of pollutants. Hydrogen peroxide limits the electron-hole recombination rate and increases the hydroxyl radical concentration at the TiO_2 surface (Didier et al., 2002). For instance, DOC increased from 55 (without oxidant) to 60% after 120 min of reaction for DCF with the presence of 0.14 mM H_2O_2 (Figure 3.20 A). DOC removal increased from 45 (without oxidant) to 50% and from 40 (without oxidant) to 52% after 120 min of reaction in the presence of 1.4 mM H_2O_2 for IBP and CBZ, respectively (3.20 B and C).

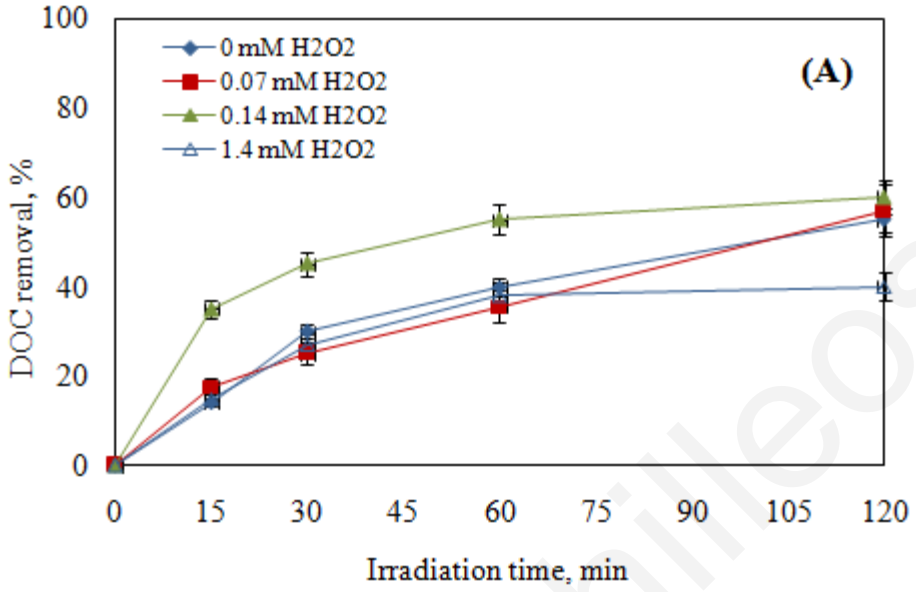

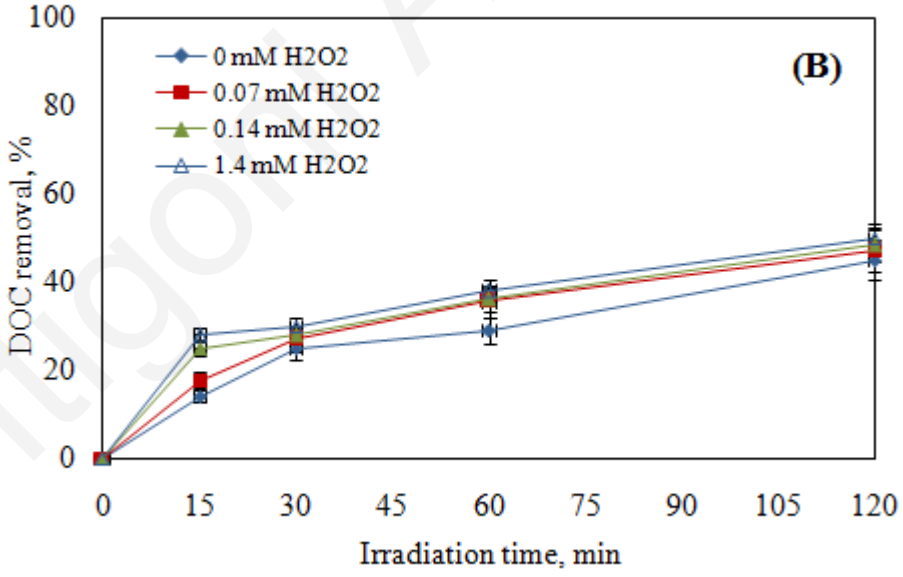

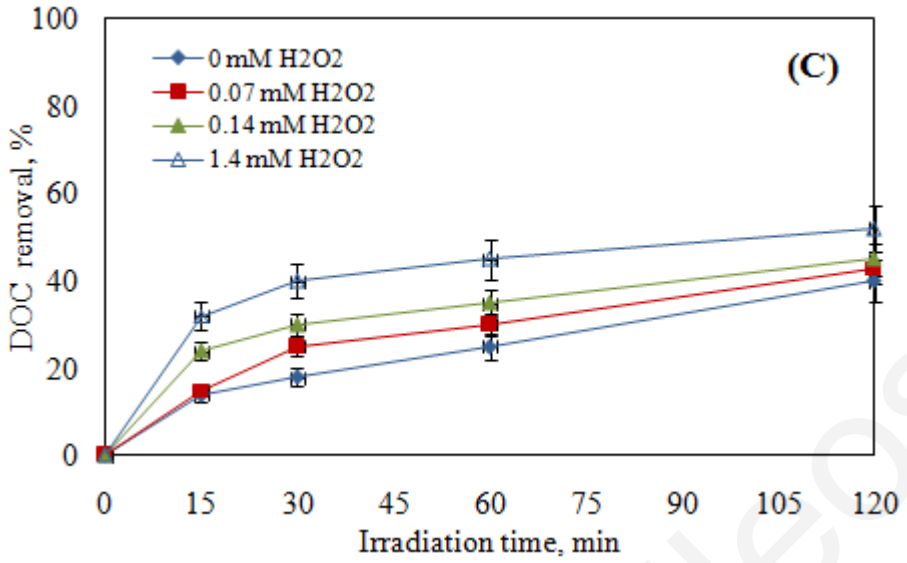

Figure 3.20: Effect of H_2O_2 addition on mineralization during the solar degradation of 10 mg/L (A) DCF, 500 mg/L TiO_2, (B) IBP, 500 mg/L TiO_2 and (C) CBZ, 100 mg/L TiO_2; in ultrapure water

3.3.6 Influence of the pH on the conversion of DCF, IBP and CBZ

All the experiments described so far were executed at solution's ambient pH; this was 5.5 for 10 mg/L DCF, IBP and 5.9 for 10 mg/L CBZ, respectively. A set of experiments was conducted adjusting the initial solution pH to 3 and 10 with the addition of the appropriate amount of HCl and NaOH, respectively. The change in solution pH affects not only the photocatalytic activity of TiO_2 but also the TiO_2 surface ionic speciation, because of the amphoteric behaviour of this semi-conductor. An increase of the pH will have a positive or negative effect on their conversion and consequently the mineralization rate of the solution (Didier et al., 2002).

According to Agustina et al. (2005), in the case of substances which are weakly acidic, the photocatalytic degradation increases at lower pH because of an increase in the adsorption. Some substances undergo hydrolysis at alkaline pH, which is one of the reasons for the increase in the photocatalytic degradation at alkaline pH values. As clearly seen in Figures 3.21 A, B and C, after 120 min of irradiation DOC removal for DCF was 60 % (at pH 3) while

at natural pH was 55%. DOC removal for IBP was 51% (at pH 3) while at natural pH was 40 %. For CBZ, DOC removal was 47% (at pH 10) while at natural pH was 45 %.

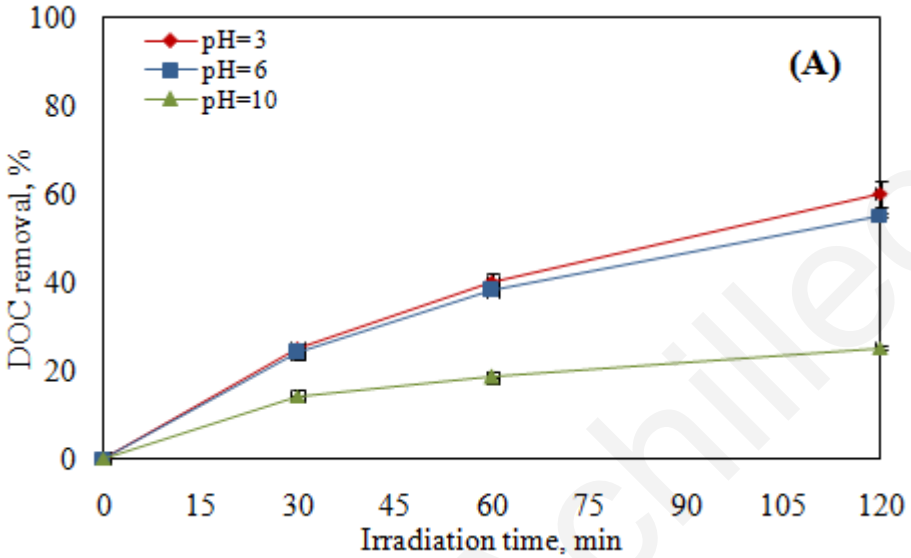

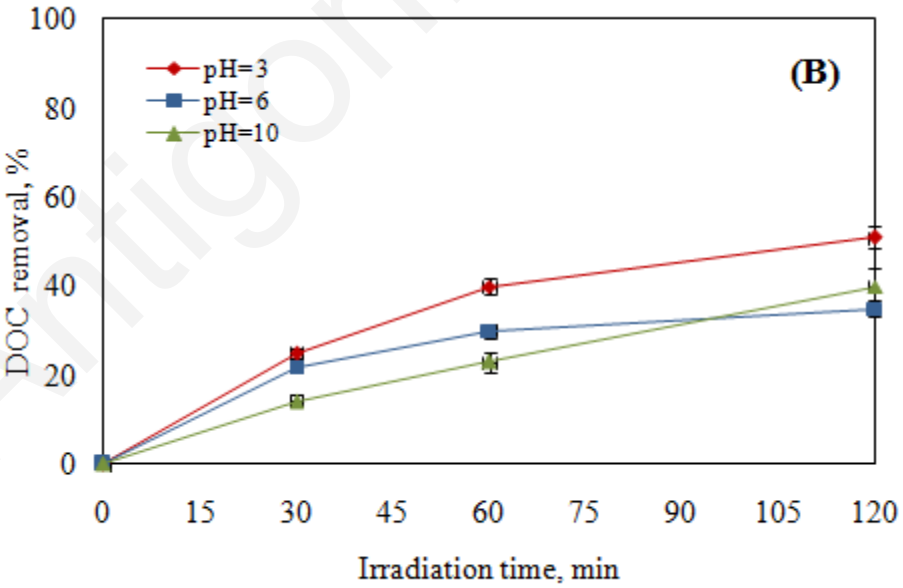

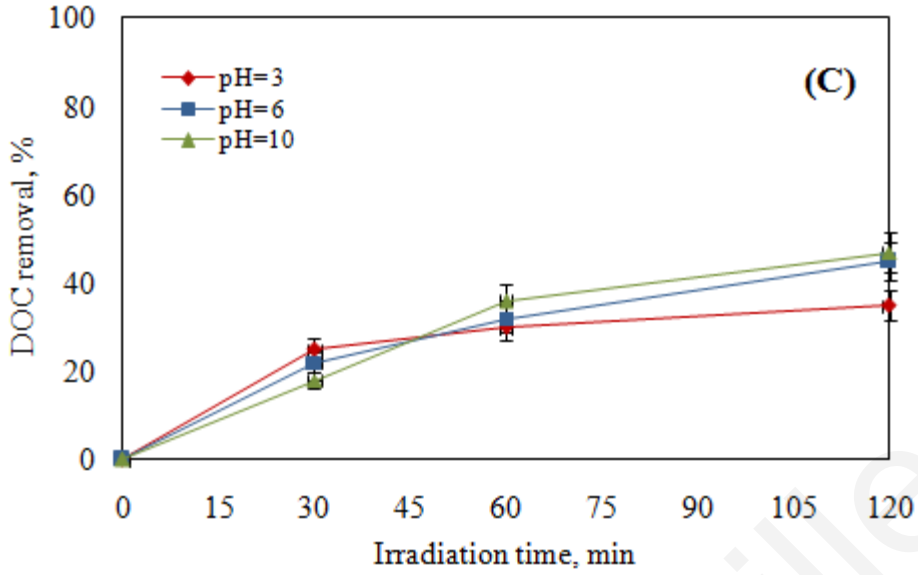

Figure 3.21: DOC removal %, Solar irradiation of 10 mg/L (A) DCF, 500 mg/L TiO_2 (B) IBP, 500 mg/L and (C) CBZ, 100 mg/L TiO_2

3.3.7 Influence of oxygen sparging

The presence of excess molecular oxygen is expected to influence photocatalytic efficiency. The photogenerated electrons react with adsorbed molecular oxygen on the TiO_2 surface leading to the formation of perhydrol radical. In addition perhydrol radical can generate hydrogen peroxide, which in turn gives rise to hydroxyl radicals (Pekakis et al., 2006).

As can be seen in Figure 3.22 A, B and C, after 120 min, the DCF conversion was 89 (with oxygen) and 76% with out oxygen, while the conversion of IBP and CBZ was 98 and 92% (with oxygen) and 62, 74% with out oxygen respectively; i.e., conversion increases with the influence of oxygen.

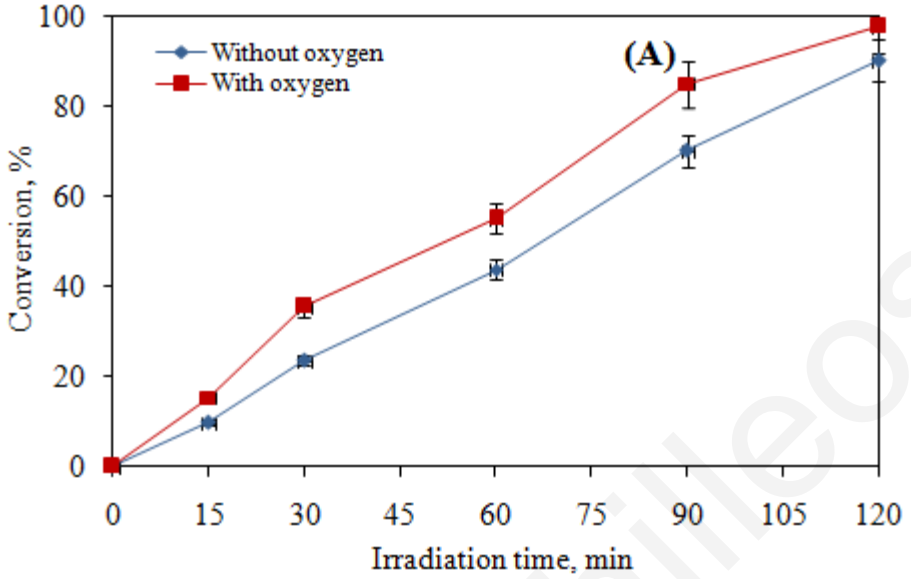

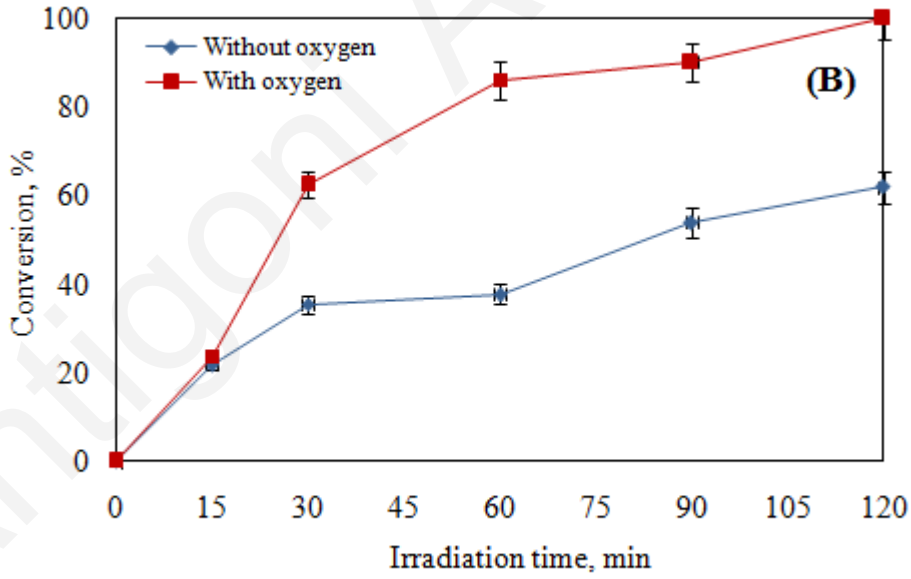

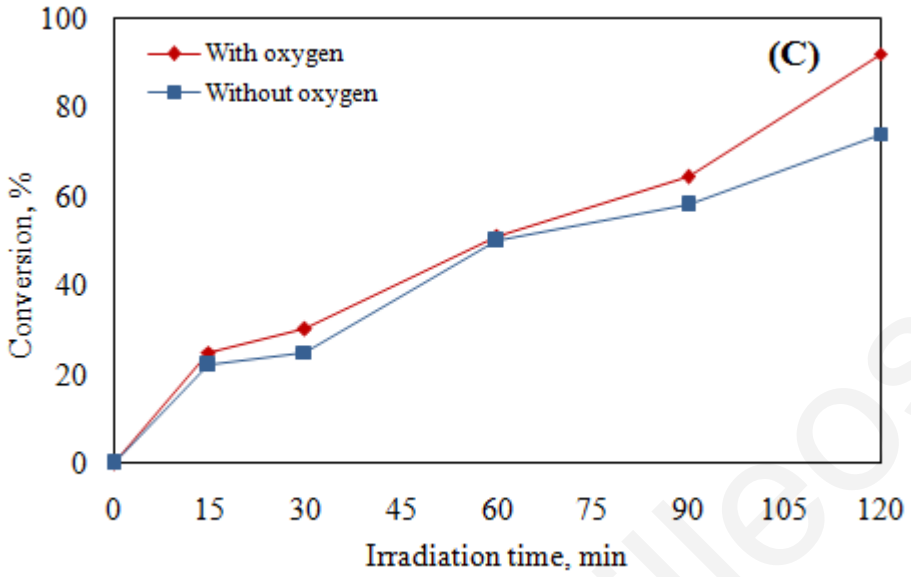

Figure 3.22: Effect of oxygen sparging, 10 mg/L (A) DCF, 500 mg/L TiO_2, (B) IBP, 500 mg/L TiO_2 and (C) CBZ, 100 mg/L TiO_2

Below in Figure 3.23, DOC removal for 10 mg/L DCF, IBP and CBZ is shown. DOC removal after oxygen sparge was 70, 42 and 65% for 10 mg/L DCF, IBP and CBZ respectively.

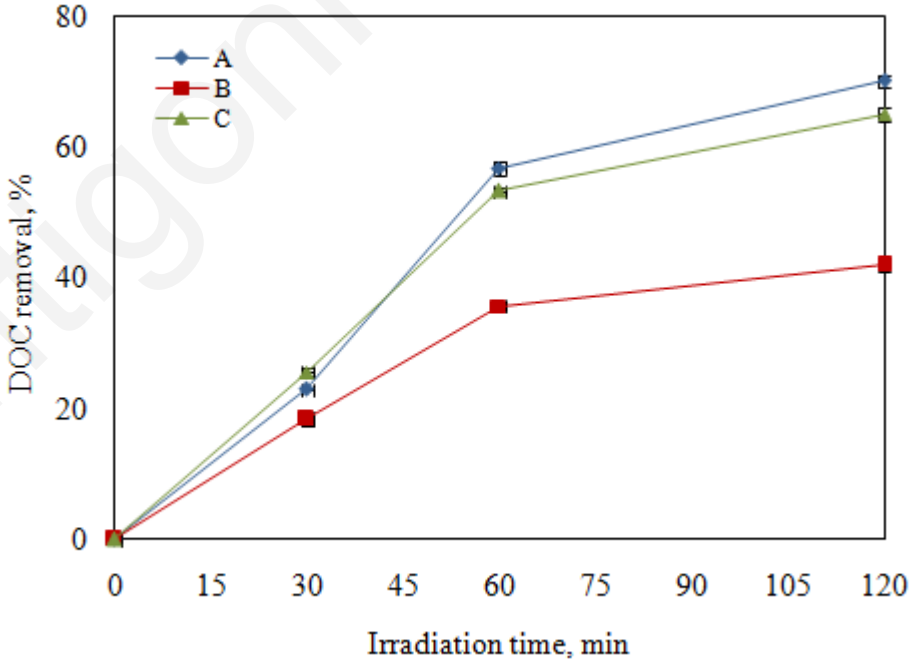

Figure 3.23: DOC removal (%), oxygen sparging on optimum catalyst loading on 10 mg/L (A) DCF, (B) IBP and (C) CBZ

3.3.8 Effect of water matrix

All runs described so far were carried out in ultrapure water. In order to evaluate the effect of water matrix on mineralization, WWTPEf and GW samples were spiked with 10 mg/L of DCF, IBP and CBZ, added varying loadings of Degussa P25 in the range 500-3000 mg/L and subject to solar irradiation; results are shown in Figures 3.24 A and B. In WWTPEf sample after 120 min DOC removal was 38, 18 and 25 % respectively for 10 mg/L DCF, IBP and CBZ with 3000 mg/L, 2000 mg/L and 3000 mg/L catalyst loading. In GW sample after 120 min DOC removal was 26, 35 and 40% respectively for 10 mg/L DCF, IBP and CBZ with 3000 mg/L catalyst loading.

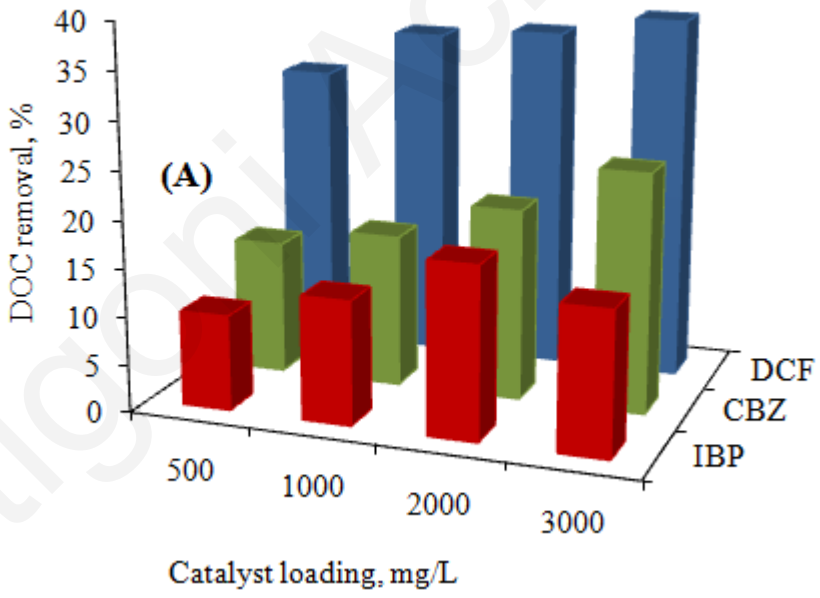

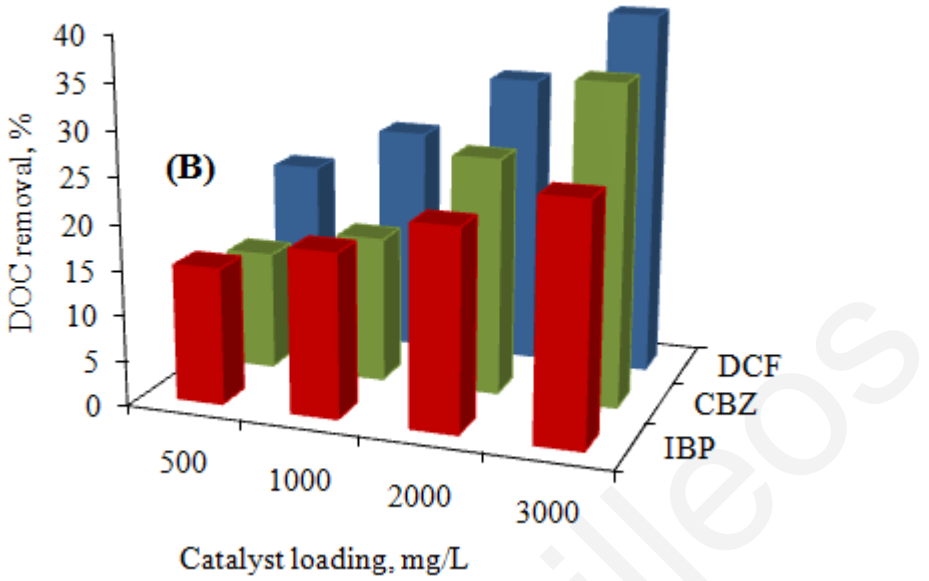

Figure 3.24: DOC removal % in water matrix spiked with 10 mg/L DCF, IBP and CBZ: (A) WWTPEf, (B) GW, under solar irradiation

Conversion after 120 min of irradiation is shown below in Table 3.8.

Table 3.8: Conversion and DOC removal in water matrix spiked with pharmaceutical compounds

Pharmaceutical compounds spiked	**WWTPEf**	**GW**
Conversion, %		
DCF 10 mg/L, 3000 mg/L TiO_2	45%	30%
IBP 10 mg/L, 3000[a] and 2000[b] mg/L TiO_2	26%	40%
CBZ 10 mg/L, 3000 mg/L TiO_2	32%	44%
DOC removal, %		
DCF 10 mg/L, 3000 mg/L TiO_2	38	26
IBP 10 mg/L, 3000[a] and 2000[b] mg/L TiO_2	18	35
CBZ 10 mg/L, 3000 mg/L TiO_2	25	40

[a]: optimum catalyst loading for WWTPEf, [b]: optimum catalyst loading for GW

Perez-Estrada et al. (2005) studied the decomposition of DCF by solar driven photo-Fenton and TiO_2 photocatalysis at a pilot plant scale. In this study only one initial concentration of DCF and one TiO_2 loading. The total decomposition of 50 mg/L of DCF took place after 200 min using 0.2 g/L TiO_2. Calza et al. (2006) investigated lower DCF concentrations in the range of 0.76-9.24 mg/L using TiO_2 loading range of 0.1-0.9 g/L. After 1h of irradiation a

complete elimination was achieved. Mendez-Arriaga et al. (2008) investigated the TiO_2 photocatalytic degradation of three NSAIDs (DCF, IBP, naproxen) at initial concentrations varying from 25-1000 mg/L under simulated solar irradiation (1000 W Philips Xe-OP lamp. Removal was 70% (expressed as TOC), achieved after 4h of irradiation using 0.1 g/L TiO_2.

In our investigation after 120 min of irradiation using 3000 mg/L TiO_2 for DOC removal was 38, 18 and 25% for DCF, IBP and CBZ and conversion was 46, 26 and 32% for DCF, IBP and CBZ respectively. This can be explained due to the irradiation time 2 h instead of 4 h and to the different reactor setups.

3.3.9 Comparison between UV-A and solar driven process efficiency

A comparison between UV-A and solar irradiation is shown below in Table 3.9. As we can see, in general, the substrate conversion is faster than mineralization to carbon dioxide and water in both processes; for instance, during UV-A irradiation, at 10 mg/L DCF with 500 mg/L catalyst loading conversion was 80% in 120 min, while mineralization was 58% in 120 min, thus indicating the formation of persistent oxidation by-products. When the experiment was performed under solar irradiation conversion and DOC removal were lower than the experiments under UV-A irradiation. This can be explained as follows: (i) the spectrum of the xenon lamp consists of just about 5% UV irradiation and, consequently, the degree of photoactivation for the titania is expected to be limited, and (ii) reactor setups for UV-A and solar irradiation experiments are different. The former offers full and uniform illumination of the reaction mixture since the lamp is located inside the vessel, while the latter yields partial illumination since the source is outside the vessel. In general however, all the parameters examined have exhibited similar effects during both types of irradiation.

3.3.10 Comparison between pharmaceuticals' behaviour under UV-A and solar driven processes at optimum conditions

A comparison between DCF, IBP and CBZ under UV-A and solar irradiation is shown below in Tables 3.9 and 3.10 after 120 min. As it was already mentioned, substrate conversion is faster than mineralization to carbon dioxide and water in both processes. Degradation refers to

the parent compound after quantification of each sample with HPLC/ESI-QqLIT-MS, during UV-A and solar irradiation.

Under UV-A irradiation the highest conversion (80%) and DOC removal (58%) was achieve with DCF 10 mg/L with 500 mg/L catalyst loading. The highest degradation (93.84%) was for CBZ 10 mg/L with 100 mg/L catalyst loading. Under solar irradiation the highest conversion (90%) and DOC removal (55%) was achieve with DCF 10 mg/L with 500 mg/L catalyst loading. The highest degradation (96%) was for IBP 10 mg/L with 500 mg/L catalyst loading.

In the presence of H_2O_2 catalyst loading under UV-A irradiation the highest conversion (95%) and DOC removal (66%) was achieve with DCF 10 mg/L with 500 mg/L catalyst loading. In the presence of H_2O_2 and catalyst under solar irradiation the highest conversion (95%) and DOC removal (60%) was achieve with DCF 10 mg/L with 500 mg/L catalyst loading.

In the presence of catalyst loading under UV-A irradiation and oxygen sparging the highest conversion (92%) was achieve with CBZ 10 mg/L with 500 mg/L and DOC removal (66%) was achieve for DCF 10 mg/L with 500 mg/L catalyst loading and CBZ 10 mg/L with 100 mg/L catalyst loading. In the presence of catalyst loading under solar irradiation and oxygen sparging the highest conversion (98%) and DOC removal (70%) was achieve with IBP 10 mg/L with 500 mg/L catalyst loading and DCF 10 mg/L with 500 mg/L catalyst loading.

From the comparison of the conversion, DOC removal and compound degradation its obvious that DOC is not completely removed in any case a fact that clearly indicates the formation of persistent oxidation products.

Table 3.9: Comparison between UV-A and solar irradiation processes under optimum process conditions

Treatment	Conversion, %	DOC removal, %
UVA-irradiation		
Photolysis experiment		
• 10 mg/L DCF	• 11%	• ~2% (for DCF, IBP and CBZ)
• 10 mg/L IBP	• 12%	
• 10 mg/L CBZ	• 7%	
Effect of catalyst loading		
• 10 mg/L DCF, 500 mg/L TiO_2	• 80%	• 58%
• 10 mg/L IBP, 500 mg/L TiO_2	• 65%	• 46%
• 10 mg/L CBZ, 100 mg/L TiO_2	• 74%	• 40%
Effect of H_2O_2 addition		
• 10 mg/L DCF, 500 mg/L TiO_2, 0.14 mM H_2O_2	• 95%	• 66%
• 10 mg/L IBP, 500 mg/L TiO_2, 1.4 mM H_2O_2	• 90%	• 58%
• 10 mg/L CBZ, 100 mg/L TiO_2, 1.4 mM H_2O_2	• 99.8%	• 56%
Influence of oxygen sparging		
• 10 mg/L DCF, 500 mg/L TiO_2	• 89%	• 66%
• 10 mg/L IBP, 500 mg/L TiO_2	• 83%	• 38%
• 10 mg/L CBZ, 100 mg/L TiO_2	• 92%	• 66%
Effect of water matrix		
• 10 mg/L DCF spiked in WWTPEf and GW, 3000 mg/L TiO_2	• 53% (WWTPEf), 42% (GW)	• 48% (WWTPEf), 20% (GW)
• 10 mg/L IBP spiked in WWTPEf with 2000 mg/L TiO_2 and GW 3000 mg/L TiO_2	• 34% (WWTPEf), 46% (GW)	• 25% (WWTPEf), 30% (GW)
• 10 mg/L CBZ spiked in WWTPEf and GW , 3000 mg/L TiO_2	• 38% (WWTPEf), 55% (GW)	• 30% (WWTPEf), 40% (GW)
Solar irradiation		
Photolysis experiment		
• 10 mg/L DCF	• 11%	• ~2% (for DCF, IBP and CBZ)
• 10 mg/L IBP	• 4%	
• 10 mg/L CBZ	• 7%	
Effect of catalyst loading		

A) 10 mg/L DCF, 500 mg/L TiO_2	• 90%	• 55%
B) 10 mg/L IBP, 500 mg/L TiO_2	• 59%	• 40%
C) 10 mg/L CBZ, 100 mg/L TiO_2	• 69%	• 45%
Effect of H_2O_2 addition		
• 10 mg/L DCF, 500 mg/L TiO_2, 0.14 mM H_2O_2	• 95%	• 60%
• 10 mg/L IBP, 500 mg/L TiO_2, 1.4 mM H_2O_2	• 80%	• 50%
• 10 mg/L CBZ, 100 mg/L TiO_2, 1.4 mM H_2O_2	• 78%	• 52%
Influence of oxygen sparging		
• 10 mg/L DCF, 500 mg/L TiO_2	• 89%	• 70%
• 10 mg/L IBP, 500 mg/L TiO_2	• 98%	• 42%
• 10 mg/L CBZ, 100 mg/L TiO_2	• 92%	• 65%
Effect of water matrix		
• 10 mg/L DCF spiked in WWTPEf and GW, 3000 mg/L TiO_2	• 45% (WWTPEf), 30% (GW)	• 38% (WWTPEf), 26% (GW)
• 10 mg/L IBP spiked in WWTPEf with 2000 mg/L TiO_2 and GW 3000 mg/L TiO_2	• 26% (WWTPEf), 40% (GW)	• 18% (WWTPEf), 35% (GW)
• 10 mg/L CBZ spiked in WWTPEf and GW , 3000 mg/L TiO_2	• 32% (WWTPEf), 44% (GW)	• 25% (WWTPEf), 40% (GW)

Table 3.10: Comparison of pharmaceutical substances under UV-A and solar irradiation at optimum conditions

Pharmaceutical compounds	Conversion, %	DOC removal, %	Degradation, %
UVA irradiation			
DCF **(**10 mg/L, 500 mg/L TiO_2)	80	58	53.3
IBP (10 mg/L, 500 mg/L TiO_2)	65	46	84.3
CBZ (10 mg/L, 100 mg/L TiO_2)	75	40	93.84
Solar irradiation			
DCF (10 mg/L, 500 mg/L TiO_2)	90	55	53
IBP (10 mg/L, 500 mg/L TiO_2)	59	40	95.8
CBZ (10 mg/L, 100 mg/L TiO_2)	69	45	50

3.4 Sonolytic degradation of pharmaceuticals

3.4.1 Effect of power density on conversion

As it is known, the ultrasound power is a major factor affecting sonochemical reactions. Figure 3.25 A, B and C shows, the effect of changing ultrasound power on DCF, IBP and CBZ degradation as a function of the sonication time at 10 mg/L initial concentration under air. As clearly seen, in Figure 3.25 A the final (i.e. after 120 min) conversion increases from 6 to 21% in terms of absorbance, in Figure 3.25 B conversion increases from 2 to 5% in terms of absorbance and in Figure 3.25 C conversion increases from 3 to 50% in terms of absorbance with increasing power density from 130 to 640 W/L. The beneficial effect of power on conversion is attributed to increased cavitational activity occurring at higher levels of power. As power increases, the number of collapsing bubbles also increases, thus leading to enhanced degradation levels.

The study of the sonolytic degradation of the pharmaceutical compounds DCF, IBP and CBZ showed that the beneficial ultrasound power density is 640 W/L. Based on these sonolytic experiments, all subsequent runs were conducted with 640 W/L. Figure 3.26 presents the sonolytic degradation of the three pharmaceutical compounds.

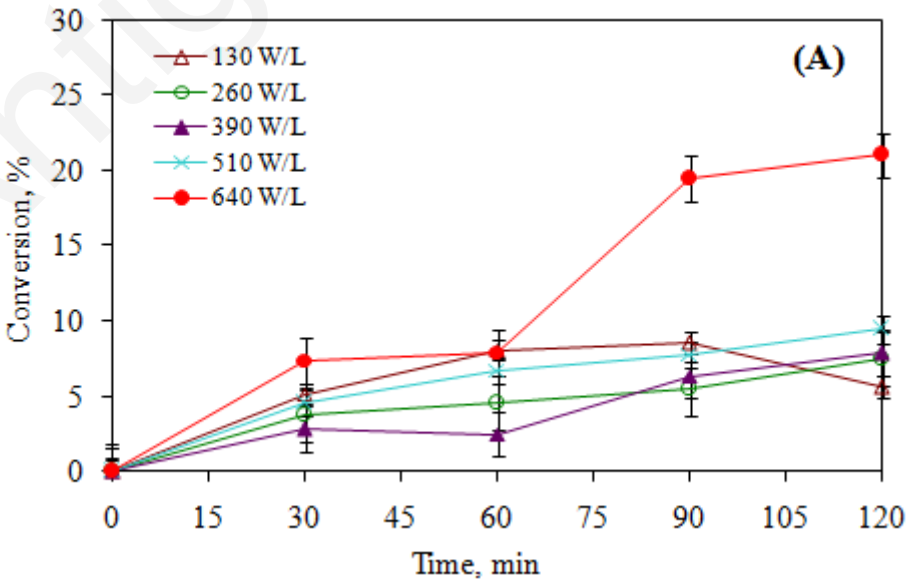

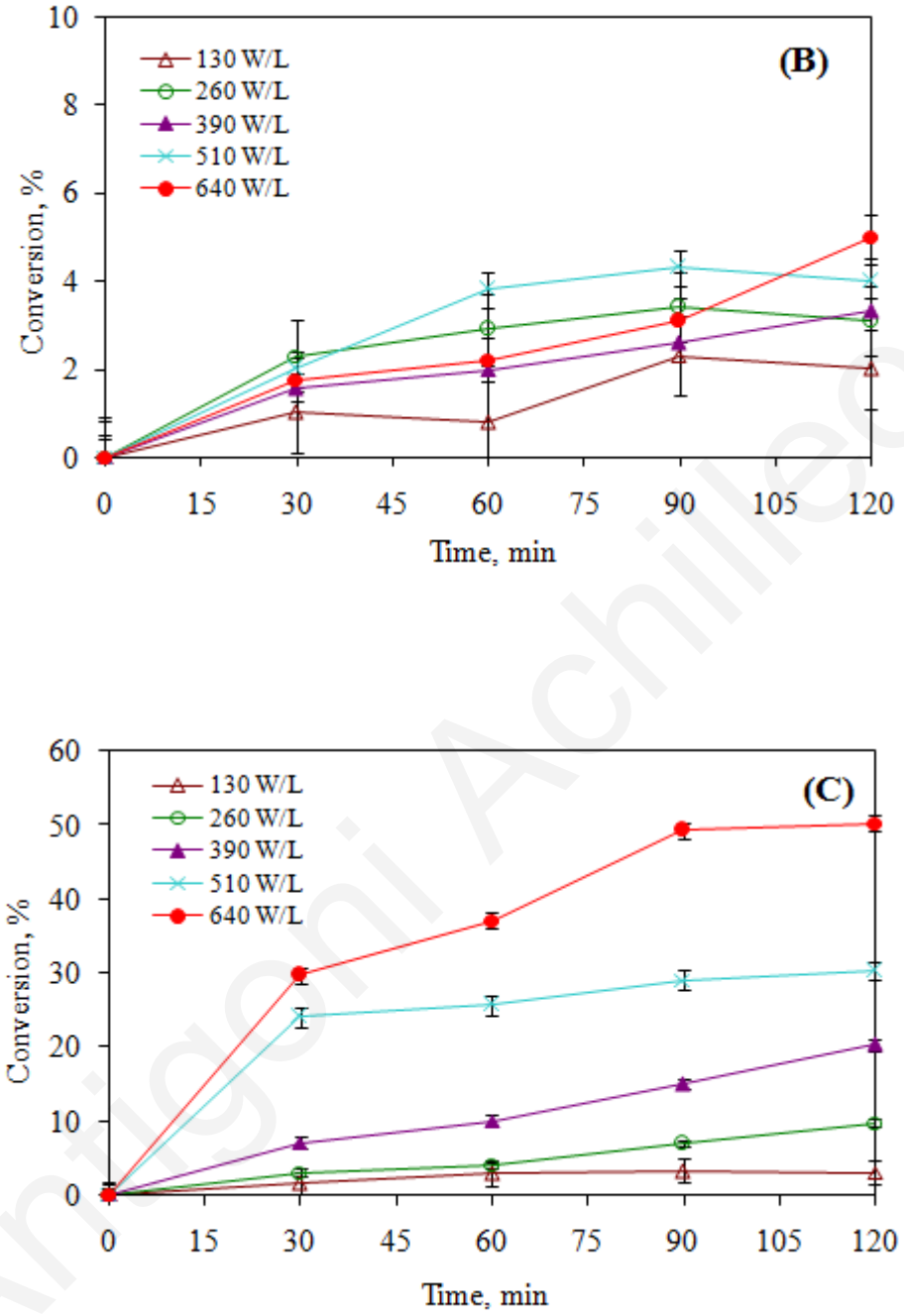

Figure 3.25: Effect of ultrasound power density on conversion at 10 mg/L (A) DCF, (B) IBP and (C) CBZ

As seen, after 120 min, the pharmaceuticals conversion was ~21, ~5 and ~50% for 10 mg/L DCF, IBP and CBZ, in terms of absorbance respectively. DOC removal was ~10.5, ~2 and ~21.3% for 10 mg/L DCF, IBP and CBZ (Figure 3.27).

As clearly seen, the photocatalytic degradation of DCF, IBP and CBZ occurs appreciably faster than sonolytic degradation under similar experimental conditions. For instance, photocatalytic removal occurs after 120 min of reaction at 500 mg/L catalyst loading for 10 mg/L DCF, IBP and 100 mg/L catalyst loading for 10 mg/L CBZ under air, was ~76%, 65~% and ~74% respectively, while sonolysis fails to achieve a significant conversion.

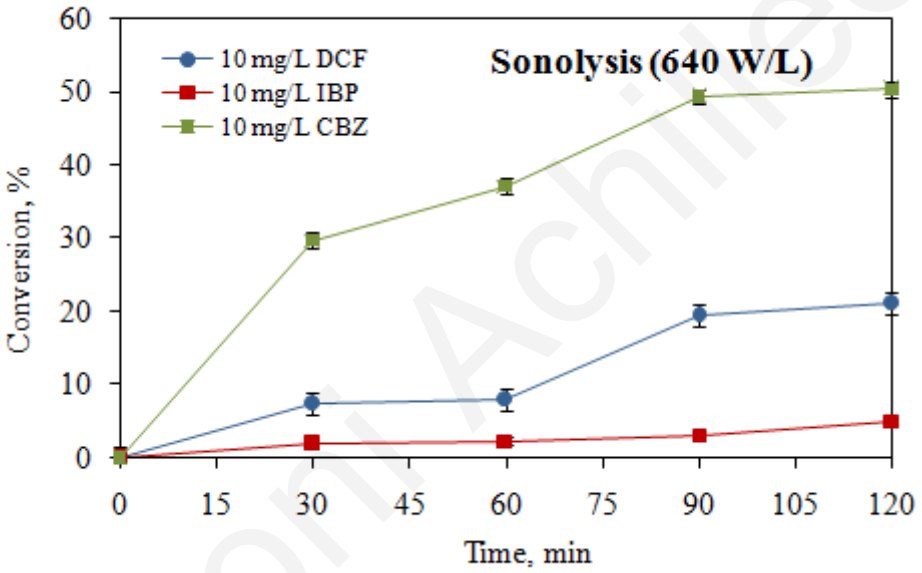

Figure 3.26: Sonolysis: Conversion–time profiles during sonolysis; C_0 = 10 mg/L; ultrasound power, 640 W/L; gas bubbled, air

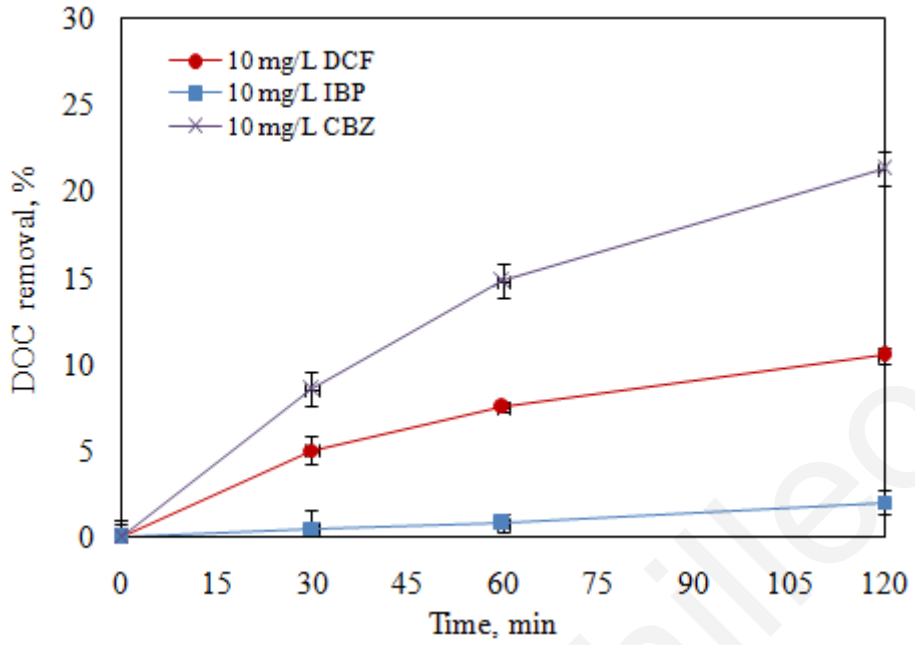

Figure 3.27: DOC removal during sonolysis; 10 mg/L DCF, IBP and CBZ; ultrasound power, 640 W/L; gas bubbled, air

Madhavan et al. (2010) studied the sonolytic degradation of IBP for the initial concentrations 0.02, 0.05, 0.07, 0.09 and 0.09 mM at 213 KHz and 55 mW/ml power and they pointed out that the degradation rate increases with an increase of initial concentration. The degradation rates obtained for the actual US powers 16, 35, 55 mW/ml were 1.04, 11.6, and 29.8 x 10^{-7} M/min respectively. It is known that the number of active cavitation bubbles increases with an increase in the acoustic power leading to an increase in the amount HO· generated which might be resposible for the observed enhacement in the degradation rates (Madhavan et al., 2010). Mendez-Arriaga et al. (2008) suggested that pyrolytic degradation of IBP is not possible due to its hydrophobic and low volatility character at pH less than its pka (4.9). Hence the degradation of IBP can occur by the hydroxyl radicals present in the bubble-liquid interface.

3.4.2 Addition of electron acceptor

In further experiments, the effect of adding H_2O_2, at various concentrations (0.07 – 1.4 mM) on DCF, IBP and CBZ conversion was studied and the results are shown in Figure 3.28 A, B and C. In general H_2O_2 is expected to promote degradation as it was mentioned before. As seen in Figure 3.28A for 10 mg/L DCF after 120 min, conversion was ~21, ~22, ~21.5 and ~28% for 0, 0.07, 0.14, 1.4 mM H_2O_2 in terms of UV absorbance. DOC removal was 12% in the presence of 1.4 mM H_2O_2 (Figure 3.29). In Figure 3.28B for 10 mg/L IBP after 120 min conversion was ~5, ~6, ~8 and ~10.5% for 0, 0.07, 0.14, 1.4 mM H_2O_2 in terms of UV absorbance. DOC removal was 5% in the presence of 1.4 mM H_2O_2 (Figure 3.29). For CBZ 10 mg/L (Figure 3.28 C) after 120 min conversion was 50, 51, 51 and 56% for 0, 0.07, 0.14, 1.4 mM H_2O_2 in terms of UV absorbance. DOC removal was 25% in the presence of 1.4 mM H_2O_2 (Figure 3.29).

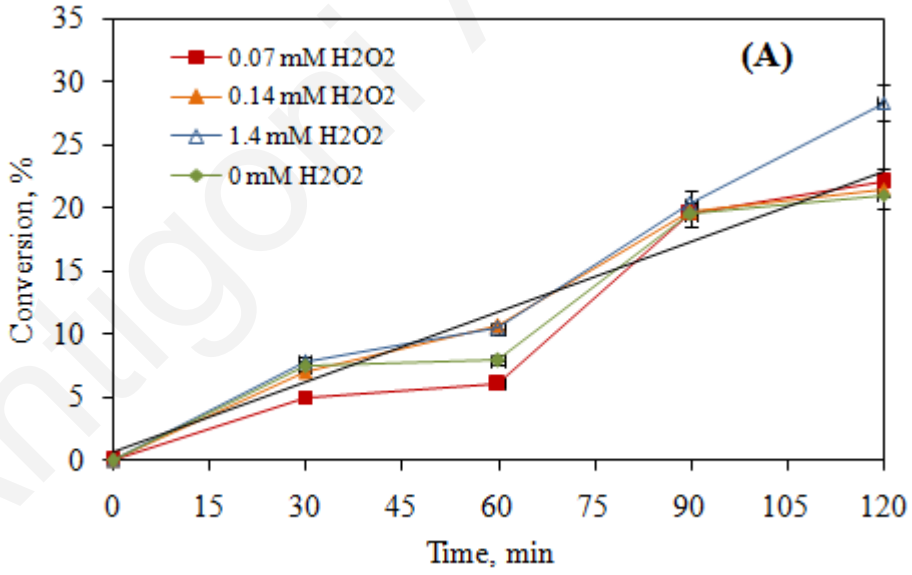

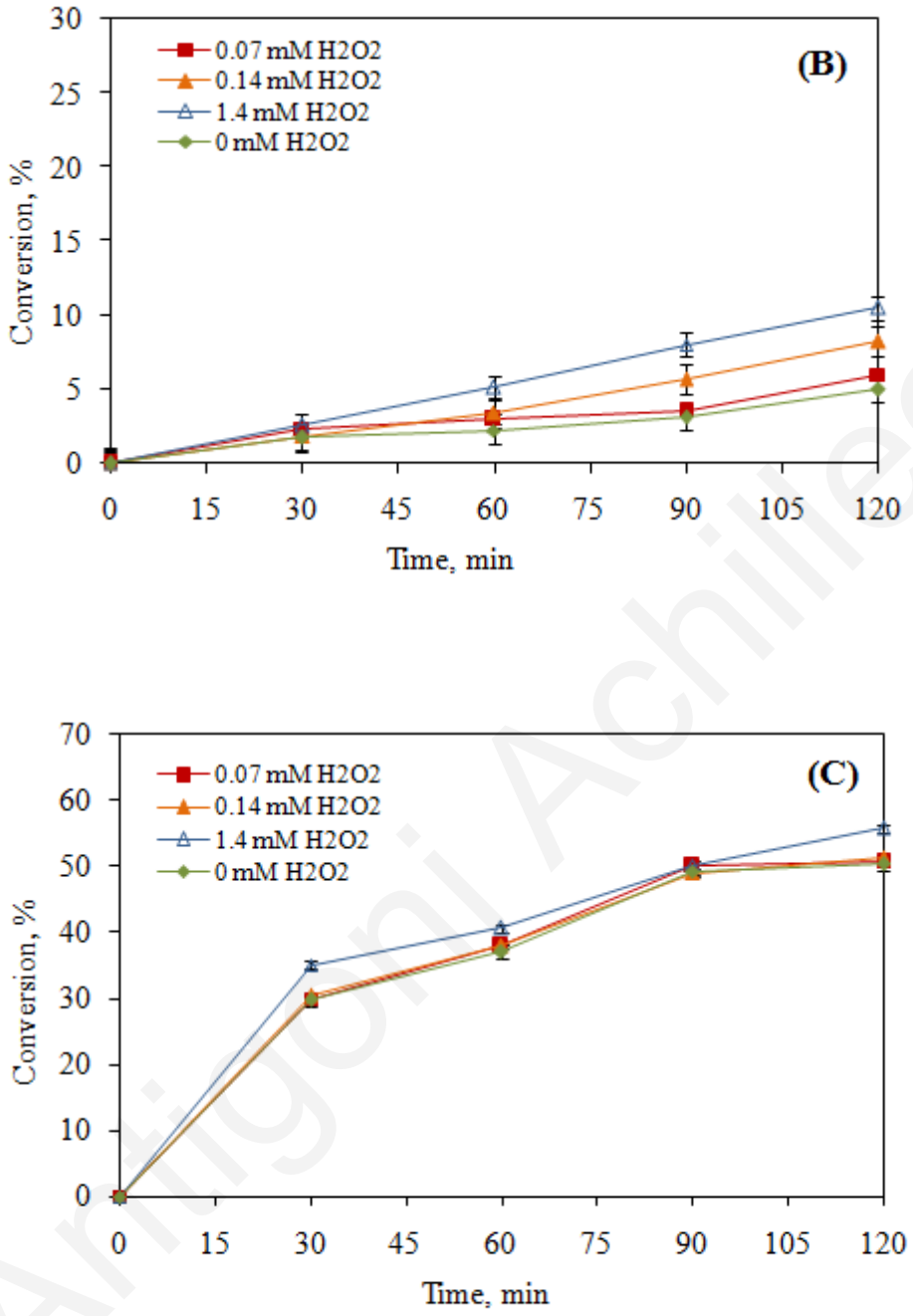

Figure 3.28: Effect of electron acceptor: Conversion–time profiles during sonolysis; C_0 = 10 mg/L (A) DCF, (B) IBP and (C) CBZ; ultrasound power, 640 W/L; gas bubbled, air

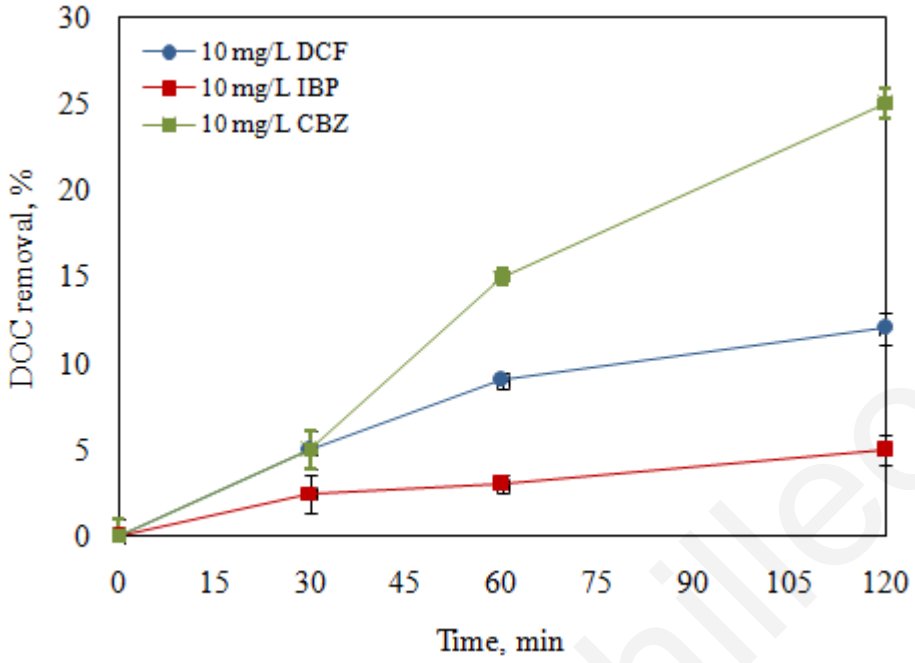

Figure 3.29: Effect of electron acceptor: DOC removal (%); 10 mg/L DCF, IBP and CBZ; ultrasound power, 640 W/L; 1.4 mM H_2O_2, gas bubbled, air

To verify that these conversions are due to combined action of ultrasound and peroxide rather than bleaching, a silent experiment was conducted showing that H_2O_2 alone does not practically contribute to degradation.

3.4.3 Effect of initial concentration of the pharmaceuticals

Figure 3.30 A, B and C shows the effect of initial DCF, IBP and CBZ concentration on conversion at 500 mg/L catalyst loading for DCF and IBP and 100 mg/L for CBZ. In Figure 3.30 A conversion decreases with increasing initial concentration i.e. at 120 min it becomes 35, 21 and 15% at 5, 10 and 20 mg/L DCF initial concentration respectively in terms of absorbance. DOC removal was 13, 10.5 and 8% at 5, 10 and 20 mg/L DCF. In Figure 3.30 B at 120 min it becomes 15, 5, 4% at 5, 10 and 20 mg/L IBP in terms of absorbance and as seen in Figure 3.30C it becomes 66, 50% at 5 and 10 mg/L CBZ initial concentration in terms of absorbance. DOC removal was 5 and 2, 1% at 5, 10 and 20 mg/L IBP. For CBZ DOC removal was 25, 21.3% at 5 and 10 mg/L after 120 min (Figure 3.31).

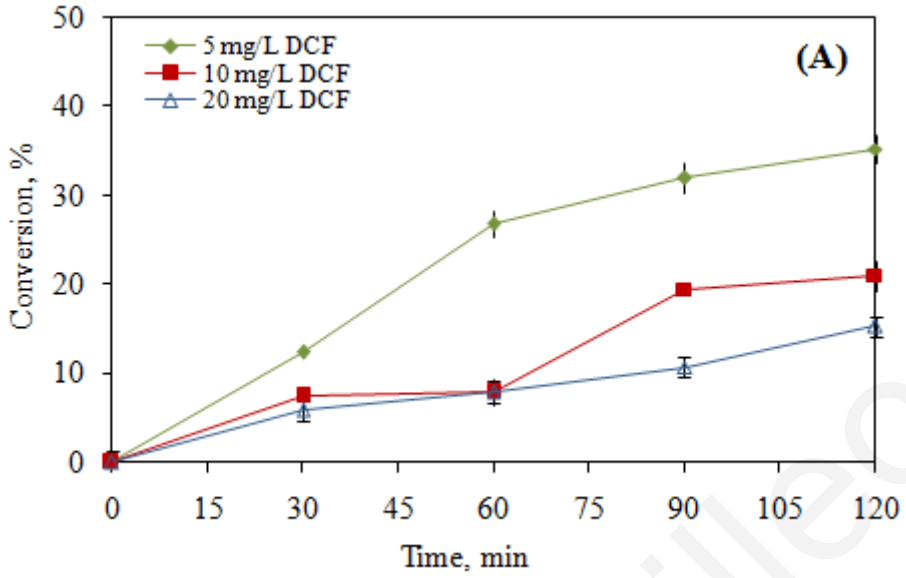

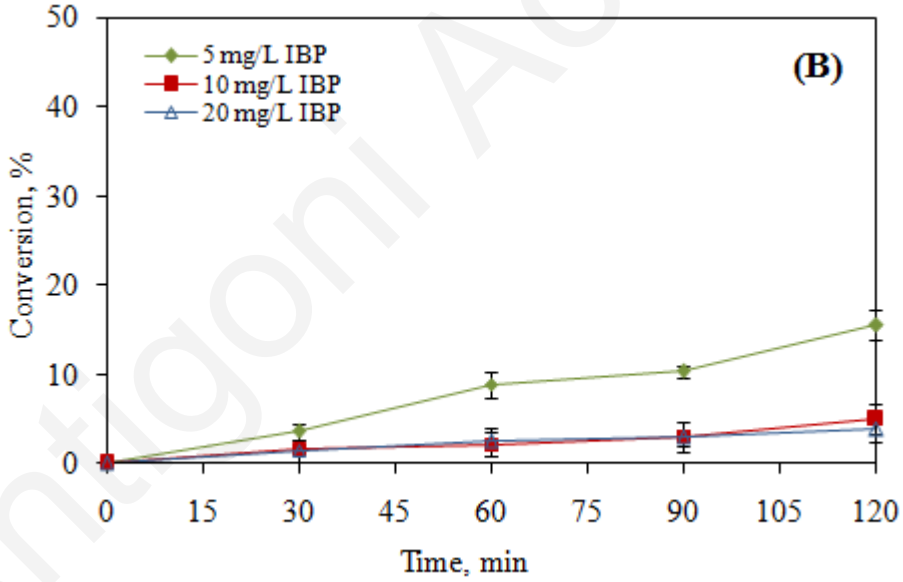

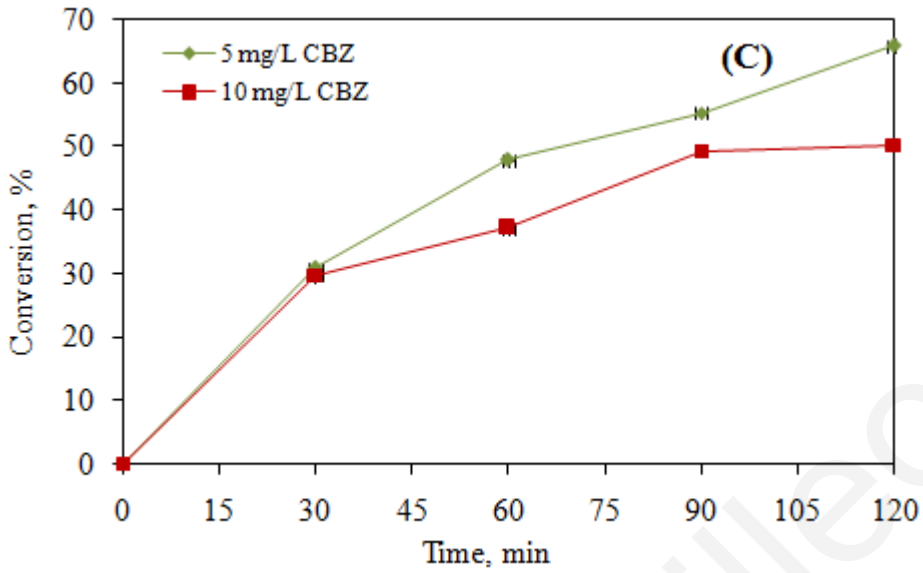

Figure 3.30: Effect of initial concentration (A) 5-20 mg/L DCF, (B) 5-20 mg/L IBP, (C) 5-10 mg/L CBZ, Conversion–time profiles during sonolysis; ultrasound power, 640 W/L; gas bubbled air

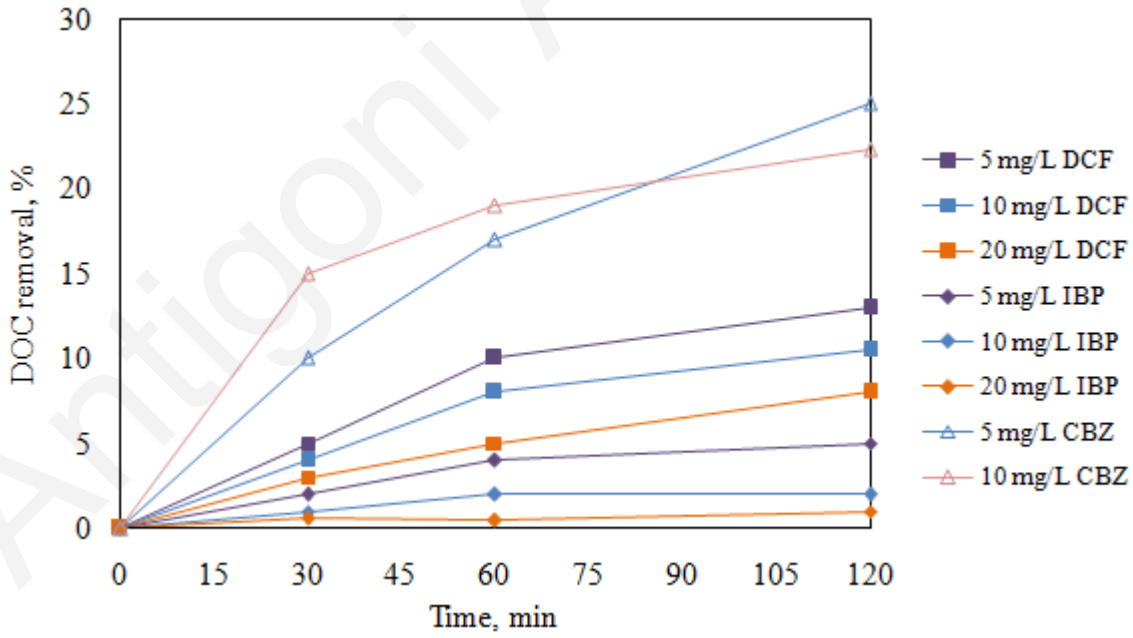

Figure 3.31: Effect of initial concentration of pharmaceutical compounds, DOC removal (%) during sonolysis; ultrasound power, 640 W/L; gas bubbled air

3.4.4 Effect of gas sparging

The presence of dissolved gases in the reaction mixture generally enhances sonochemical activity as gases act as nucleation sites for cavitation. Reactivity decreases in the order: Ar>O_2 air>He>N_2 no gas. There are three of gases that can affect soochemical activity, namely: (i) the polytropic ratio (i.e. specific heat ratio) since the maximum temperatures and pressures achieved upon bubble collapse increase with increasing ratio. In this respect, monoatomic gases are expected to be more effective than polyatomic gases since the former have greater polytropic ratios than the latter, (ii) gas thermal conductivity. Although bubble collapse is modeled as adiabatic, there is always a small amount of heat dissipated upon collapse, therefore gases with low thermal conductivities should reduce heat dissipation, thus favoring increased collapsed temperatures and consequently increasing sonochemical activity, (iii) gas solubility. As solubility increases more nucleation sites become available, thus facilitating cavitation.

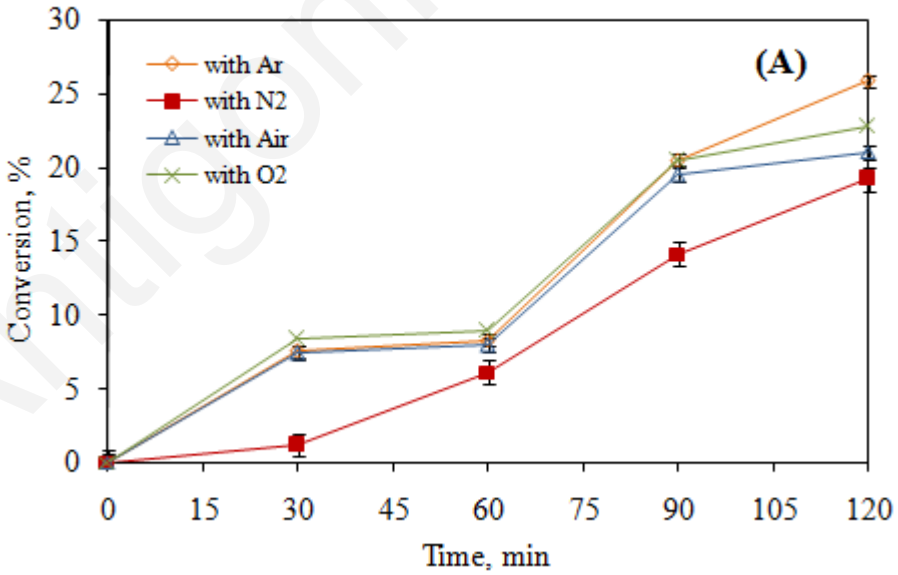

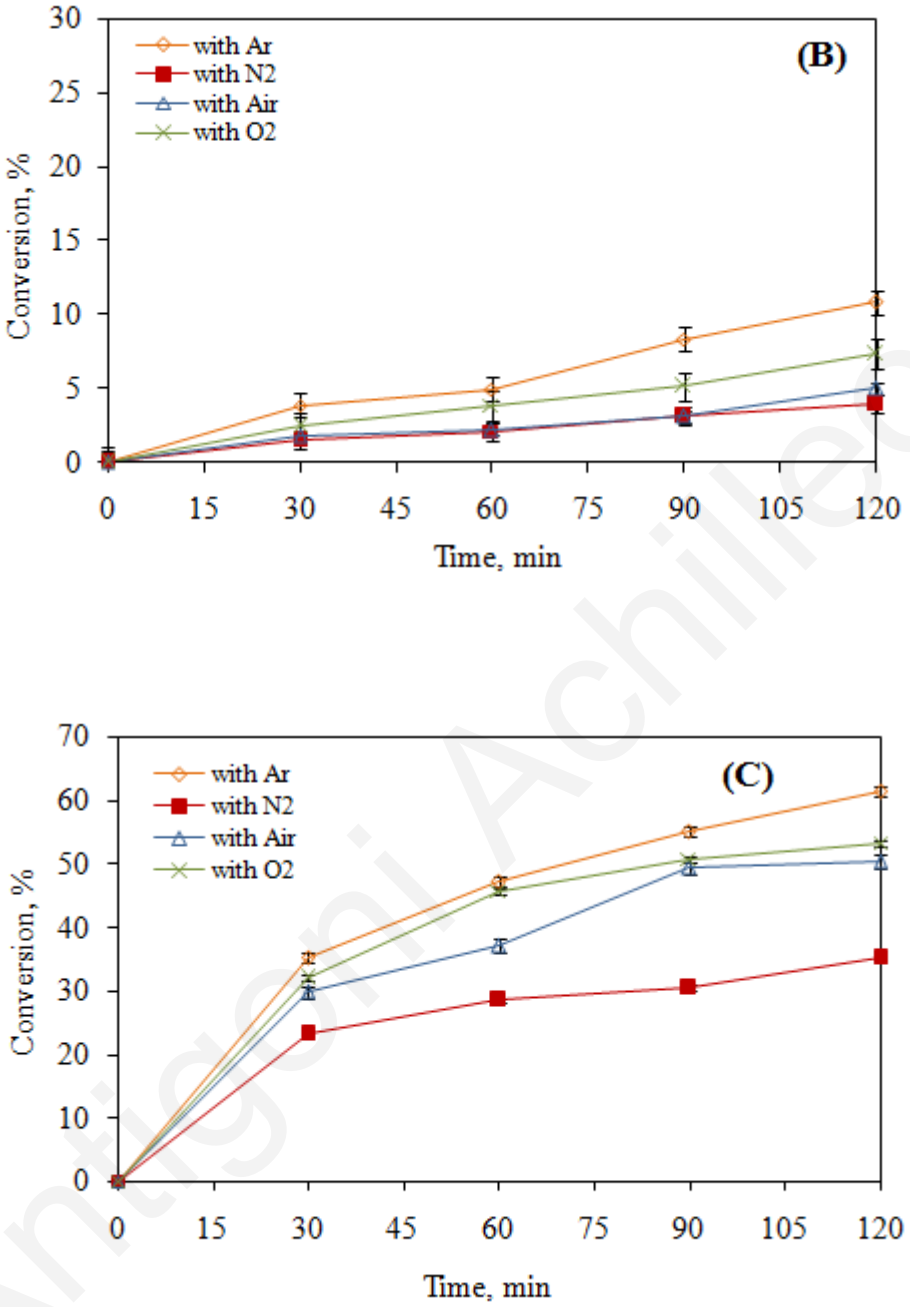

Figure 3.32: Effect of gas sparge, Conversion–time profiles during sonolysis; 10 mg/L (A) DCF, (B) IBP, (C) CBZ; ultrasound power 640 W/L; gas bubbled

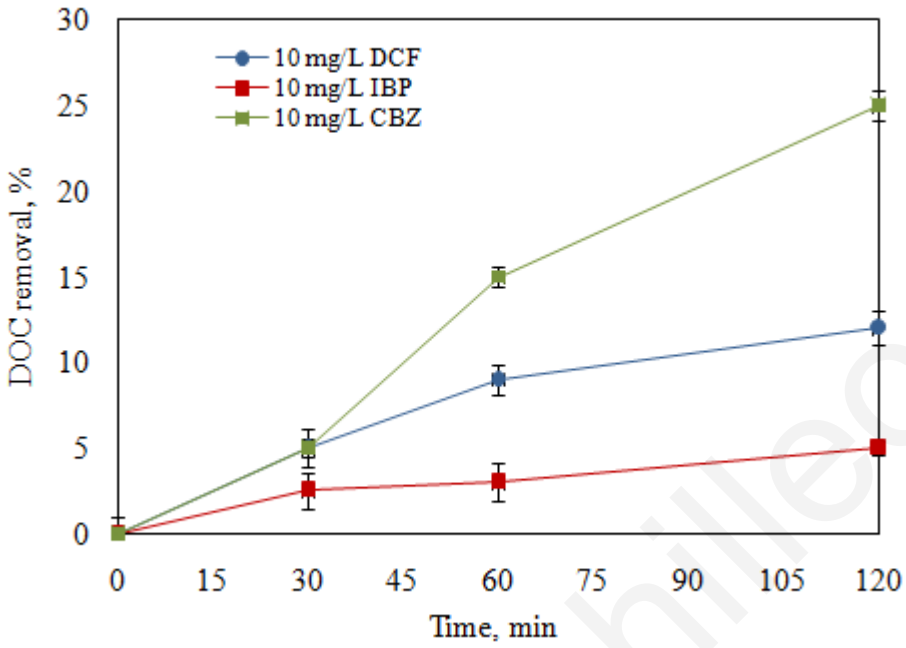

Figure 3.33: Effect of argon sparge, DOC removal (%) during sonolysis; 10 mg/L DCF, IBP and CBZ; ultrasound power 640 W/L

In Figures 3.32 A, B and C argon is substancially effective leading to 26, 11 and 61% conversion after 120 min for 10 mg/L DCF, IBP and CBZ and this is due to the fact that it has the greater polytropic ratio (1.67) and solubility in water (5.6 ml in 100 ml H_2O) as well as the lower thermal conductivity (0.18 mW/cm/K at 27˚C) than any other gas tested (Thompson and Doraiswamy, 1999; Adewuyi et al., 2005). DOC removal was 12, 5 and 25% after 120 min with argon sparging (Figure 3.33).

Table 3.11: Properties of sparging gases. *Adapted from Lide (2006). **Calculated from the respective values for nitrogen and oxygen

Gas	Polytropic ratio	Solubility in water at 25°C, 1 atm (mol fraction)	Thermal conductivity at 27°C (mW/(m.K))
*Argon	1.67	$2.75\ 10^{-5}$	17.9
*Oxygen	1.4	$2.5\ 10^{-5}$	26.3
*Nitrogen	1.4	$1.3\ 10^{-5}$	25.8
**Air	1.4	$1.45\ 10^{-5}$	25.9

3.4.5 Effect of water matrix

All runs described so far were conducted in ultrapure water (DW). To evaluate the effect of water matrix on mineralization, 10 mg/L DCF, IBP and CBZ were spiked in single solutions in WWTPEf and GW pumping from a well, while keeping their concentration constant at 10 mg/L added varying loadings of Degussa P25 in the range 500-3000 mg/L. In Figure 3.34 A and B, DOC removal was 8, 2, and 10% for 10 mg/L DCF, IBP and CBZ spiked in WWTPEf with 3000 mg/L catalyst loading. For GW spiked with the above concentrations of drugs, DOC removal was 11, 3.5 and 15% with 3000 mg/L catalyst loading.

Experiments were also carried out in the presence of 0.07-3 mM H_2O_2. The addition of H_2O_2 did not practically improve the reduction of DOC (i.e. only about 3% greater than without peroxide), thus indicating the stability of the wastewater matrix.

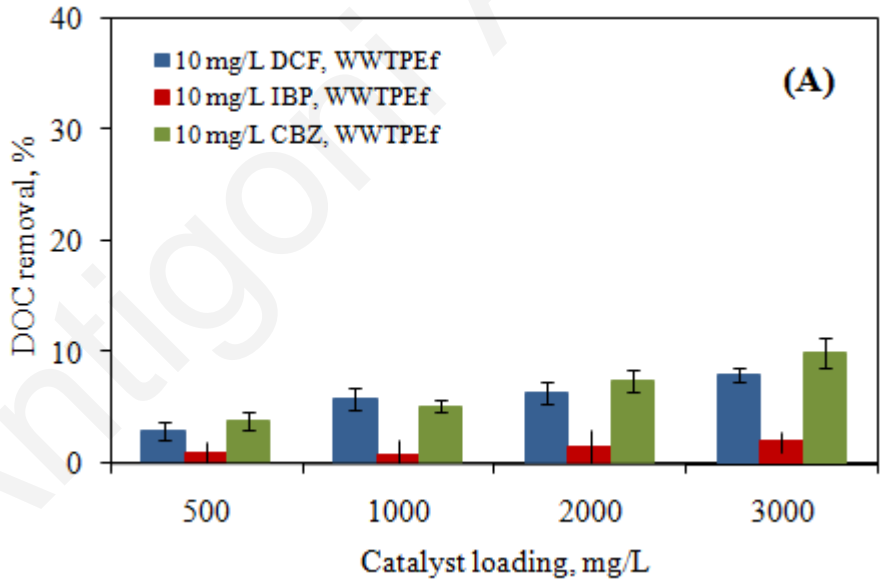

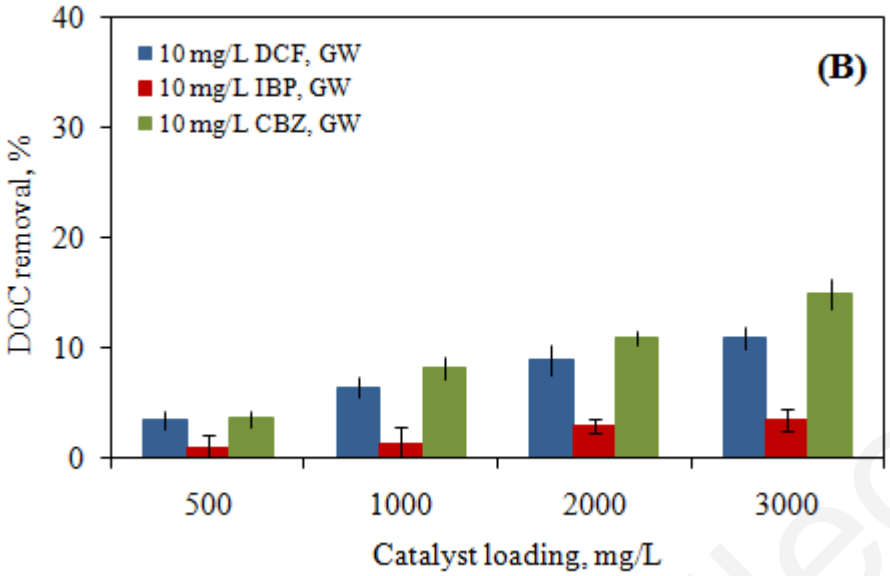

Figure 3.34: DOC removal - Effect of water matrix, Sonolysis of spiked samples (A) WWTPEf, 640 W/L, (B) GW, 640 W/L

3.5 Sonophotocatalytic (US + UV + TiO_2) conversion of DCF, IBP and CBZ

In further experiments, pharmaceuticals degradation by means of simultaneous combined ultrasound and ultraviolet irradiation in the presence of TiO_2 was studied. As mentioned before, the ultrasound power is a major factor affecting sonochemical reactions. As p

ower increases, the number of collapsing bubbles also increases, thus leading to enhanced degradation levels.

Although photocatalysis and sonolysis have been extensively employed individually for the degradation of several organic species in water, their combined use (i.e. sonophotocatalysis) has received appreciably less attention. Process integration may be favorable in eliminating the disadvantages associated with each individual process, thus increasing degradation rates. For instance, in heterogeneous catalytic systems, the use of ultrasound creates conditions of increased turbulence in the liquid, thus decreasing mass transfer limitations and increasing the surface area available due to catalyst fragmentation and de-agglomeration.

Some of the reasons for the enhancement of decomposition efficiency are reported as follows (Tokumoto et al., 2008):
(1) Catalyst particles are physically dispersed by ultrasonic treatment
(2) Enhancement of mass transfer between the bulk liquid and the surface of the catalyst and renewal of the fluid film near the surface of the catalyst
(3) Formation of HO· radicals from hydrogen peroxide, which is produced by the reaction with photocatalyst.

For that reason at first, the sonophotocatalytic experiments were carried out with ultrasound density 640 W/L at 500 mg/L catalyst loading for DCF and IBP and 100 mg/L catalyst loading for CBZ. As clearly seen (Figures 3.35) after 120 min, the conversion of 10 mg/L DCF, IBP and CBZ was ~21, ~5 and ~50% in terms of absorbance for 640 W/L respectively. In general, the conversion for these

pharmaceuticals may be due to the fact that high temperature, pyrolytic reactions inside or around the cavitation bubble does not occur to an appreciable extent since DCF, IBP and CBZ soluble in water; in this light, hydroxyl radical-induced reactions in the liquid bulk are likely to be the main degradation mechanism as follows:

$$H_2O + \text{ultrasound} \rightarrow H^{\cdot} + HO^{\cdot} \quad (3.5)$$

$$DCF, IBP, CBZ + HO^{\cdot} \rightarrow \text{intermedia tes} + HO^{\cdot} \rightarrow \text{end} - \text{products} \quad (3.6)$$

Sonophotocatalytic DCF, IBP and CBZ removal occurs after 120 min of reaction at 500 mg/L catalyst loading for DCF and IBP and 100 mg/L for CBZ under air, was ~80.4, ~75 and ~78%, respectively. It was found that the destruction in the combined process was more significant than in the UV photocatalysis or sonolysis alone. Figure 3.36A, B and C shows the pharmaceuticals conversion by the combination of the processes. It was found that the destruction in the combined process was more significant than in the UV-A photocatalysis or sonolysis alone.

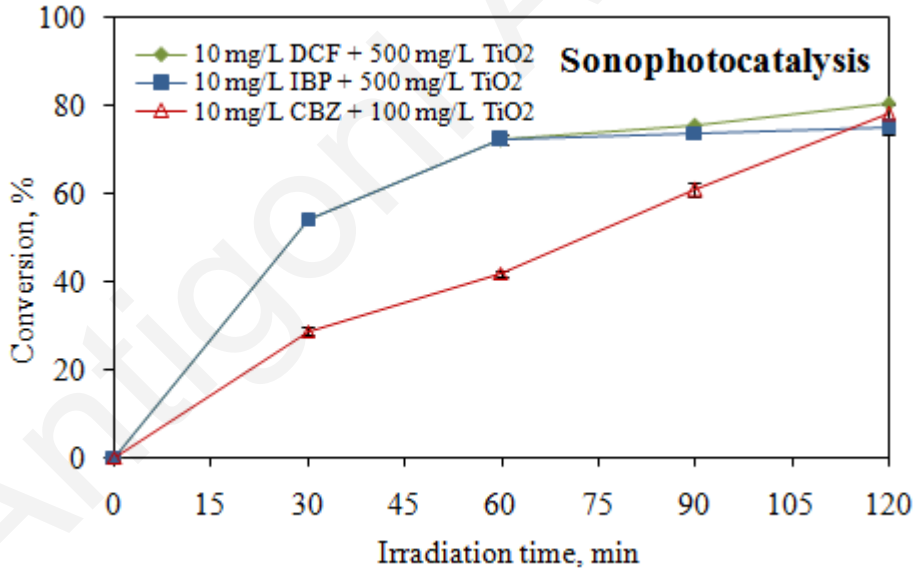

Figure 3.35: Pharmaceuticals (DCF, IBP and CBZ): Conversion–time profiles during sonophotocatalysis; C_0 = 10 mg/L; ultrasound power, 640 W/L; gas bubbled, air

Efficiency was found to follow the order: Sonolysis < sonocatalysis< photocatalysis < sonophotocatalysis. After 120 min, as seen in Figure 3.36 A, 21% of DCF was degraded using sonolysis alone, 76% was eliminated by photocatalysis, 21.3% was

eliminated by sonocatalysis and ~80% with sonophotochemical process. In Figure 3.35B, 10 mg/L IBP was degraded using sonolysis alone 5%, 21% was eliminated by sonocatalysis, 65% was eliminated by photocatalysis and 75% was eliminated by sonophotocatalysis. In Figure 3.36 C, 10 mg/L CBZ was degraded using sonolysis alone 50%, 52% was eliminated by sonocatalysis, 74% was eliminated by photocatalysis and 78% was eliminated by sonophotocatalysis.

The beneficial effect of coupling photocatalysis with sonolysis may be attributed to several reasons, namely (Mrowetz et al., 2003; Gogate and Pandit, 2004; Shimizu et al., 2007): (i) increased production of hydroxyl radicals in the reaction (ii) enhanced mass transfer of organics between the liquid phase and the catalyst surface, (iii) catalyst excitation by ultrasound-induced luminescence and (iv) increased catalytic activity due to ultrasound de-aggregating catalyst particles, thus increasing surface area (Berberidou et al., 2007).

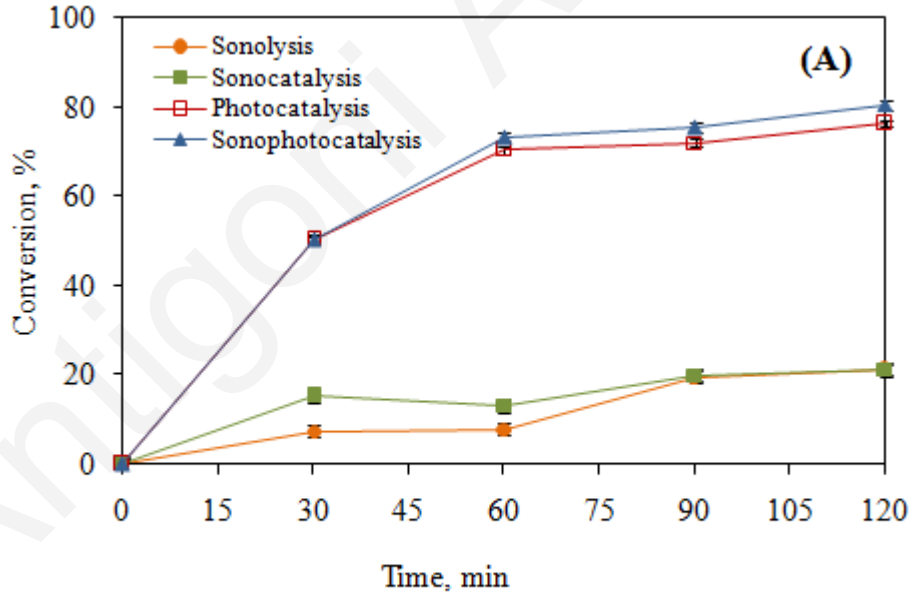

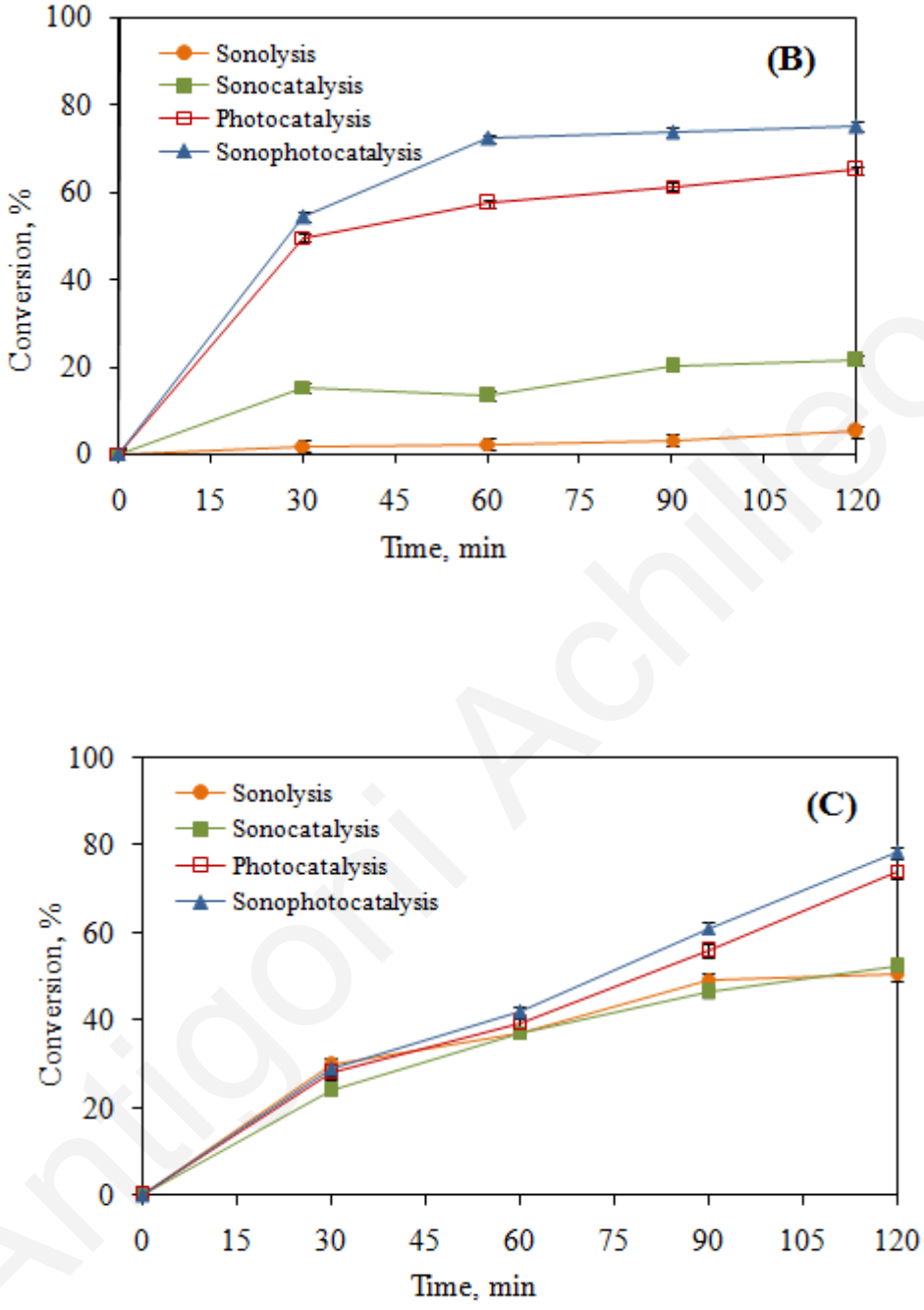

Figure 3.36: Conversion–time profiles during UV-A photocatalysis, sonolysis, sonocatalysis and sonophotocatalysis,; ultrasound power, 640 W/L; gas bubbled, air, (A) 10 mg/L DCF, 500 mg/L TiO_2, (B) 10 mg/L IBP, 500 mg/L TiO_2, (C) 10 mg/L CBZ, 100 mg/L TiO_2

In Table 3.12 the concentration profile during photocatalysis (uva irradiation) and sonophotocatalysis with uva irradiation of each pharmaceutical compound with concentration ~10 mg/L in the optimum catalyst loading determined with HPLC/ESI-QqLIT-MS is shown.

Table 3.12: Comparison of compounds; Concentration profile during photocatalysis and sonophotocatalysis

Pharmaceutical compound/ Process	**Irradiation time, min**				
	0	**15**	**30**	**60**	**120**
DCF					
PC	8.97	4.30	4.56	3.84	4.19
SPC	10.53	4.78	0.73	0.43	0.01
IBP					
PC	9.40	2.40	3.30	2.60	1.50
SPC	10.2	2.6	0.17	0.02	0.02
CBZ					
PC	9.99	8.31	6.67	2.89	0.62
SPC	9.53	4.52	2.58	1.47	0.67

From the concentration profile we can see that the degradation of DCF using uva irradiation was 52.1 and 54.6% with sonophotocatalysis in the first 15 min. After 120 min the degradation of DCF was similar with the degradation in 15 min (53.3%) with uva irradiation. In sonophotocatalysis a significant enhacement in the degradation of DCF (99.9%) was observed in 120 min

The degradation of IBP was 74.1 and 74.5% in the first 15 min using photocatalysis and sonophotocatalysis respectively. In 120 min of experiment the degradation of IBP was 84.3 and 99.8% using photocatalysis and sonophotocatalysis respectively.

CBZ degradation was 16.8 and 93.8% in 15 and 120 min of photocatalysis. In sonophotocatalysis experiment the degradation was 52.6 and 93% in 15 and 120 min.

Similar to this study Madhavan et al. (2010) in their study pointed that when both US and UV were combined (sonophotocatalysis) a significant enhacement in the degradation (85% in 15 min) of IBP was observed. About 24% increment in the degradation under the same processing time suggests that the hydroxyl radicals

formed by both the advanced oxidation processes, photocatalysis and sonolysis are involved in the sonophotocatalytic degradation of IBP.

Below in Table 3.13 a comparison of conversion (%), DOC removal (%) and degradation (%) between heterogeneous photocatalysis under UV-A irradiation and sonophotocatalysis is shown.

Table 3.13: Comparison of conversion (%), DOC removal (%) and degradation (%) of pharmaceutical substances between heterogeneous photocatalysis under UV-A irradiation and sonophotocatalysis at optimum conditions

Pharmaceutical compounds	Conversion, %	DOC removal, %	Degradation, %
UVA irradiation			
DCF **(**10 mg/L, 500 mg/L TiO_2)	80	58	53.3
IBP (10 mg/L, 500 mg/L TiO_2)	65	46	84.3
CBZ (10 mg/L, 100 mg/L TiO_2)	75	40	93.84
Sonophotocatalysis			
DCF **(**10 mg/L, 500 mg/L TiO_2)	80.4	63	99.9
IBP (10 mg/L, 500 mg/L TiO_2)	75	55	99.8
CBZ (10 mg/L, 100 mg/L TiO_2)	78	40	93

As shown, with the combination of heterogeneous photocatalyis and sonolysis a significant enhancement in the conversion, DOC removal and degradation was observed except for CBZ for which removal values remained almost the same.
In Table 3.14 a comparison of each pharmaceutical compound per process is shown.

Table 3.14: Comparison of each pharmaceutical compound per process

Pharmaceutical compounds	Conversion, %	DOC removal, %	Degradation, %
DCF (10 mg/L, 500 mg/L TiO_2)			
UVA irradiation	80	58	53.3
Solar irradiation	90	55	53
Sonolysis*	21	10.5	Was not determined
Sonocatalysis	21.3	12	Was not determined
Sonophotocatalysis	80.4	63	99.9
IBP (10 mg/L, 500 mg/L TiO_2)			
UVA irradiation	65	46	84.3
Solar irradiation	59	40	95.8
Sonolysis*	5	2	Was not determined
Sonocatalysis	21	10	Was not determined
Sonophotocatalysis	75	55	99.8
CBZ (10 mg/L, 100 mg/L TiO_2)			
UVA irradiation	75	40	93.84
Solar irradiation	69	45	50

Sonolysis*	50	21.3	Was not determined
Sonocatalysis	52	25	Was not determined
Sonophotocatalysis	78	40	93

*only 10 mg/L of pharmaceutical compound

Table 3.14 shows that sonophotocatalysis is the best combination to achieve the highest DOC removal for IBP and DCF, the highest conversion for IBP and CBZ (Figure 3.37) and the highest degradation for DCF and IBP. The highest degradation of CBZ was achieved under UV-A irradiation and the highest conversion for DCF was achieved under solar irradiation (Figure 3.37).

In Figure 3.37, a comparison of the efficiency of each process applied and assessed for DCF, IBP and CBZ conversion is shown. Photocatalysis and sonophotocatalysis achieve faster and higher conversion than sonolysis and sonocatalysis for DCF and IBP. The results for CBZ showed again the same behaviour of the processes but clearly in less pronounced way since the trends and final removal percentages are more closed. This indicates that not all compounds behave the same way under the same oxidation processes.

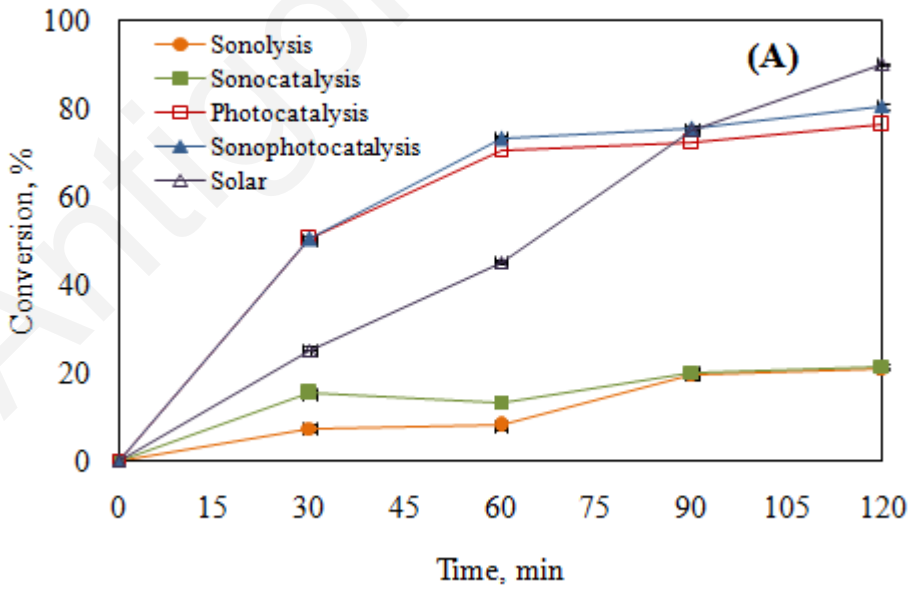

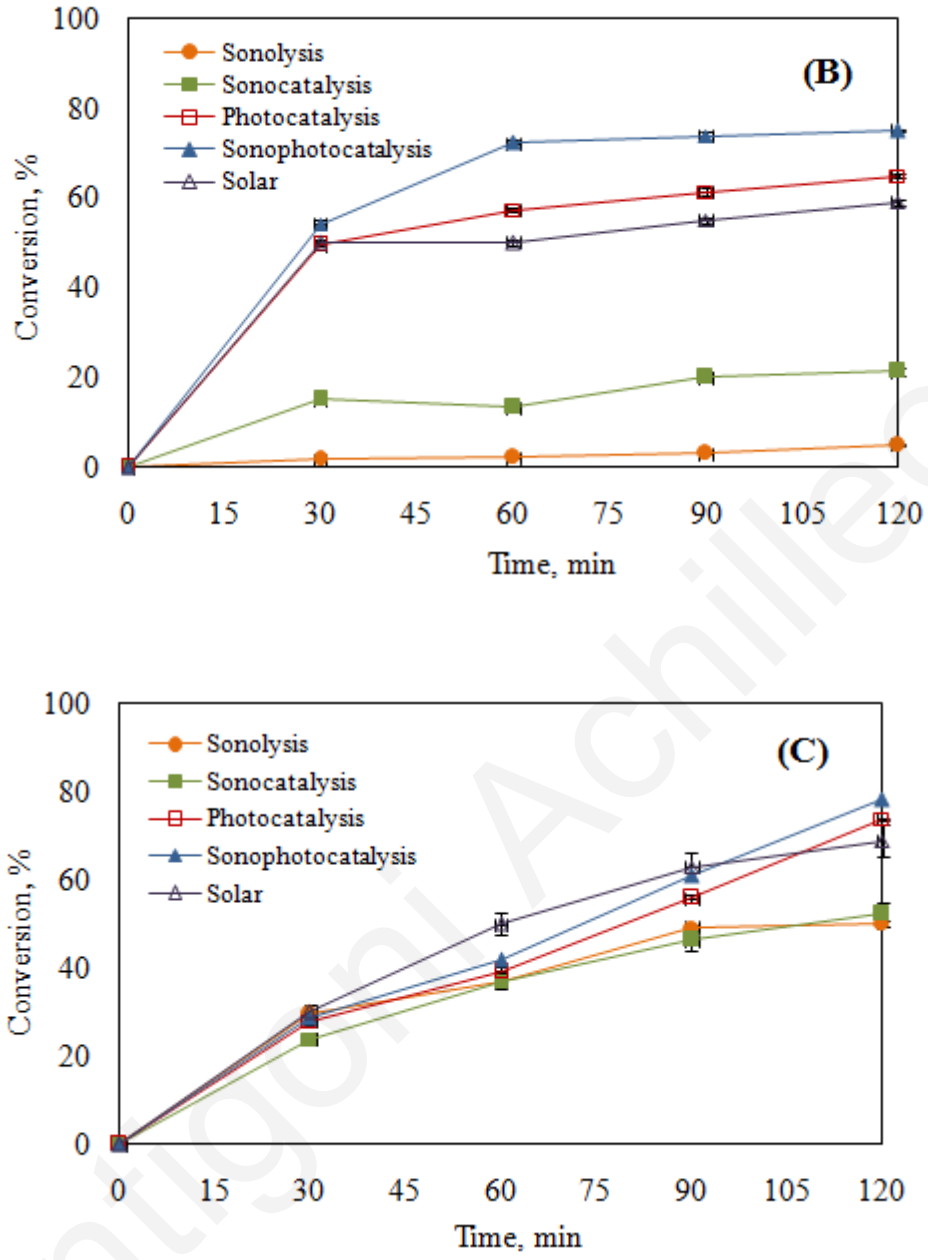

Figure 3.37: Comparison of each pharmaceutical compound per process (A) DCF, (B) IBP and (C) CBZ

3.6 Kinetics

The rate and efficiency of the photocatalytic reaction depend on a number of factors. One such important factor is adsorption of the substrate onto the surface on the catalyst (Dalrymple et al., 2007). This mechanism requires that the contaminant adsorbs on the catalyst surface for efficient oxidation. The adsorption-desorption process is characterized by the transfer of the reactants in the aqueous phase to the surface, adsorption of the reactants, reaction in the adsorbed phase, desorption of the products and removal of the products from the interface region

It is well documented in the literature (Thompson and Doraiswamy, 1999; Adewuyi, 2001; Hapeshi et al., 2010) that most photocatalytic degradation reactions can be modelled by a power law kinetic expression, i.e.

$$-\frac{dC}{dt} = k_{app}C^{n} \tag{3.7}$$

where k_{app} is an apparent rate constant, C is the substrate concentration and n is the order of reaction that typically takes values between 0 and 1.

Recent publications have shown that a pseudosteady state analysis may be applied. Plotting ln Co/C versus time represents a straight line, the slope of which upon linear regression equals the apparent first-order rate constant kapp, thus implying that the decomposition kinetics of DCF, IBP and CBZ perfectly fits first order kinetics (Figure 3.38A, B, C and D). Table 3.15 lists the values of *k*app and the linear regression coefficients for pseudo-first-order kinetics of DCF, IBP, and CBZ conversion. According to these values the appropriate first-order relationship appears to fit well.

Table 3.15: Kinetic parameters for the optimum loading TiO_2

Drug	**Optimum loading TiO_2 for each pharmaceutical**		
UV-A irradiation	**Kapp (1/min)**	**R^2**	**$t_{1/2}$ (min)**
DCF: 10 mg/L, TiO_2: 500 mg/L	0.0195	0.9543	36
IBP: 10 mg/L, TiO_2: 500 mg/L	0.0246	0.9511	28
CBZ: 10 mg/L, TiO_2: 100 mg/L	0.0175	0.9827	40
Solar irradiation	**Kapp (1/min)**	**R^2**	**$t_{1/2}$ (min)**
DCF: 10 mg/L, TiO_2: 500 mg/L	0.0154	0.9744	45
IBP: 10 mg/L, TiO_2 : 500 mg/L	0.0085	0.9775	82
CBZ: 10 mg/L, TiO_2 : 100 mg/L	0.006	0.9623	116
Sonolysis	**Kapp (1/min)**	**R^2**	**$t_{1/2}$ (min)**
DCF: 10 mg/L, ampl. 50%	0.002	0.891	346.50
IBP: 10 mg/L, ampl. 50%	0.001	0.974	693
CBZ: 10 mg/L, ampl. 50%	0.003	0.979	231
Sonophotocatalysis	**Kapp (1/min)**	**R^2**	**$t_{1/2}$ (min)**
DCF: 10 mg/L, TiO_2: 500 mg/L	0.04	0.9355	17.33
IBP: 10 mg/L, TiO_2 : 500 mg/L	0.0488	0.9866	14.20
CBZ: 10 mg/L, TiO_2 : 100 mg/L	0.046	0.977	15.07

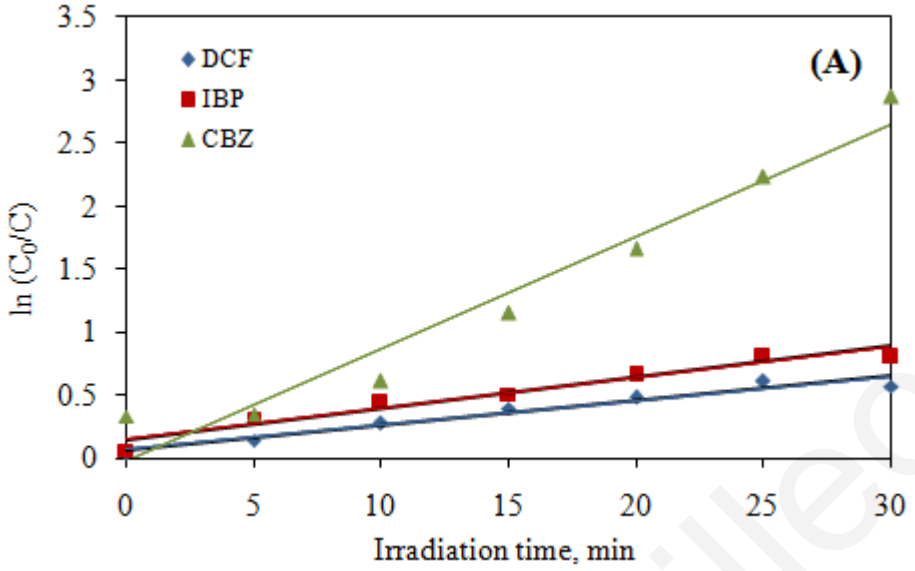

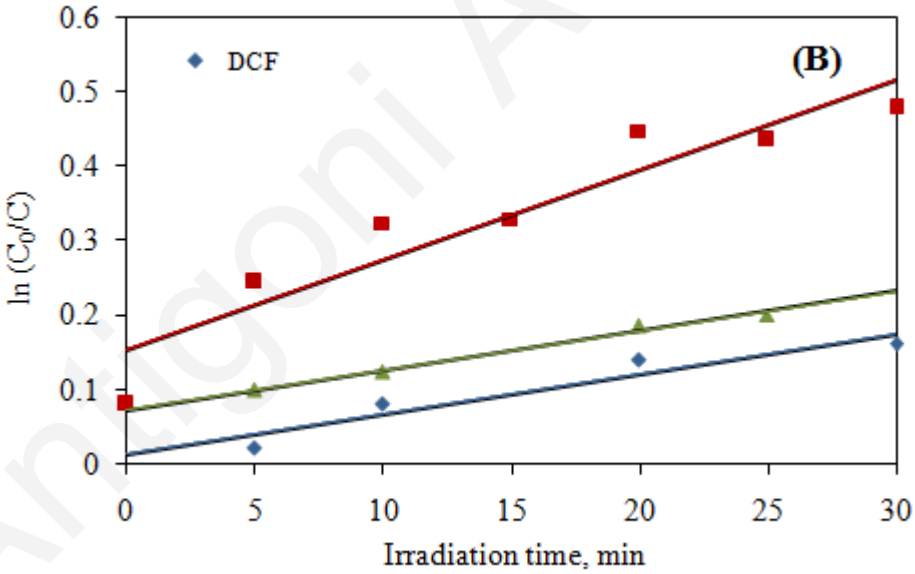

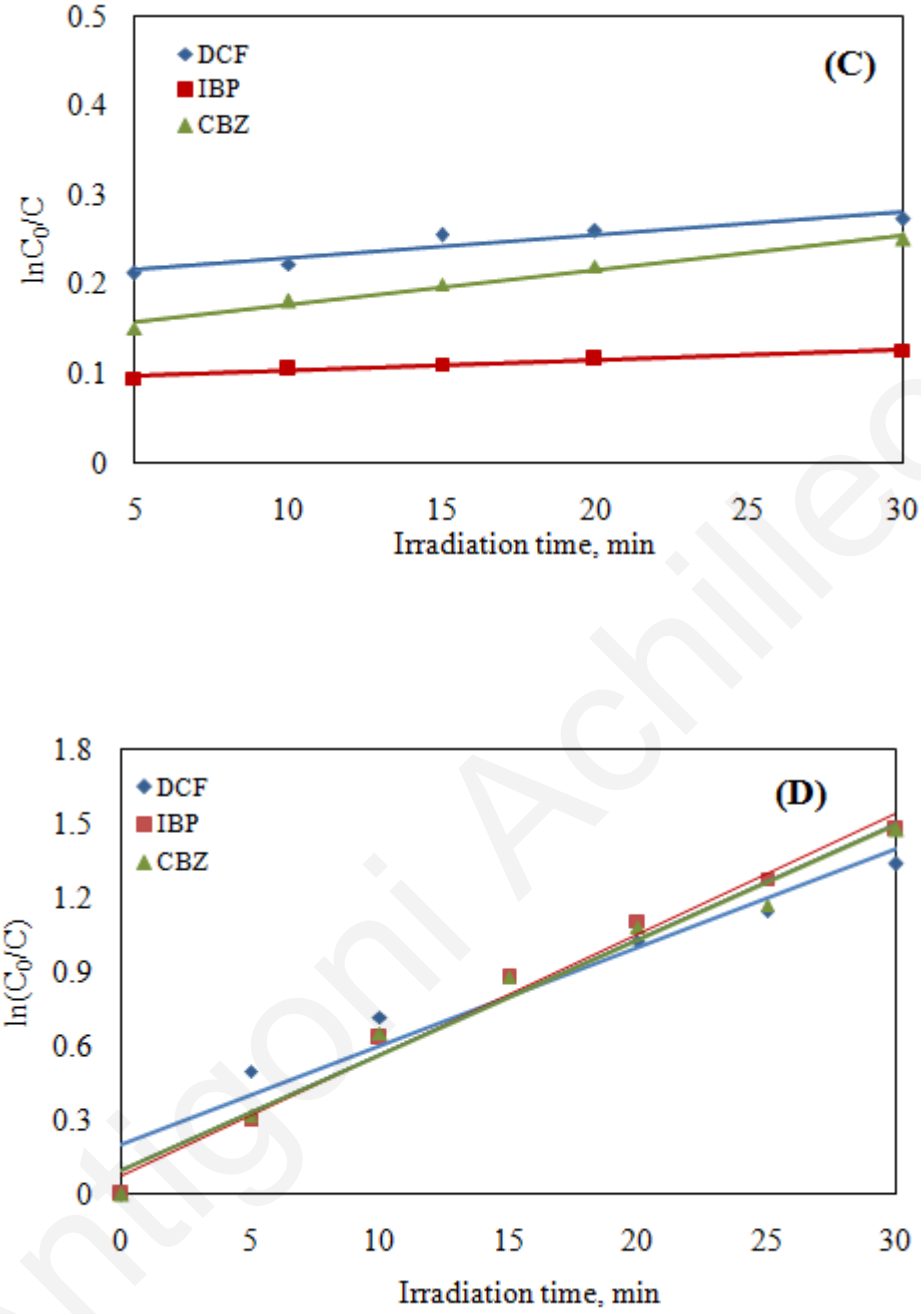

Figure 3.38: Kinetics for 10 mg/L DCF, IBP and CBZ under (A) UVA irradiation, (B) solar irradiation, (C) sonolysis and (D) sonophotocatalysis

3.7 Toxicity

DCF and IBP at 10 mg/L initial concentration with 500 mg/L Degussa P25 TiO_2 and CBZ at 10 mg/L initial concentration with 100 mg/L catalyst loading were treated with photocatalysis, sonolysis and sonophotocatalysis and toxicity was monitored as a function of treatment and exposure times, as seen in Figures 3.38-3.40. The dissolved oxygen and pH was measured at the end of each test and in the control sample. The dissolved oxygen concentration in controls was in compliance with the validity criterion and a minimum 6 mg/L of dissolved oxygen was supplied by air filtered through activated carbon. The pH was adjusted to 7±0.5.

Blank samples containing titania only without DCF, IBP and CBZ were tested to exclude the possibility that toxicity is owing to catalyst particles.

In heterogeneous photocatalysis under UV-A irradiation (Figure 3.39 A) the unoxidized DCF was slightly toxic. In 24 and 48 h toxicity increased in 15 min. This can be explained due to the TPs appearance in the first 15 min. After 15 min toxicity decreased until 60 min and then increased in 120 min. This can be explained because TPs remained in the solution during the whole experiment. Some of them appeared and disappeared in different irradiation times.

In heterogeneous photocatalysis under solar irradiation figure 3.39 B the unoxidized DCF was not toxic in 24 h and 40% toxic in 48 h. After 15 min toxicity increased, decreased in 30 min, increased in 60 min and slightly decreased in 120 min in 24 and 48 h. In solar irradiation experiment TPs appeared in the first 15 min and remained until 120 min in the solution with different relative intensities.

Sonolysis experiments (Figures 3.39 C, 3.40 C and 3.41 C) were not investigated for TPs. Experiments for the investigation of TPs were conducted only for heterogeneous photocatalysis under UV-A and solar irradiation and sonophotocatalysis. The scope was to investigate TPs formation only to the treatments with the highest efficiency. Allthough TPs were not investigated the difference between conversion and DOC removal indicates the formation of transformation products. Toxicity in the solution might be due to the TPs and the presence of the parent compound.

In sonophotocatalysis experiment (Figure 3.39 D) the unoxidized DCF was slightly toxic in 24 and 48 h. Toxicity increased in the first 15 min decreased until 60 min and increased again in 120 min in 24 and 48 h. In the first 15 min TPs are formed and their intensities were higher compared to other irradiation times. The intensities of TPs increased and decreased during the experiment. Some TPs appeared after 30 min and some disappeared after 30 or 60 min.

This profile is typical for model solutions of organic pollutants since early degradation by-products are responsible for individual and synergistic toxic effects that are greater than that of the initial compound (Mantzavinos et al., 2004); at longer treatment times, toxicity decreases to acceptable levels as toxic intermediates are degraded further. Interestingly, the sample taken after 120 min of reaction is highly toxic, thus implying that some of the deep oxidation end-products accumulating in the reaction mixture introduce severe inhibition. A similar trend was observed by Rizzo et al. (2009) who investigated the toxicity of photocatalytically treated DCF (20 mg/L of substrate in the presence of 1600 mg/L TiO_2) to *Daphnia magna* and *P. subcapitata*.

In heterogeneous photocatalysis under UV-A irradiation (Figure 3.40 A) the unoxidized IBP was slightly toxic, increased in 15 min, decreased in 30 min, increased slightly in 60 and 120 min after 24 and 48 h. In the first 15 min seven TPs are formed and remained in the solution in different intensities for 120 min.

In heterogeneous photocatalysis under solar irradiation (Figure 3.40 B) the unoxidized IBP was slightly toxic, decreased in 15 min, non toxic in 30 min, increased slightly in 60 and 120 min after 24 h. In 48 h the solution was toxic in the first 30 min decreased in 60 min and increased again in 120 min. In the first 15 min seven TPs are formed and remained in the solution in different intensities for 120 min.

In sonophotocatalysis experiment (Figure 3.40 D) the unoxidized IBP was slightly toxic in 24 and toxic in 48 h. Toxicity increased in the first 15 min, decreased in 30, increased slightly in 60 min and remained at the same levels until 120 min in 24 h. In 48 h the solution was toxic in 120 min. In 15 min we have the highest values in the intensities of the TPs compared to the other irradiation times. In 30 min of irradiation the intensities of the TPs decreased and after 30 min TPs disappeared. Toxicity in the

solution after 30 min is due to the toxicity observed form the parent compound which was at the same levels as the unoxidized solution.

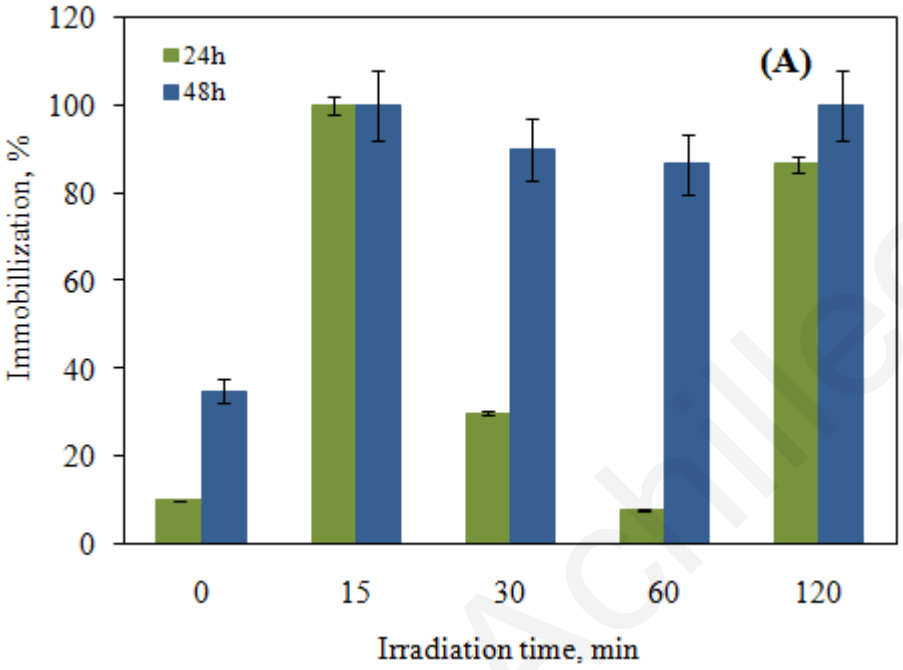

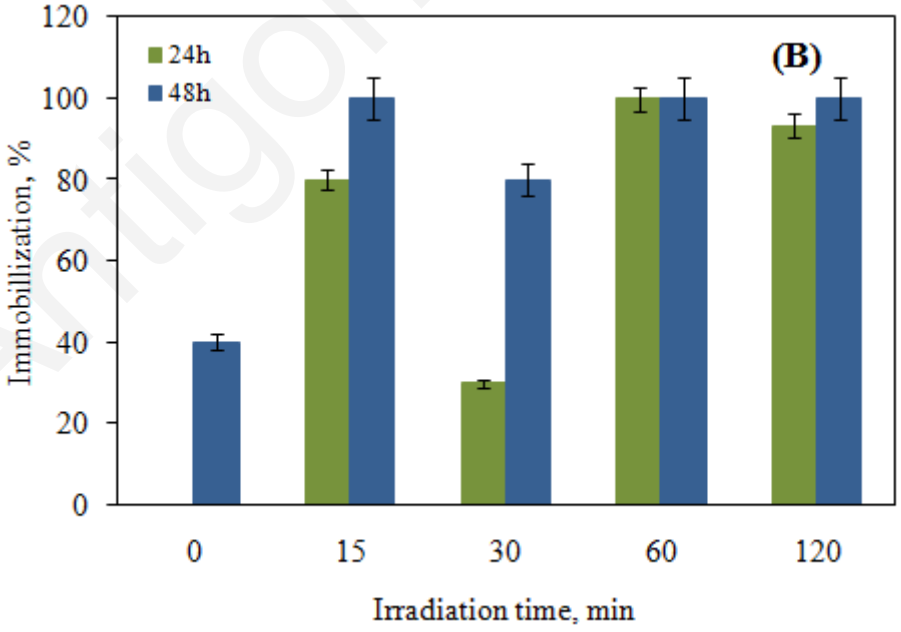

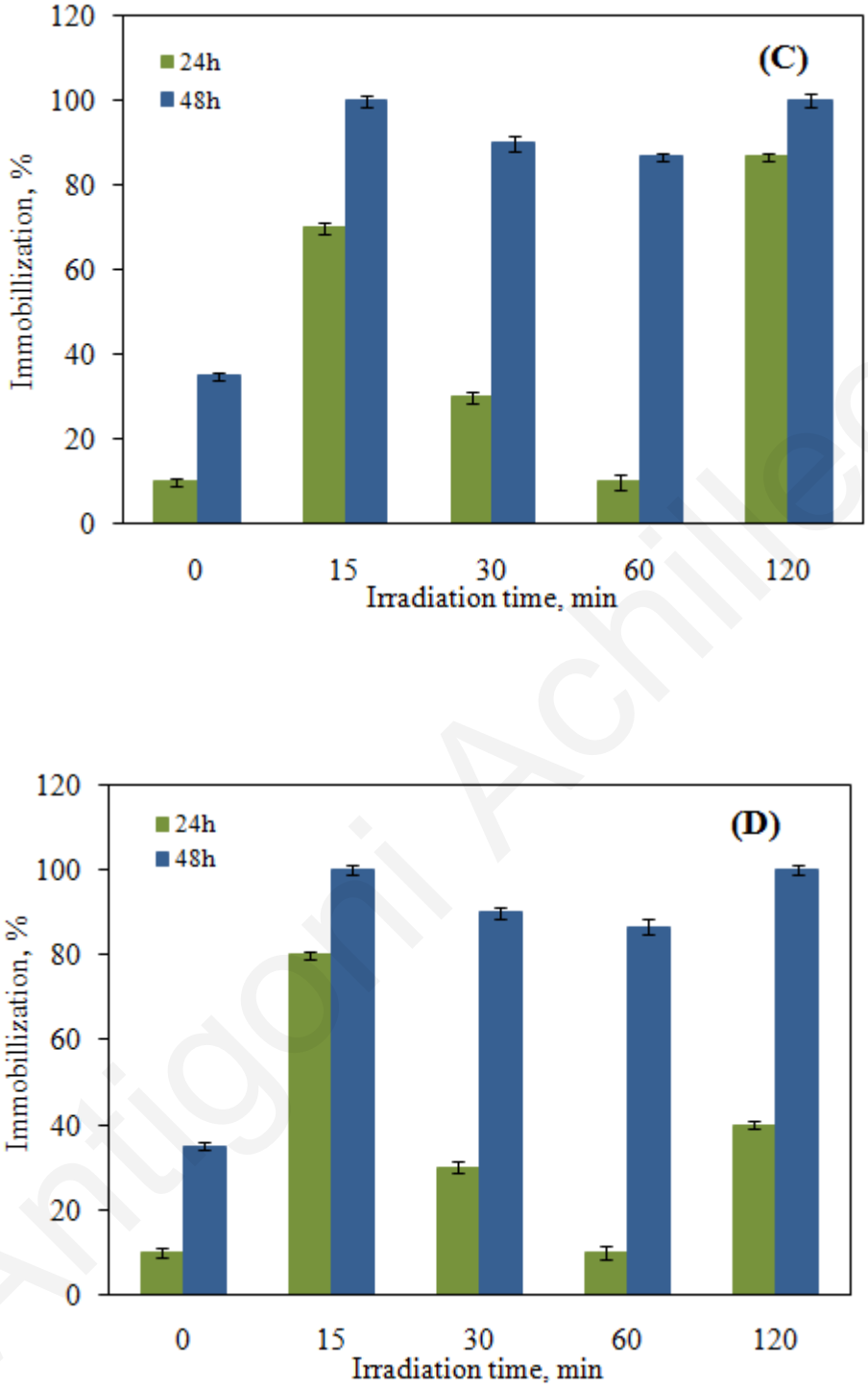

Figure 3.39: Toxicity, DCF 10 mg/L, 500 mg/L TiO_2, 500 W/L, (A) 9W UV-A irradiation, 500 mg/L TiO_2, (B) solar irradiation, 500 mg/L TiO_2, (C) sonolysis, (D) 9W UV-A irradiation, sonophotocatalysis, 500 mg/L TiO_2

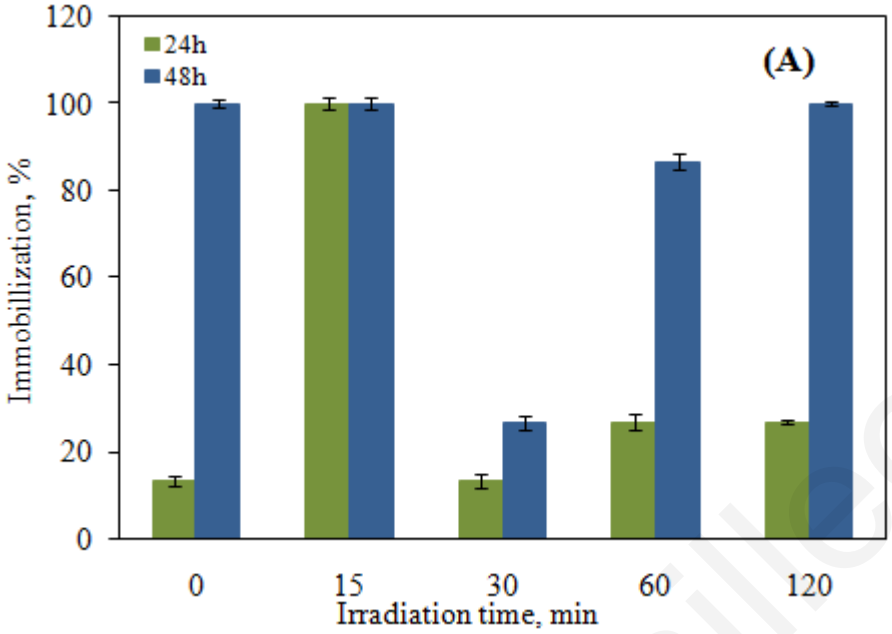

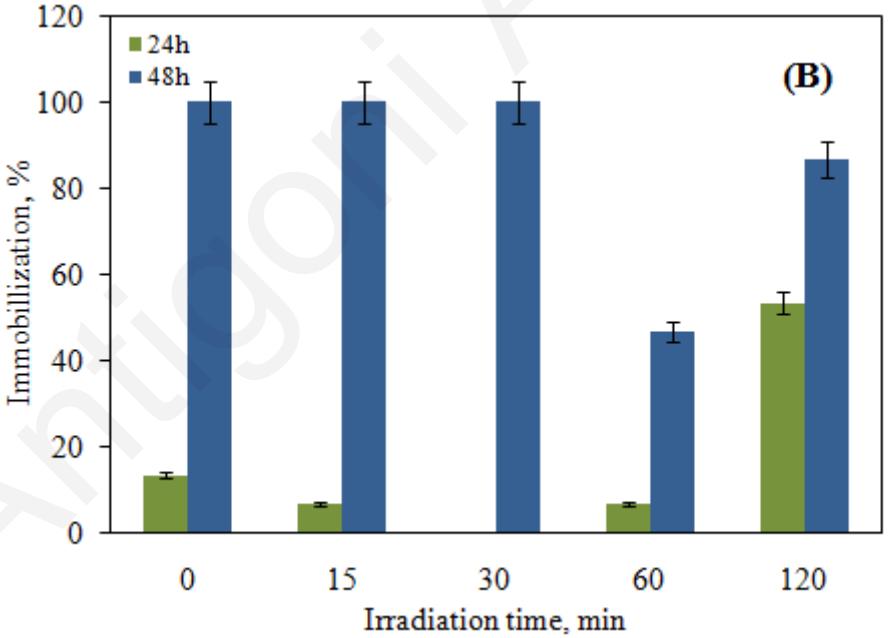

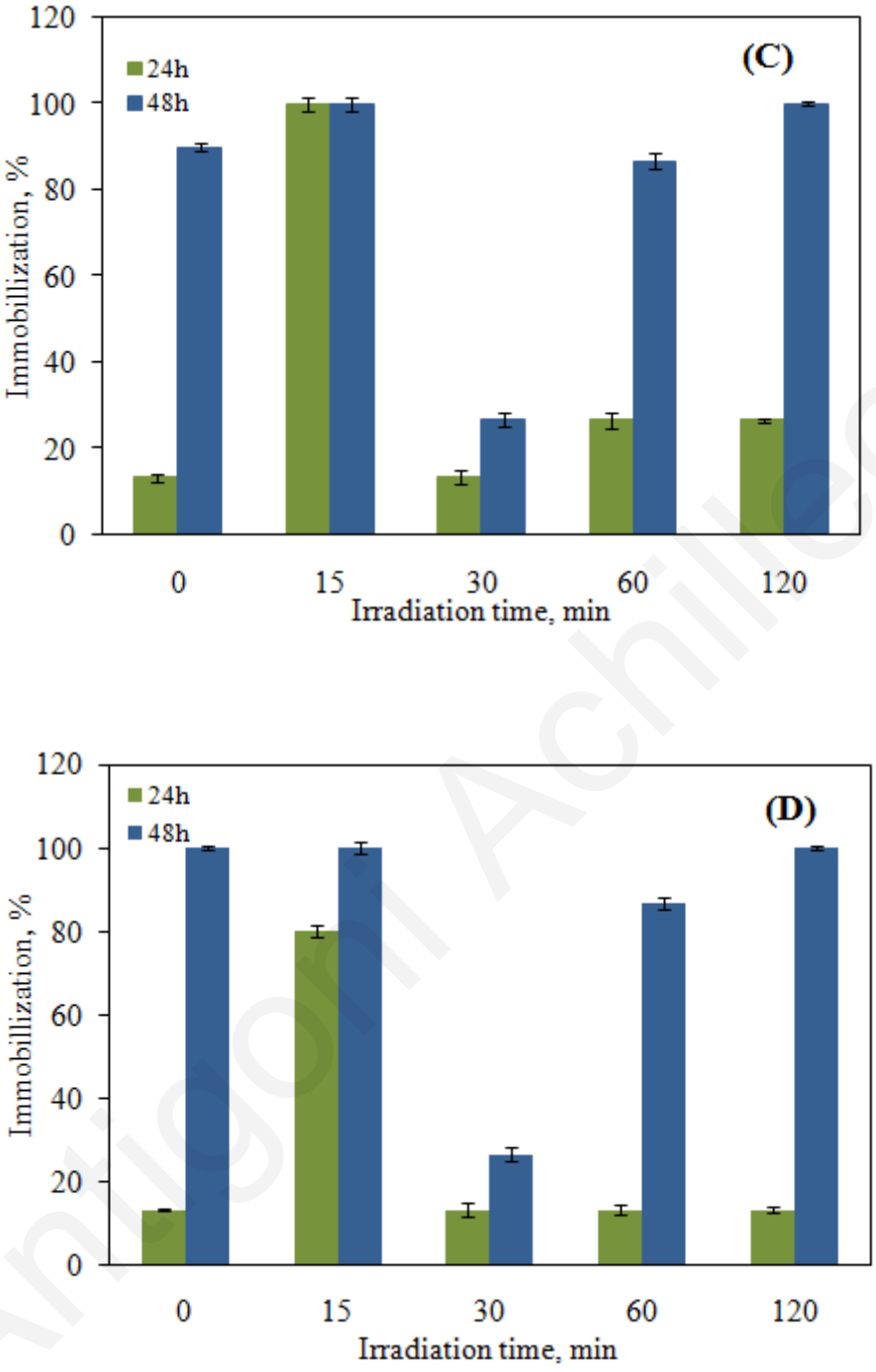

Figure 3.40: Toxicity, IBP 10 mg/L, 500 mg/L TiO_2, 500 W/L, (A) 9W UV-A irradiation, 500 mg/L TiO_2, (B) solar irradiation, 500 mg/L TiO_2, (C) sonolysis, (D) 9W UV-A irradiation, sonophotocatalysis, 500 mg/L TiO_2

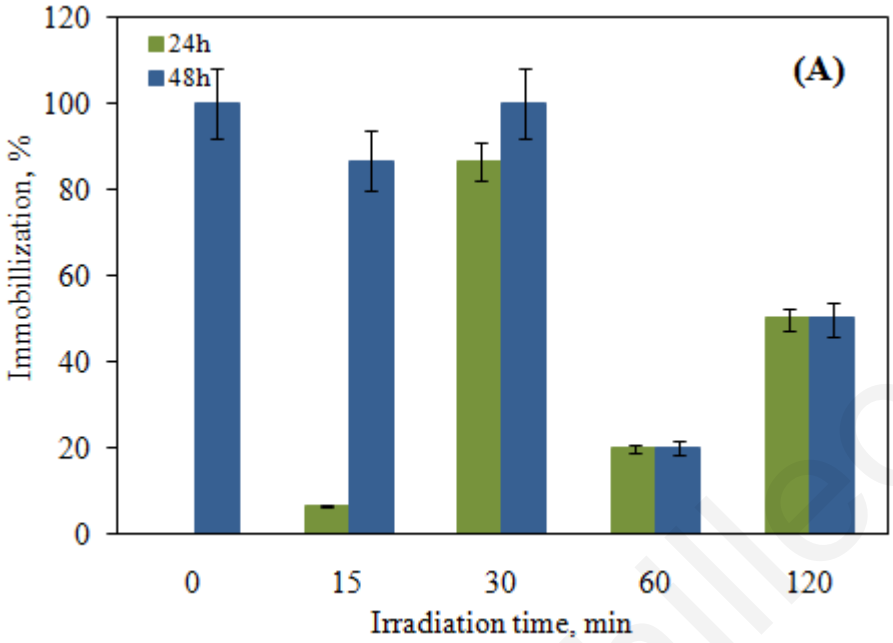

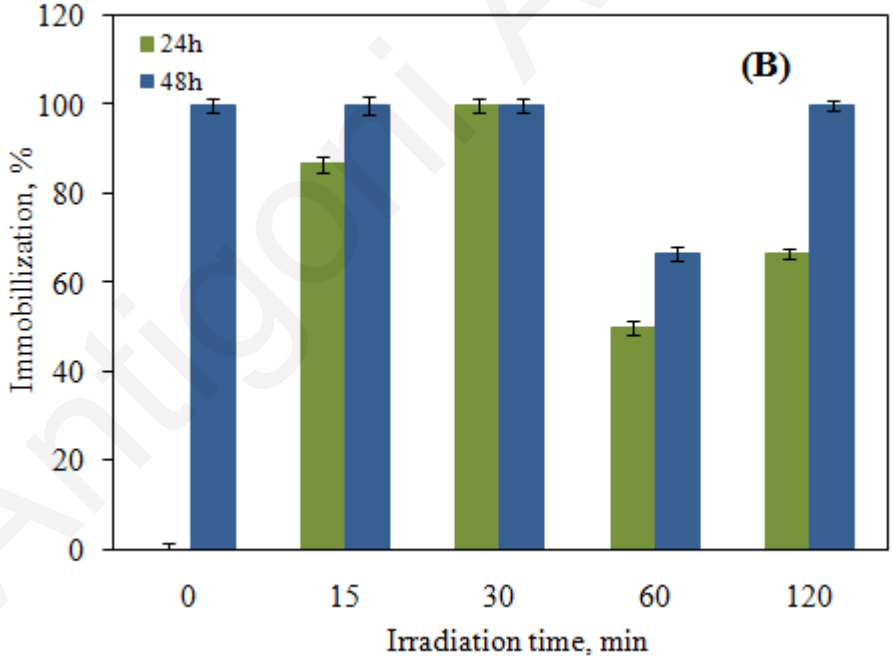

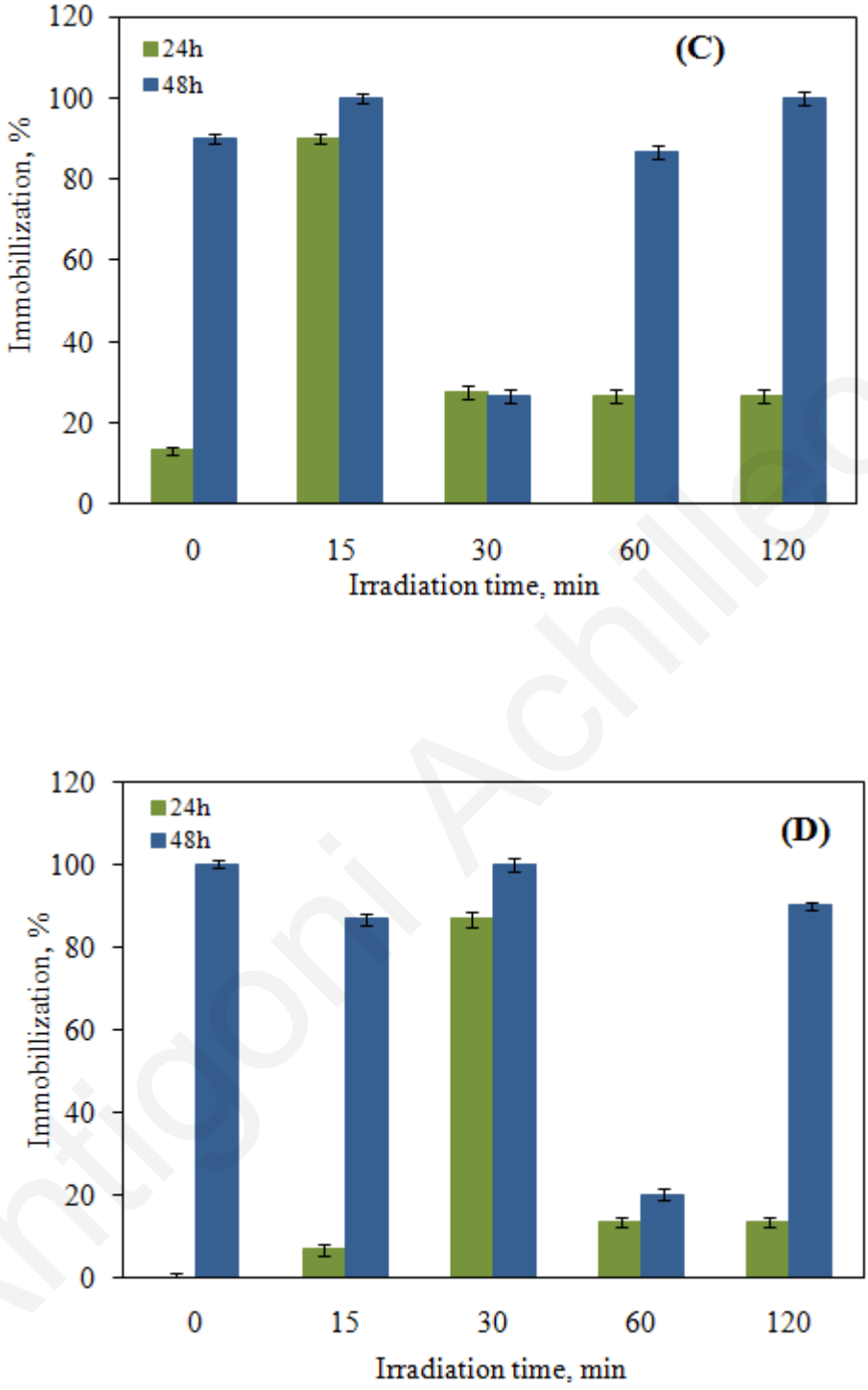

Figure 3.41: Toxicity, CBZ 10 mg/L, (A) 9W UV-A irradiation, 100 mg/L TiO_2, (B) solar irradiation, 100 mg/L TiO_2, (C) sonolysis, 500 W/L, (D) 9W UV-A irradiation, sonophotocatalysis, 100 mg/L TiO_2

The untreated CBZ samples were found non-toxic in 24 and 48 h in undiluted samples and toxic at 48 h of exposure at *Daphnia magna* with solar irradiation. Toxicity after 15 and 30 min of UV-A and solar irradiation increases at 24 h exposure. Toxicity after 60 and 120 min of UV-A and solar irradiation decreased and then increased at 24 and 48h (Figures 3.41A and B).

In sonophotocatalysis experiments (Figure 3.41 D) the untreated samples were found non-toxic at 24h and toxic at 48h of exposure. At 15 min toxicity increased slightly at 24h and decreases at 48 h of exposure. At 30 min toxicity increased, decreased in 60 min and in 120 min toxicity remains constant at 24h.

This is not surprising because if we can see in section 3.8.1 the profile of CBZ transformation products, TPs appeared in the first 15 min and after 120 min remain in the solution. So toxicity might be due to these transformations.

Toxic samples were diluted 80%, 40%, 20% and 10% times. Toxicity decreased as dilution increased. At 10% and 20% dilution all samples were not toxic.

3.8 Identification of transformation products by mass spectrometry

3.8.1 Carbamazepine

Structural elucidation and interpretation of the fragmentation pathways of CBZ and the detected TPs was acquired by using a hybrid mass detector QqToF, which combines the advantages of the ion separation as well as the detection principle of the ToF and the fragmentation obtained with MS (MS^2). QqToF permits the acquisition of full-scan product ion spectra, with the accurate mass of the product ions, thus yielding results of much higher degree of certainty making it useful for structure elucidation of unknown compounds, as well as for identifying target compounds (Kosjek et al., 2009).

Possible elemental compositions, based on accurate mass, were calculated using the Elemental Composition Calculator embedded into the MassLynx v4.1. software. A maximum deviation of ±10ppm from a measured accurate mass was accepted, and parameters were set in relation to CBZ structure. Additionally, the option "even electron only" was selected for precursor ions and "odd- and even- electrons" for product ions. It is worth to point out that, on the basis of the MS2 mass fragmentation patterns alone, a definitive assignment of TPs structure was not possible. The TPs structures were tentatively elucidated by coupling MS data with knowledge on the reactivity of investigated oxidants. For identification of TPs (Tables 3.16-3.17), in support to the proposed chemical structures, confirmatory methods were also used including matching the TP fragmentation patterns with those held in the NIST mass spectral library or published mass spectra and, where possible, a comparison of the compound's chromatographic and mass spectrometric behavior with that of a commercially available authentic compound.

Tables 3.18-3.26 show the summary of the data related to the calculated and measured masses of fragment ions of CBZ and its TPs determined in ESI(+)-MS^2 experiments on the QqToF instrument, together with the error between them, the proposed empirical formula corresponding to the compounds identified and the corresponding double bond equivalents (DBEs) (the number of rings and double bonds present in the molecule) given by the software. The data presented in Tables 3.18-3.26, were

obtained under optimized conditions of collision energy and cone voltage of the QqToF-MS. The TPs was in some cases confirmed with the presence of sodium adducts as additional peaks together with the peak of the protonated molecule. Most of the accurate mass results were found with an error of less than 2 ppm, thus providing a high degree of certainty in the assignment of formulas.

Table 3.16: Structure elucidation of CBZ and its TPs

Transformation products	**$[M+H]^+$**	**Chemical structure (incl. positive charge) (The most possible have been assigned)**
CBZ	237	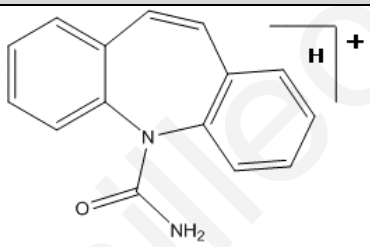
TP 252	253	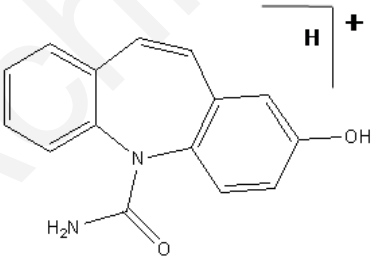
TP 252	253	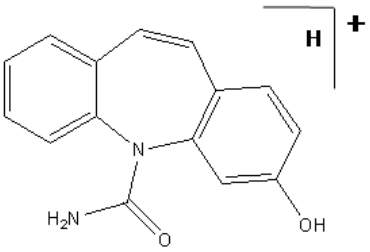
TP 267	267	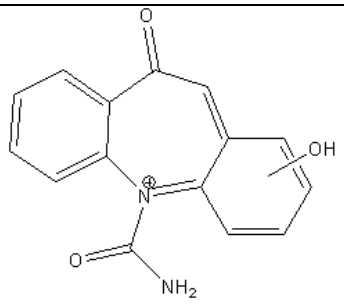 or

		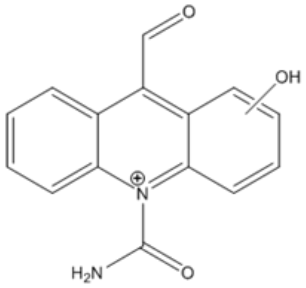
TP 251	251	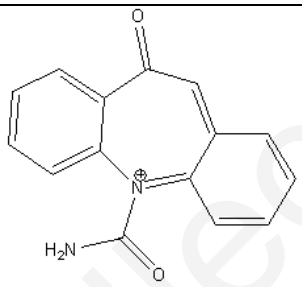
TP 225	226	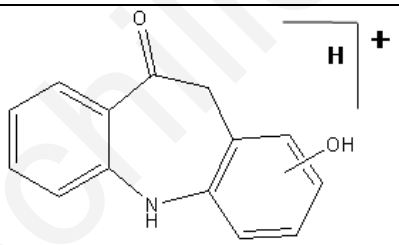 or 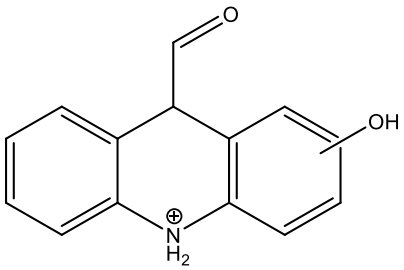
TP 223	224	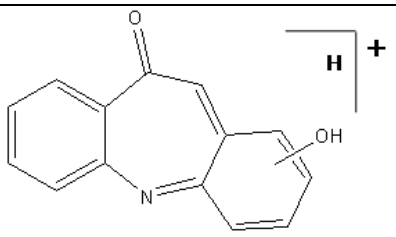 or 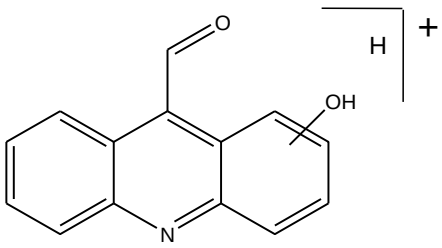

TP 270	271	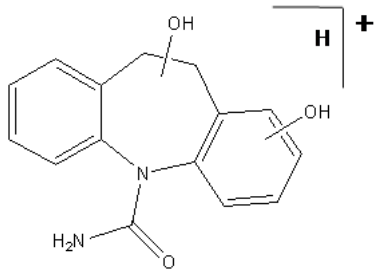 or 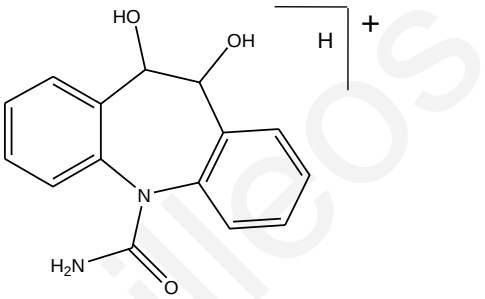
TP 268	269	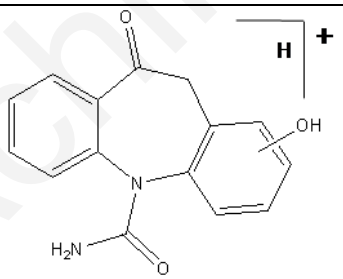

The screening of the treatment samples in (+) ESI scan mode allowed to confirm the formation of eight TPs (Figures 3.42-3.44). All of the identified products, except one (TP225), are eluted before the main peak of CBZ at 5 min (Table 3.17), indicating the formation of smaller and more polar products when compared to the parent compound.

Table 3.17: Accurate mass measurements of the transformation products (TP) of carbamazepine (CBZ) as determined by UPLC–(+)ESI-QqToF-MS in full scan mode

Compound	Ion	Elemental composition	Meas. Mass	Calc. Mass	Error (mDa)	Error (ppm)	DBE
CBZ	$[M+H]^+$	$C_{15}H_{13}N_2O$	237.1035	237.1028	0.7	3	10.5
	$[M+Na]^+$	$C_{15}H_{12}N_2ONa$	259.085	259.0847	0.3	1.2	10.5
2-OH-CBZ	$[M+H]^+$	$C_{15}H_{13}N_2O_2$	253.0996	253.0977	1.9	7.5	10.5
	$[M+Na]^+$	$C_{15}H_{12}N_2O_2Na$	275.0787	275.0796	-0.9	-3.3	10.5
3-OH-CBZ	$[M+H]^+$	$C_{15}H_{13}N_2O_2$	253.0987	253.0977	1	4	10.5
	$[M+Na]^+$	$C_{15}H_{12}N_2O_2Na$	275.0801	275.0796	0.5	1.8	10.5
TP 251	M^+	$C_{15}H_{11}N_2O_2$	251.0829	251.0821	0.8	3.2	11.5
TP 267	M^+	$C_{15}H_{11}N_2O_3$	267.0783	267.077	1.3	4.9	11.5
TP 225	$[M+H]^+$	$C_{14}H_{12}NO_2$	226.0872	226.0868	0.4	1.8	9.5
	$[M+Na]^+$	$C_{14}H_{11}NO_2Na$	248.0698	248.0687	1.1	4.4	9.5
TP 223	$[M+H]^+$	$C_{14}H_{10}NO_2$	224.0728	224.0712	1.6	7.1	10.5
TP 268	$[M+H]^+$	$C_{15}H_{13}N_2O_3$	269.0957	269.0926	3.1	11.5	10.5

	$[M+Na]^+$	$C_{15}H_{12}N_2O_3Na$	291.075	291.0746	0.4	1.4	10.5
TP 270	$[M+H]^+$	$C_{15}H_{15}N_2O_3$	271.1077	271.1083	-0.6	-2.2	9.5
	$[M+Na]^+$	$C_{15}H_{14}N_2O_3Na$	293.091	293.0902	0.8	2.7	9.5

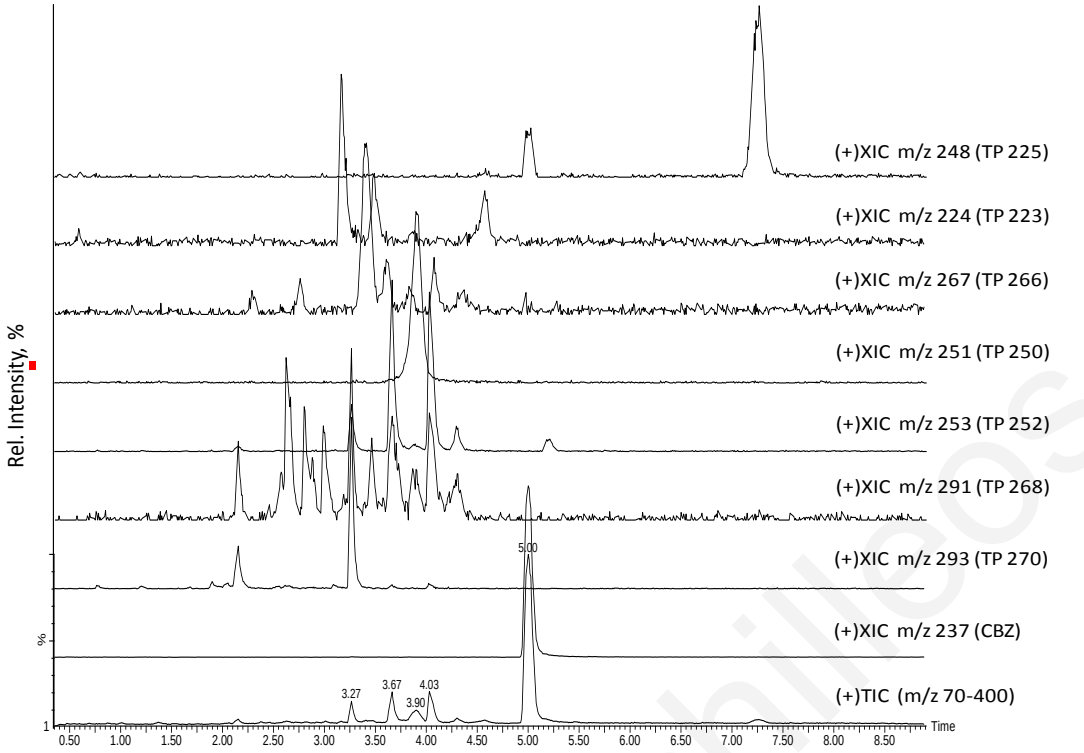

Figure 3.42: Total ion chromatogram (TIC) and extracted ion chromatograms (XIC) of CBZ (10 mg/L) after 30 min with photocatalysis UV-A

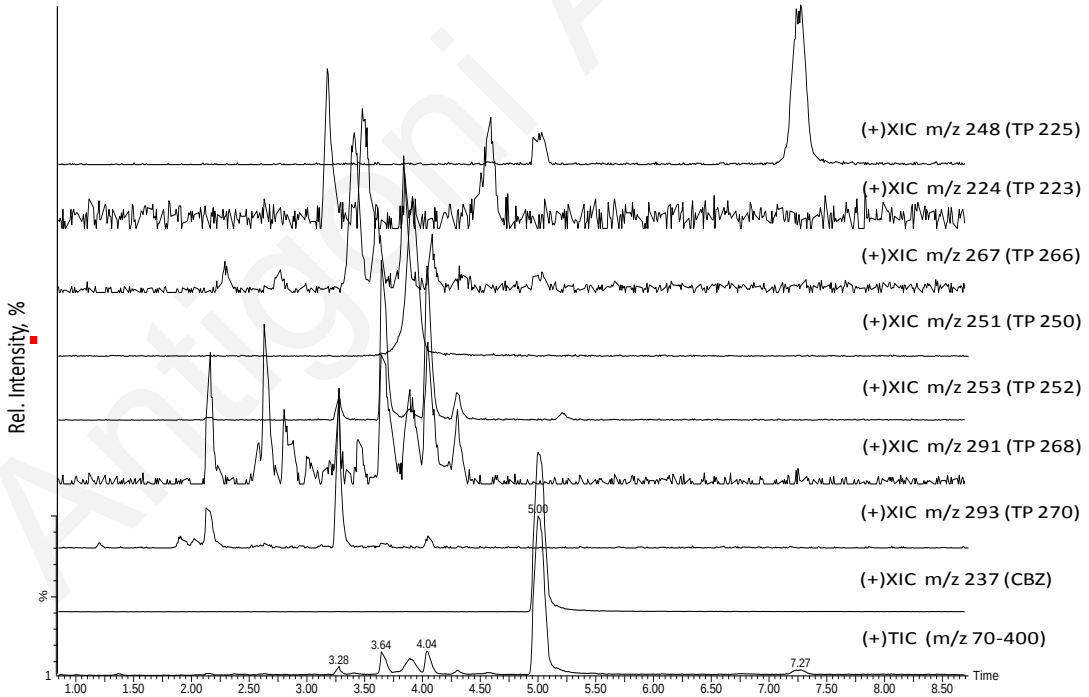

Figure 3.43: Total ion chromatogram (TIC) and extracted ion chromatograms (XIC) of CBZ (10 mg/L) after 120 min with solar irradiation

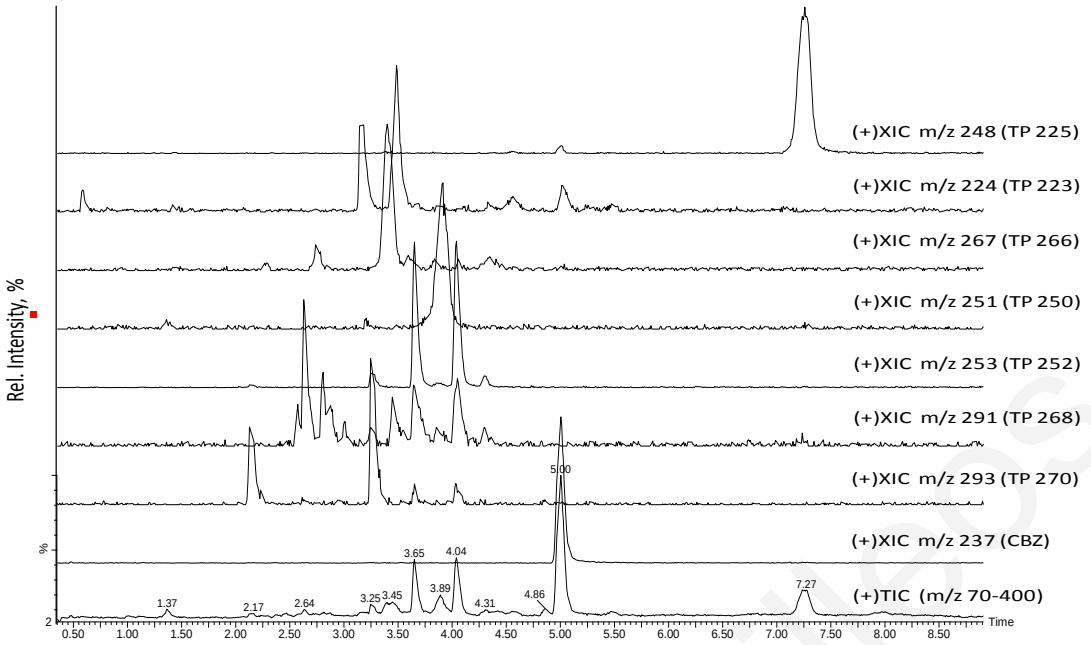

Figure 3.44: Total ion chromatogram (TIC) and extracted ion chromatograms (XIC) of CBZ (10 mg/L) after 60 min with sonophotocatalysis

In Figure 3.44, the TIC shows the peak of CBZ at t_R = 5.0 min that exhibited a molecular ion peak at *m/z* 237. The collision-induced-dissociation experiments with CBZ (molecular ion $[M + H]^+$ 237) (Figure 3.45, Table 3.18) revealed the formation of only two fragment ions at m/z 220 and 194, as a consequence of the loss of ammonia and CONH group (43 Da), respectively.

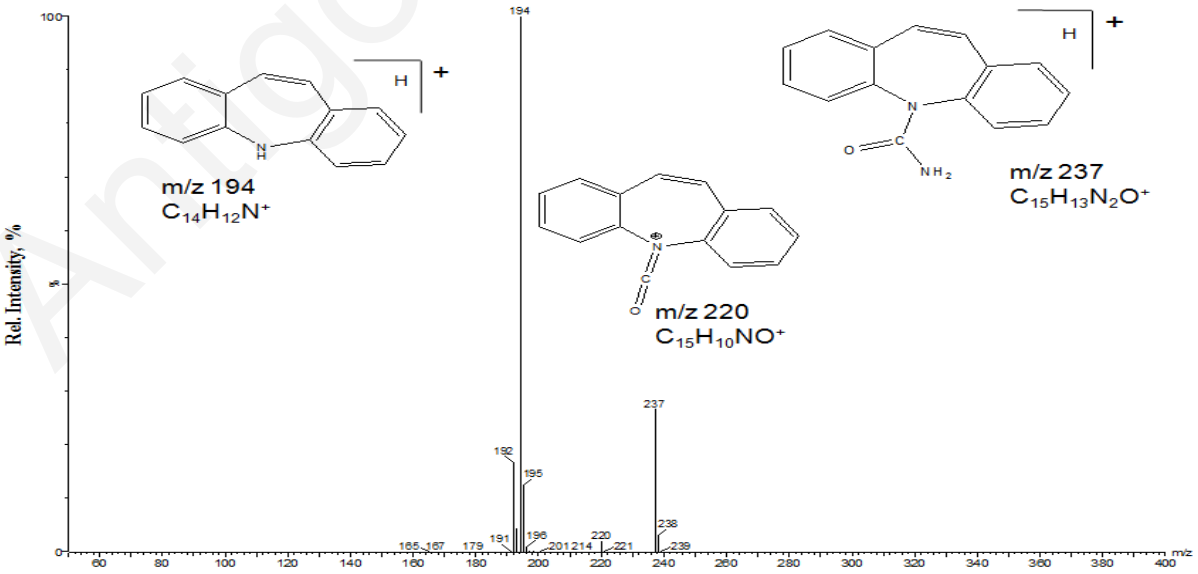

Figure 3.45: Spectra obtained in ESI(+)-MS^2 experiments at QqToF instrument for CBZ and proposed fragmentation patterns

Table 3.18: Accurate mass measurements of CBZ as determined by UPLC–(+)ESI-QqToF-MS in product ion mode

Elemental composition	Meas. Mass	Calc. Mass	Error (mDa)	Error (ppm)	DBE
$C_{15}H_{13}N_2O$	237.1038	237.1028	1	4.2	10.5
$C_{15}H_{10}NO$	220.0752	220.0762	-1	-4.7	11.5
$C_{14}H_{12}N$	194.0975	194.097	0.5	2.6	9.5

The approach to identify TPs using LC-QqToF-MS was as usual by screening the total ion chromatogram, acquired in full-scan mode and then selecting a specific protonated molecule for further product ion scans. The MS^2 experiments improved the selectivity of the analyses, providing the structural information together with accurate mass measurements of product ions, and thus allowed the precision in the low ppm range (Reemtsma, 2003). Thus, searching in full scan mode, numerous suspected species were found in the TIC, at retention times between 2 and 5.5 min (Table 3.20).

By utilizing the capabilities of the QqTOF mass spectrometer, two TPs have been unequivocally identified as mono-hydroxylated CBZ derivatives. The identity of theses TPs was ultimately confirmed by analyzing the commercially available authentic standard of the proposed compound, which matched the retention time and fragmentation pattern of the protonated molecule. The difference of 16 Da when compared to the molecular ion of CBZ suggested that these intermediates were generated through hydroxylation of the primary molecule. The first one (t_R = ~3.65 min), has been as assigned as 2-OH-CBZ, while the second one (t_R = ~4.03 min) as 3-OH-CBZ. The theoretical accurate mass of these species (253.0977) gave a unique elemental composition of $C_{15}H_{13}N_2O_2^+$. Additionally, the protonated form of the target TPs is also accompanied by one sodium adduct giving a positive charged ion at m/z 275.0796 (Table 3.17). The two spectra (MS^2 fragmentation of the molecular ion $[M + H]^+$ 253) are almost identical and rendered intense signals at m/z 236 and 210, corresponding to the loss of ammonia and CONH group, respectively. The strong signal observed at m/z 208 would be attributed to the intra-molecular stabilization.

It is worth pointing out that the formation of 2- and 3-hydroxylated derivatives of CBZ has been reported in the metabolism of CBZ by the cytochrome P450 in mammals (Mandrioli et al., 2001; Pearce et al., 2002) as well as in the two model fungi *Cunninghamella elegans* and *Umbelopsis ramanniana* used to study mammalian metabolism for many drugs (Kang et al., 2008).

Table 3.19: Retention time (chromatography) and elemental composition of CBZ and its TPs under different treatment process: solar driven catalysis (S), sonophotocatalysis (SPC) and UV-A light driven photocatalysis (PC)

Compound	Elemental composition	LC retention time, min		
		PC	SPC	S
CBZ	$C_{15}H_{13}N_2O$	5.00	5.00	5.00
2-OH-CBZ	$C_{15}H_{13}N_2O_2$	3.67	3.65	3.64
3-OH-CBZ	$C_{15}H_{13}N_2O_2$	4.03	4.04	4.04
TP 251	$C_{15}H_{11}N_2O_2$	3.91	3.92	3.92
TP 267	$C_{15}H_{11}N_2O_3$	3.41	3.40	a) 3.41 b) 3.60 c) 3.84
TP 225	$C_{14}H_{12}NO_2$	7.27	7.26	7.27
TP 223	$C_{14}H_{10}NO_2$	a) 3.17 b) 3.48	a) 3.18 b) 3.48	a) 3.18 b) 3.49
TP 268	$C_{15}H_{13}N_2O_3$	a) 2.62 b) 2.80 c) 2.99 d) 3.27 e) 3.47 f) 3.67 g) 4.03	a) 2.62 b) 2.80 c) 3.27 d) 3.47 e) 3.67	a) 2.62 b) 2.80 c) 3.27 d) 3.47 e) 3.67 f) 4.03
TP 270	$C_{15}H_{15}N_2O_3$	a) 3.28	a) 2.13 b) 3.25	a) 2.13 b) 3.28

a, b, c etc. are isomers of a TP that eluted at different retention times

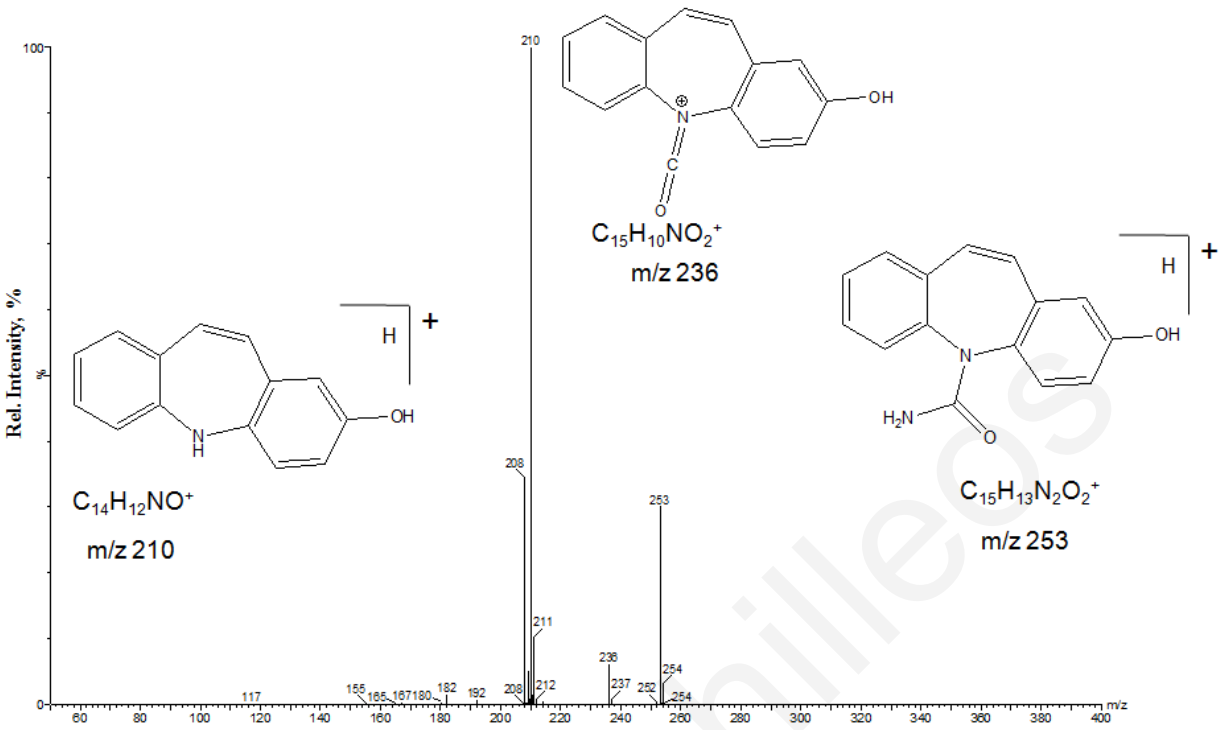

Figure 3.46: 2-OH-CBZ in product ion mode and proposed fragmentation patterns

Table 3.20: Accurate mass measurements of 3-OH-CBZ as determined by UPLC–(+)ESI-QqToF-MS in product ion mode

Elemental composition	Meas. Mass	Calc. Mass	Error (mDa)	Error (ppm)	DBE
$C_{15}H_{13}N_2O_2$	253.0975	253.0977	-0.2	-0.8	10.5
$C_{15}H_{10}NO_2$	236.0696	236.0712	-1.6	-6.8	11.5
$C_{14}H_{12}NO$	210.092	210.0919	0.1	0.5	9.5
$C_{13}H_{10}N$	180.0818	180.0813	0.5	2.8	9.5

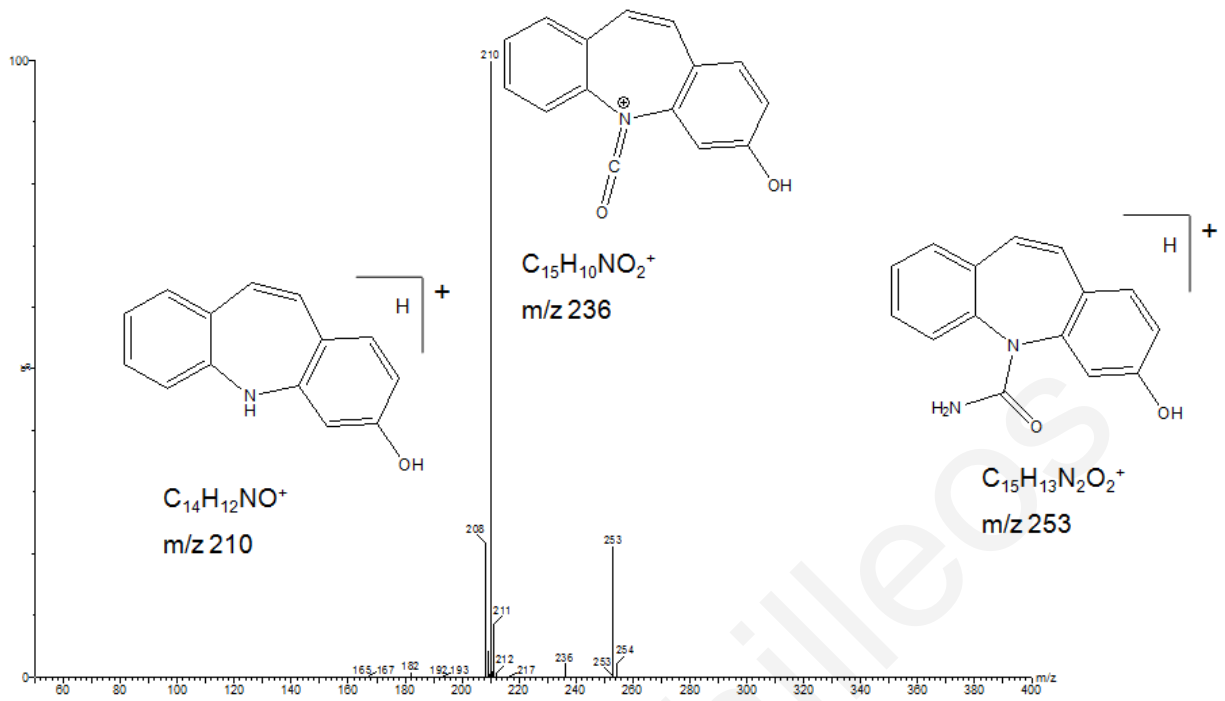

Figure 3.47: 3-OH-CBZ in product ion mode and proposed fragmentation patterns

Table 3.21: Accurate mass measurements of 3-OH-CBZ as determined by UPLC-(+)ESI-QqToF-MS in product ion mode

Elemental composition	Meas. Mass	Calc. Mass	Error (mDa)	Error (ppm)	DBE
$C_{15}H_{13}N_2O_2$	253.0971	253.0977	-0.6	-2.4	10.5
$C_{15}H_{10}NO_2$	236.0718	236.0712	0.6	2.5	11.5
$C_{14}H_{12}NO$	210.0916	210.0919	-0.3	-1.4	9.5
$C_{13}H_{10}N$	180.0815	180.0813	0.2	1.1	9.5

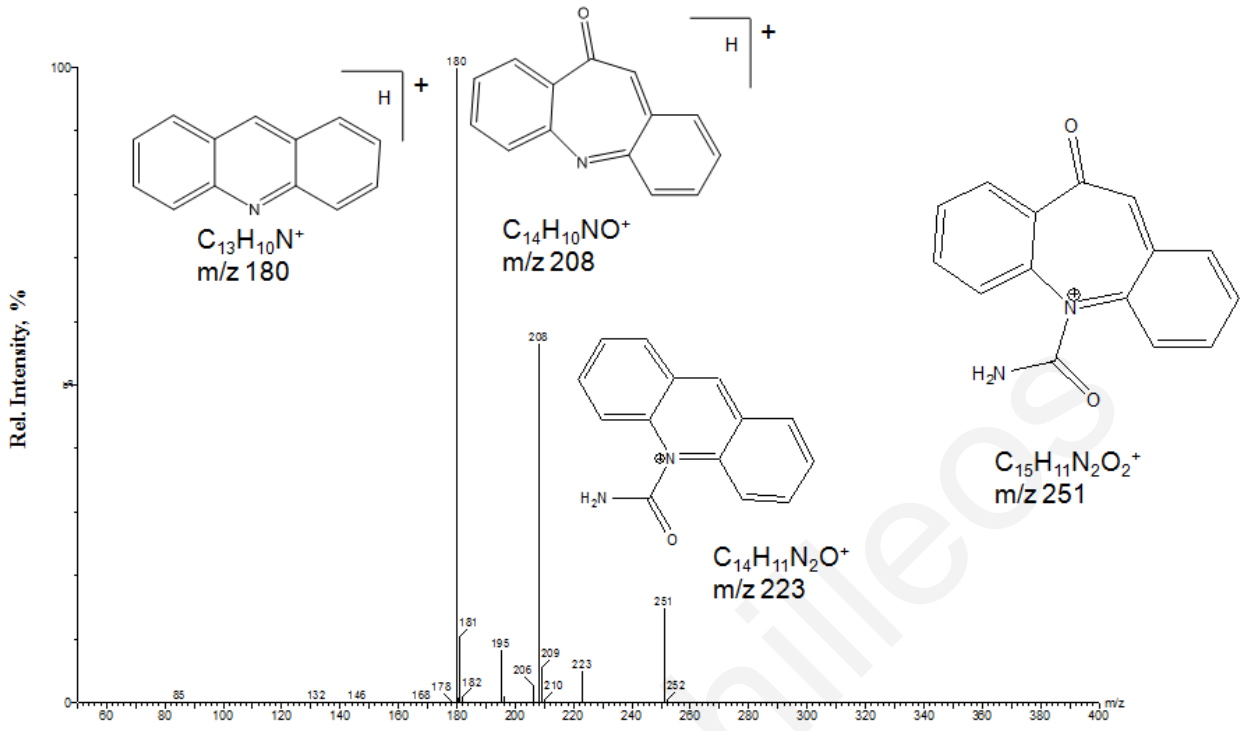

Figure 3.48: TP251 in product ion mode and proposed fragmentation patterns

The next TP derivative identified provided a protonated molecular ion at *m/z* 251. Based on the best-fit formula of $C_{15}H_{11}N_2O_2^+$ and the mass difference of 2 amu compared to the OH-CBZ TPs, the elemental composition may be rationalized by the formation of keto or epoxy CBZ -derivatives. Determined double-bond equivalency (DBE), which represents the number of rings and double bonds present in the molecule, is also consistent with the proposed structure (Figure 3.48). The structure ($C_{15}H_{11}N_2O_2^+$) of this product was also confirmed by the appearance of three characteristic fragments. The loss of 28 Da, typical for the elimination of CO, led to the appearance of the highest mass ion at *m/z* 223, which with further loss of CONH group resulted in the *m/z* 180 fragment ion. The third one exhibited the product ion with mass m/z of 208.0762, resulting from the loss of CONH group from the molecular ion at *m/z* 251.

Table 3.22: Accurate mass measurements of TP 251 as determined by UPLC-(+)ESI-QqToF-MS in product ion mode

Elemental composition	Meas. Mass	Calc. Mass	Error (mDa)	Error (ppm)	DBE
$C_{15}H_{11}N_2O_2$	251.0819	251.0821	-0.2	-0.8	11.5
$C_{14}H_{11}N_2O$	223.0869	223.0871	-0.2	-0.9	10.5
$C_{14}H_{10}NO$	208.0771	208.0762	0.9	4.3	10.5
$C_{13}H_{10}N$	180.0815	180.0813	0.2	1.1	9.5

As far as TP 267 is concerned, ESI-MS^2 spectra patterns are consistent with hydroxcarbamazepine-9-carboxaldehyde (Figure 3.49 A) or hydroxy-10-oxo-4aH-dibenzo[b,f]azepine-5(10H)-carboxamide (Figure 3.49 B). The loss of 43 Da typical for CONH group led to the appearance of the fragment ion at m/z 224, which with further loss of 28 Da (loss of CO) resulted in a very stable fragment ion at m/z 196.

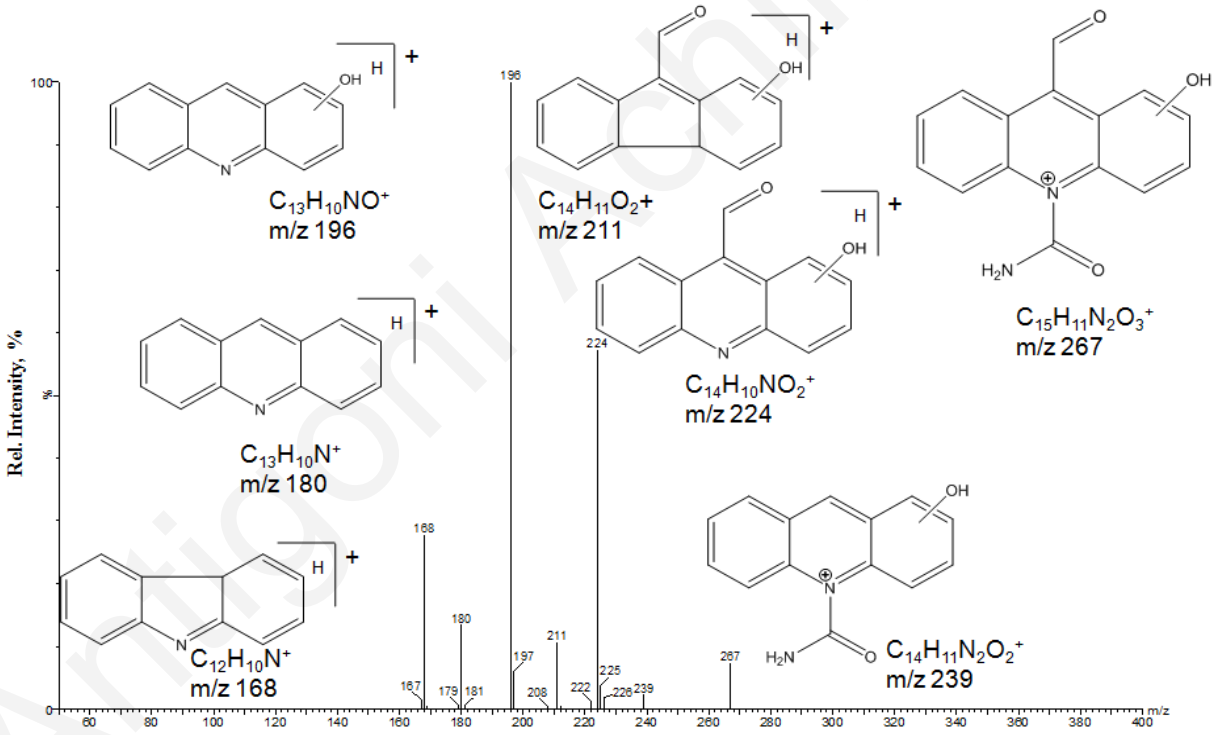

Figure 3.49 A: TP267 in product ion mode and proposed fragmentation patterns

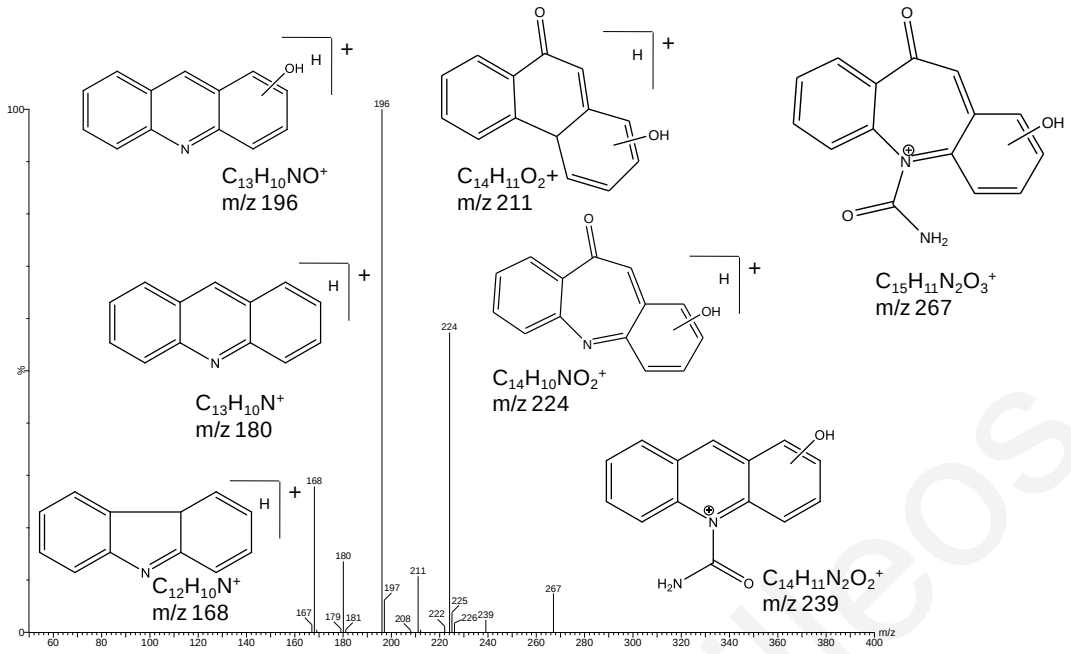

Figure 3.49 B: TP267 in product ion mode and proposed fragmentation patterns

Table 3.23: Accurate mass measurements of TP 267 as determined by UPLC-(+)ESI-QqToF-MS in product ion mode

Elemental composition	Meas. Mass	Calc. Mass	Error (mDa)	Error (ppm)	DBE
$C_{15}H_{11}N_2O_3$	267.0775	267.077	0.5	1.9	11.5
$C_{14}H_{11}N_2O_2$	239.084	239.0821	1.9	8.1	10.5
$C_{14}H_{10}NO_2$	224.0719	224.0712	0.7	3.1	10.5
$C_{14}H_{11}O_2$	211.0711	211.0759	-4.8	-22.8	9.5
$C_{13}H_{10}NO$	196.0753	196.0762	-0.9	-4.6	9.5
$C_{13}H_{10}N$	180.0822	180.0813	0.9	5	9.5
$C_{12}H_{10}N$	168.0805	168.0813	-0.8	-4.9	8.5

The ESI-MS^2 spectra patterns of TP 224 are consistent with 2-hydroxyacridine-9-carbaldehyde (Figure 3.50A) or hydroxy-10H-dibenzo[b,f]azepin-10-one. The spectra is characterized by the fragment ion at m/z 206 that arises from the loss of a water molecule, which reinforces the presence of the OH group on the proposed structure. The ion at m/z 178 corresponds to a combined loss of water and CO group from the protonated molecule.

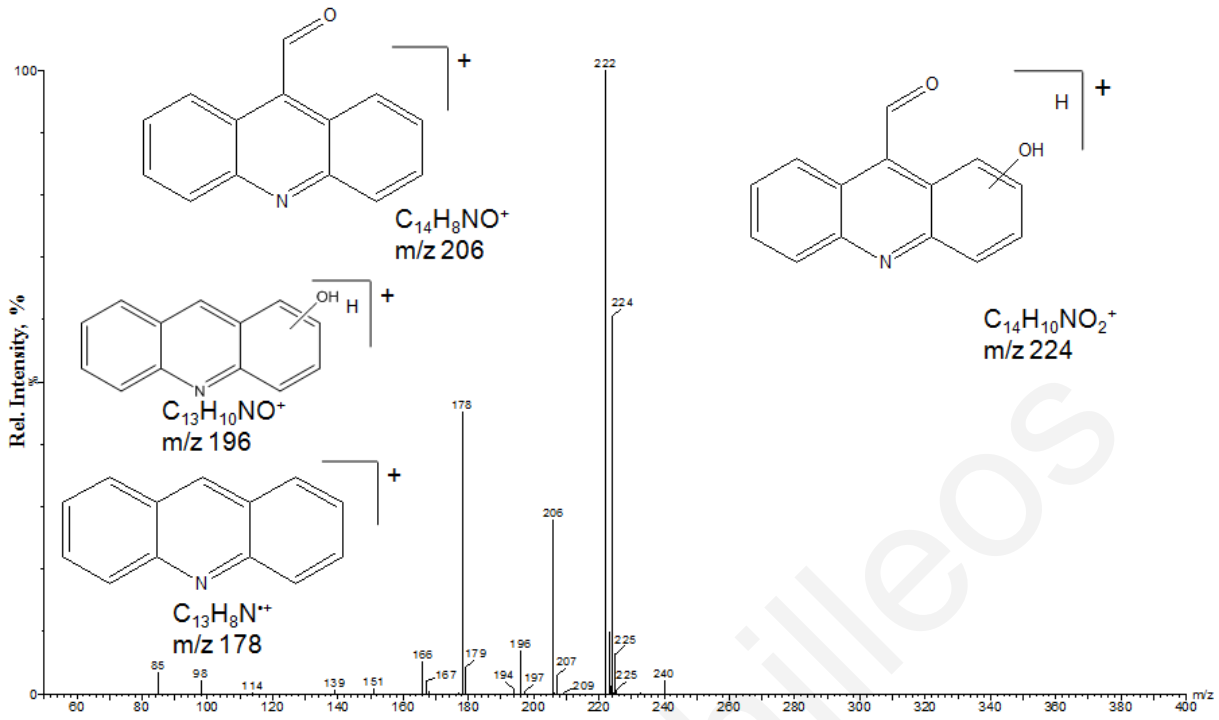

Figure 3.50 A: TP223 in product ion mode and proposed fragmentation patterns

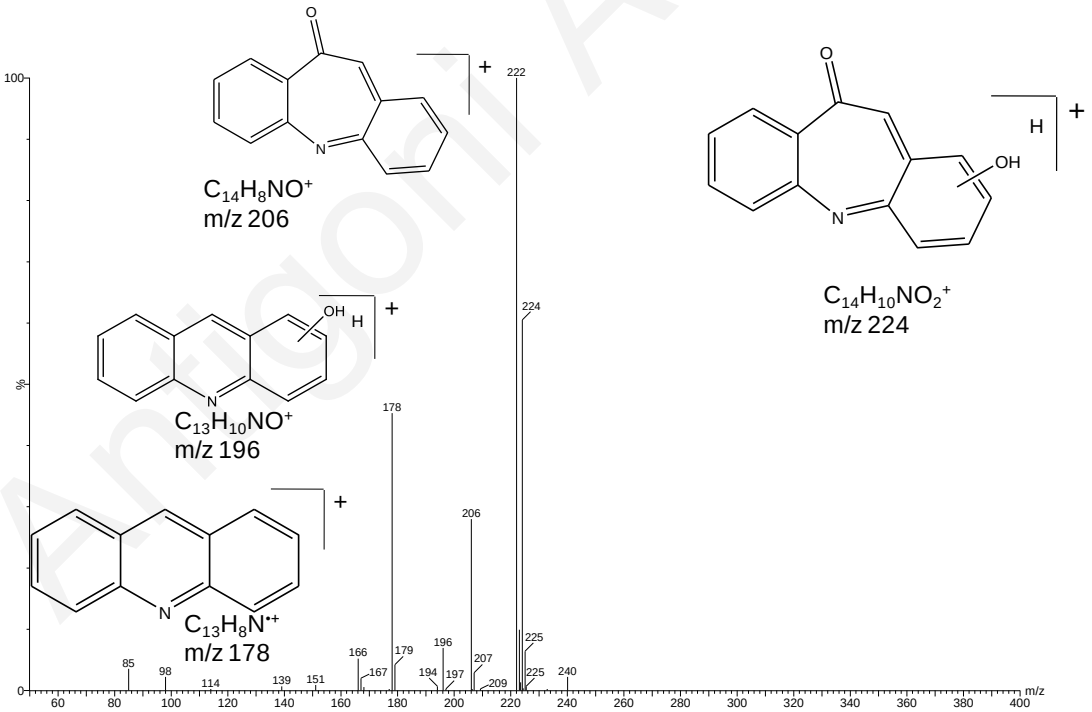

Figure 3.50 B: TP223 in product ion mode and proposed fragmentation patterns

Table 3.24: Accurate mass measurements of TP 224 as determined by UPLC-(+)ESI-QqToF-MS in product ion mode

Elemental composition	Meas. Mass	Calc. Mass	Error (mDa)	Error (ppm)	DBE
$C_{14}H_{10}NO_2$	224.0696	224.0712	-1.6	-7.1	10.5
$C_{14}H_8NO$	206.0596	206.0606	-1	-4.9	11.5
$C_{13}H_{10}NO$	196.0759	196.0762	-0.3	-1.5	9.5
$C_{13}H_8N$	178.0659	178.0657	0.2	1.1	10.5

As regards, TP 226, the ESI-MS^2 spectrum of m/z 226 showed sequential losses of 18, 28 and 46, eventually leading to the fragment ions at m/z 208, 198 and 180, therewith demonstrating again the individual and combined loss of water and CO from the protonated molecule (Figure 3.51 A & B).

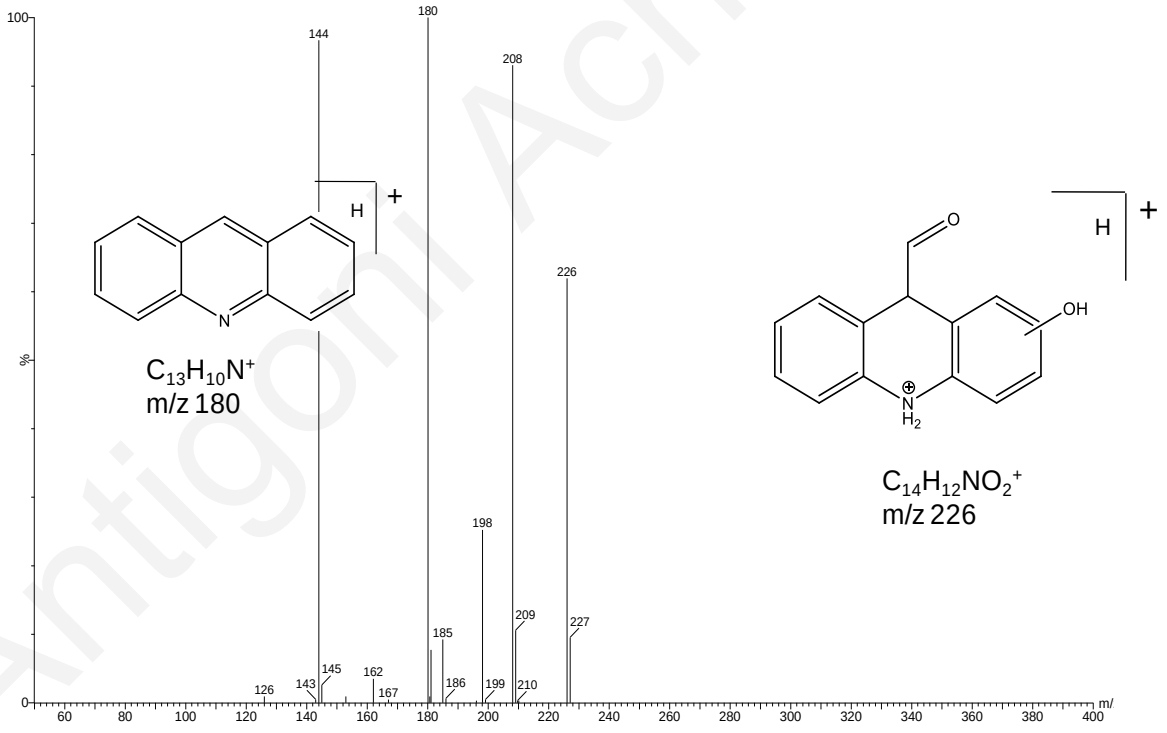

Figure 3.51 A: TP225 in product ion mode and proposed fragmentation patterns

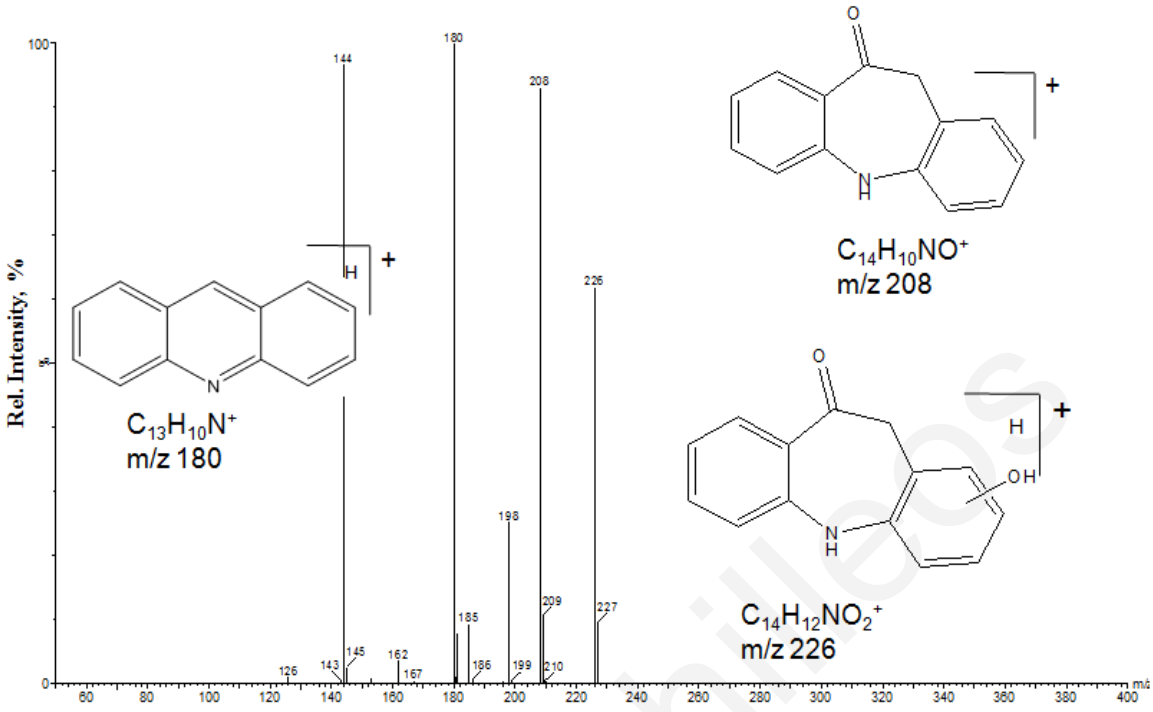

Figure 3.51 B: TP225 in product ion mode and proposed fragmentation patterns

Table 3.25: Accurate mass measurements of TP 226 as determined by UPLC-(+)ESI-QqToF-MS in product ion mode

Elemental composition	Meas. Mass	Calc. Mass	Error (mDa)	Error (ppm)	DBE
$C_{14}H_{12}NO_2$	226.0859	226.0868	-0.9	-4	9.5
$C_{14}H_{10}NO$	208.0756	208.0762	-0.6	-2.9	10.5
$C_{13}H_{12}NO$	198.0932	198.0919	1.3	6.6	8.5
$C_{13}H_{10}N$	180.0811	180.0813	-0.2	-1.1	9.5

The next TP isomers identified provided a protonated molecular ion at m/z 269 (Figure 3.52). Looking closely at the LC chromatogram, up to seven peaks have been detected with m/z 269 with slight different fragmentation pattern as well as different relative abundance for the more significant fragments. In all cases, their ESI-MS^2 spectrum is rendered by the characteristic fragment at m/z 226, representing the cleavage of $COHNH_2$. Further loss of CO in the fragment ion m/z 226 afforded the signal at m/z 196. As in the case of OH-CBZ the strong signal observed at m/z 224 would be attributed to the intramolecular cyclization of the TP 226. A proposed mechanism is depicted in the following scheme:

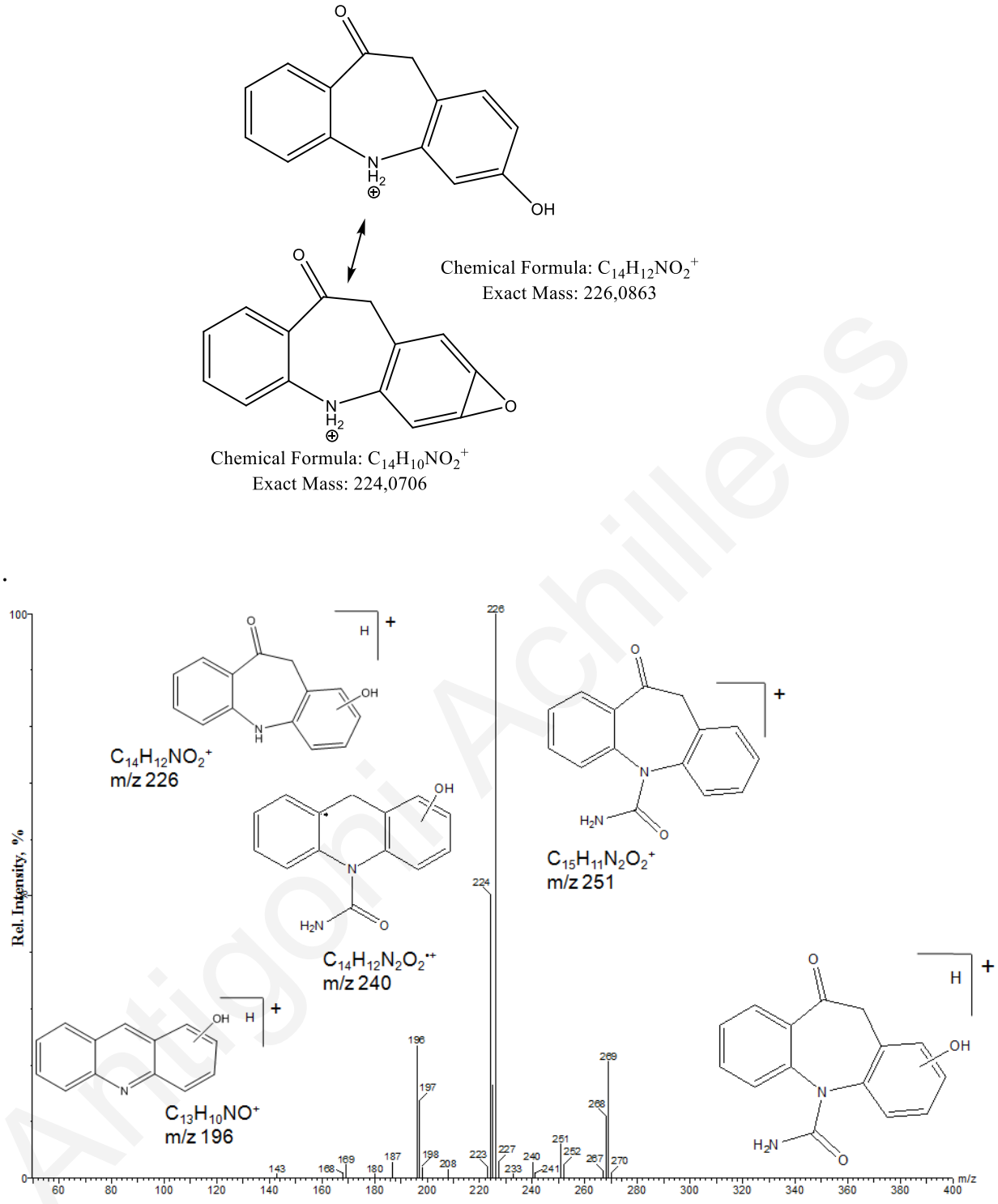

Figure 3.52: TP268 in product ion mode and proposed fragmentation patterns

Table 3.26: Accurate mass measurements of TP 269 as determined by UPLC-(+)ESI-QqToF-MS in product ion mode

Elemental composition	Meas. Mass	Calc. Mass	Error (mDa)	Error (ppm)	DBE
$C_{15}H_{13}N_2O_3$	269.092	269.0926	-0.6	-2.2	10.5
$C_{15}H_{11}N_2O_2$	251.0823	251.0821	0.2	1	11.5
$C_{14}H_{12}N_2O_2$	240.0903	240.0899	0.4	1.8	10.0
$C_{14}H_{12}NO_2$	226.0847	226.0868	-2.1	-9.3	9.5
$C_{14}H_{10}NO_2$	224.0723	224.0712	1.1	5.1	10.5
$C_{13}H_{10}NO$	196.0741	196.0762	-2.1	-10.7	9.5

Continuous HO• attack on the CBZ molecule could lead to the formation of more hydroxylated (TP 271, m/z 271). The difference of 32 amu with respect to the parent molecule numerically corresponds to a double HO• substitution and these products are assigned to be dihydroxy-CBZ derivatives. Although, the oxidation of the aromatic ring of hydroxycarbamazepine is expected to yield up to 4 isomers with the OH function in different positions, only one isomer has been detected in the case of PC treatment and two isomers in the case of SP and S treatment The MS^2 spectrum of TP 271 at t_R = 3.28 was featured by a less intense fragment ions at m/z 253 related to a first OH loss. Two possible structures with relevant fragmentation patters would be assigned for this TP (Figures 3.53 A & B). As in the case of TP 253, characteristic fragments at m/z 236, 210 and 180 have been observed. However, the MS^2 fragmentation pattern using the m/z 271 precursor ion was not consistent (different intense signals) with that observed in the MS^2 mass spectrum of TP 253. Based on this fragment profile, as well as on previous published spectra regarding the dihydroxy-CBZ derivatives, it can be assumed that hydroxylation in the aromatic rings represents a less favorable pathway and that occurs preferentially on the azepine moiety with the major product being the 10,11-dihydroxy-10,11-dihydro-5H-dibenzo[*b*,*f*]azepine-5-carboxamide (10,11-dihydro-10,11-dihydroxycarbamazepine). Furthermore, determined double-bond equivalency (DBE), which represent on the number of rings and double bonds present in the molecule, is also consistent with the proposed structure.

It should be noted that this compound was also detected as a TP of CBZ by an improved Fenton's process (Ghauch et al., 2011) while an analogue product was identified in metabolic studies (Bernus et al., 1995; Miao and Metcalfe, 2003). In

general, 10,11-dihydro-10,11-dihydroxycarbamazepine, is considered one of the most important metabolite of CBZ and its presence has been confirmed in the environment, at higher concentrations than the parent drug (Miao et al., 2003; Petrovic et al., 2005). For example, 10,11-dihydro-10,11-dihydroxycarbamazepine was detected in the STP influent and effluent at 1571.7 and 1325.0 ng/L, respectively, compared with carbamazepine at 368.9 and 426.2 ng/L in the STP influent and effluent, respectively. In surface water, 10,11-dihydro-10,11-dihydroxycarbamazepine and CBZ were detected at concentrations of 2.2 and 0.7 ng/L, respectively. As in the case of the parent drug (CBZ) concentrations of 10,11-dihydro-10,11-dihydroxycarbamazepine were similar in the influent and effluent, indicating little removal during sewage treatment (Miao et al., 2003).

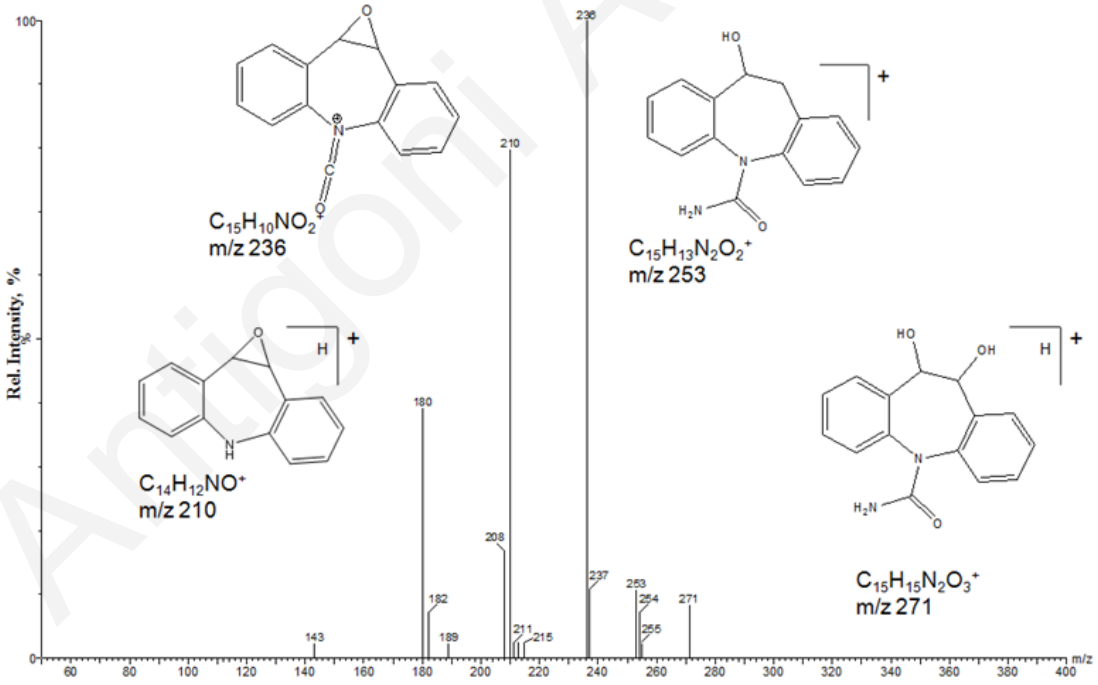

Figure 3.53 A: TP270 in product ion mode and proposed fragmentation patterns

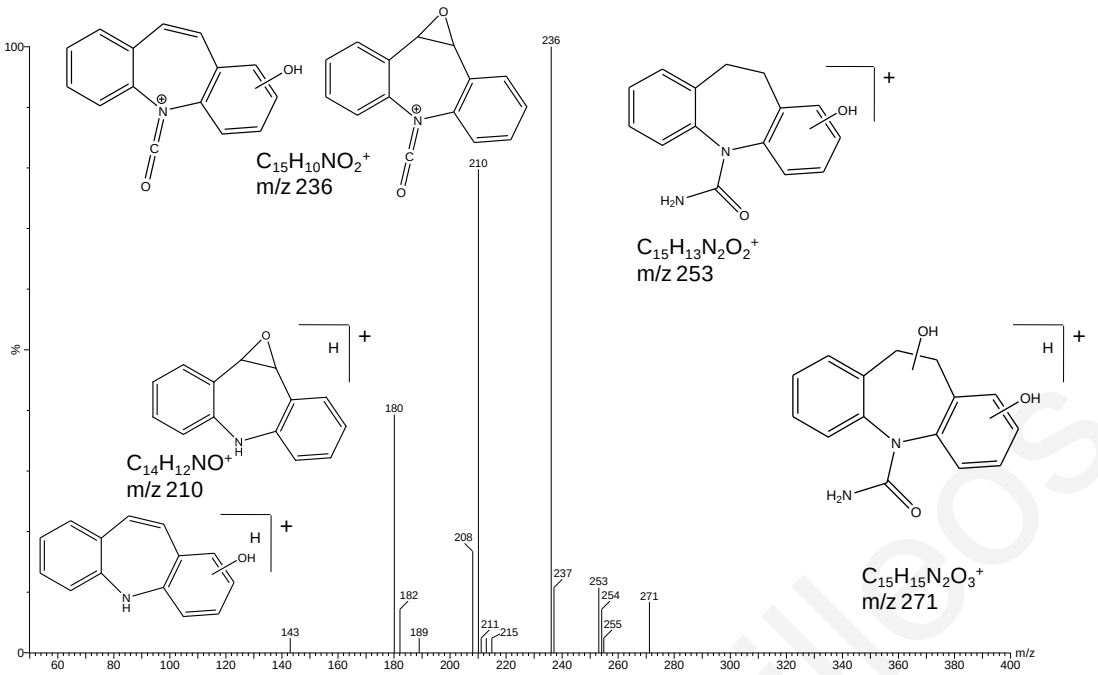

Figure 3.53 B: TP270 in product ion mode and proposed fragmentation patterns

Table 3.27: Accurate mass measurements of TP 271 as determined by UPLC–(+)ESI-QqToF-MS in product ion mode

Elemental composition	Meas. Mass	Calc. Mass	Error (mDa)	Error (ppm)	DBE
$C_{15}H_{15}N_2O_3$	271.1109	271.1083	2.6	9.7	9.5
$C_{15}H_{13}N_2O_2$	253.0995	253.0977	1.8	7.1	10.5
$C_{15}H_{10}NO_2$	236.0708	236.0712	-0.4	-1.7	11.5
$C_{14}H_{12}NO$	210.0898	210.0919	-2.1	-10	9.5
$C_{13}H_{10}N$	180.08	180.0813	-1.3	-7.2	9.5

Overall, the identified CBZ TPs are in accordance with previously published studies (Chiron et al., 2006; Kosjek et al., 2009; Calisto et al., 2011; Marco-Urrea et al., 2010). However, it is worth to point out that despite the same fragmentation pattern, in some cases, other structural isomers are proposed by the authors. For example, two different structural isomers have been proposed for TP 251 by Chiron et al. (2006), Lanhua Hu et al. 2009 and Calisto et al., 2011, as shown below.

.

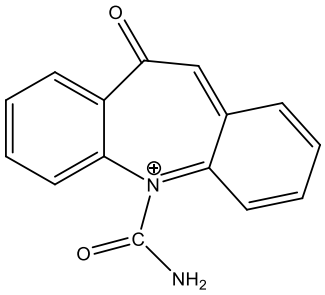

(Present study)

251

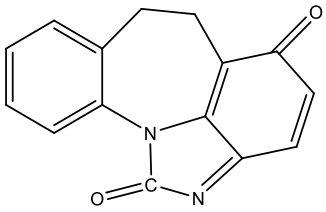

(Chiron et al., 2006, Lanhua Hu et al. 2009)

251

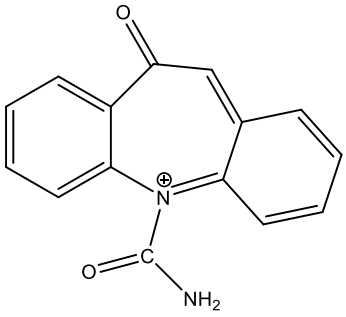

(Present study)

251

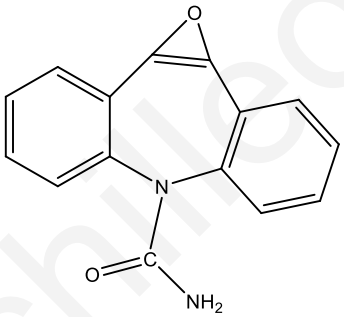

(Calisto et al., 2011)

251

It is apparent that by MS/MS, from spectra, we can only tentatively assign structures to their TPs. Thus, for their confirmation it would be good to combine various instrumental techniques.

Based on the above, further investigation is needed to confirm with certainty the structure of CBZ TPs. ^{1}H NMR methods or labeling experiments could be used in this direction in order to fully capitalize the structural elucidation of the CBZ TPs.

3.8.1.1 Profile of CBZ TPs

The formation of CBZ TPs was depicted in Figures 3.54 A, B and C. Profile of TPs was expressed as relative area (A/A_0) measured by integration of LC-MS peaks of the corresponding TP (A) and the parent drug in the control treatments at different irradiation times, since due to the lack of authentic analytical standards for the newly identified products their quantitative determination was not possible. In Figures 3.55, 3.56 and 3.57 the concentration profile of CBZ, 2-OH-CBZ, 3-0H-CBZ was depicted.

CBZ, 2-OH and 3-OH were quantified on QTRAP (as explained in quantitative analysis).

In heterogeneous photocatalysis (Figure 3.54A) with UV-A irradiation, TPs appear during 15 min of irradiation and remain during the whole experiment with different areas. At the beginning of the experiment the parent compound had an area of 3994. TP250 also had an area of 4 in 0 min of the experiment. In 15 min fifteen TPs appeared and TP270 and 2-OH-CBZ with highest areas. At the end of the experiment the areas decreased but the TPs remained in the solution. The area of the parent compound decreased during the experiment. TP268c and TP270 appear only in heterogeneous photocatalysis with UV-A irradiation and not in solar irradiation.
In solar irradiation (Figure 3.54 B), TPs appear also during 15 min of irradiation and remain with different areas during the whole experiment. At the beginning of the experiment the parent compound had an area of 3616. TP250 also had an area of 8 in 0 min of the experiment. 2-OH-CBZ and TP250 reached a maximum area of 86 and 82 respectively in 15 min. At the end of the experiment the areas decreased but the TPs remained in the solution. TP270a and TP270b appeared only in solar irradiation and sonophotocatalysis experiments.

In sonophotocatalysis (Figure 3.54 C), TPs appeared also during 15 min of irradiation and disappeared after 30 min of irradiation except TP250 appeared from the beginning of the experiment. TP223a, TP268e, TP268f and TP268g remain constant after 30 min of irradiation. TP266a, TP266b and TP266c appeared only in sonophotocatalysis.

From the quantification of the parent compound the degradation under UV-A, solar irradiation and sonophotocatalysis was 93.8%, 50 and 93%. Comparing the three processes the lowest degradation was with solar irradiation. The concentration of 2-OH-CBZ and 3-OH-CBZ for UV-A irradiation and sonophotocatalysis were approximately 0.35 and 0.5 mg/L in 15 min and at the end of the experiments their concentration decreased. For 2-OH-CBZ and 3-OH-CBZ the concentratons were in 120 min 0.096 and 0.135 respectively under UV-A irradiation and sonophotocatalysis. In solar irradiation the concentrations of the above TPs increased. For example in 15

min of irradiation the concentrations were 0.150 and 0.214 mg/L and after 120 min the concentrations were 0.358 and 0.590 mg/L.

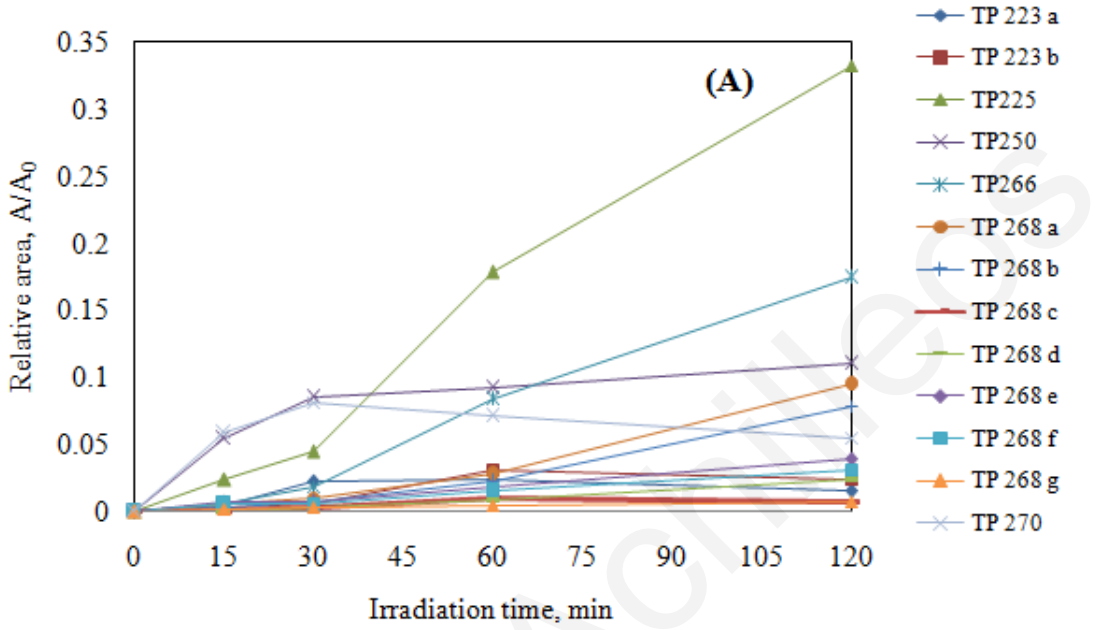

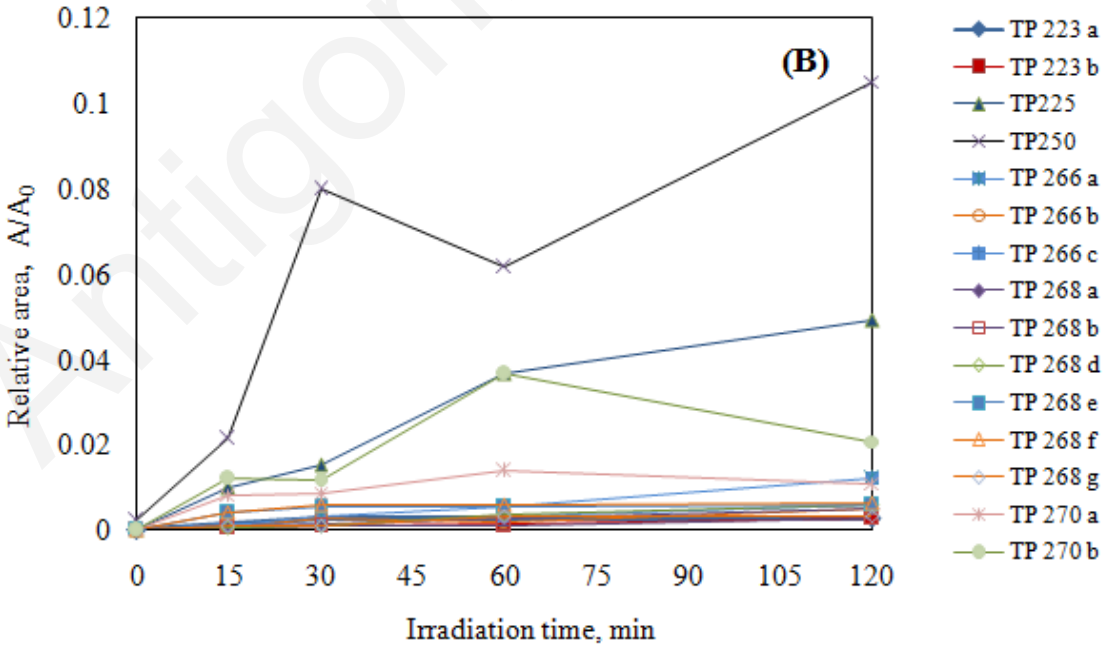

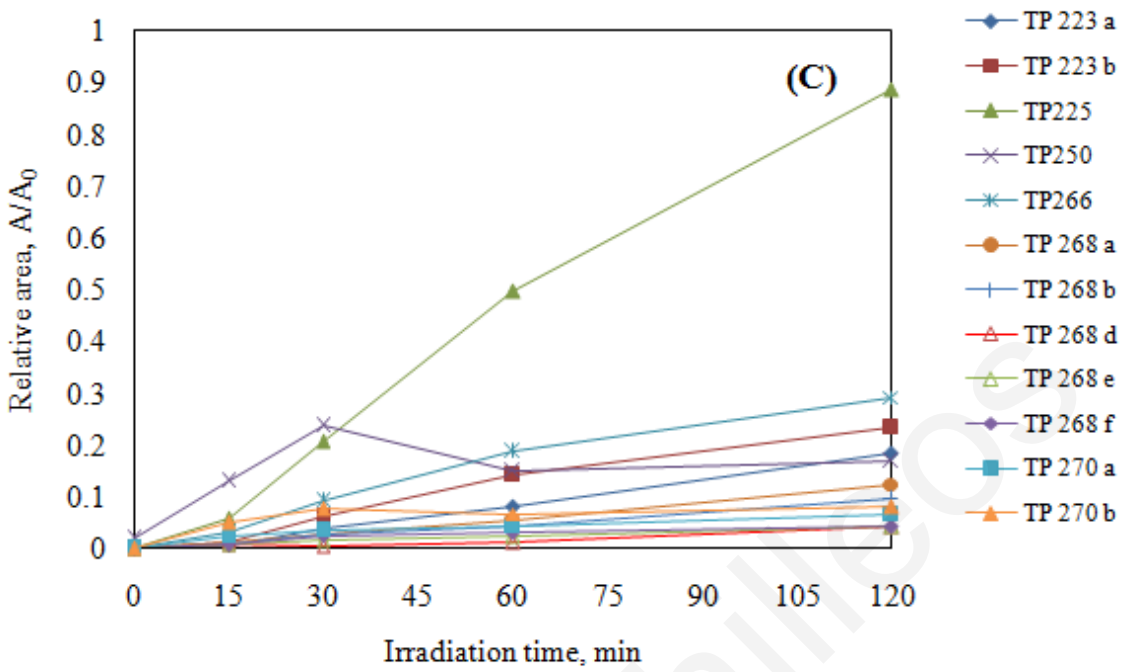

Figure 3.54: Profile of TPs (A) uva irradiation, (B) solar irradiation, (C) sonophotocatalysis, CBZ 10 mg/L, 100 mg/L catalyst loading

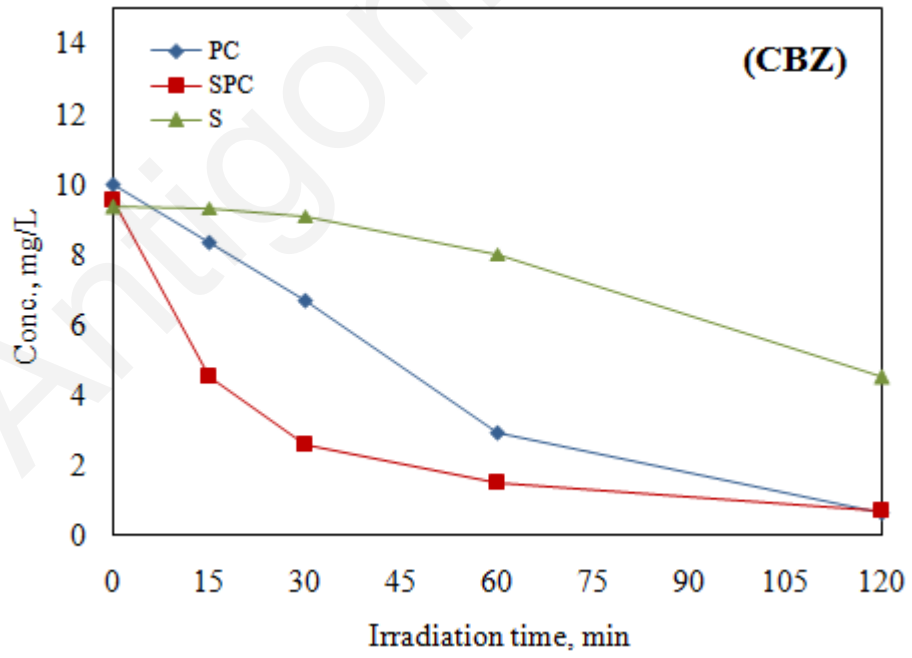

Figure 3.55: Concentration profile of CBZ 10 mg/L, 100 mg/L catalyst loading, during uva irradiation (PC), solar irradiation (S) and sonophotocatalysis (SPC)

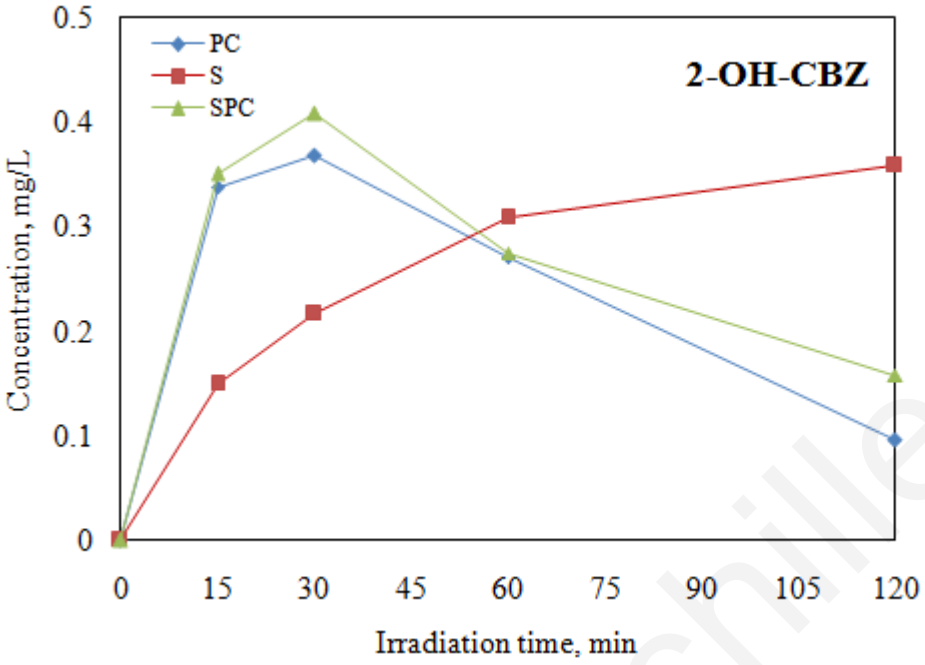

Figure 3.56: Concentration profile of 2-0H-CBZ, during uva irradiation (PC), solar irradiation (S) and sonophotocatalysis (SPC)

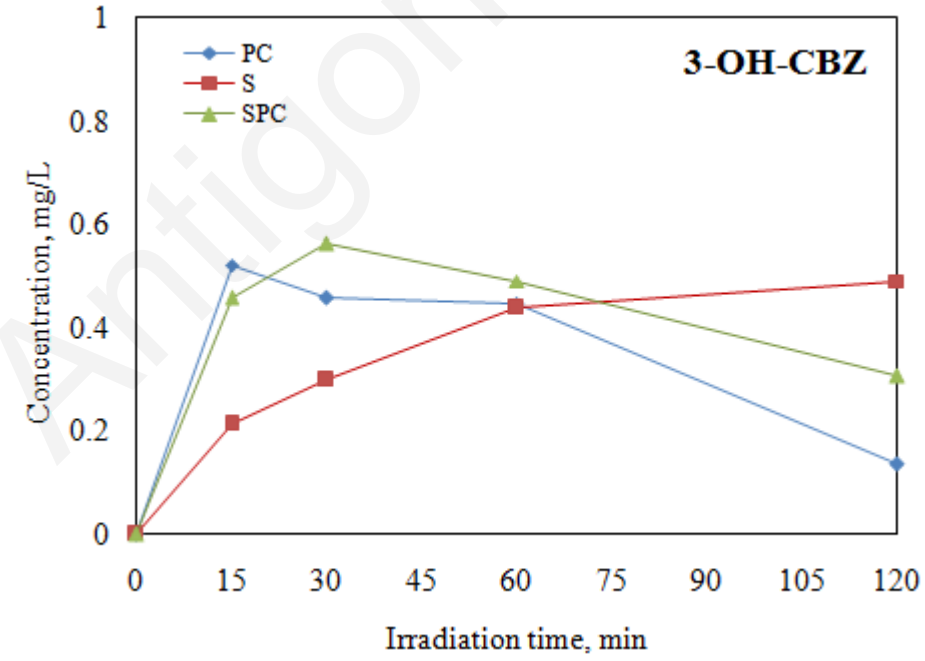

Figure 3.57: Concentration profile of 3-0H-CBZ, during uva irradiation (PC), solar irradiation (S) and sonophotocatalysis (SPC)

3.8.1.2 Mechanism of CBZ photocatalytic degradation

An overall view of carbamazepine degradation pathway is provided in Fig. 3.58. This scheme is merely indicative and is not intended to provide a comprehensive representation of the actual complexities of the degradation process.

On the basis of the foregoing results of the HPLC/ESI-QqLIT-MS and UPLC/ESI-QqToF-MS experiments and previous studies on the oxidation of CBZ (Vogna et al. 2004; Chiron et al., 2006; Hu et. Al, 2009; Li et al., 2011) two main routes (Figure 3.57) can be drawn as major steps during the transformation processes.

In the first pathway, initial attack of •OH to the aromatic ring moieties leading to hydroxylated derivatives. The last TPs were further oxidized and transformed to the formation of smaller and more oxidized molecules, such as anthranilic acid, salicylic acid, catechol and other intermediates.

In parallel reaction pathway, the hydroxylation of CBZ is occurred at the 10 position to give a radical intermediate that can evolve to give 10,11-epoxycarbamazepine. Subsequent oxidation or opening of epoxide ring would give a labile species that suffers facile ring contraction to give 9-acridine-9-carboxaldehyde. This latter would decompose to yield hydroxy-acridine.

The proposed mechanism is in accordance with previous published studied (Vogna et al. 2004; Chiron et al., 2006, Li et al., 2011).

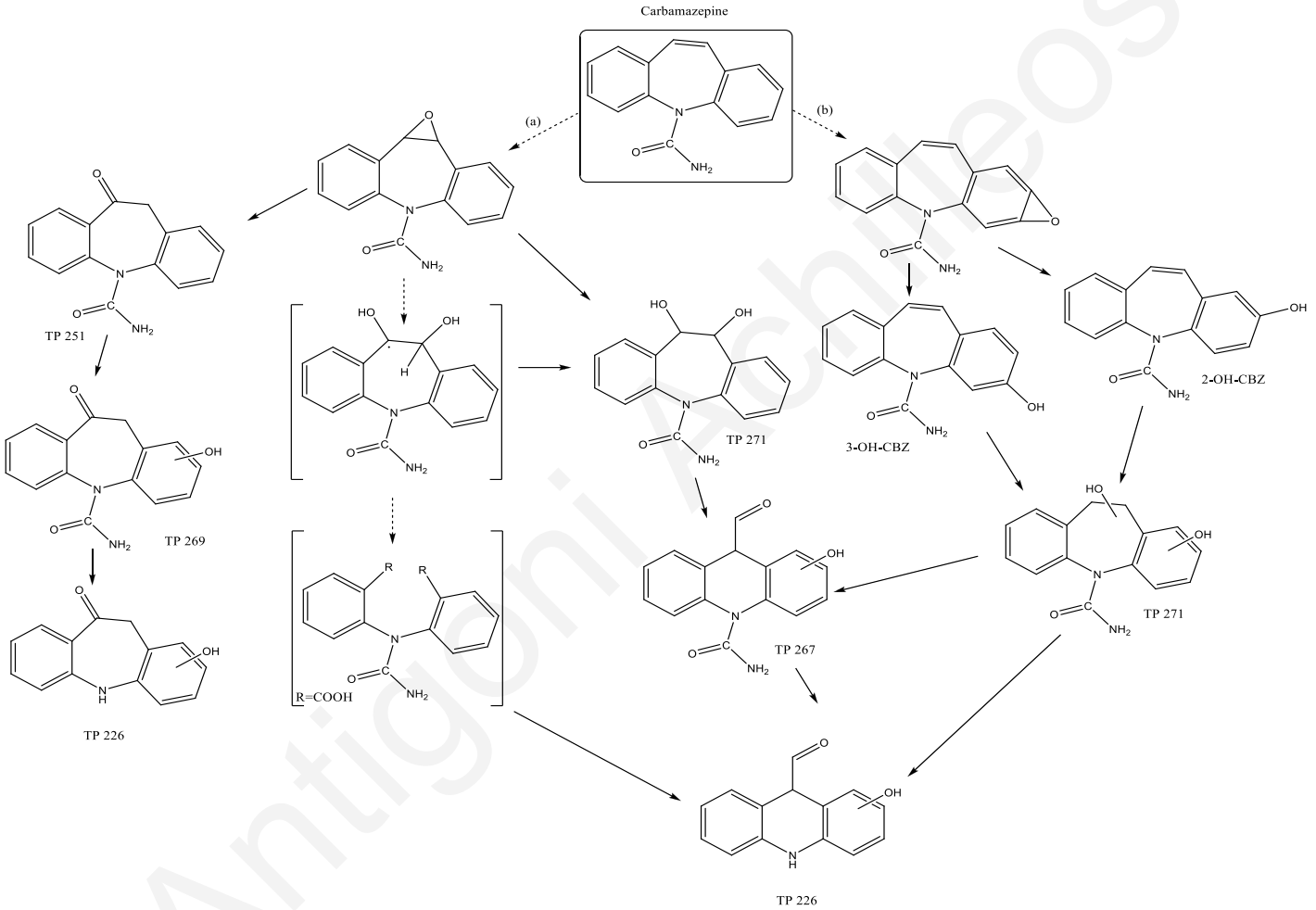

Figure 3.58: Proposed degradation pathway of CBZ

3.8.2. Ibuprofen

In order to identify reaction TPs of Ibuprofen (IBP) degradation, samples collected at various time intervals were analyzed by means of HPLC/ESI-QqLIT-MS and UPLC/ESI-QqToF-MS. Structural elucidation and interpretation of the fragmentation pathways of IBP and the detected TPs, were acquired by using a hybrid mass detector QqToF in the ESI(-) mode. The results indicate that all the tested treatments (S, SPC, PC) lead to degradation of the IBP and end up in the formation of a number of products including among others substituted phenols and aromatic carboxylic acids.

Tables 3.28-3.29 show the summary of the data related to the calculated and measured masses of fragment ions of IBP and its TPs determined in ESI(-)-MS^2 experiments on the QqToF instrument, together with the error between them, the proposed empirical formula corresponding to the compounds identified and the corresponding DBEs. The data presented in Tables 3.30-3.37, were obtained under optimized conditions of collision energy and cone voltage of the QqToF-MS. Most of the accurate mass results were found with an error of less than 2 ppm, thus providing a high degree of certainty in the assignment of formulas.

Table 3.28: Structure elucidation of IBP and its TPs (Experiments: solar (S), sonophotocatalysis (SPC) and photocatalysis(PC)).

Transformation products	$[M-H]^-$	Chemical structure (incl. negative charge)
IBP	205	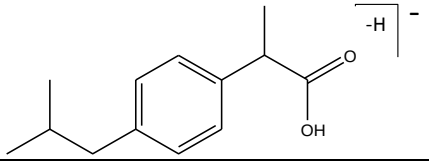
TP 134	133	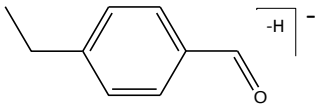
TP 150	149	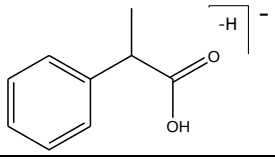
TP 176	175	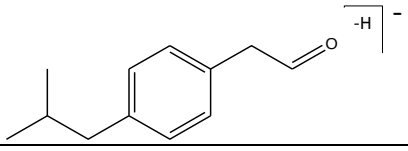

		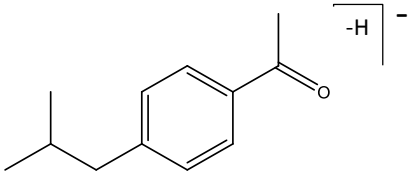
TP 178	177	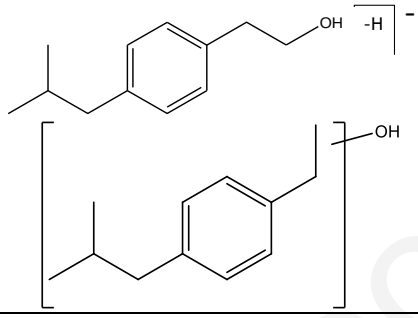
TP 222	221	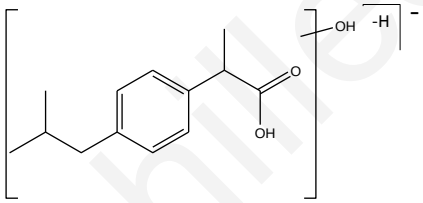
TP 208	207	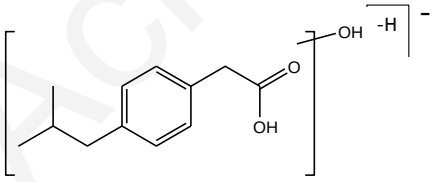
TP 192	191	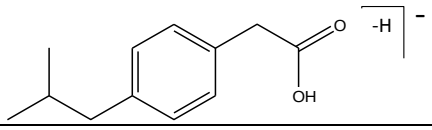

The screening of the treatment samples in (-)ESI scan mode allowed to confirm the formation of seven TPs (Figures 3.59-3.61). All of the identified products, except two (TP 208 and TP 192), are eluted before the main peak of IBP at 4.73 min (Table 3.28), indicating the formation of smaller and more polar products when compared to the parent compound.

Table 3.29: Accurate mass measurements of the transformation products (TP) of Ibuprofen (IBP) as determined by UPLC–(-)ESI-QqToF-MS in full scan mode

Compound	Ion	Elemental composition	Meas. Mass	Calc. Mass	Error (mDa)	Error (ppm)	DBE
IBP	$[M-H]^-$	$C_{13}H_{17}O_2$	205.1205	205.1229	-2.4	-11.7	5.5
TP134	$[M-H]^-$	C_9H_9O	133.0647	133.0653	-0.6	-4.5	5.5
TP150	$[M-H]^-$	$C_9H_9O_2$	149.0595	149.0603	-0.8	-5.4	5.5
TP176	$[M-H]^-$	$C_{12}H_{15}O$	175.1110	175.1123	-1.3	-7.4	5.5
TP178	$[M-H]^-$	$C_{12}H_{17}O$	177.1240	177.1279	-3.9	-22	4.5
TP222	$[M-H]^-$	$C_{13}H_{17}O_3$	221.1163	221.1178	-1.5	-6.8	5.5
TP208	$[M-H]^-$	$C_{12}H_{15}O_3$	207.1003	207.1021	-1.8	-8.7	5.5
TP192	$[M-H]^-$	$C_{12}H_{15}O_2$	191.1059	191.1072	-1.3	-6.8	5.5

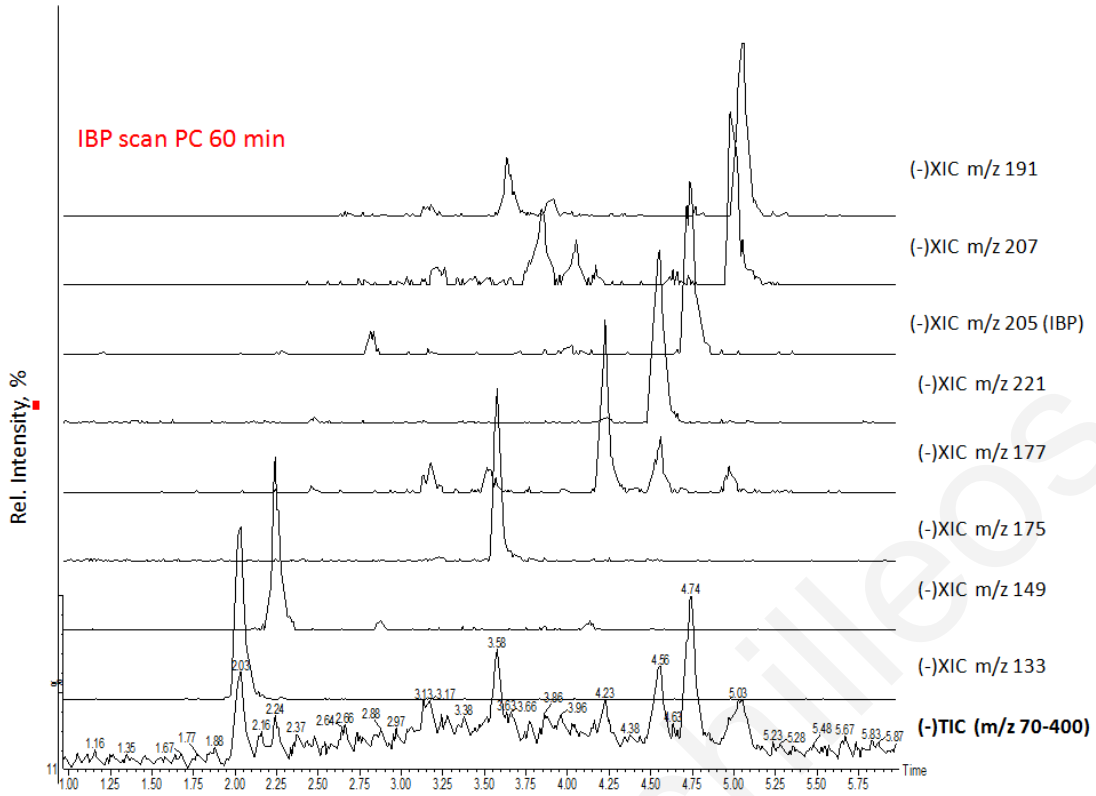

Figure 3.59: Total ion chromatogram (TIC) and extracted ion chromatograms (XIC) of IBP (10 mg/L) after 60 min under UV-A photocatalysis

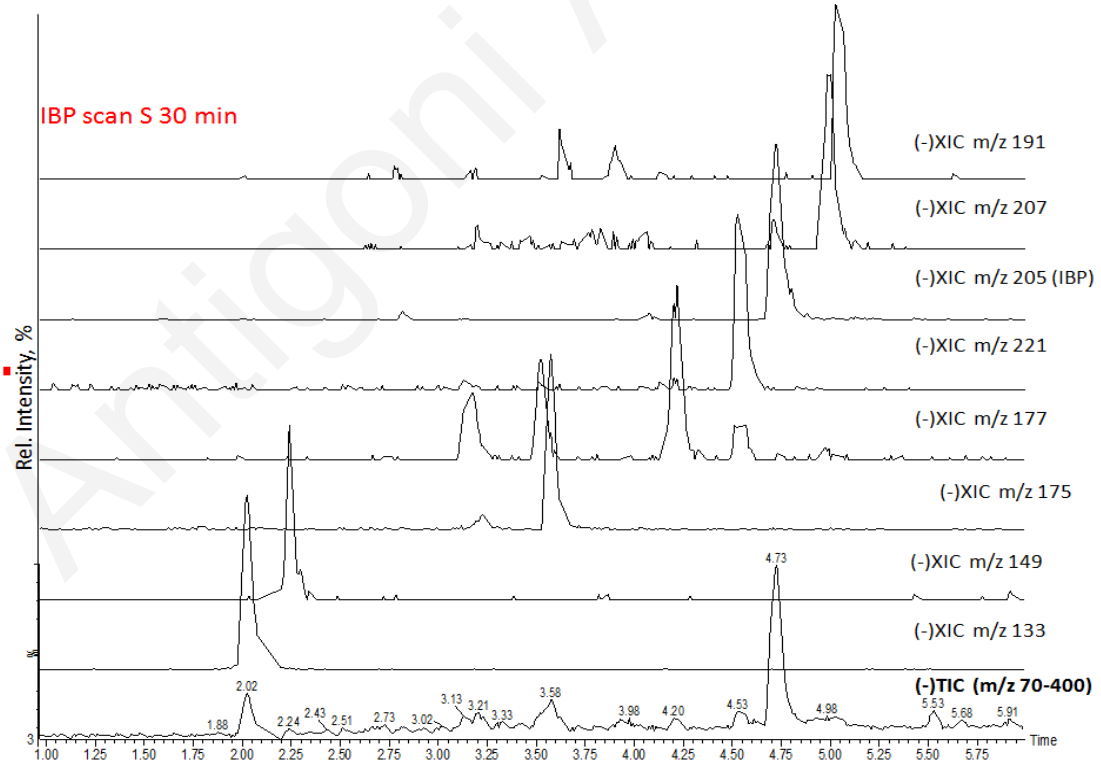

Figure 3.60: Total ion chromatogram (TIC) and extracted ion chromatograms (XIC) of IBP (10 mg/L) after 30 min under solar-driven photocatalysis

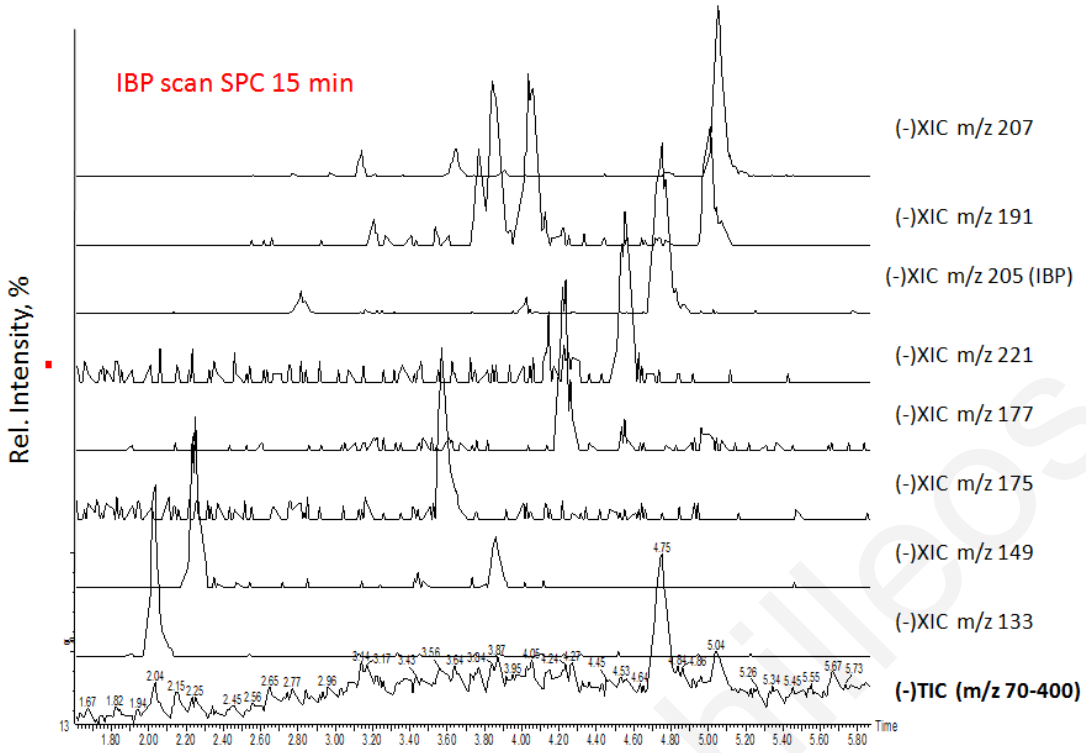

Figure 3.61: Total ion chromatogram (TIC) and extracted ion chromatograms (XIC) of IBP (10 mg/L) after 15 min under sonophotocatalysis

In Figure 3.61, the TIC shows the peak of IBP at t_R = 4.75 min that exhibited a molecular ion peak at *m/z* 205. The collision-induced-dissociation experiments with IBP (molecular ion $[M - H]^-$ 205) (Figure 3.62, Table 3.30) revealed the formation of only one characteristic fragment ion at m/z 161, as a consequence of the typical loss of CO_2 (44 Da).

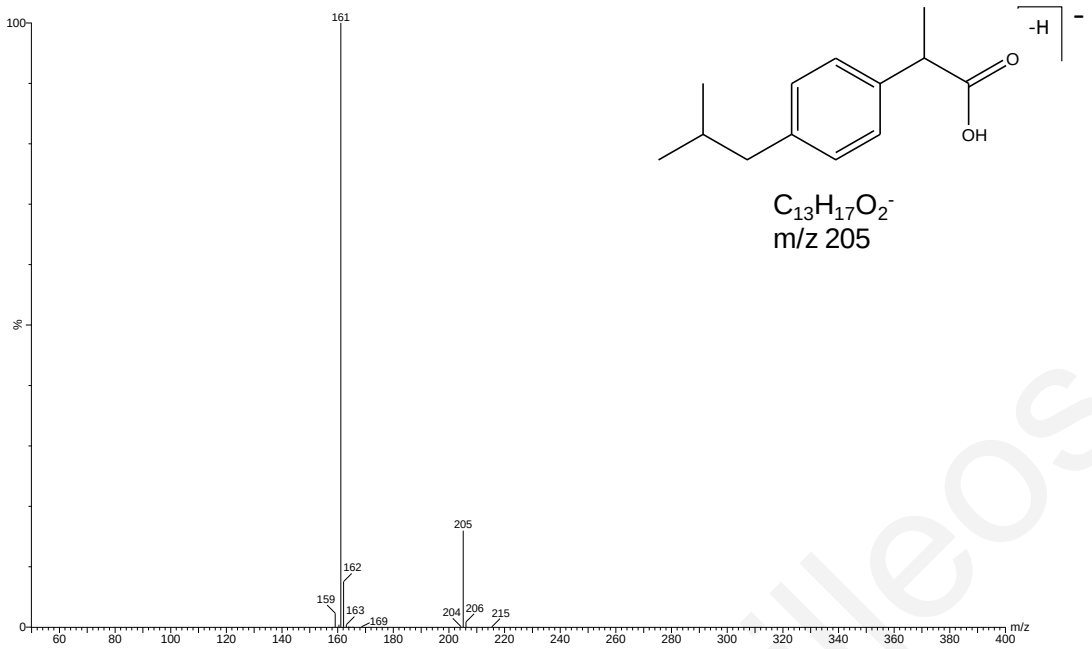

Figure 3.62: Spectra obtained in ESI(-)-MS^2 experiments at QqToF instrument for IBP and proposed fragmentation patterns

Table 3.30: Accurate mass measurements of IBP as determined by UPLC–(-)ESI-QqToF-MS in product ion mode

Mass	Calc. Mass	mDa	ppm	DBE	Formula
161.1311	161.133	-1.9	-11.8	4.5	$C_{12}H_{17}$
205.1212	205.1229	-1.7	-8.3	5.5	$C_{13}H_{17}O_2$

Compound TP 221, appearing at t_R = 4.53, yielded a m/z ratio of 221.1183 with an error smaller than 2.5 ppm. This accurate mass corresponds to the formula $C_{13}H_{17}O_3$, which is consistent with the mono- hydroxylated product of IBP, a known IBP metabolite. The spectra (MS^2 fragmentation of the molecular ion $[M - H]^-$ 221) showed decarboxylation to m/z 177. Although more isomers could be expected taking into account the free sites in the IBP molecule, only one of them was finally detected and identified during the tested treatment processes. In general, there are two principal options for this structural feature, either hydroxylation on the methylpropyl moiety or hydroxylation on the phenylcarboxylic moiety. Based on the MS^2 experiments performed at QqToF, we conclude that hydroxylation takes place preferentially on the

aromatic ring. This is also supported by the key fragment at m/z 93 which indicates that methylpropyl and carboxylic moieties of the IBP structure were intact. The theoretical accurate mass of this fragment (93.034) gave a unique elemental composition of C_6H_5O- (error -0.4 ppm). A second evidence comes from the presence of strong signal with accurate mass of 119.0506 (C_8H_7O- / 7.6 ppm) which can be easily assigned to elimination of isobutyl (58 Da) and carboxylic (44 Da) group from the primary compound (TP 221).

It should be noted that OH-IBP isomers have been also detected as photoproducts (Méndez-Arriaga et al., 2008; 2010; Zheng et al., in press), and as microbial transformation intermediates of IBP (Quintana et al., 2010). Furthermore, analogue isomers were identified in metabolic studies (Kepp et al., 1997) and in raw wastewaters as a human metabolite (Stumpf et al., 1998; Buser et al., 1999). However, in all cases, oxidation of isopropyl chain of IBP, yielding 2-hydroxy IBP and/or 1-hydroxy IBP is proposed by the authors. To the best of our knowledge a plausible structure of OH-IBP by addition of a OH group on the aromatic ring is tentatively identified and proposed in the present study for the first time.

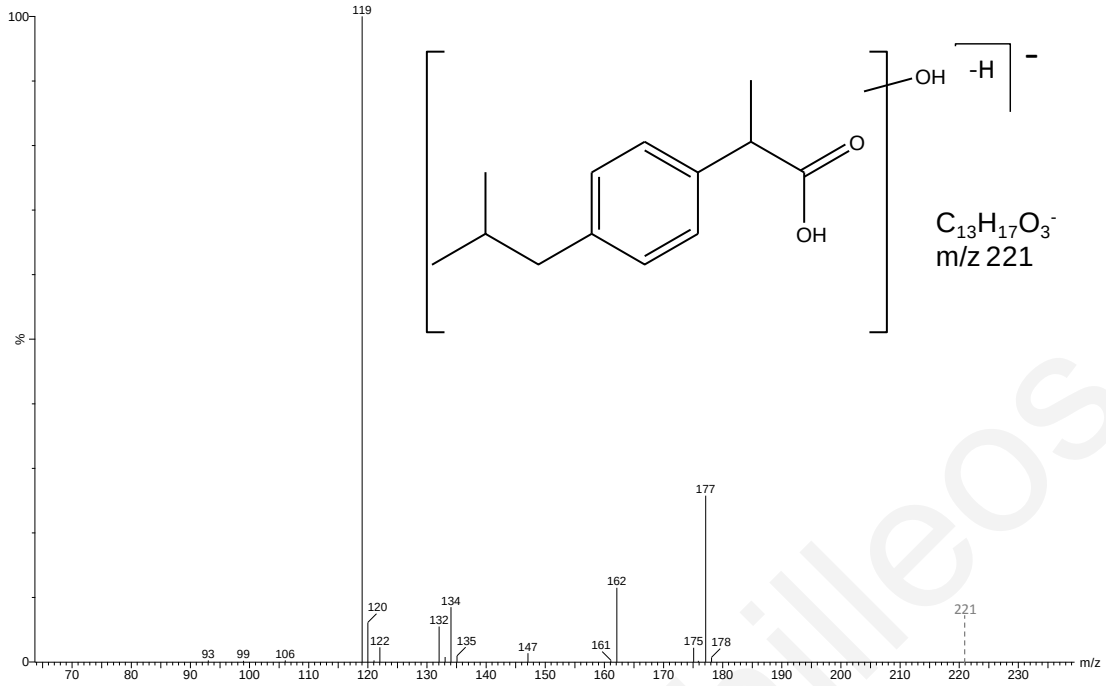

Figure 3.63: TP 222 in product ion mode

Table 3.31: Accurate mass measurements of TP 222 as determined by UPLC–(-)ESI-QqToF-MS in product ion mode

Mass	Calc. Mass	mDa	ppm	DBE	Formula
93.034	93.034	0	-0.4	4.5	C_6H_5O
119.0506	119.0497	0.9	7.6	5.5	C_8H_7O
122.0358	122.0368	-1	-8	5	$C_7H_6O_2$
132.0542	132.0575	-3.3	-25.1	6	C_9H_8O
134.0719	134.0732	-1.3	-9.4	5	$C_9H_{10}O$
147.0817	147.081	0.7	4.8	5.5	$C_{10}H_{11}O$
162.1033	162.1045	-1.2	-7.2	5	$C_{11}H_{14}O$
177.1274	177.1279	-0.5	-3.1	4.5	$C_{12}H_{17}O$
221.1183	221.1178	0.5	2.4	5.5	$C_{13}H_{17}O_3$

The ESI-MS^2 spectra patterns of TP 192 are consistent with 4-(1-carboxyethyl) benzoic acid. Evidence that in IBP degradation, direct demethylation takes place in parallel reaction with the hydroxylation process. The spectrum is characterized by the fragment ion at m/z 148 that arises from the typical loss of CO_2.

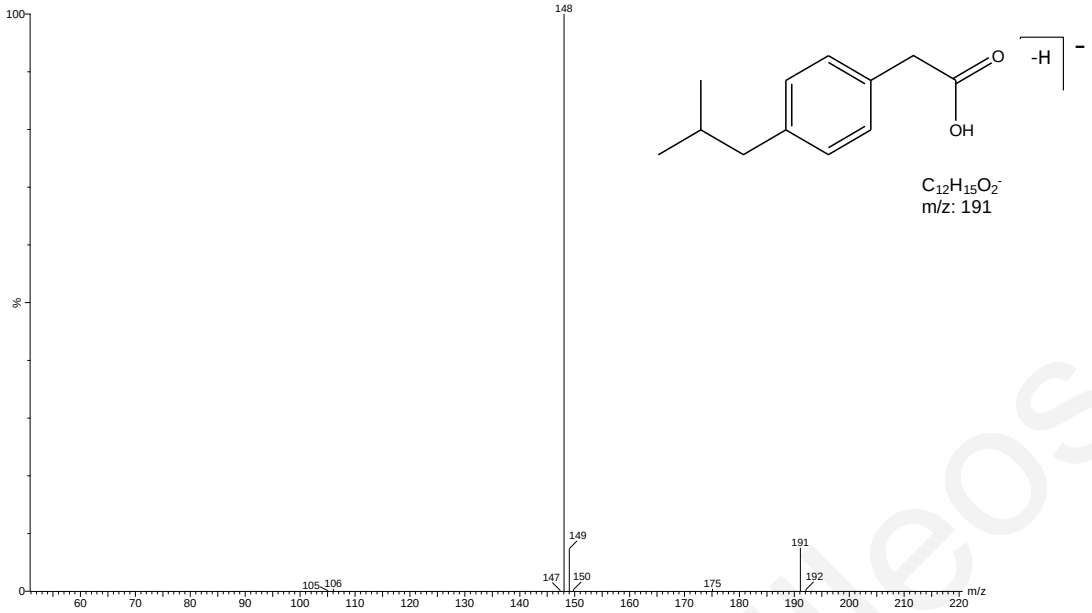

Figure 3.64: TP 192 in product ion mode and proposed fragmentation patterns

Table 3.32: Accurate mass measurements of TP 192 as determined by UPLC-(-)ESI-QqToF-MS in product ion mode

Mass	Calc. Mass	mDa	ppm	DBE	Formula
105.0333	105.034	-0.7	-6.7	5.5	C_7H_5O
148.0513	148.0524	-1.1	-7.6	6	$C_9H_8O_2$
175.1073	175.1123	-5.0	-28.5	5.5	$C_{12}H_{15}O$
191.1061	191.1072	-1.1	-5.8	5.5	$C_{12}H_{15}O_2$

The next TP derivative identified provided a molecular ion at *m/z* 207. Based on the best-fit formula of $C_{12}H_{15}O_3^-$ and the mass difference of 16 amu compared to the TP 191, the elemental composition may be rationalized by the formation of hydroxyl - demethylated IBP derivative. The loss of 43 Da, for the elimination of isopropyl radical, led to the appearance of the highest mass ion at m/z 164, which with further loss of methyl group resulted in the m/z 150 fragment ion.

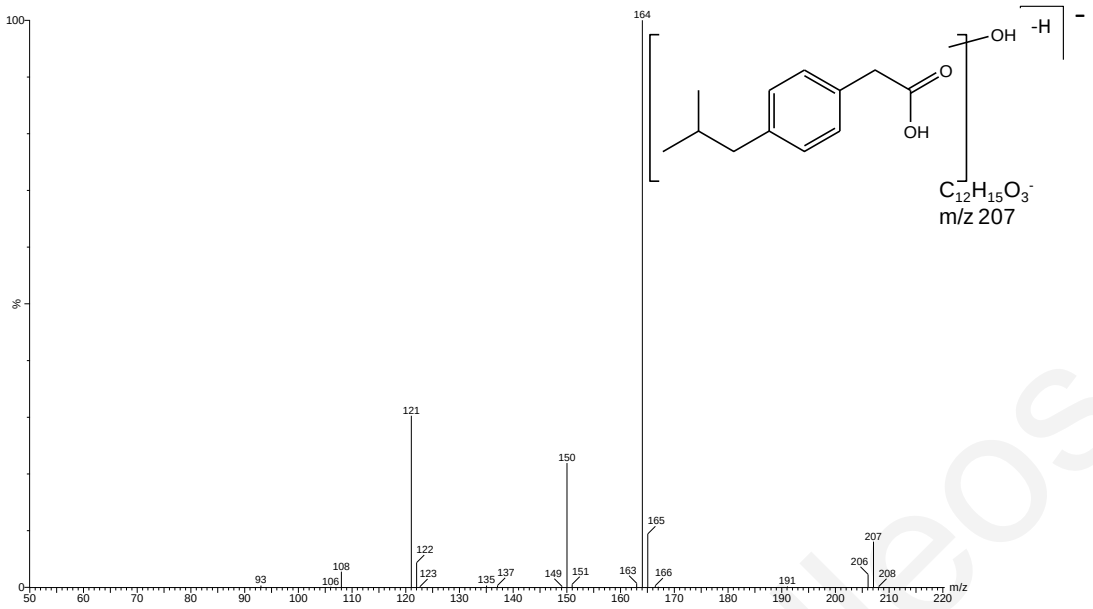

Figure 3.65: TP208 in product ion mode

Table 3.33: Accurate mass measurements of TP 208 as determined by UPLC-(-)ESI-QqToF-MS in product ion mode

Mass	Calc. Mass	mDa	ppm	DBE	Formula
93.0329	93.034	-1.1	-12.3	4.5	C_6H_5O
106.0453	106.0419	3.4	32.4	5	C_7H_6O
121.0293	121.029	0.3	2.9	5.5	$C_7H_5O_2$
135.0453	135.0446	0.7	5.1	5.5	$C_8H_7O_2$
150.0306	150.0317	-1.1	-7.3	6	$C_8H_6O_3$
164.0500	164.0473	2.7	16.2	6	$C_9H_8O_3$
191.0697	191.0708	-1.1	-5.9	6.5	$C_{11}H_{11}O_3$
207.101	207.1021	-1.1	-5.4	5.5	$C_{12}H_{15}O_3$

Decarboxylation of TP 221 led to the formation of TP 178 with m/z 177 molecular ion. The spectra is characterized by the fragment ion at m/z 119 that arises from the combined loss of isobutyl moiety and hydrogen abstraction.

This product (TP 177) has been also identified as major photoproduct under photo-Fenton (Méndez-Arriaga et al. 2010) and photocatalytic TiO_2 degradation of IBP (Méndez-Arriaga et al. 2008) as well as under degradation with gamma irradiation process (Zheng et al., in press).

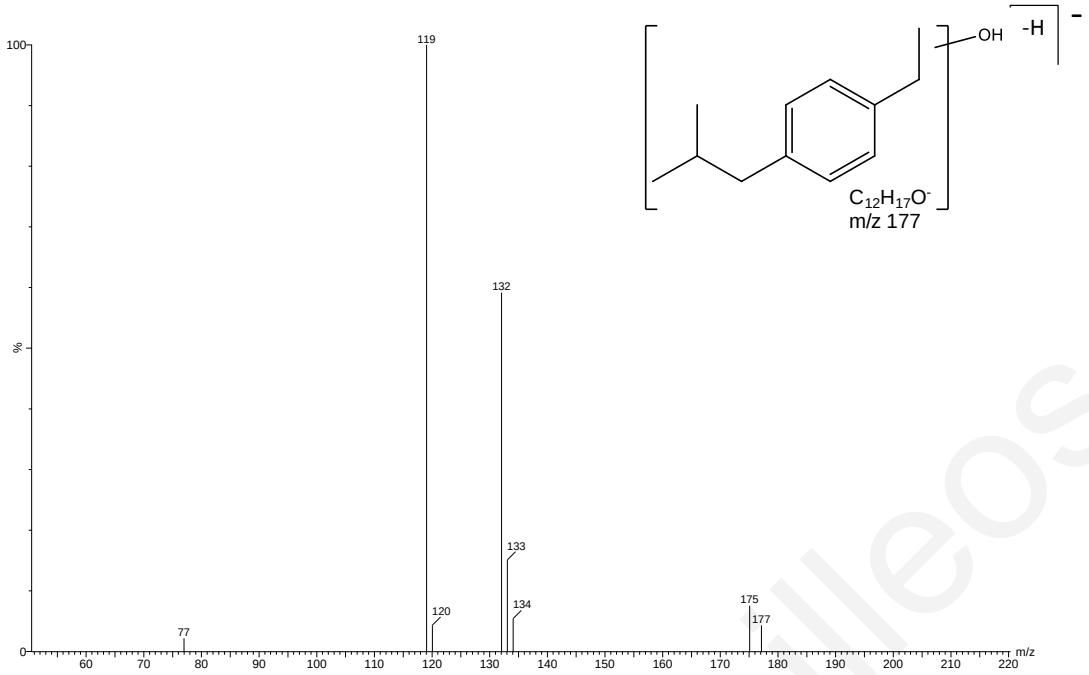

Figure 3.66: TP 178 in product ion mode

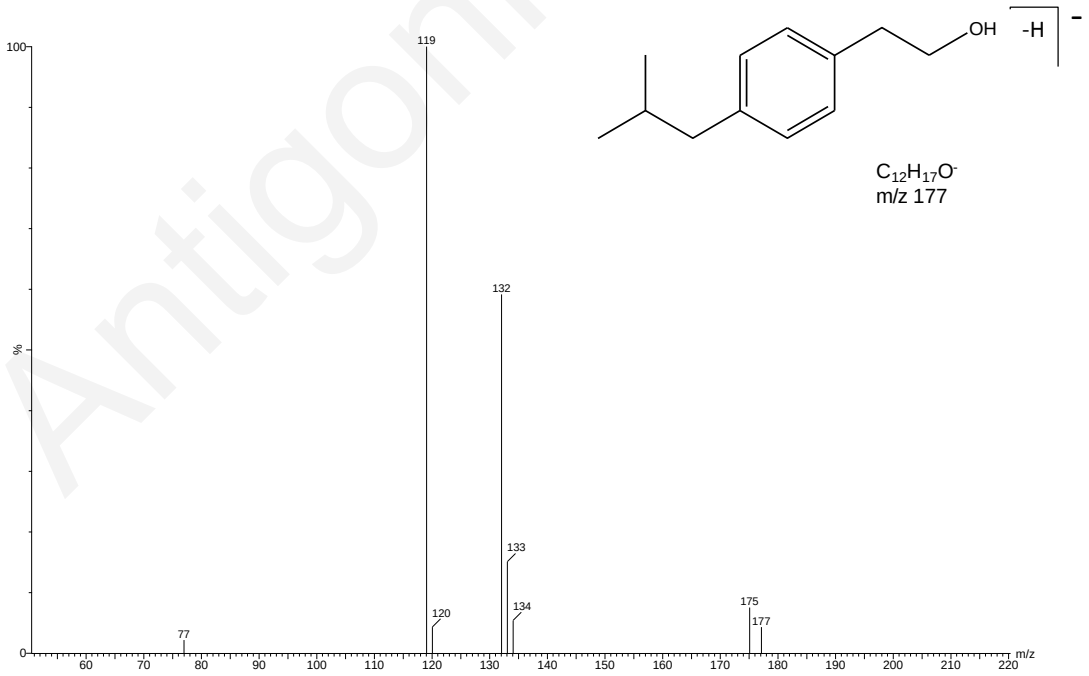

Figure 3.67: TP 177 in product ion mode

Table 3.34: Accurate mass measurements of TP 178 as determined by UPLC-(-)ESI-QqToF-MS in product ion mode

Mass	Calc. Mass	mDa	ppm	DBE	Formula
119.0492	119.0497	-0.5	-4.1	5.5	C_8H_7O
132.0568	132.0575	-0.7	-5.4	6	C_9H_8O
134.0726	134.0732	-0.6	-4.5	5	$C_9H_{10}O$
162.1059	162.1045	1.4	8.9	5	$C_{11}H_{14}O$
177.1284	177.1279	0.5	2.6	4.5	$C_{12}H_{17}O$

The next TP identified provided a molecular ion at m/z 175 (TP 176). Based on the best-fit formula of $C_{12}H_{15}O$ and the mass difference of 2 amu compared to the TP 178, the elemental composition may be rationalized by the formation of keto-derivative.

Based on the MS^2 spectrum of this product that shows the presence of characteristic fragment ion at m/z 147 corresponding to the loss of two methyl groups, which with further detachment of $CH_2C=O$ moiety and hydrogen abstraction resulted in the m/z 103 fragment ion, the structure of 4-isobutylacetophenone would be proposed as more predominated. The formation of 4-isobutylacetophenone (TP 176) has been also reported as main IBP intermediate by the photo-Fenton (Méndez-Arriaga et al. 2010), and photocatalytic sonolytic and sonophotocatalytic (Madhavan et al., 2010) degradation of IBP. Furthermore, Caviglioli et al. (2002), observed its formation during the oxidative degradation of IBP using permanganate solution.

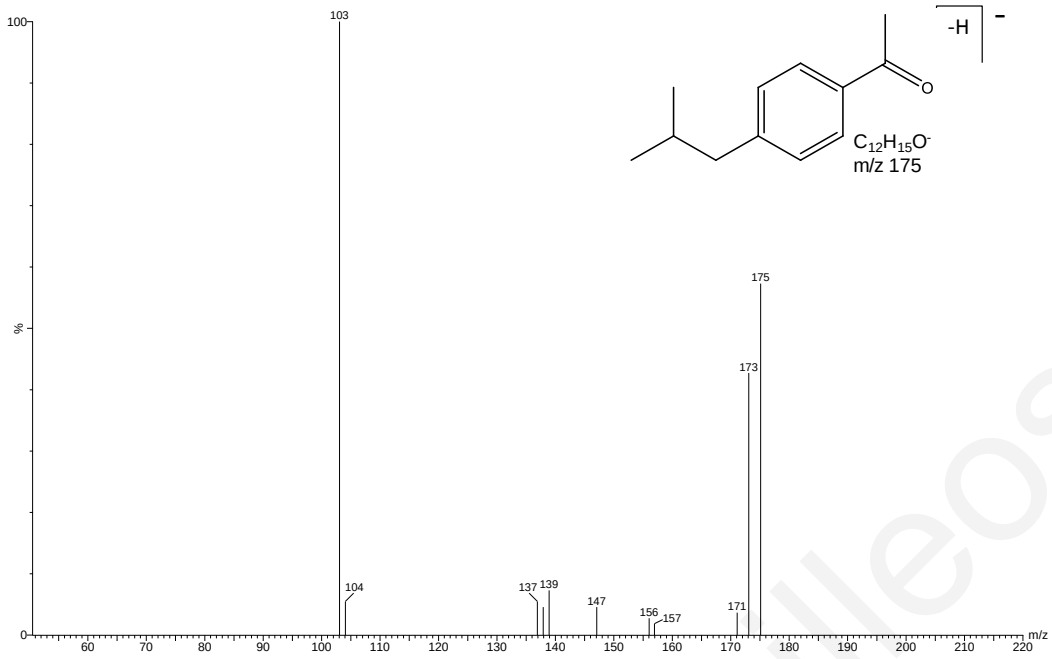

Figure 3.68: TP 176 in product ion mode

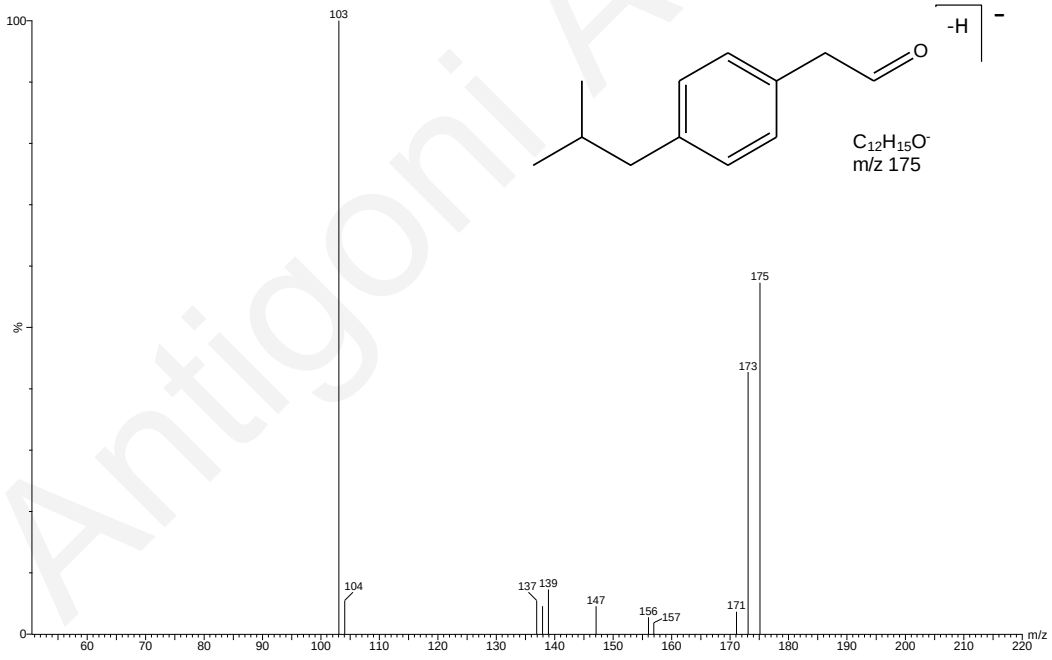

Figure 3.69: TP 176 in product ion mode

Table 3.35: Accurate mass measurements of TP 176 as determined by UPLC-(-)ESI-QqToF-MS in product ion mode

Mass	Calc. Mass	mDa	PPM	DBE	Formula
103.0551	103.0548	0.3	3.2	5.5	C_8H_7
147.0814	147.081	0.4	2.8	5.5	$C_{10}H_{11}O$
156.0575	156.0575	0	0	8	$C_{11}H_8O$
171.0815	171.081	0.5	2.9	7.5	$C_{12}H_{11}O$
173.095	173.0966	-1.6	-9.2	6.5	$C_{12}H_{13}O$
175.1108	175.1123	-1.5	-8.6	5.5	$C_{12}H_{15}O$

Also, the product with the m/z value 133 may correspond to 4-ethylbenzaldehyde. The loss of 28 Da, typical for CO group led to the appearance of the fragment ion at m/z 105.

The strong signals observed at m/z 131 and m/z 103 would be attributed to the intramolecular cyclization of the TP 134, as presented in the following scheme.

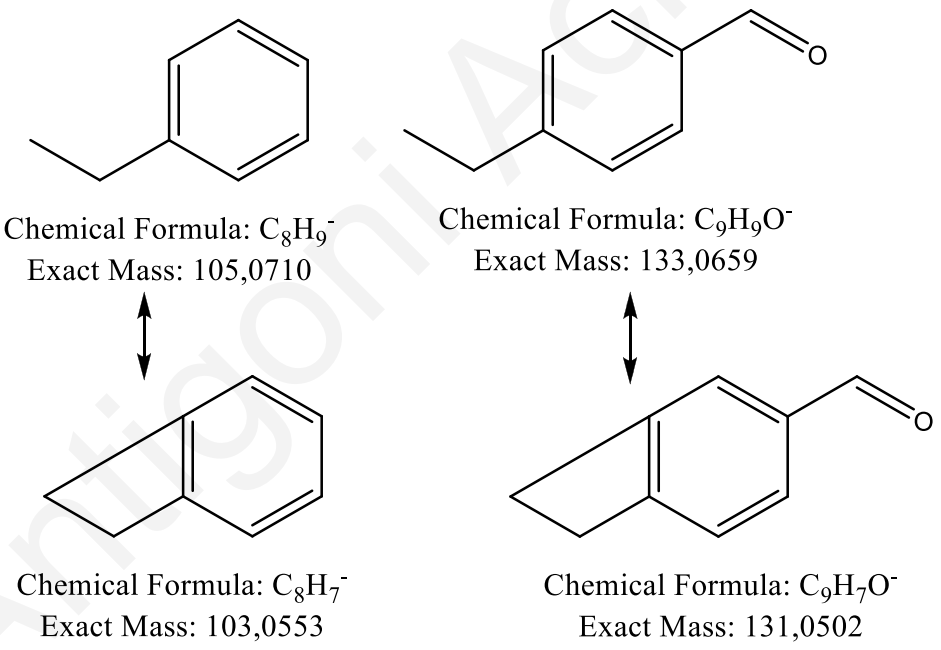

This product (TP 134) has been also reported as main IBP intermediate by the photoelectron-Fenton (Skoumal et al., 2009), photo-Fenton (Méndez-Arriaga et al., 2010) and photocatalytic (Méndez-Arriaga et al., 2008; Madhavan et al., 2010), sonolytic and sonophotocatalytic (Madhavan et al., 2010) degradation of IBP as well as by gamma irradiation process (Zheng et al., in press).

Figure 3.70: TP 134 in product ion mode

Table 3.36: Accurate mass measurements of TP 134 as determined by UPLC-(-)ESI-QqToF-MS in product ion mode

Mass	Calc. Mass	mDa	ppm	DBE	Formula
103.0549	103.0548	0.1	1	5.5	C_8H_7
105.0355	105.034	1.5	14.3	5.5	C_7H_5O
131.0489	131.0497	-0.8	-6.1	6.5	C_9H_7O
133.0648	133.0653	-0.5	-3.8	5.5	C_9H_9O

Finally, the last detected intermediate product of photocatalytic degradation of IBP was TP 150, with the molecular ion m/z 149. It was assumed that TP 150 was a consequence of cleavage of isobutyl moiety from the primary molecule (m/z 205). The loss of 15 Da typical for methyl group resulted in a very stable fragment ion at m/z 134.

To the best of our knowledge this compound TP 150 was the only one from the aforementioned TPs that have been identified by adopting solar, photocatalytic and sonophotocatalytic processes and have not been found with in vivo metabolic experiments and other advanced oxidation studies.

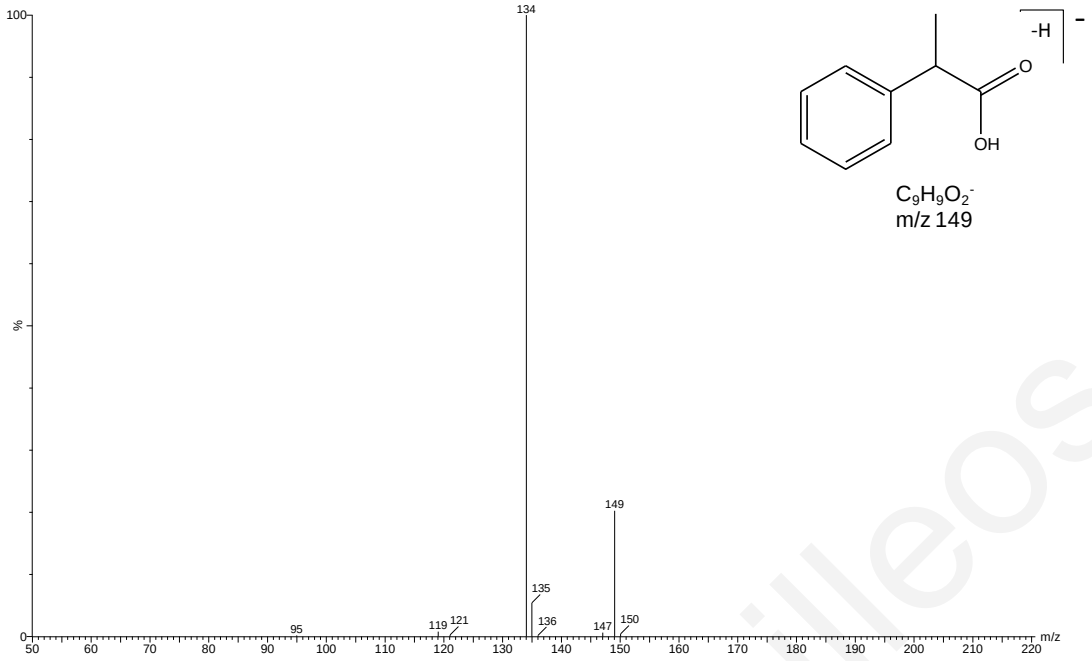

Figure 3.71: TP 150 in product ion mode

Table 3.37: Accurate mass measurements of TP 150 as determined by UPLC-(-)ESI-QqToF-MS in product ion mode

Mass	Calc. Mass	mDa	ppm	DBE	Formula
119.0487	119.0497	-1.0	-8.3	5.5	C_8H_7O
134.0365	134.0368	-0.3	-2.1	6	$C_8H_6O_2$
149.0605	149.0603	0.2	1.3	5.5	$C_9H_9O_2$

3.8.2.1 Profile of IBP TPs

The formation of IBP TPs was depicted in Figures 3.71A, B and C was expressed as relative intensity (Relative Intensity TPs /Relative Intensity IBP) measured by integration of LC-MS peaks of the corresponding TP (Relative Intensity) and the parent drug in the control treatments at different irradiation times, since due to the lack of authentic analytical standards for the newly identified products their quantitative determination was not possible.

In heterogeneous photocatalysis with uva irradiation (Figure 3.72 A), TPs appear during 15 min of irradiation and remain with different intensities during the whole experiment. TP133 and TP221 reach a maximum relative intensity of 70 and 60 respectively while the relative intensity of the parent compound was 26 at 15 min of

irradiation and 100 (0 min of irradiation). At 30 min of irradiation the relative intensities of the TPs were higher than the intensities in 15 min. TP149, TP177b, TP177c, TP177e, TP221 and TP191a relative intensities remained stable. TP177e relative intensity remained stable during the irradiation time of the whole experiment. In 120 min of irradiation TP133 had the highest relative intensity and TP177a the lowest. The relative intensity of the parent compound decreased during the experiment.

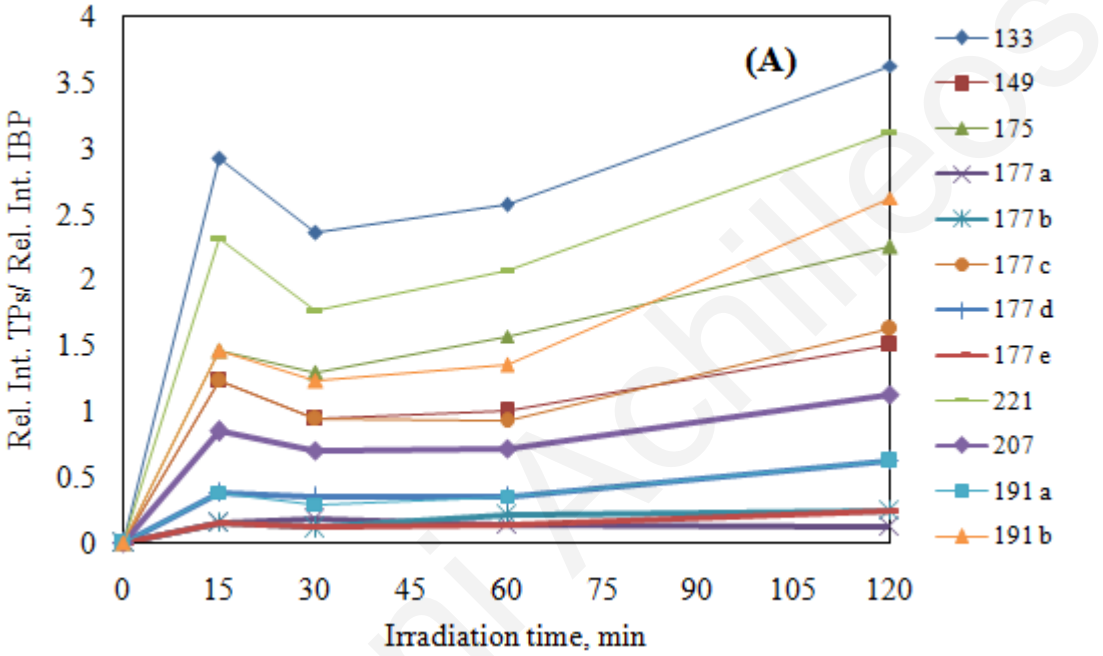

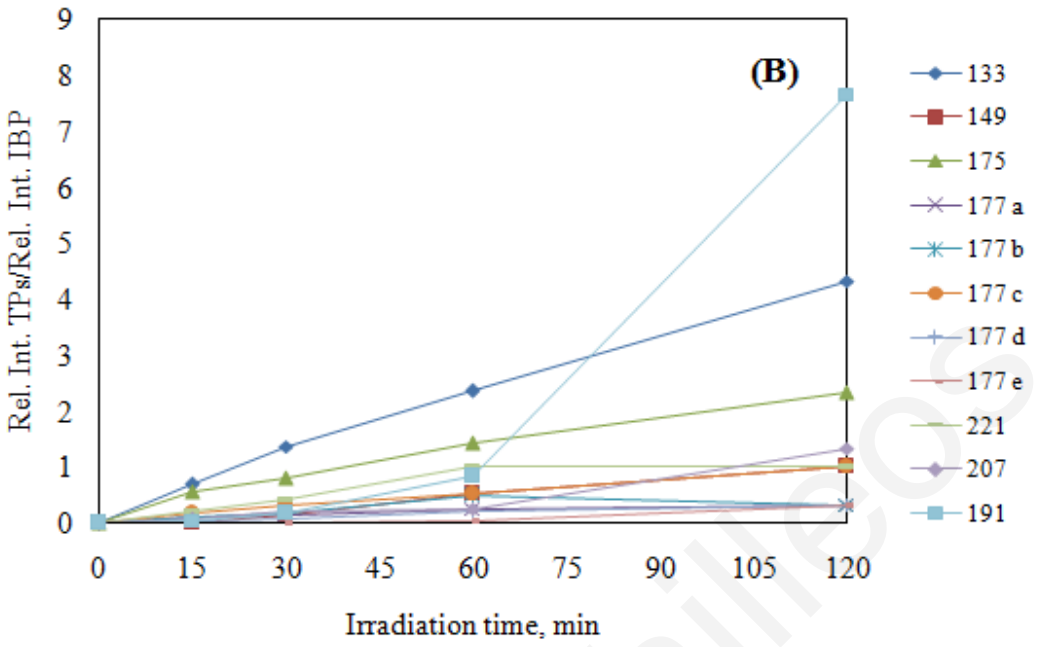

In solar irradiation (Figure 3.72 B), TPs appear also during 15 min of irradiation and remain with different intensities during the whole experiment. TP133 and TP175 reach a maximum relative intensity of 60 and 48 respectively while the relative intensity of the parent compound was 86 at 15 min of irradiation and 116 (0 min of irradiation). At 30 min of irradiation the relative intensities of the TPs were higher than the intensities in 15 min. TP133 and TP175 have the highest relative intensities. TP177e appeared in the first 60 min. In 120 min the relative intensities of the TPs and the parent compound decreased except TP191b. The relative intensity of the TP191b was the highest. The relative intensity of the parent compound decreased during the experiment.

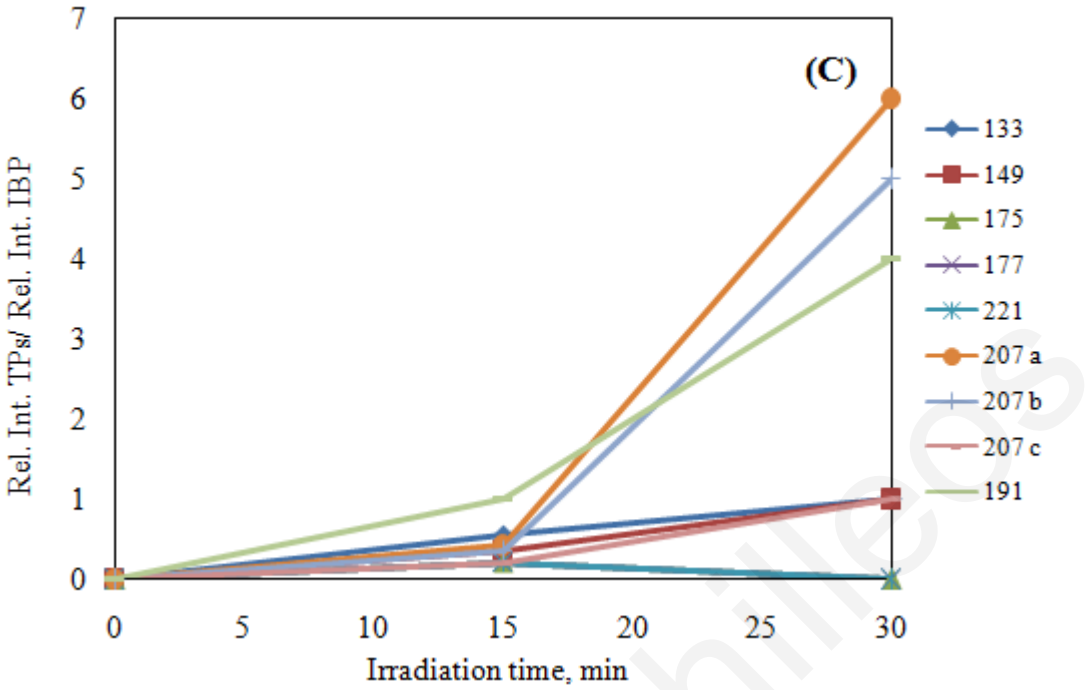

Figure 3.72: Profile of TPs (A) uva irradiation, (B) solar irradiation, (C) sonophotocatalysis, IBP 10 mg/L, 500 mg/L catalyst loading

In sonophotocatalysis (Figure 3.72 C), TPs appeared also during 15 min of irradiation and disappeared after 30 min of irradiation. TP175, TP177 and TP221 appear during 15 min and disappear after 15 min.

Below in Figure 3.73 the concentration profile of IBP 10 mg/L with the presence of 500 mg/L TiO_2 is shown. The degradation of IBP during photocatalyisis under uva, solar irradiation and sonophotocatalysis was 84.3, 95.8 and 99.8% in 120 min respectively.

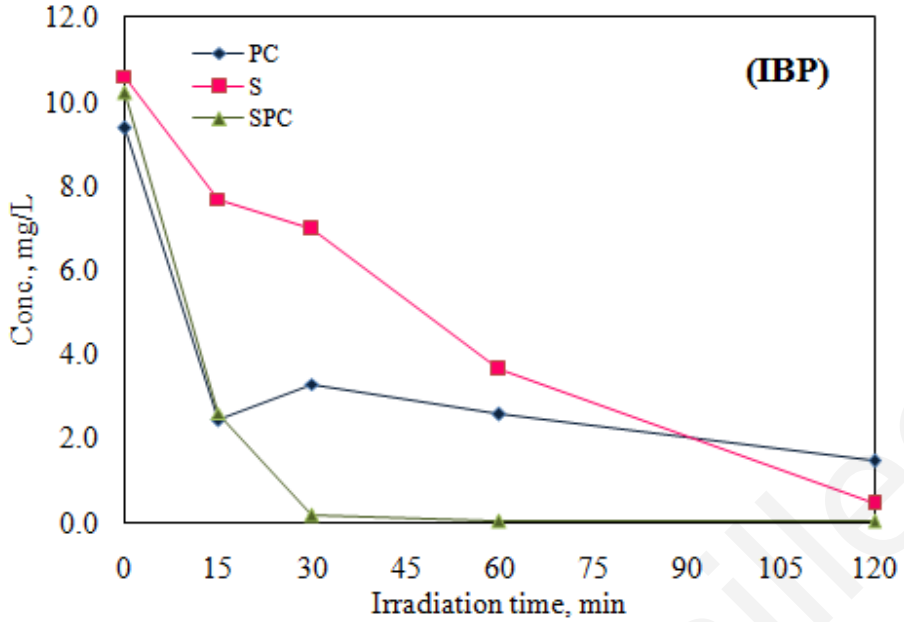

Figure 3.73: Concentration profile of IBP 10 mg/L, 500 mg/L catalyst loading, during uva irradiation (PC), solar irradiation (S) and sonophotocatalysis (SPC)

3.8.2.2 Mechanism of IBP photocatalytic degradation

Overall, no differences were observed in the type of TPs identified among experiments carried - solar, photocatalysis and sonophotocatalysis. However, it is worth to point out that five isomers were identified for the TP 178 in the case of S and PC, while only one in the case of SPC. Furthermore, two isomers of TP 191 were identified in the case of PC and only one in the case of S and SPC. Finally, as regards TP 208, three isomers were identified only in the case of SPC.

On the basis of the foregoing results of the HPLC/ESI-QqLIT-MS and UPLC/ESI-QqToF-MS experiments and previous studies on the oxidation (Caviglioli et al., 2002; Méndez-Arriaga et al., 2008, 2010; Madhavan et al. 2010; Zheng et al., in press), biodegradation (Quintana et al., 2005) and metabolism of IBP (Stumpf et al., 1998; Buser et al., 1999; Marco-Urrea et al., 2009) three competitive pathways (Figure 3.74) can be drawn, in which hydroxylation, demethylation, decarboxylation, cleavage of isobutyl moiety, and oxidation of hydroxyl groups are described as major steps during the transformation processes.

In the first pathway, either the methylpropyl or the phenylcarboxylic moiety of the IBP molecule is attacked by HO• to form mono-hydroxylated species (TP 221). The last TPs were either further oxidized or induced the loss of the carboxylic moiety leading to the formation of decarboxylated derivatives (TP 177, TP 175), which further transformed to TP 134.

In parallel reaction pathway, a methyl group of IBP molecule is attacked by HO• to form demethylated intermediates (TP 191). These TPs undergoes the same mechanism, via hydroxylation (TP 207), oxidation, demethylation and decarboxylation and finally transformed to lower molecular weight products before mineralization.

In the third pathway, the transformation can initially proceed through the detachment of isobutyl group by leading to the formation of 2-phenylpropanoic acid (TP 150).

All the above-described intermediates were further transformed by an oxidative opening of the aromatic ring, giving rise to the formation of smaller and more oxidized molecules, such as short carboxylic acids (e.g. formic, etc).

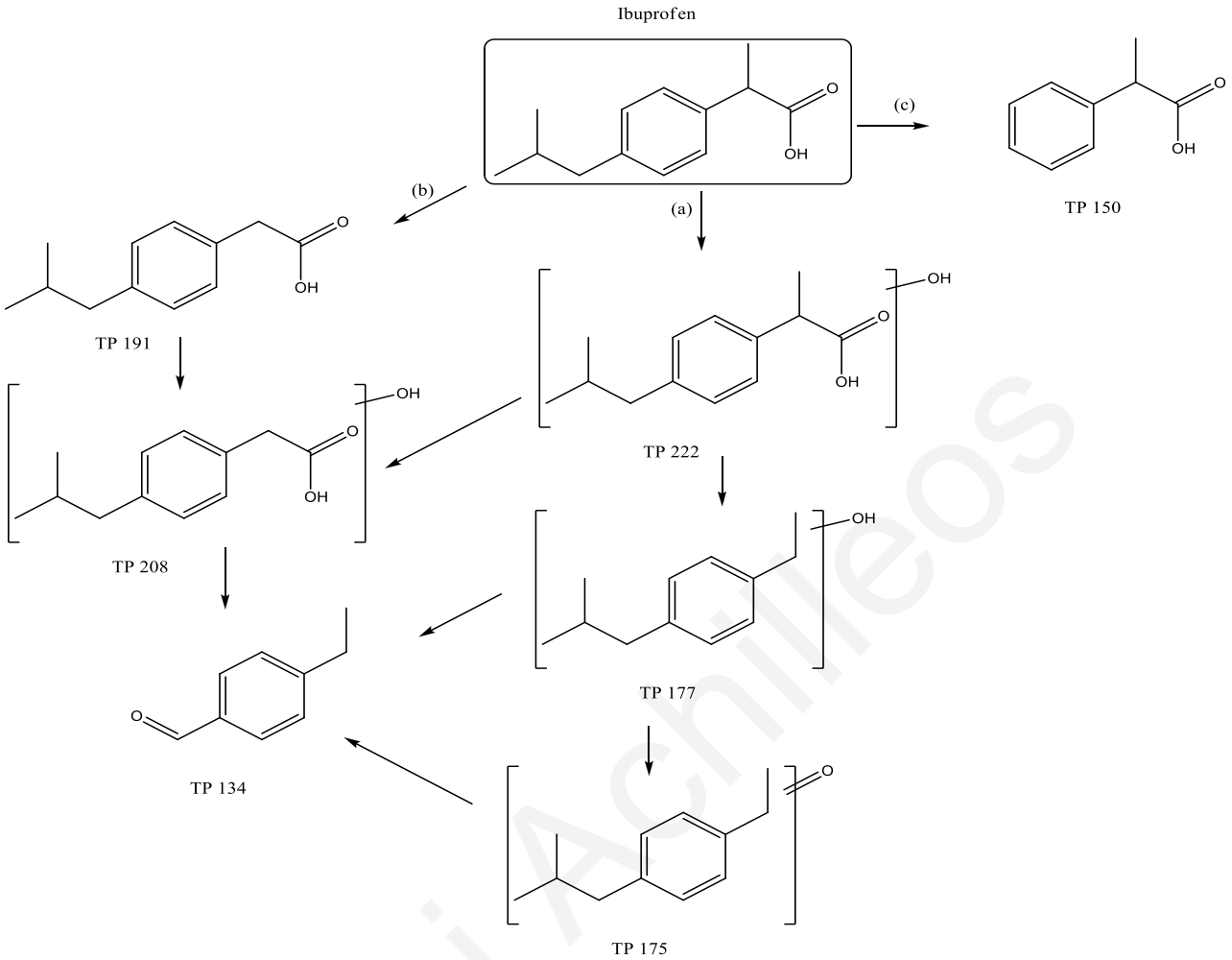

Figure 3.74: Proposed transformation pathway of IBP in aqueous solution by solar (S), sonophotocatalysis (SPC) and photocatalysis (PC)).

3.8.3 Diclofenac

The screening of the treated samples in (+)ESI scan mode allowed to confirm the formation of eleven TPs with retention times shorter than that of the parent compound (Figure 3.79). The results indicate that all the tested treatments (S, SPC, PC) degrades the DCF and results in the formation of a number of products.

Tables 3.38-3.39 show the summary of the data related to the calculated and measured masses of fragment ions of DCF and its TPs determined in ESI(+)-MS^2 experiments on the QqToF instrument, together with the error between them, the proposed empirical formula corresponding to the compounds identified and the corresponding DBEs. The data presented in Tables 3.38-3.39 were obtained under optimized conditions of collision energy and cone voltage of the QqToF-MS. Most of the accurate mass results were found with an error of less than 2 ppm, thus providing a high degree of certainty in the assignment of formulas.

Table 3.38: Structure elucidation of DCF and its TPs (Experiments: solar (S), sonophotocatalysis (SPC) and photocatalysis(PC))

Transformation products	$[M+H]^+$	Chemical structure or elemental composition (incl. positive charge)	Confirmation / comments
DCF	296	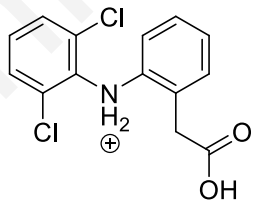	YES Diclofenac (DCF) Confirmed with standard
TP 311(A)	312	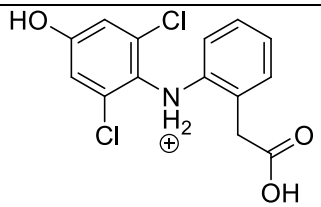	YES 4'-hydroxy-diclofenac Confirmed with standard
TP 311(B)	312	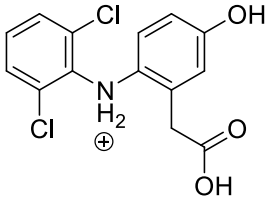	YES 5-hydroxy-diclofenac Confirmed with standard
TP 327(A)	328		YES 4',5-dihydroxy-

		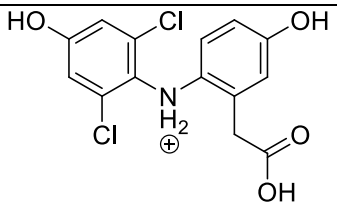	diclofenac Confirmed with standard
TP 327(B)	328	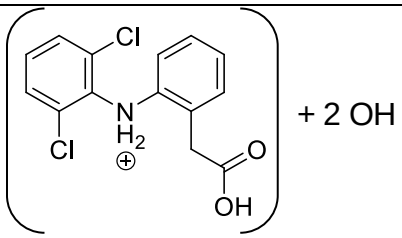 + 2 OH	YES X,Y-dihydroxy-diclofenac NOT CONFIRMED with standard
TP 279	280	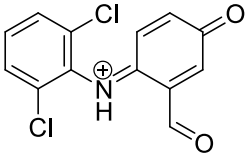	Chemical Formula and Structure NOT CONFIRMED
TP 281	282	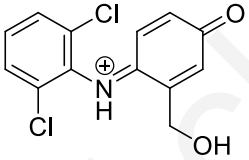	NOT CONFIRMED with standard
TP 313	314	**NOT IDENTIFIED**	**NOT IDENTIFIED**
TP 307	308	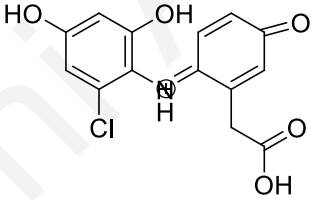	Not confirmed MS2 with very low sensitivity NOT CONFIRMED with standard
TP 211	212	**NOT IDENTIFIED**	**NOT IDENTIFIED**
TP 191	192	**NOT IDENTIFIED**	**NOT IDENTIFIED**
TP 293	294	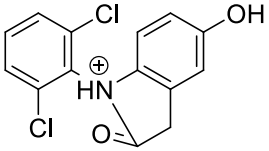 Exact Mass: 294,0083	Chemical Formula and Structure NOT CONFIRMED NOT CONFIRMED with standard
TP 177	178	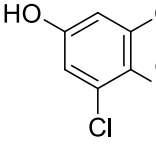 Chemical Formula: $C_6H_6Cl_2NO^+$ Exact Mass: 177.9821	NOT CONFIRMED with standard
TP 265 (A) (B)	266		NOT CONFIRMED with standard

		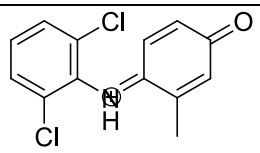 Exact Mass: 266,0134	

In order to elucidate the chemical structures of TPs, first the mass behaviour of the parent compound was studied and afterwards compared with the mass fragmentation of detected TPs. In most cases, they were easily recognizable by the presence, in the mass spectrum, of the resolved isotopic cluster characteristic of compounds that contain chlorine atoms in the molecule. The screening of the treatment samples in (+)ESI scan mode allowed to confirm the formation of thirteen TPs (Figures 3.75-3.78). All of the identified products, except two (TP 280 & TP 282), are eluted before the main peak of DCF at 3.82 min (Table 3.39), indicating the formation of smaller and more polar products when compared to the parent compound. Some of these compounds have already been reported by other authors as products of DCF ozonation, photo-Fenton, electro-oxidation, heterogeneous catalytic oxidation, photolysis and solar degradation ((Vogna et al., 2004; Calza et al., 2006; Hohmann et al., 2007; Hartmann et al. 2008; Coelho et al., 2009; Zhao et al., 2009; Madhavan et al. 2010).

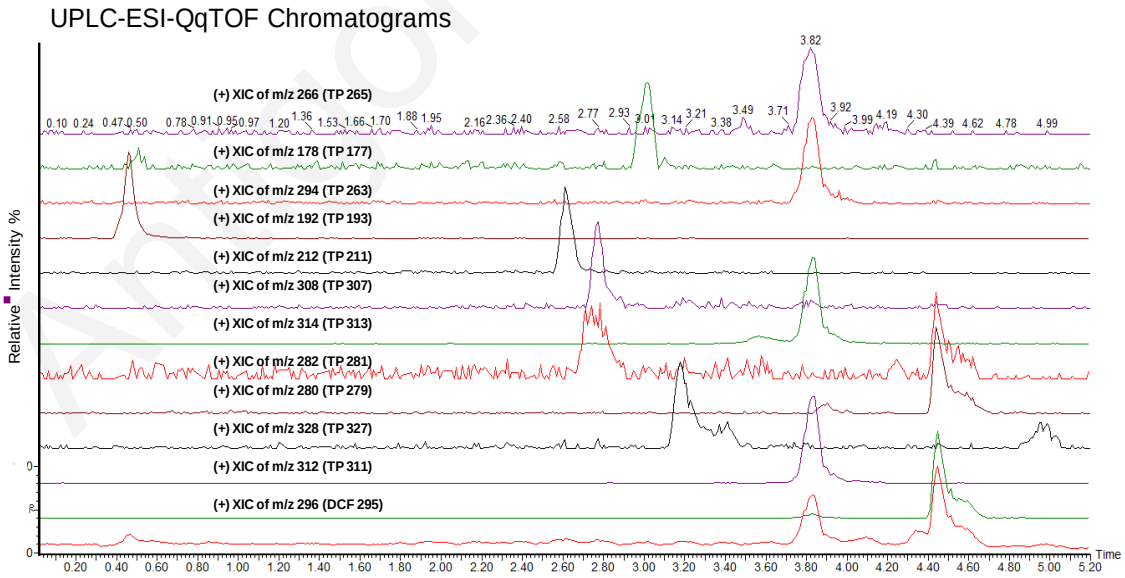

Figure 3.75: Total ion chromatogram (TIC) and extracted ion chromatograms (XIC) of DCF (10 mg/L) after 60 min with photocatalysis UV-A

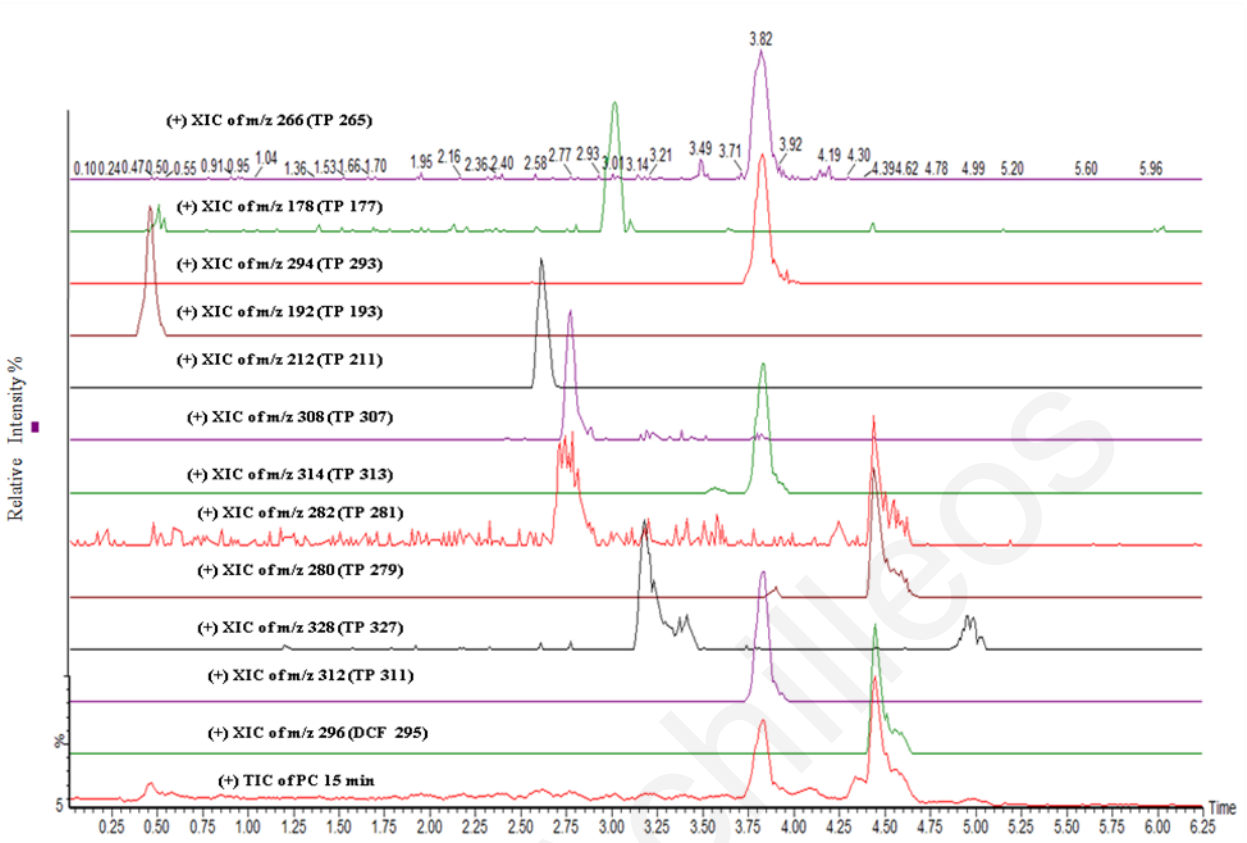

Figure 3.76: Total ion chromatogram (TIC) and extracted ion chromatograms (XIC) of DCF (10 mg/L) after 15 min with photocatalysis UV-A

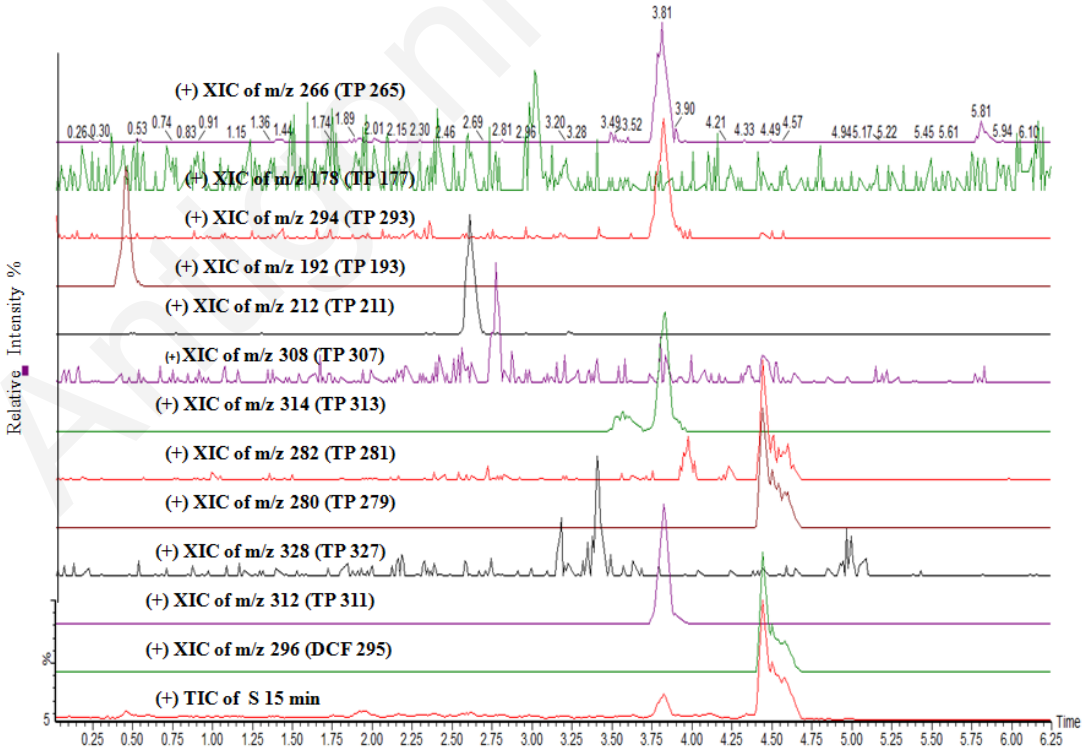

Figure 3.77: Total ion chromatogram (TIC) and extracted ion chromatograms (XIC) of DCF (10 mg/L) experiment after 15 min with solar

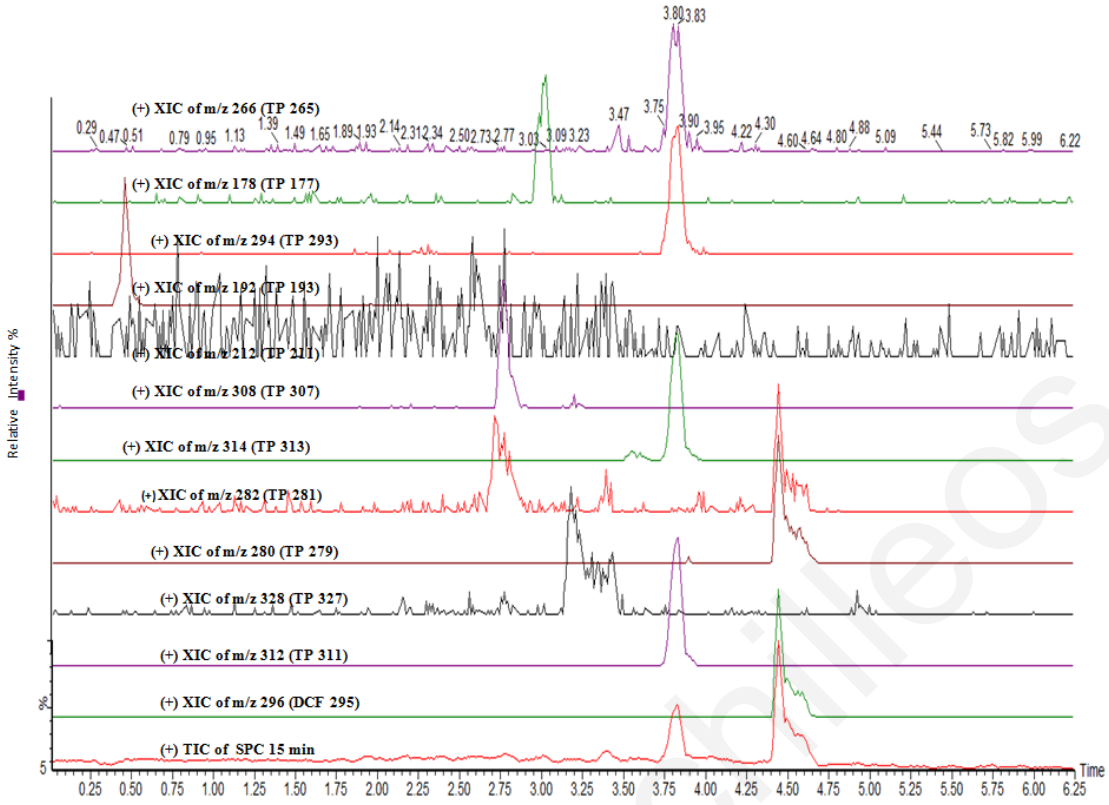

Figure 3.78: Total ion chromatogram (TIC) and extracted ion chromatograms (XIC) of DCF (10 mg/L) experiment after 15 min with sonophotocatalysis

In Figure 3.75, the TIC shows the peak of DCF at t_R = 3.83 min that exhibited a molecular ion peak at *m/z* 296. In the (+)ESI mode (Fig. 3.79), the product ion profile of the protonated molecule, m/z 296, derives from the sequential loss of H_2O (m/z 278) and CO (m/z 250) followed by cleavage of the chlorine atoms as radicals (m/z 215 and 180), which was corroborated through pseudo-MS^3 experiments by selecting the fragment ions m/z 278, 250, and 215, generated by in-source CID, in the Q1 analyzer followed by further fragmentation in the collision cell (spectra not shown).

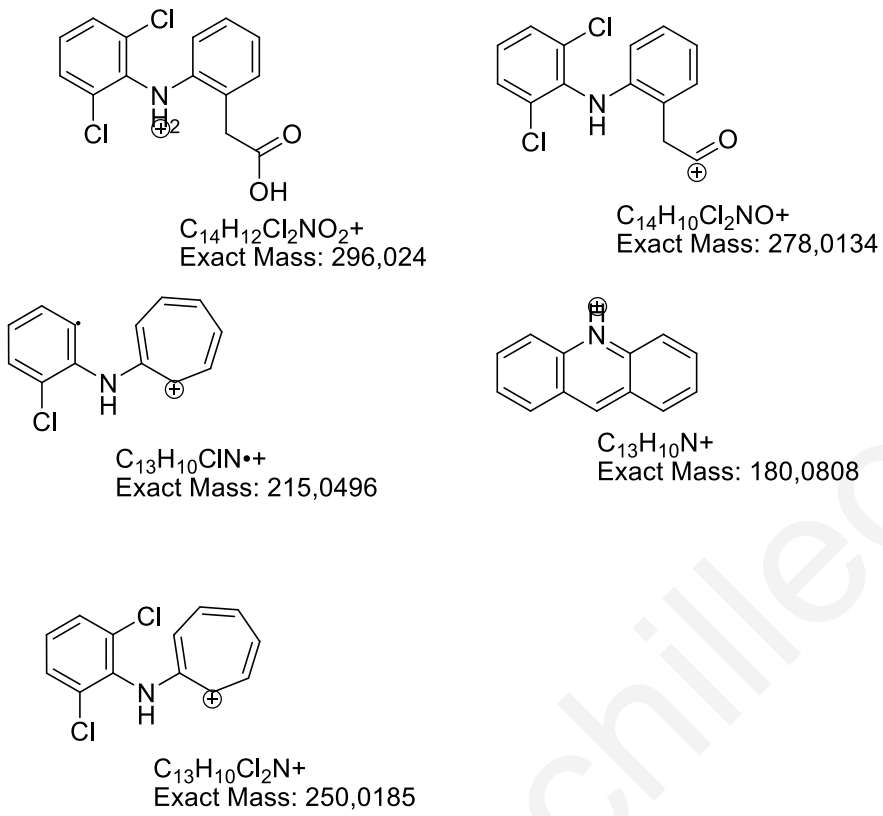

Figure 3.79: Proposed mass fragmentation pathway of diclofenac (DCF)

Table 3.39: Accurate mass measurements of the transformation products (TP) of Diclofenac (DCF) as determined by UPLC–(+)ESI-QqToF-MS in full scan mode

Compound	Ion	Elemental composition	Meas. Mass	Calc. Mass	Error (mDa)	Error (ppm)	DBE
DCF	$[M+H]^+$	$C_{15}H_{13}N_2O$	296.0251	296.0245	0.6	2.0	8.5
4'-OH-DCF	$[M+H]^+$	$C_{14}H_{12}NO_3Cl_2$	312.0197	312.0194	0.3	1.0	8.5
5-OH-DCF	$[M+H]^+$	$C_{14}H_{12}NO_3Cl_2$	312.0197	312.0194	0.2	1.0	8.5
4',5-diOH-DCF	$[M+H]^+$	$C_{14}H_{12}NO_4\ Cl_2$	328.0167	328.0143	2.4	7.3	8.5
X,Y-diOH-DCF	$[M+H]^+$	$C_{14}H_{12}NO_4\ Cl_2$	328.0127	328.0143	-1.6	-4.9	8.5
TP 279	$[M+H]^+$	$C_{13}H_8NO_2\ Cl_2$	-	-	-	-	-
TP 281	$[M+H]^+$	$C_{13}H_{10}NO_2\ Cl_2$	282.0062	282.0089	-2.7	-9.6	8.5
TP 307	M^+	$C_{15}H_{11}N_2O_3$	308.0339	308.0326	1.3	4.2	9.5
TP 293	$[M+H]^+$	$C_{14}H_{12}NO_2$	-	-	-	-	-
TP 177	$[M+H]^+$	$C_{14}H_{11}NO_2Na$	177.9825	177.9826	-0.1	-0.6	3.5
TP 265	$[M+H]^+$	$C_{14}H_{10}NO_2$	266.0167	266.0139	2.8	10.5	8.5

The formation of hydroxylated derivatives was confirmed by the presence of compounds whose formula showed an increase of one of more oxygen atoms with respect to the formula of DCF, without changes in the DBE. The first two of them, labeled TP 311(A) and TP 311(B) in Table 3.38, yielded an accurate mass m/z of 312.0189. This accurate mass corresponded to the formula $C_{14}H_{11}NO_3Cl_2$ (neutral molecule), which is consistent with the mono- hydroxylated product of DCF, which are known DCF metabolites, named as 4'-hydroxy diclofenac and 5-hydroxy diclofenac, respectively. 4-OH-DCF and to a minor extent 5-OH-DCF are the major metabolites of oxidative diclofenac metabolism in humans, which is catalyzed by different types of cytochromes in the hepatocytes. The 4-OH-DCF metabolite is produced by the cytochrome P-450 isoenzyme CYP2C9 (Leemann et al., 1993), whereas 5-hydroxylation of the most electron-rich aromatic ring of the drug is catalysed by several cytochromes, including CYP3A4, CYP2C8, and CYP2C19 (Shen et al., 1999). The identity of theses TPs was ultimately confirmed by analyzing the commercially available authentic standard of the proposed compound, which matched the retention time and fragmentation pattern of the protonated molecule.

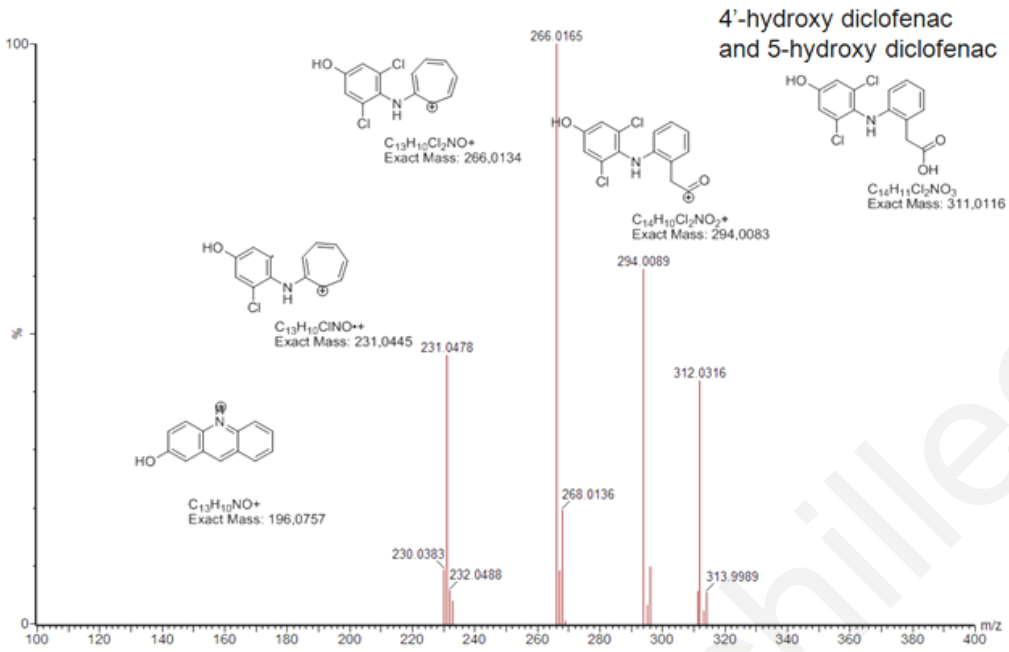

Figure 3.80: 4-OH-DCF and 5-OH-DCF, in product ion mode and proposed fragmentation patterns

The two spectra (MS^2 fragmentation of the molecular ion $[M + H]^+$ 312) are almost identical and rendered intense signal at m/z 294 corresponding to the loss of water, which with further loss of CO resulted in the m/z 266 fragment ion. The loss of 35 Da, typical for the elimination of one chlorine atom, led to the appearance of the less mass ion at m/z 231, which with further loss of the second chlorine atom resulted in the m/z 196 fragment ion (Figure 3.80).

It should be noted that 4-OH-DCF and 5-OH-DCF were among the TPs when DCF was irradiated with ultrasound (Hartmann et al. 2008; Madhavan et al. 2010). 5-OH-DCF was also reported as TP under electro-oxidation of DCF (Zhao et al., 2009). OH-DCF isomers were also detected as photoproducts under ozonolisis (Coelho et al., 2009), photo-fenton degradation (Pérez-Estrada et al., 2005) as well as under photocatalytic conditions (Vogna et al., 2004; Calza et al., 2006; Hohmann et al., 2007).

Considering the mass difference between the parent molecule and TPs 328 (Table 1), the m/z increases of 32 Da, the TPs 328 are indicative of di-hydroxylated diclofenac species. As in the case of TP 312, the product ion spectrum of the di-hydroxy-DCF (m/z 328) characterized by stepwise elimination of H_2O (m/z 310), CO (m/z 282), and two Cl molecules (m/z 247 and 212) (Figure 3.81).

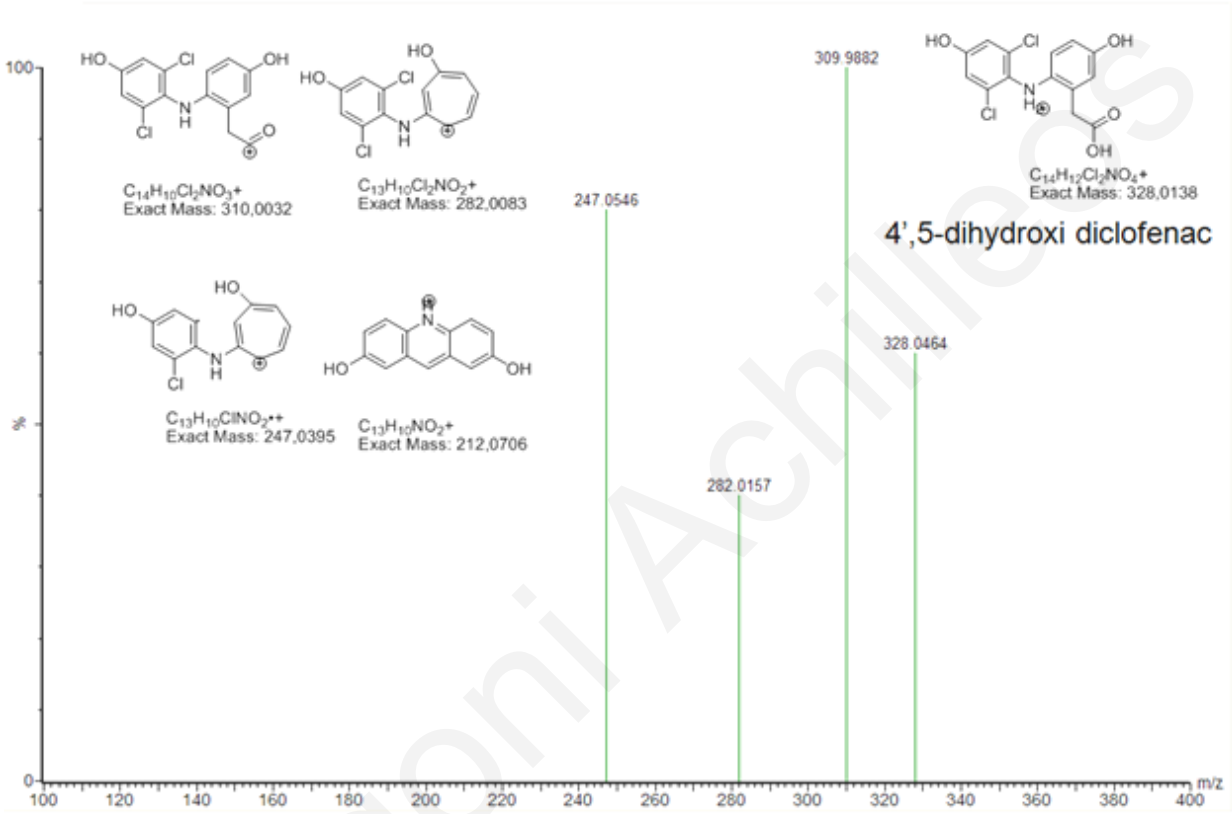

Figure 3.81: 4-,5-dihydroxy-DCF, in product ion mode and proposed fragmentation patterns

The next TP derivatives identified provided a molecular ion at m/z 266 (TP 265 (A) & (B)). Based on the best-fit formula of $C_{13}H_{10}NOCl_2$ (protonated molecule) a plausible structure corresponded to a loss of CO_2 (44 Da) and hydrogen abstraction from the hydroxylated DCF derivatives (m/z 312). The ESI-MS^2 spectra patterns of TP 266 is characterized by a strong signals at m/z 231 which corresponds to the loss of one chlorine atom (35 Da)

Further, hydroxylation of the latter TPs with m/z 266 results to the formation of the TP 281 with accurate mass of m/z 282.0083, which was further transformed to TP 279. Analogous to mono and dihydroxy-DCF derivatives, TP 279 (Figure 3.82)

showed the protonated molecule $[M + H]^+$ with m/z 280 and the successive elimination of CO and one chlorine atom to form fragment ions at m/z 252 and m/z 217, respectively. Based on the best-fit formula of $C_{13}H_8NO_2Cl_2$ (protonated molecule) and the mass difference of 2 amu compared to the hydroxylated TP 281, the elemental composition may be rationalized by the formation of keto-derivative.

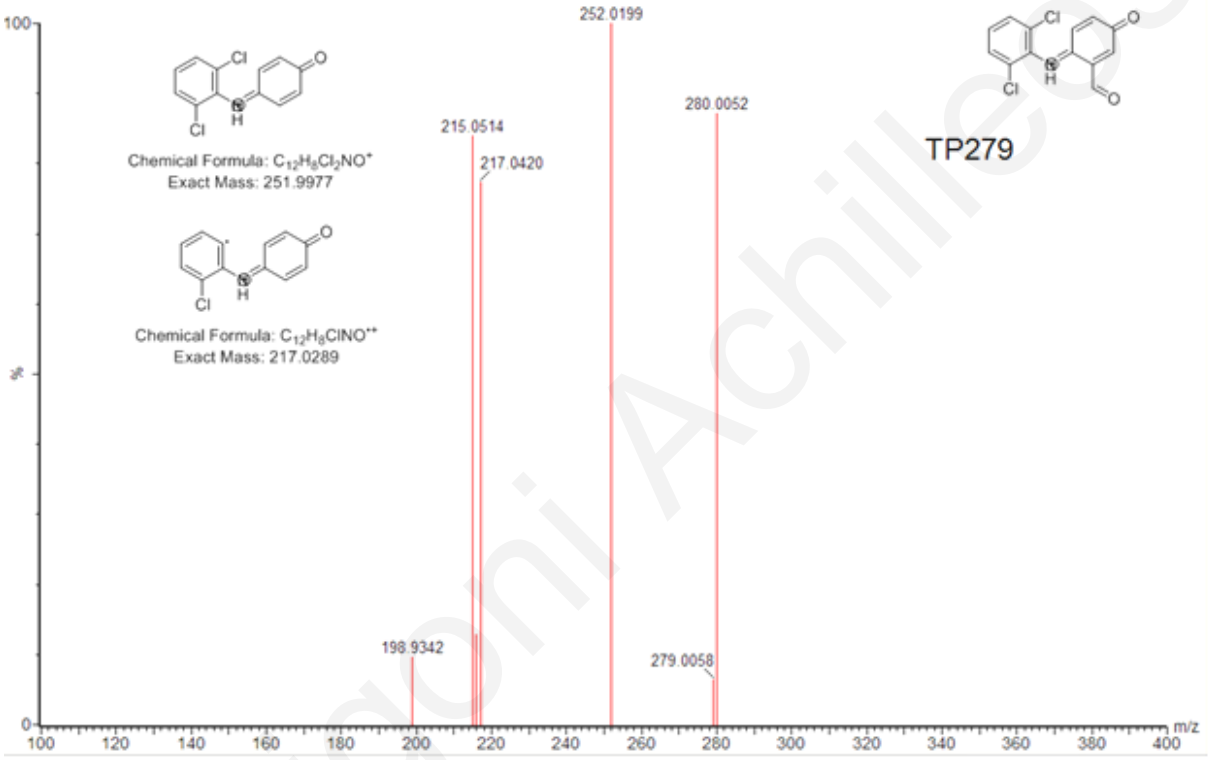

Figure 3.82: TP 279 in product ion mode and proposed fragmentation patterns

The chromatographic peak at 3.82 min (TP 293) indicated a decrease in molecular mass for 18 Da from TP 311, suggesting a dehydratation of the hydroxy-DCF. The MS/MS spectrum of m/z 294 showed a neutral loss of CO (28 Da), producing a fragment at m/z 266, and a loss of Cl at m/z 231.

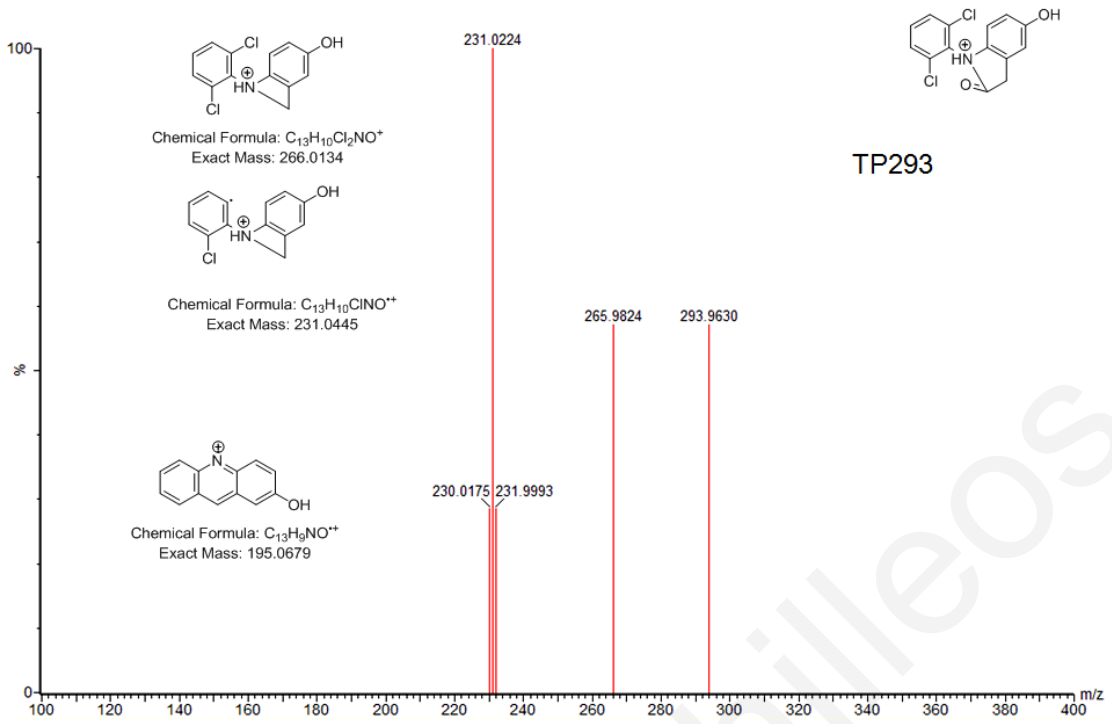

Figure 3.83: TP 293 in product ion mode and proposed fragmentation patterns

Finally, the last detected intermediate product of photocatalytic degradation of DCF was TP 177, with the molecular ion m/z 178. It was assumed that TP 177 coming from the opening of the nonchlorinated ring, after oxidation-hydroxylation and/or hydrolysis, followed by a further decarboxylation step. Based on the presence of the fragment with accurate mass of 143.0130 (C_6H_6ClNO, protonated molecule) which result from the loss of OH group we can conclude that hydroxylation takes place on the nitrogen atom and not on the chlorinated aromatic ring (Figure 3.83). This TP was also proposed by Pérez-Estrada et al., 2005 under the solar photodegradation of DCF, in aqueous solutions by photo-Fenton reaction as well as by Coelho et al., 2009 under the degradation of DCF in aqueous solution by ozonation.

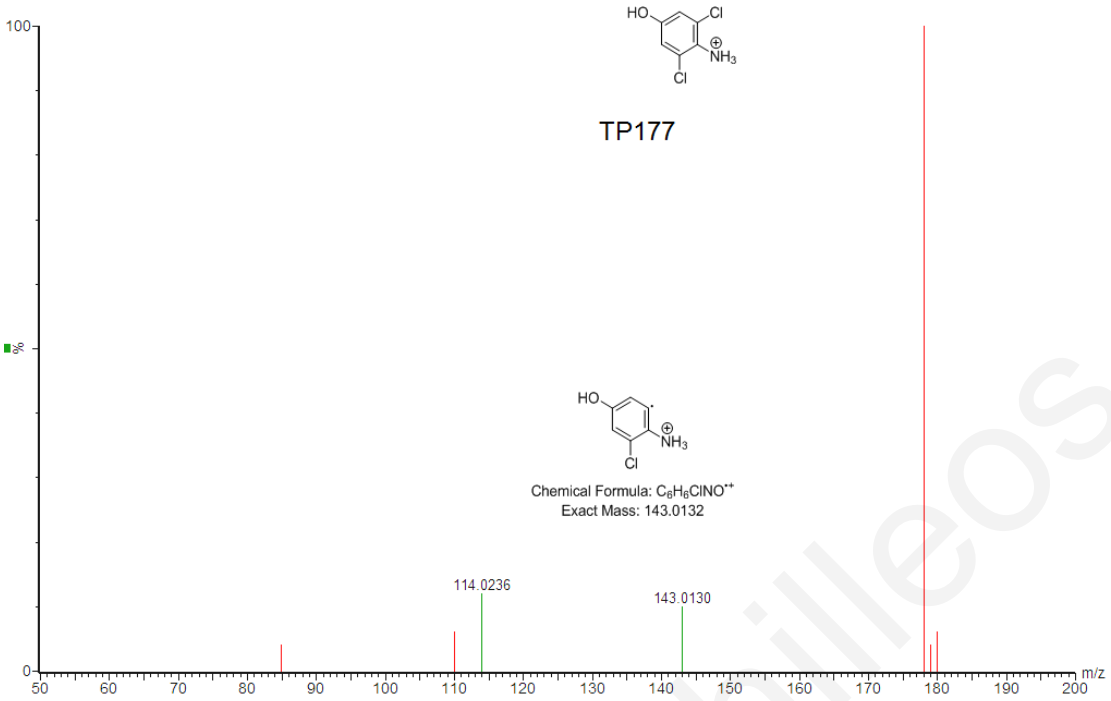

Figure 3.84: TP 177 in product ion mode and proposed fragmentation patterns

It is worth mentioning that additional peaks in the TIC at t_R 0. 45, 2.60, 255 and 2.80 min were considered as unknown TPs U192, U212, U308 and U314, respectively (Table 3.38), because their concentration increased and decreased as a function of the reaction time. For these compounds it is difficult to find a match with a formula, which could be chemically coherent with DCF and only the m/z was obtained.

3.8.3.1 Profile of DCF TPs

The formation of DCF TPs was depicted in Figures 3.85 A, B and C. Profile of TPs was expressed as relative area (A/A_0) measured by integration of LC-MS peaks of the corresponding TP (A) and the parent drug in the control treatments at different irradiation times, since due to the lack of authentic analytical standards for the newly identified products their quantitative determination was not possible. In Figure 3.86 the concentration profile of DCF was depicted.

4-OH-DCF appeared in the first 15 min in PC and S experiment and remained until 120 min. In SPC experiment appeared in the first 15 min and disappeared after 60 min.

5-OH-DCF appeared in the first 15 min in all experiments remained until 120 min in the PC experiment. In S experiment disappeared in 30 min, appeared in 60 min and remained until 120 min of the experiment. In SPC remained until the first 30 min of the experiment and then disappeared.

TP32 appeared in the first 15 min in all experiments and remained until 120 min in the PC and S experiment. In SPC experiment disappeared after 60 min of the experiment.

TP328 exists from the start (0 min) to all of the experiments. In PC experiment disappeared in the first 30 min, appeared again in 60 min and remained until the 120 min of the experiment. In S and SPC remained in the solution until 120 min of the experiment.

TP280 appeared in 0 min and remained until the end of PC and S experiments. In SPC experiments disappeared after 60 min.

TP281A appeared in 0 min and remained until the end of PC and S experiments. In SPC experiments disappeared after 60 min.

TP281B appeared in the first 15 min of the experiments. In PC experiment remained until 120 min. In S experiment disappeared after 30 min of irradiation and in SPC experiment disappeared after 15 min.

TP281C in PC experiment appeared in the first 30 min and remained until 120 min of irradiation. In S experiment appeared in the first 15 min and remained until 120 min of irradiation. In SPC experiment did not appear.

TP313A in PC experiment appeared in 0 min and remained until the end of irradiation. In SPC and S experiments appeared in the first 15 min and remained until 120 min of irradiation.

TP313B in PC, S and SPC experiments appeared in the first 15 min and remained until the end of the experiment (120 min).

TP307 in S and PC experiments appeared in the first 15 min and remained until the end of the experiment (120 min). In SPC experiment appeared in the first 15 min and disappeared after 30 min.

TP211 in PC experiment appeared in 0 min and remained until the end of irradiation. In SPC experiment did not appear. In S experiment appeared in 0 min and remained until the first 15 min. After 30 min disappeared and appeared again in 60 min and remained until 120 min of irradiation.

TP191 in all experiments appeared from 0 min and remained until 120 min of irradiation.

TP293 in S and PC experiments appeared in the first 15 min and remained in the solution until 120 min. In SPC experiment appeared in the first 15 min and disappeared after 60 min.

TP177 in PC experiments appeared in 0 min and remained until 120 min of irradiation. In S experiment appeared in the first 15 min, disappeared after 30 min and appeared again in 60 min until 120 min of irradiation. In SPC experiment appeared in the first 15 min and disappeared after 30 min.

TP265A appeared in the first 15 min and remained in the solution until 120 min. In S experiment appeared in the first 15 min, disappeared after 30 min and appeared again in 60 min until 120 min of irradiation. In SPC appeared in the first 15 min and disappeared after 60 min.

TP265B in PC experiment did not appear, in SPC experiment appeared in 0 min, disappeared in 15- 60 min and in 120 min appeared. In S experiment appeared in 0 min, disappeared in 15 min, appeared in 30 min and after 60 min disappeared.

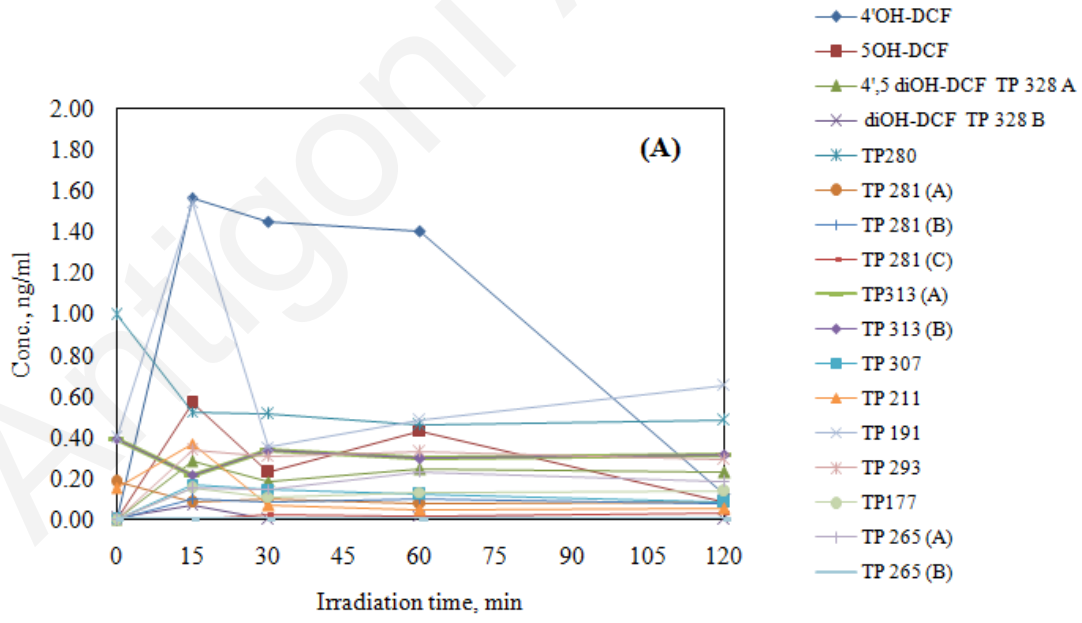

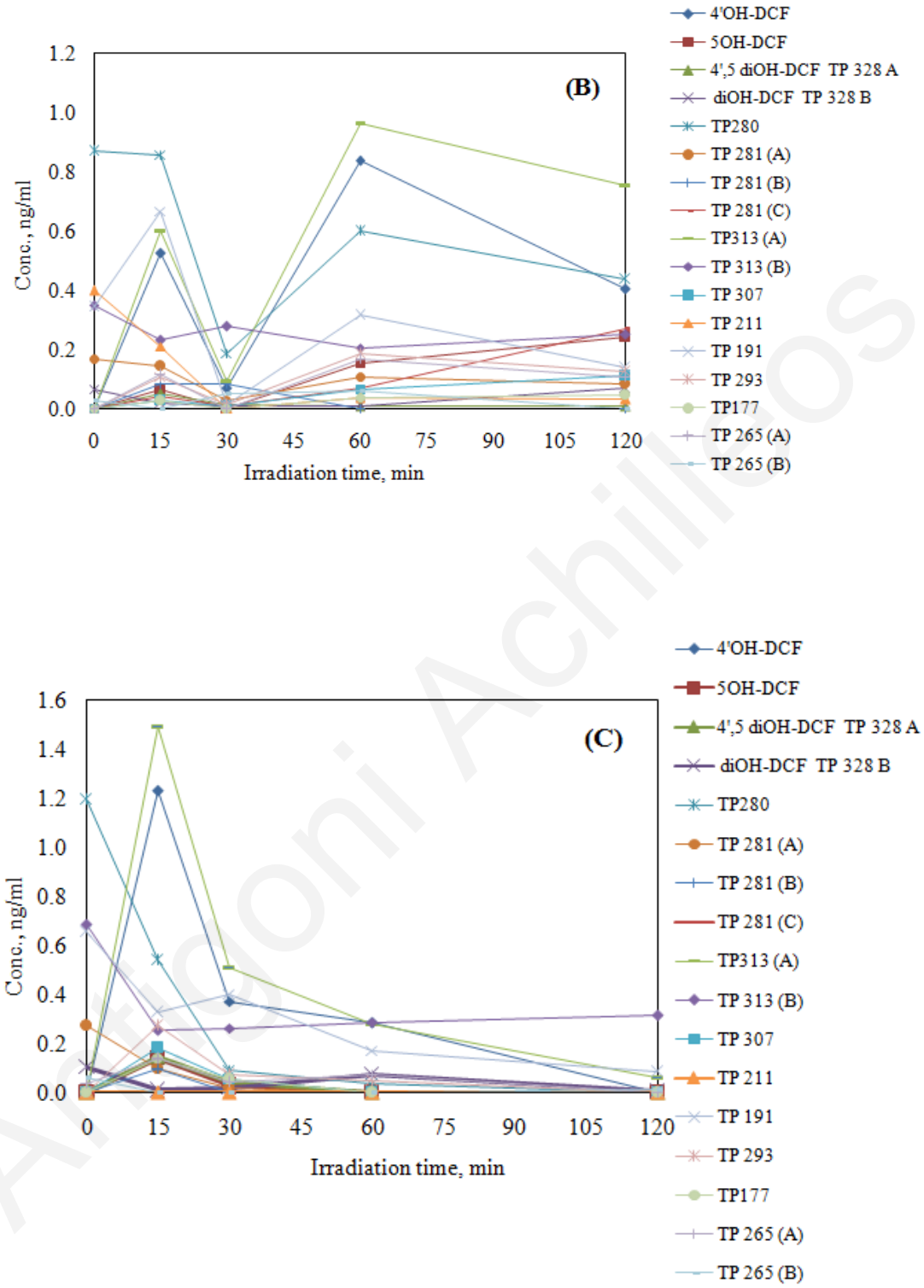

Figure 3.85: Profile of TPs (A) UV-A irradiation, (B) solar irradiation, (C) sonophotocatalysis, DCF 10 mg/L, 500 mg/L catalyst loading

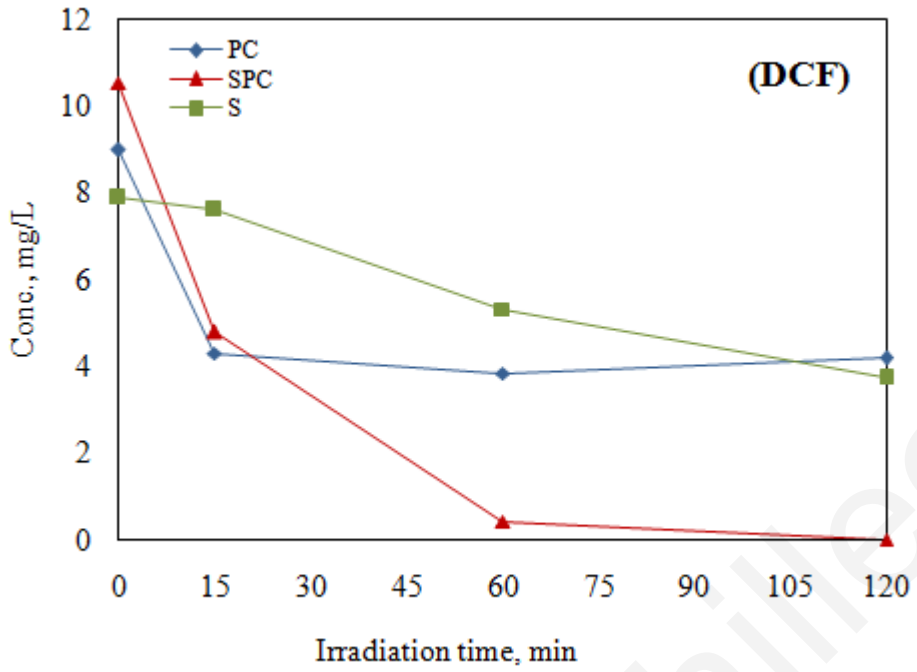

Figure 3.86: Concentration profile of DCF 10 mg/L, 500 mg/L catalyst loading, during UV-A irradiation (PC), solar irradiation (S) and sonophotocatalysis (SPC)

In Figure 3.86 the degradation of DCF in SPC, S and PC experiment is 99.9, 52.8 and 53.3% after 120 min

3.8.3.2 Mechanism of DCF photocatalytic degradation

On the basis of the foregoing results of the HPLC/ESI-QqLIT-MS and UPLC/ESI-QqToF-MS experiments and previous studies on the oxidation ((Vogna et al., 2004; Calza et al., 2006; Hohmann et al., 2007; Hartmann et al. 2008; Coelho et al., 2009; Zhao et al., 2009; Madhavan et al. 2010) a possible degradation pathway is proposed (Figure 3.87).

Product analysis suggests that oxidation of DCF, under the experimental conditions used, mainly proceeds by hydroxylation reactions (a) and cleavage of the C–N bond (b). Decarboxylation, cyclization and ring opening reactions in the phenylacetic acid moiety also occur in the further steps of the transformation processes.

Hydroxylation reactions are common in most of the oxidative processes. Thus •OH radical attack lead to the formation of mono hydroxylated species (4-OH-DCF, 5-OH-DCF) as the first step in the DCF degradation (Calza et al., 2006). The last TPs either

were further oxidized (TP 327(A) & (B), TP 294) and/or induced the loss of the carboxylic moiety leading to the formation of decarboxylated derivatives (TP 266), which further transformed to TP 279 and TP 281.

The appearance of TP 177 also points to the cleavage of the C–N bond of DCF as a preferential route, which originates a series of C–N cleavage products such as the formation of 2,6-dichlorophenol and 4-chlorocathecol on one hand, while cathecol and hydroquinone are probably formed from the other aromatic ring, through the loss of the lateral chain (Calza et al., 2006).

All the above described intermediates were further transformed by an oxidative opening of the aromatic ring, giving rise to the formation of smaller and more oxidized molecules, such as short carboxylic acids (Zhao et al., 2009).

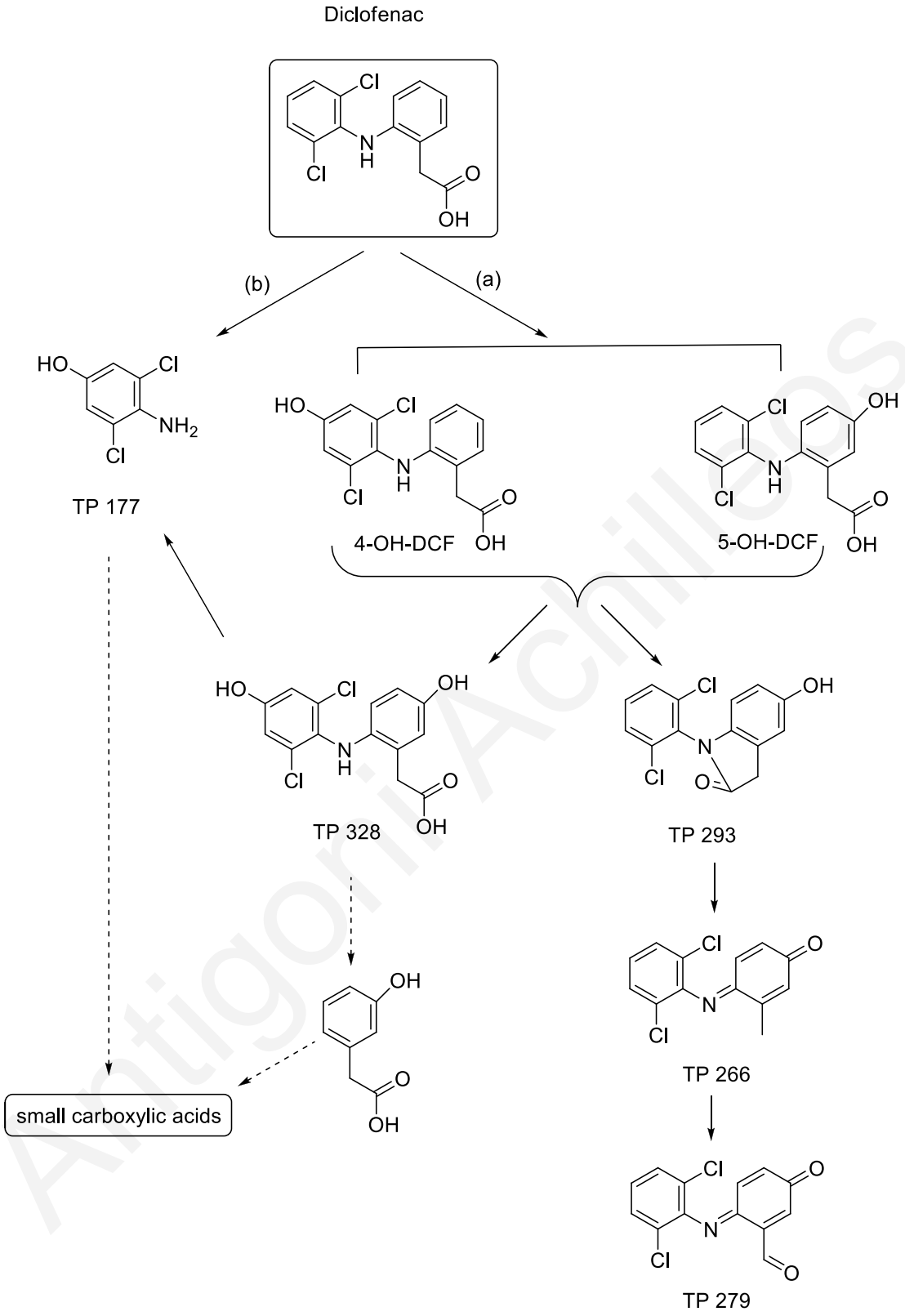

Figure 3.87.: Proposed transformation pathway of DCF in aqueous solution by solar (S), sonophotocatalysis (SPC) and photocatalysis (PC)). Structures with dot lines represent TPs that were not detected but are proposed based on previous studies

CHAPTER 4
CONCLUSIONS – SUGGESTIONS FOR FUTURE WORK

Pharmaceuticals constitute one category of xenobiotic compounds that raises a lot of concern because they are designed to be biologically active and most often escape urban wastewater treatment plants intact, retaining also their biological activity. Due to their special physico-chemical characteristics, pharmaceuticals are characterized as special pollutants and their fate and behavior cannot be simulated by any other group of chemicals, like for example with that of pesticides.

The major findings of this thesis are summarized below:

- Heterogeneous photocatalysis under UV-A or solar irradiation and sonophotocatalysis appears to be a promising treatment method for the removal of DCF, IBP and CBZ, particularly taking into account that the actual environmental concentrations of the pharmaceuticals will be much lower than those studied in this thesis. In any case the formation of TPs must be considered because there are cases where these are more toxic than the parent compounds.
- Following the collection and elaboration of data regarding the pharmaceutical products' consumption in the Cyprus market, information concerning the volumes of sales of the commercial drugs of the public hospitals and private pharmacies, the quantities of the ten active pharmaceutical ingredients with the highest consumption volumes in Cyprus were determined. The major finding is that the quantities of drugs consumed by hospitals are very high and according to the Pharmaceutical Services, at least until 2005, the situation was partly and not fully controlled and monitored.
- Predicted Environmental Concentrations (PECs) should only be used as rough estimates and should always be followed by Measured Environmental Concentrations (MECs). In comparison, PECs substantially differed from MECs, particularly when there were not enough data to estimate the environmental fate of the molecule. Predictive models might therefore be useful for studying pharmaceuticals in the environment, providing enough experimental data available on the environmental fate of the molecules

- Results of photolysis experiments under UV-A irradiation did not show any significant conversion for DCF, IBP and CBZ after 120 min. The conversion for 5, 10, 20 mg/L DCF after 120 min of UV-A irradiation was 27, 11 and 10%. The conversion for 5, 10, 20 mg/L IBP was after 120 min of irradiation 15, 12 and 15%. The conversion for 5, 10 mg/L CBZ was 20 and 7% after 120 min of irradiation. Moreover, DOC measurements did not show any significant removal (~ 2%) for any of the substances under UV-A irradiation. In photolysis experiments under solar irradiation the conversion efficiency was 27.4, 11, and 10.2% for 5, 10 and 20 mg/L DCF. The conversion efficiency was 6,4 and 3.5% for 5, 10, 20 mg/L IBP. The conversion efficiency was 4.5 and 7% for 5 and 10 mg/L CBZ. DOC removal was maximum at ~1.4%.
- Heterogeneous photocatalysis under UV-A and solar irradiation process performance is affected by several factors such as the type and concentration of catalyst, initial pharmaceutical concentration, addition of oxidant and the water matrix (i.e. addition of extra oxidants, presence of other organics etc). Degussa P25 shows higher photoactivity than the other catalysts employed in this study. The optimum catalyst loading was 500 mg/L for 10 mg/L DCF and IBP and 100 mg/L for 10 mg/L CBZ. Increasing the initial pharmaceutical concentration conversion decreases. With the addition of H_2O_2 in the range 0.07-1.4 mM DOC removal and conversion increased. More importantly, the matrix appears to have a detrimental effect on mineralization and this can be explained in terms of increased initial carbon concentration, the presence of species like chlorides and carbonates/bicarbonates that may act as scavengers of hydroxyl radicals and other reactive moieties and finally the increased solution pH which affects adversely mineralization. The highest DOC removal (58%) and conversion (80%) was achieved for DCF under UV-A irradiation. The highest DOC removal (55%) and conversion (90%) was achieved for DCF under solar irradiation
- Low frequency ultrasound is not capable of sufficiently degrading DCF, IBP and CBZ in aqueous solutions. Operating conditions, such as applied ultrasound power, contact time, substrate concentration and the presence of dissolved gases can all affect treatment performance in a positive or adverse side. The study of the sonolytic degradation of the pharmaceutical compounds DCF, IBP and CBZ showed that the beneficial ultrasound power density is 640 W/L. The effect of adding H_2O_2, at various

concentrations (0.07–1.4 mM) on DCF, IBP and CBZ enhanced conversion and DOC removal. The effect of initial DCF, IBP and CBZ concentration on conversion at 500 mg/L catalyst loading for DCF and IBP and 100 mg/L for CBZ showed that conversion decreases with increasing initial concentration. The presence of dissolved gases in the reaction mixture generally enhances sonochemical activity as gases act as nucleation sites for cavitation. Reactivity decreases in the order: Ar>O_2 air>He>N_2 no gas. The highest DOC removal (21.3%) and conversion (50%) was achieved for CBZ.

- With sonophotocatalysis the highest DOC removal (63%) and conversion (80.4%) was achieved for DCF 10 mg/L with catalyst loading 500 mg/L.
- The decomposition kinetics of DCF, IBP and CBZ perfectly fits first order kinetics.
- The quantification with HPLC/ESI-QqLIT-MS of the treated spiked samples of DCF, IBP and CBZ showed a 53.3, 53 and 99.9% degradation of 10 mg/L DCF under UV-A and solar irradiation and sonophotocatalysis. For 10 mg/L IBP the degradation was 84.3, 95.8 and 99.8% under UV-A and solar irradiation and sonophotocatalysis. For 10 mg/L CBZ the degradation was 93.8, 50 and 93% under UV-A and solar irradiation and sonophotocatalysis.
- The phototransformation of pharmaceuticals proceeds usually through the formation of long-lived intermediate species. Major degradation pathways usually include hydroxylation, isomerization, dehalogenation, dealkylation, cyclization, decarboxylation, dimerization and ring opening (for aromatic compounds), leading to corresponding derivatives as well as carboxylic acids. The screening of the treatment samples in (+) ESI scan mode allowed to confirm the formation of eight TPs in CBZ, nine TPs in DCF and seven TPs in IBP treated samples under UV-A and solar irradiation and sonophotocatalysis.
- The toxicity tests are useful analytical tools for the toxicity screening of chemical compounds and as an early warning system to monitor the performance of wastewater treatment plants. The toxicity tests showed to have discriminatory ability to distinguish between different degrees of toxicity, and the toxic specificity of the compounds on target organisms. Fresh water microorganisms *Daphnia magna* are more sensitive to pharmaceuticals degradation by-products than to DCF, IBP and CBZ. This is a point of concern should the treated solutions be discharged in aquatic receivers. Toxic samples were diluted to 80%, 40%, 20% and 10%. Toxicity decreased as dilution increased. At 10% and 20% dilution all samples were not toxic.

Toxicity was directly related with the TPs appearance and disappearance in the solution.

This research work could be extended in various others directions so as to be able to obtain important information for:

- The development of heterogeneous photocatalysis technology that can utilize solar radiation as a source of photons to activate the catalyst on a pilot scale to assess economic viability
- The design of photocatalytic reactor systems that could enhance potentially the performance with regard to rates and efficiency
- The behavior of mixtures of pharmaceuticals under such treatment processes
- Toxicity assessment using other species so as to assess more organisms, plants and endpoints
- The assessment of the potential synergistic effects of transformation products towards various organisms

BIBLIOGRAPHY

Abellan M., Dillert R., Gimenez J., Bahnemann D., (2009). Evaluation of two types of TiO_2-based catalysts by photodegradation of DMSO in aqueous suspension, Journal of Photochemistry and Photobiology A: Chemistry 202, 164-171.

Achilleos A., Hapeshi E., Xekoukoulotakis N., Mantzavinos D., Kassinos D., (2010). Factors affecting diclofenac decomposition in water by UV-A/TiO_2 photocatalysis, Chemical Engineering Journal 161, 53-59.

Adewuyi G., (2005). Sonochemistry in environmental remediation. Heterogeneous sonophotocatalytic oxidation processes for the treatment of pollutants in water. Environmental Science and Technology 39, 8557-8570.

Agustina T., Ang H., Vareek V., (2005). A review of synergistic effect of photocatalysis and ozonation on wastewater treatment, Journal of Photochemistry and Photobiology C: Photochemistry Reviews 6, 264-273.

Alder A., Schaffner C., Majewsky M., Klasmeier J., Fenner K., (2010). Fate of b-blocker human pharmaceuticals in surface water: Comparison of measured and simulated concentrations in the Glatt Valley Watershed, Switzerland, Water Research 44, 936-948.

Andreozzi R., Caprio V., Insola A., Longo G., Tufano V., (2000). Photocatalytic oxidation of 4-nitrophenol in aqueous TiO_2 slurries: an experimental validation of literature kinetic models, Journal Chemical Technology Biotechnology 75, 131-136.

Andreozzi R., Caprio V., Marotta R., Vogna D., (2003a). Paracetamol oxidation from aqueous solution by means of ozonation and H_2O_2/UV system, Water Research 37, 993-1004.

Andreozzi R., Marotta R., Paxeus N., (2003b). Pharmaceuticals in STP effluents and their solar photodegradation in aquatic environment, Chemosphere 50, 1319-1330.

Andreozzi R., Raffaele M., Nicklas P., (2002). Pharmaceuticals in STP effluents and their solar photodegradation in aquatic environment, Chemosphere 50, 1319-1330.

Anipsitakis P., Dionysiou D., (2004). Transition metal/UV-based advanced oxidation technologies for water decontamination, Applied Catalysis B: Environmental 54, 155-163.

Arnold W. and McNeill K., V50, (2007). In Barcelo D. and Petrovic M. (ed) Analysis, Fate and Removal of pharmaceuticals in the water cycle, 361-385.

Arslan-Alaton I., Dogruel S., (2004). Pre-treatment of penicillin formulation effluent by advanced oxidation processes, Journal of Hazardous Materials 112, 105-113.

Ashton D., Hilton M., Thomas K., (2004). Investigating the environmental transport of human pharmaceuticals to streams in the United Kingdom, Science of the Total Environment 333, 167-184.

Augugliaro V., García-López E., Loddo V., Malato-Rodríguez S., Maldonado I., Marcì G., Molinari R., Palmisano L., (2005). Degradation of lincomycin in aqueous medium: Coupling of solar photocatalysis and membrane separation, Solar Energy 79, 402-408.

Augugliaro V., Litter M., Palmisano L., Soris J., (2006). The combination of heterogenous photocatalysis with cheical and physical operations: A tool for improving the photoprocess performance, Journal of Photochemistry and Photobiology C: Photochemistry Reviews 7, 127-144.

Baran W., Jolanta Sochacka J., Wardas W., (2006). Toxicity and biodegradability of sulfonamides and products of their photocatalytic degradation in aqueous solutions, Chemosphere 65, 1295-1299.

Belgiorno V., Rizzo L., Fatta D., Rocca C., Lofrano G., Nikolaou N., Naddeo V., Meric S., (2007). Review on endocrine disrupting –emerging compounds in urban wastewater: occurence and removal by photocatalysis and ultrasonic irradiation for wastewater reuse, Desalination 215, 166-176.

Bendz D., Paxeus A., Ginn R., Loge J., (2005). Occurrence and fate of pharmaceutically active compounds in the environment, a case study: Hoje River in Sweden, Journal of Hazardous Materials 122, 195-204.

Berberidou C., Poulios I., Xekoukoulotakis N.P., Mantzavinos D., (2007). Sonolytic, photocatalytic and sonophotocatalytic degradation of malachite green in aqueous solutions, Applied Catalysis B 74, 63-72.

Bernus I., Hooper W., Dickinson R., Eadie M., (1995). Metabolism of carbamazepine and co-administered anticonvulsants during pregnancy, Epilepsy Research 21, 65-75.

Bickley R., Gonzalez-Carreno T., Lees J., Palmisano L., Tilley R., (1991). A structural investigation of titanium dioxide photocatalysts, Journal of Solid State Chemistry 92, 178-190.

Bixio D., Thoeye C.,De Koning J., Joksimovic D., Savic D., Wintgens T., Melin T., (2006). Wastewater Reuse in Europe, Desalination 187, 89-101.

Boggara M., Faraone A., Krishnamoorti R., (2010). Effect of pH and Ibuprofen on the Phospholipid Bilayer Bending Modulus, Journal of Physical Chemistry B 114, 8061–8066.

Bound J. P., Voulvoulis N. (2004). Pharmaceuticals in the aquatic environment—a comparison of risk assessment strategies, Chemosphere 56, 1143–1155.

Bound J., Vourvoulis N., (2005). Household disposal of pharmaceuticals as a pathway contamination in the United Kingdom, Environmental Health Perspectives 113, 1705-1711.

Bound P., Voulvoulis N., (2006). Predicted and measured concentrations for selected pharmaceuticals in UK rivers: Implications for risk assessment, Water Research 40, 2885-2892.

Buerge J., Buser R., Poiger T., Müller D., (2006). Occurrence and fate of the cytostatic drugs cyclophosphamide and ifosfamide in wastewater and surface waters, Environmental Science and Technology 40, 7242–7250.

Buser H., Poiger T., Müller M., (1999). Occurrence and Environmental Behavior of the Chiral Pharmaceutical Drug Ibuprofen in Surface Waters and in Wastewater, Environmental Science and Technology 33, 2529-2535.

Calamari D., Zuccato E., Castiglioni S., Bagnati R., Fanelli R., (2003). Strategic Survey of Therapeutic Drugs in the Rivers Po and Lambro in Northern Italy, Environmental Science and Technology 37, 1241-1248.

Calisto V., Domingues M., Erny G., Esteves V., (2011). Direct photodegradation of carbamazepine followed by micellar electrokinetic chromatography and mass spectrometry, Water Research 45, 1095-1104.

Calza P., Medana C., Pazzi M., Baiocchi C., Pelizzetti E., (2004). Photocatalytic transformations of sulphonamides on titanium dioxide, Applied Catalysis B: Environmental 53, 63-69.

Calza P., Sakkas V., Medana C., Baiocchi C., Dimou A., Pelizzetti E., Albanis T., (2006). Photocatalytic degradation study of diclofenac over aqueous TiO_2 suspensions, Applied Catalysis B: Environmental 67, 197-205.

Calza P., Sakkas V., Villioti A., Massolino C., Boti V., Pelizzetti E., Albanis T., (2008). Multivariate experimental design for the photocatalytic degradation of imipramine: Determination of the reaction pathway and identification of intermediate products, Applied Catalysis B: Environmental 84, 379-388.

Carballa M., Omil F., Lema J., (2005). Removal of cosmetic ingredients and pharmaceuticals in sewage primary treatment, Water Research 39, 4790-4796.

Castiglioni S., Bagnati R., Calamari D., Fanelli R., Zuccato E., (2005). A multiresidue analytical method using solid-phase extraction and high-pressure liquid chromatography tandem mass spectrometry to measure pharmaceuticals of different therapeutic classes in urban wastewaters, Journal of Chromatography A 1092, 206-215.

Castiglioni S., Bagnati R., Fanelli R., Pomati F., Calamari D., Zuccato E., (2006). Removal of Pharmaceuticals in Sewage Treatment Plants in Italy, Environmental Science and Technology 40, 357-363.

Castiglioni S., Fanelli R., Calamari D., Bagnati R., Zuccato E., (2004). Methodological approaches for studying pharmaceuticals in the environment by comparing predicted and measured concentrations in River Po, Italy. Regulatory Toxicology and Pharmacology 39, 25-32.

Caviglioli G., Valeria P., Brunella P., Sergio C., Attilia A., Gaetano B., (2002). Identification of degradation products of Ibuprofen arising from oxidative and thermal treatments Journal of Pharmaceutical and Biomedical Analysis 30, 499-509.

Chatzisymeon E., Stypas E., Bousiios S., Xekoukoulotakis N., Mantzavinos D., (2008). Photocatlytic treatment of black table olive processing wastewater, Journal of Hazardous Materials 154, 1090-1097.

Chatzitakis A., Berberidou C., Paspaltsis I., Kyriakou G., Sklaviadis T., Poulios I., (2008). Photocatalytic degradation and drug activity reduction of Chloramphenicol, Water Research 42, 386-394.

Chiron S., Minero C., Vione D., (2006). Photodegradation Processes of the Antiepileptic Drug Carbamazepine, Relevant To Estuarine Waters, Environmental Science and Technology 40, 5977-5983.

Choi K., Kim Y., Park J., Park C., Kim M., Kim H., Kim P., (2008). Seasonal variations of several pharmaceutical residues in surface water and sewage treatment plants of Han River, Korea, Science of the Total Environment 405, 120-128.

Chong M., Jin B., Chow C., Saint C., (2010). Recent developments in photocatalytic water treatment technology: A review, Water Research 44, 2997-3027.

Clara M., Strenn B., Gans O., Martinez E., Kreuzinger N., Kroiss H., (2005). Removal of selected pharmaceuticals, fragrances and endocrine disrupting compounds in a membrane bioreactor and conventional wastewater treatment plants, Water Research 39, 4797-4807.

Cochran W., (2002). Fast Gas Chromatography–Time-of-Flight Mass Spectrometry of Polychlorinated Biphenyls and Other Environmental Contaminants, Journal of Chromatographic Science 40, 254-268.

Coelho A., Sans C., Agüera A., Gómez M., Esplugas S., Dezotti M., (2009). Effects of ozone pre-treatment on diclofenac: Intermediates, biodegradability and toxicity assessment, Science of the Total Environment 407, 3572–3578.

Collin J., Gianluca P., Awang B., Duduku K., (2009). Sonophotocatalysis in advanced oxidation process: A short review, Ultrasonics Sonochemistry 16, 583-589.

Connors A., Amidon L., Stella J., (1986). Chemical Stability of Pharmaceuticals: A Handbook for Pharmacists, second ed., Wiley-Interscience.

Cunningham L. V., Buzby M., Hutchinson T., Mastrocco F., Parke N., Roden N., (2006). Effects of human pharmaceuticals on aquatic life: next steps, Environmental Science and Technology 40, 3456-3462.

Cunningham VI (2008) In Kummerer K (ed) Pharmaceuticals in the environment, Springer, 23-33.

Cunningham, J., Al-Sayyed, G., Srijaranai S., (1994). Adsorption of model pollutants onto TiO_2 particles in relation to photoremedation of contaminated water. In: Helz, G., Zepp, R., Crosby, D. (Eds.), Aquatic and Surface Photochemistry. CRC, Press, Boca Raton, FL, pp. 317–348 (Chapter 22).

Cyprus Water Development Department 2011: Provision of data by the personnel of the department.

Dalrymple OK, Yeh H Daniel, Trotz MA, (2007). Removing pharmaceuticals and endocrine disrupting compounds from wastewater by photocatalysis, Journal of Chemical Technology and Biotechnology 82, 121-134.

Daughton C., Ternes T., (1999). Pharmaceuticals and Personal Care Products in the Environment: Agents of subtle change?, Environmental Health Perspectives 107, 907-938.

Doll T., Frimmel F., (2004). Kinetic study of photocatalytic degradation of carbamazepine, clofibric acid, iomeprol and iopromide assisted by different TiO2 materials-determination of intermediates and reaction pathways, Water Research 38, 955-964.

Doll T., Frimmel F., (2005a). Cross-flow microfiltration with periodical back-washing for photocatalytic degradation of pharmaceutical and diagnostic residues–evaluation of the long-term stability of the photocatalytic activity of TiO_2, Water Research 39, 847-854.

Doll T., Frimmel F., (2005b). Photocatalytic degradation of carbamazepine, clofibricacid and iomeprol with P25 and Hombikat UV100 in the presence of natural organic matter (NOM) and other organic water constituents, Water Research 39, 403-411.

Doll T., Frimmel F., (2005c). Removal of selected persistent organic pollutants by heterogenous photocatalysis in water, Catalysis Today 101, 195-202.

Dollery C., ed. (1991). "Therapeutic Drugs", Edinburgh: Churchill Livingstone.

Dominguez C., Garcia J., Pedraz A., Torres A., Galan A., (1998). Photocatalytic oxidation of organic pollutants in water, Catalysis Today 40, 85-101.

Eichhorn P., Ferguson P., Perez S., Aga D., (2005). Application of Ion Trap-MS with H/D Exchange and QqTOF-MS in the Identification of Microbial Degradates of Trimethoprim in Nitrifying Activated Sludge, Analytical Chemistry 77, 4176-4184.

EMEA, 2006. Note for guidance on environmental risk assessment of medicinal products for human use. CMPC/SWP/4447/draft, London: The European Agency for the Evaluation of Medicinal Products.

Emery J., Papadaki M, Freitas dos Santos M., Mantzavinos D., (2005). Extent of sonochemical degradation and change of toxicity of a pharmaceutical precursor (triphenylphosphine oxide) in water as a function of treatment conditions, Environmental International 31, 207-211.

Emilio C., Litter M., Marinus K., Bouchard M., Colbeau-Justin C., (2006). Phenol degradation on platinized-TiO_2 photocatalysts related to charge-carrier dynamics, Langmuir 22, 3606-3613.

Fatta D, Achilleos A, Nikolaou A, Meriç S., (2007). Analytical methods for tracing pharmaceutical residues in water and wastewater, Trends in Analytical Chemistry 26, 515-533.

Fatta-Kassinos D., Hapeshi E., Achilleos A., Meric S., Gros M., Petrovic M., Barcelo D., (2010). Existence of pharmaceutical compounds in tertiary treated urban wastewater that is utilized for reuse applications, Water Resource Management 25, 1183-1193.

Fent K., Weston A., Caminada D., (2006). Review Ecotoxicology of human pharmaceuticals, Aquatic Toxicology 76, 122-159.

Fernandez C., Doncel M., Carbonell J., Tarazona J., (2010). Occurrence of pharmaceutically active compounds in surface waters of the henares-jarama-tajo river system (Madrid, Spain) and a potential risk characterization, Science of the Total Environment 408, 543-551.

Ghauch A., Baydoun H., Dermesropian P., (2011). Degradation of aqueous carbamazepine in ultrasonic/Fe^0/H_2O_2 systems, Chemical Engineering Journal, Article in Press, Corrected Proof.

Gogate P., Pandit A., (2004). A review of imperative technologies for wastewater treatment I: oxidation technologies at ambient conditions, Advances in Environmental Research 8, 501-551.

Gomez M., Martinez Bueno M., Lacorte S., Fernandez-Alba A., Aguera A., (2007). Pilot survey monitoring pharmaceuticals and related compounds in a sewage treatment plant located on the Mediterranean coast, Chemosphere 66, 993-1002.

Gomez MJ, Martínez Bueno MJ, Lacorte S, Fernández-Alba AR, Agüera A. (2006). Pilot survey monitoring pharmaceuticals and related compounds in a sewage treatment plant located on the Mediterranean coast, Chemosphere 66, 993-1002.

Gros M., Petrović M., Barceló D., (2006). Development of a multi-residue analytical methodology based on liquid chromatography–tandem mass spectrometry (LC–MS/MS) for screening and trace level determination of pharmaceuticals in surface and wastewaters, Talanta 70, 678-690.

Gros M., Petrović M., Barcelo D., (2007). Wastewater treatment plants as a pathway for aquatic contamination by pharmaceuticals in the Ebro river basin (Northeast Spain), Environmental Toxicology and Chemistry 26, 1553-1562.

Grujic S., Vasiljevic T., Lausevic M., (2009). Determination of multiple pharmaceutical classes in surface and ground waters by liquid chromatography–ion trap–tandem mass spectrometry, Journal of Chromatography A 1216, 4989-5000.

Grung M., Källqvist T., Sakshaug S., Skurtveit S., Thomas V., (2008). Environmental assessment of Norwegian priority pharmaceuticals based on the EMEA guideline, Ecotoxicology and Environmental Safety 71, 328-340.

Hada M, Takino M, Yamagami T, Daishima S, Yamaguchi K. (2000). Trace analysis of pesticide residues in water by high-speed narrow-bore capillary gas chromatography-mass spectrometry with programmable temperature vaporizer, Journal of Chromatography A 874, 81–90.

Halling-Sørensen B., Nors Nielsen S., Lanzky P., Ingerslev F., Holten Lützhoft H., Jorgensen S., (1998). Occurrence, fate and effects of pharmaceutical substances in the environment- A review, Chemosphere 36, 357-393.

Hapeshi E., Achilleos A., Vasquez M., Michael I., Xekoukoulotakis N., Mantzavinos D., Kassinos D., (2010). Drugs degrading photocatalytically: Kinetics and mechanisms of ofloxacin and atenolol removal on titania suspensions, Water Research 44, 1737-1746.

Hartmann J., Bartels P., Mau U., Witter M., Tumpling W., Hofmann J., Nietzschmann E., (2008). Degradation of the drug diclofenac in water by sonolysis in presence of catalysts, Chemosphere 70, 453-461.

Heberer T., (2002a). Occurrence, fate, and removal of pharmaceutical residues in the aquatic environment: a review of recent research data. Toxicological Letters, 131, 5-17.

Heberer T., (2002b). Trackling persistent pharmaceutical residues from municipal sewage to drinking water, Journal of Hydrology 266, 175-189.

Heberer T., Feldmann D., Reddersen K., Altmann H., (2001a). Removal of pharmaceutical residues and other persistent organics from municipal sewage and surface waters applying membrane filtration, Water Resources 18-29.

Heberer T., Fuhrmann B., Schmidt-Baumler K., Tsipi D., Koutsouba V., Hiskia A., (2001b). Occurrence of Pharmaceutical Residues in Sewage, River, Ground, and Drinking Water in Greece and Berlin (Germany), ACS Symposium Series, Vol. 79.

Heberer T., Reddersen K., Feldmann D., Zimmermann T., (2000). From municipal sewage to drinking water: Fate and removal of pharmaceutical residues in the aquatic system of Berlin. Lecture at the eleventh annual meeting of the american college of Toxicology (AcTox), November 13th-15th, San Diego, USA.

Hernandez F., Ibanez M., Pozo A., Sancho J., (2008). Investigating the presence of pesticide transformation products in water by using liquid chromatography-mass spectrometry with different mass analyzers, Journal of Mass Spectrometry 43, 173-184.

Hernando D., Mezcua R. Fernández-Alba R., Barcelo D., (2006). Environmental risk assessment of pharmaceutical residues in wastewater effluents, surface waters and sediments, Talanta 69, 334-342.

Herrmann J., (2010). Photocatalysis fundamentals revisited to avoid several misconceptions, Applied Catalysis B: Environmental 99, 461-468.

Herrmann J., Duchamp C., Karkmaz M., Hoai B., Lachheb H., Puzenat E., Guillard C., (2007). Environmental green chemistry as defined by photocatalysis, Journal of Hazardous Materials 146, 624-629.

Hilton M., Thomas K., (2003). Determination of selected human pharmaceutical compounds in effluent and surface water samples by high-performance liquid chromatography–electrospray tandem mass spectrometry, Journal of Chromatography A 1015, 129-141.

Himmelsbach M., Buchberger W., Klampfl C., (2006). Determination of antidepressants in surface and waste water samples by capillary electrophoresis with electrospray ionization mass spectrometric detection after preconcentration using off-line solid-phase extraction, Electrophoresis 27, 1220-1226.

Hochstrat R. and Wintgens T.,(2003). AQUAREC, Report on Milestone M3.I, Draft of wastewater reuse potential estimation, Interim report.

Hochstrat R., Wintgens T., Melin T., Jeffrey P., (2006). Assessing the European wastewater reclamation and reuse potential- a scenario analysis, Desalination 188, 1-8.

Höfl C., Sigl G., Specht O., Wurdack I., Wabner D., (1997). Oxidative degradation of aox and cod by different advanced oxidation processes: A comparative study with two samples of a pharmaceutical wastewater, Water Science and Technology 35, 257-264.

Hofmann J., Freier U., Wecks M., Hohmann S., (2007). Degradation of diclofenac in water by heterogeneous catalytic oxidation with H2O2, Applied Catalysis B: Environmental 70, 447–451.

Hu L, Flanders M., Miller L., Strathmann J., (2007). Oxidation of sulfamethoxazole and related antimicrobial agents by TiO_2 photocatalysis, Water Research 41, 2612-2626.

Hua I., Hochemer R., Hoffmann M., (1995). Sonolytic hydrolysis of p-nitrophenyl acetate: The role of supercritical water, Journal of Physical Chemistry 99, 2335-2342.

Hugget B., Khan A., Foran M., Schlenk D., (2003). Determination of beta-adrenergic receptor blocking pharmaceuticals in United States wastewater effluent, Environmental Pollution 121, 199-205.

Huschek G., Hansen P., Maurer H., Krengel D., Kayser A., (2004). Environmental risk assessment of medicinal products for human use according to European Commission recommendations, Environmental Toxicology 19, 226-240.

Hyotylainen T, Kallio M, Hartonen K, Jussila M., Palonen S, Riekkola M., (2002). Modulator design for comprehensive two-dimensional gas chromatography: Quantitative analysis of polyaromatic hydrocarbons and polychlorinated biphenyls, Analytical Chemistry 74, 4441-4446.

International Water Management Institute (IWMI), 2009. Reducing our water footprint. Water Figures: quarterly newsletter of the International Water Management Institute (IWMI), 1. 8p.

Jones A., Voulvoulis N., Lester N., (2002). Aquatic environmental assessment of the top 25 English prescription pharmaceuticals. Water Research 36, 5013-5022.

Jones O., Voulvoulis N., Lester J., (2007). The occurrence and removal of selected pharmaceutical compounds in a sewage treatment works utilising activated sludge treatment, Environmental Pollution 145, 738-744.

Joss A., Keller E., Alder C., Gobel A., McArdell S., Ternes T., Siegrist H., (2005). Removal of pharmaceuticals and fragrances in biological wastewater treatment, Water Research 39, 3139–3152.

Kampa E., Vidaurre R., Laaser C., Dworak T., (2010). Chapter 2, Policy framework at EU level, Pharmaceuticals in the environment, IWA Publishing.

Kanabar D., Dale S., Rawat M., (2007). A review of ibuprofen and acetaminophen use in febrile children and the occurrence of asthma-related symptoms, Clinical Therapeutics 29, 2716-2723.

Kang S., Kang S., Hur H., (2008). Identification of fungal metabolites of anticonvulsant drug carbamazepine, Applied Microbiology and Biotechnology 79, 663-669.

Kaniou S., Pitarakis K., Barlagianni I., Poulios I., (2005). Photocatalytic oxidation of sulfamethazine, Chemosphere 60, 372-380.

Kasprzyk-Hordern B., Dinsdale R., Guwy A., (2007). Multi-residue method for the determination of basic/neutral pharmaceuticals and illicit drugs in surface water by solid-phase extraction and ultra performance liquid chromatography–positive electrospray ionisation tandem mass spectrometry, Journal of Chromatography A 1161, 132-145.

Kassinos D., Bester K., Kummerer K., (2010a). Xenobiotics in the urban water cycle, Mass flows, Environmental Processes, Mitigation and Treatment strategies, Springer.

Kassinos D., Kalavrouziotis I., Koukoulakis P., Vasquez M., (2010b). The risks associated with wastewater reuse and xenobiotics in the agroecological environment, Science of the Total Environment xxx, xxx-xxx.

Kassinos D., Meric S., Nikolaou A., (2011). Pharmaceutical residues in environmental waters and wastewater: current state of knowledge and future research, Analytical Bioanalytrical Chemistry, 251-275.

Kepp D., Sidelmann U., Tjornelund J., Hansen S., (1997). Simultaneous quantitative determination of the major phase I and II metabolites of ibuprofen in biological fluids by high-performance liquid chromatography on dynamically modified silica, Journal of Chromatography B: Biomedical Sciences and Applications 696, 235-241.

Khetan K., Collins J., (2007). Human pharmaceuticals in the aquatic environment: a challenge to green chemistry. Chemical Reviews 107, 2319-2364.

Klauson D., Babkina J., Stepanova K., Krichevskaya M., Preis S., (2010). Aqueous photocatalytic oxidation of amoxicillin, Catalysis Today 151, 39-45.

Klavarioti M., Mantzavinos D., Kassinos D., (2009). Removal of residual pharmaceuticals from aqueous systems by advanced oxidation processes, Environment International 35, 402-417.

Konstantinou I., Lambropoulou D., Albanis T., (2009). In Fatta-Kassinos D., Kummerer K. (ed.) Xenobiotics in the urban water cycle, 179-194.

Kositzi M., Poulios I., Malato S., Caceres J., Campos A., (2004). Solar photocatalytic treatment of synthetic municipal wastewater**,** Water Research 38, 1147-1154.

Kosjek T., Andersen H., Kompare B., Ledin A., Heath E., (2009). Fate of carbamazepine during water treatment, Environmental Science and Technology 43, 6256-6261.

Kosjek T., Heath E., Kompare B., (2007a). Removal of pharmaceutical residues in a pilot wastewater treatment plant, Analytical Bioanalytrical Chemistry 387, 1379-1387.

Kosjek T., Heath E., Petrovic M., Barcelo D., (2007b). Mass spectrometry for identifying pharmaceutical biotransformation products in the environment, Trends in Analytical Chemistry 26, 1076-1085.

Kostopoulou M., Nikolaou A., (2008). Analytical problems and the need for sample preparation in the determination of pharmaceuticals and their metabolites in aqueous environmental matrices, Trends in Analytical Chemistry 27, 1023-1035.

Kritikos D., Xekoukoulotakis N., Psillakis E., Mantzavinos D., (2007). Photocatalytically degradation of reactive black 5 in aqueous solutions: Effect of operating conditions and coupling with ultrasound irradiation, Water Research 41, 2236-2246.

Kuhn H., Braslavsky S, Schmidt R., (2004). Chemical Actinometry (Iupac Technical Report), Pure Applied Chemistry 76, 2105-2146.

Kuhn H., Braslavsky S., Schmidt R., (1989). Chemical actinometry, Pure and Applied Chemistry 61, 187-210.

Kümmerer K., (2004). Pharmaceuticals in the environment: sources, fate, effects and risks.

Kümmerer K., (2009). The presence of pharmaceuticals in the environment due to human use – present knowledge and future challenges, Journal of Environmental Management 90, 2354-2366.

Lambropoulou D., Konstantinou I., Albanis T., Fernandez-Alba A., (2011). Photocatalytic degradation of the fungicide Fenhexamid in aqueous TiO_2 suspensions: Identification of intermediates products and reaction pathways, Chemosphere 83, 367–378.

Landsdorp D., Vree B., Janssen J., Guelen J., (1990). Pharmacokinetics of rectal diclofenac and its hydroxy metabolites in man, International Journal of Clinical Pharmacology Therapeutic Toxicology 28, 298-302.

Lanhua H., Heather M., Osmarily B., Matthew S., Kelly K., Timothy S., (2009). Oxidation of carbamazepine by Mn (VII) and Fe (VII): Reaction kinetics and mechanism, Environmental Science and Technology, 43, 509–515.

Lepoint T., Mullie F., (1994). What exactly is cavitation chemistry?, Ultrasonics Sonochemistry 1, S13-S22.

Lindberg H., Olofsson I., Rendahl P., Johansson I., Tysklind M., Andersson V., (2006). Behavior of fluoroquinolones and trimethoprim during mechanica, chemical and active sludge treatment of sewage water and digestion of sludge, Environmental Science and Technology 40, 1042-1048.

Lindberg H., Wennberg P., Johansson I., Tysklind M., Andersson V., (2005). Screening of human antibiotic substances and determination of weekly mass flows in five sewage treatment plants in Sweden, Environmental Science and Technology 39, 3421-3429.

Lindqvist N., Tuhkanen T., Kronberg L., (2005). Occurrence of acidic pharmaceuticals in raw and treated sewages and in receiving waters, Water Research 39, 2219-2228.

Löffler D, Meller M, Römbke J, Ternes T., (2004). Environmental Research of the federal ministry of the Environment, Nature, Conservation and Nuclear safety. Behaviour of selected human and veterinary pharmaceuticals in aquatic compartments and soil, Research Report 299, 67 401/01.

Madhavan J., Grieser F., Ashokkumar M., (2010). Combined advanced oxidation processes for the synergistic degradation of ibuprofen in aqueous environments, Journal of Hazardous Materials 178, 202-208.

Mahamuni N., Adewuyi Y., (2009). Optimization of the Synthesis of Biodiesel via Ultrasound-Enhanced Base-Catalyzed Transesterification of Soybean Oil Using a Multifrequency Ultrasonic Reactor, Energy fuels 23, 2757-2766.

Malato S., (2009). Abatement of ibuprofen by solar photocatalysis process: Enhancement and scale up, Catalysis Today 144, 112–116.

Malygina T., Preis S., Kallas J., (2005). The role of pH in aqueous photocatalytic oxidation of β-estradiol, International Journal of Photoenergy 7, 187-191.

Mandrioli R., Albani F., Casamentia G., Sabbionia C. Raggi M., (2001). Simultaneous high-performance liquid chromatography determination of carbamazepine and five of its metabolites in plasma of epileptic patients, Journal of Chromatography B: Biomedical Sciences and Applications 762, 2109-116.

Mantzavinos D., Psillakis E., (2004). Enhancement of biodegradability of industrial wastewaters by chemical oxidation pre-treatment, Journal of Chemical Technology and Biotechnology 79, 431-454.

Marco-Urrea E., Radjenović J., Caminal G., Petrović M., Vicent T., Barcelo D., (2010). Oxidation of atenolol, propranolol, carbamazepine and clofibric acid by a biological Fenton-like system mediated by the white-rot fungus *Trametes versicolor*, Water Research 44, 521-532.

Margulis M., (1992). Fundamental aspects of sonochemistry**,** Ultrasonics 30, 152-155.

Marin J., Sancho J., Pozo O., Lopez F., Hernandez F., (2006). Quantification and confirmation of anionic, cationic, and neutral pesticides and transformation products in water by on-line solid phase extraction-liquid chromatography-tandem mass spectrometry, Journal of Chromatography A 1133, 204-214.

Martin S., Herrmann H., Choi W., Hoffmann M., (1994). Time-resolved microwave conductivity. Part 1. TiO_2 phtoreactivity and size quantization, Journal of the Chemical Society, Faraday Transactions 21, 3315-3322.

Martindale W., ed. (1993). "Martindale: The Extra Pharmacopoeia", 13th edition, The Pharmaceutical Press, London.

Memarian H., Farhadi A., (2008). Sono-thermal oxidation of dihydropyrimidinones, Ultrasonics Sonochemistry 15, 1015-1018.

Mendez-Arriaga F., Esplugas S., Gimenez J., (2008a). Photocatalytic degradation of non-steroidal anti-inflammatory drugs with TiO_2 and simulated solar irradiation, Water Research 42, 585-594.

Mendez-Arriaga F., Esplugas S., Giménez J., (2010). Degradation of the emerging contaminant ibuprofen in water by photo-Fenton, Water Research 44, 589-595.

Mendez-Arriaga F., Torres-Palma R., Petrier C., Esplugas S., Gimenez J., Pulgarin C., (2009). Mineralization enhancement of a recalcitrant pharmaceutical pollutant in water by advanced oxidation hybrid processes, Water Research 43, 3984-3991.

Mendez-Arriaga F., Torres-Palma R., Pétrier C., Esplugas S., Gimenez J., Pulgarin C., (2008b). Ultrasonic treatment of water contaminated with ibuprofen Water Research 42, 4243-4248.

Miao S., Yang J., Metcalfe D., (2005). Carbamazepine and its metabolites in wastewater and in biosolids in a municipal wastewater treatment plant Environmental Science and Technology 39, 7469-7475.

Miao X. and Metcalfe C., (2003). Determination of Carbamazepine and Its Metabolites in Aqueous Samples Using Liquid Chromatography−Electrospray Tandem Mass Spectrometry, Analytical Chemistry 75, 3731–3738.

Moffat A.C., J.V. Jackson, M.S. Moss and B. Widdop, eds. (1986). "Clarke's Isolation and Identification of Drugs", 2nd edition, The Pharmaceutical Press, London.

Moldovan Z., (2006). Occurrences of pharmaceutical and personal care products as micropollutants in rivers from Romania, Chemosphere 64, 1808-1817.

Molinari R., Pirillo F., Loddo V., Palmisano L., (2006). Heterogeneous photocatalytic degradation of pharmaceuticals in water by using polycrystalline TiO_2 and a nanofiltration membrane reactor, Catalysis Today 118, 205-213.

Mompelat S., Bot B., Thomas O., (2009). Occurrence and fate of pharmaceutical products and by-products, from resource to drinking water, Environment International 35, 803-814.

Mrowetz M., Pirola C., Selli E., (2003). Degradation of organic water pollutants through sonophotocatalysis in the presence of TiO_2, Ultrasonics Sonochemistry 10, 247-254.

Mrowetz M., Selli E., (2005). Enhanced photocatalytic formation of hydroxyl radicals on fluorinated TiO_2, Physical Chemistry Chemical Physics 7, 1100-1102.

Munoz D., Martin J., Santos J., Aparicio I., Alonso E., (2010). Occurrence, temporal evolution and risk assessment of pharmaceutically active compounds in Donana Park (Spain), Journal of Hazardous Materials 183, 602-608.

Munoz I., Peral J., Ayllon A., Malato S., Passarinho P., Domenech X., (2006). Life cycle assessment of a coupled solar photocatalytic-biological process for wastewater treatment, Water Research 40, 3533-3540.

Naddeo V., Belgiorno V., Kassinos D., Mantzavinos D., Meric S., (2010). Ultrasonic degradation, mineralization and detoxification of diclofenac in water: Optimization of operating parameters, Ultrasonics Sonochemistry17, 179-185.

Naddeo V., Meriç S., Kassinos D., Belgiorno V., Guida M., (2009). Fate of pharmaceuticals in contaminated urban wastewater effluent under ultrasonic irradiation, Water Research 43, 4019-4027.

Nakada N., Shinohara H., Murata A., Kiri K., Managaki S., Sato N., Takada H., (2007). Removal of selected pharmaceuticals and personal care products (PPCPs) and endocrine-disrupting chemicals (EDCs) during sand filtration and ozonation at a municipal sewage treatment plant, Water Research 41, 4373–4382.

Nakajima T., Gupta V., Ohzawa Y., Groult H., Mazej Z., Zemv B., (2004). Influence of cointercalated HF on the electrochemical behaviour of highly fluorinated graphite, Journal of Power of Sources 137, 80-87.

Nakashima T., Kimizuka N., (2003). Interfacial Synthesis of Hollow TiO_2 Microspheres in Ionic Liquids, Journal of the America Chemical Society 125, 6386-6387.

Nasuhoglu D., Viviane Yargeau V., Berk D., (2011). Photo-removal of sulfamethoxazole (SMX) by photolytic and photocatalytic processes in a batch reactor under UV-C radiation (λmax=254 nm), Journal of Hazardous Materials 186, 67-75.

Neppolian B., Doronila A., Grieser F., Ashokkumar M., (2009). Simple and Efficient Sonochemical Method for the Oxidation of Arsenic (III) to Arsenic (V), Environmental Science and Technology 43, 6793-6798.

Neppolian, B., Choi, H. C., Sakthivel, S., B. Arabindoo, B., Murugesan, V., (2002). Solar/UV-induced photocatalytic degradation of three commercial textile dyes, Journal of Hazardous Materials 89, 303-317.

Nghiem D., Schafer I., Elimelech M., (2005). Pharmaceutical retention mechanisms by nanofiltration membranes, Environmental Science and Technolology 39, 7698-7705.

Nikolaou A, Meric S, Fatta D., (2007). Occurrence patterns of pharmaceuticals in water and wastewater environments, Analytical Bioanalytical Chemistry 387, 1225-1234.

Ohko Y., Luchi K., Niwa C., Tatsuma T., Nakashima T., Iguchi T., Kubota Y., Fujishima A., (2002). 17β-Estradiol Degradation by TiO_2 Photocatalysis as a Means of Reducing Estrogenic Activity, Environmental Science and Technology 36, 4175-4181.

Ollers S., Singer H., Fassler P., Muller S., (2001). Simultaneous quantification of neutral and acidic pharmaceuticals and pesticides at the low-ng/L level in surface and waste water, Journal of Chromatography A 911, 225-234.

Papadam T., Xekoukoulotakis P. N., Poulios I., Mantzavinos D., (2007). Photocatalytic transformation of acid orange 20 and Cr(VI) in aqueous TiO_2 suspensions, Journal of Photochemistry and Photobiology A: Chemistry 186, 308-315.

Paxeus N., (2004). Removal of selected non-steroidal anti-inflammatory drugs (NSAIDs), gemfibrozil, carbamazepine, β-blockers, trimethoprim and triclosan in conventional wastewater treatment plants in five EU countries and their discharge to the aquatic environment, Water Science and Technology 50, 253-260.

Pearce R., Uetrecht J., Leeder J., (2005). Pathways of carbamazepine bioactivation in vitro: II. The role of human cytochrome P450 enzymes in the formation of 2-hydroxyiminostilbene, Drug metabolism and disposition 33, 1819-1826.

Pekakis P., Xekoukoulotakis N., Mantzavinos D., (2006). Treatment of textile dyehouse wastewater by TiO_2 photocatalysis, Water Research 40, 1276-1286.

Peng H., Yu A., (2008a). High frame rate ultrasonic imaging through Fourier transform using an arbitrary known transmission field, Computers and Electrical Engineering 34, 141–147.

Peng X., Yu Yiyi, Tang C., Tan J., Huang Q., Wang Z., (2008b). Occurrence of steroid estrogens, endocrine-disrupting phenols, and acid pharmaceutical residues in urban riverine water of the Pearl River Delta, South China, Science of the Total Environment 397, 158-166.

Perez- Estrada A., Maldonado I., Gernjak W., Aguera A., Fernandez-Alba R., Ballesteros M., Malato S., (2005). Decomposition of diclofenac by solar driven photocatalysis at pilot plant scale, Catalysis Today 101, 219-226.

Pérez S, Eichhorn P., Barcelo D., (2007a). Structural Characterization of Photodegradation Products of Enalapril and Its Metabolite Enalaprilat Obtained under Simulated Environmental Conditions by Hybrid Quadrupole-Linear Ion Trap-MS and Quadrupole-Time-of-Flight-MS, Analytical Chemistry 79, 8293-8300.

Perez S., Barcelo D., (2007b). Application of advanced MS techniques to analysis and identification of human and microbial metabolites of pharmaceuticals in the aquatic environment, Trends in Analytical Chemistry 26, 494-514.

Perez S., Barcelo D., (2008). First evidence for occurrence of hydroxylated human metabolites of diclofenac and aceclofenac in wastewater using QqLIT-MS and QqTOF-MS, Analytical Chemistry 80, 8135-8145.

Pérez S., Eichhorn P., Celiz M., Aga D., (2006). Structural Characterization of Metabolites of the X-ray Contrast Agent Iopromide in Activated Sludge Using Ion Trap Mass Spectrometry, Analytical Chemistry 78, 1866-1874.

Perez-Estrada A., Malato S., Gernjak W., Aquera A., Thurman M., Ferrer I., (2005). Photo-fenton degradation of diclofenac: Identification of the main intermediates and degradation pathway, Environmental Science and Technology 39, 8300-8306.

Petrovic M., Barcelo D., (2007). LC-MS for identifying photodegradation products of pharmaceuticals in the environment, Trends in Analytical Chemistry 26, 486-493.

Petrovic M., Farré M., Lopez de Alda M., Perez S., Postigo C., Köck M., Radjenovic J., Gros M., Barcelo D., (2010). Recent trends in the liquid chromatography–mass spectrometry analysis of organic contaminants in environmental samples, Journal of Chromatography A 1217, 4004-4017.

Petrovic M., Gros M., Barcelo D., (2006). Multi-residue analysis of pharmaceuticals in wastewater by ultra-performance liquid chromatography-quadrupole-time of-flight mass spectrometry, Journal of Chromatography A 1124, 68-81.

Petrovic M., Hernando M., Silvia Diaz-Gruz M., Barcelo D., (2005). Liquid chromatography-tandem mass spectrometry for the analysis of pharmaceutical residues in environmental samples: a review, Journal of Chromatography A 1067, 1-14.

Pharem, (2008). Development and application of innovative advanced oxidation processes for the removal of active organic compounds in urban wastewaters and monitoring of toxicity, AEIFO/0506/16.

Pozo O., Sancho J., Ibanez M., Hernandez F., Niessen W., (2006). Confirmation of organic micropollutants detected in environmental samples by liquid chromatography tandem mass spectrometry: Achievements and pitfalls, Trends in Analytical Chemistry 25, 1030-1042.

Quintana J., Reemtsma T., (2004). Sensitive determination of acidic drugs and triclosan in surface and wastewater by ion-pair reverse-phase liquid chromatography/tandem mass spectrometry, Rapid communications in Mass Spectrometry 18, 765-774.

Quintana J., Weiss S., Reemtsma T., (2005). Pathways and metabolites of microbial degradation of selected acidic pharmaceutical and their occurrence in municipal wastewater treated by a membrane bioreactor, Water Research 39, 2654-2664.

Radjenovic J., Pérez S., Petrovic M., Barcelo D., (2008). Identification and structural characterization of biodegradation products of atenolol and glibenclamide by liquid chromatography coupled to hybrid quadrupole time –of-flight and quadrupole ion trap mass spectrometry, Journal of Chromatography A 1210, 142-153.

Radjenovic J., Petrovic M., Barcelo D., (2009). Fate and distribution of pharmaceuticals in wastewater and sewage sludge of the conventional activated sludge (CAS) and advanced membrane bioreactor (MBR) treatment, Water Research 43, 831-841.

Rafqah S., Wong-Wah-Chung P., Nelieu S., Einhorn J., Sarakha M., (2006). Phototransformation of triclosan in the presence of TiO_2 in aqueous suspension: Mechanistic approach, Applied Catalysis B: Environmental 66, 119-125.

Ragaini F., Cenini S., Gasperini M., (2001). Reduction of nitrobenzene to aniline by CO/H_2O, catalysed by Ru3(CO)12/chelating diimines, Journal of Molecular Catalysis A: Chemical 174, 51–57.

Reemtsma T., (2003). Liquid chromatography–mass spectrometry and strategies for trace-level analysis of polar organic pollutants, Journal of Chromatography A 1000, 477-501.

Rincón A., Pulgarin C., (2004). Effect of pH, inorganic ions, organic matter and H_2O_2 on E. coli K12 photocatalytic inactivation by TiO_2: Implications in solar water disinfection, Applied Catalysis B: Environmental 51, 283-302.

Rizzo L., Meric S., Kassinos D., Guida M., Russo F., Belgiorno V., (2009). Degradation of diclofenac by TiO_2 photocatalysis: UV absorbance kinetics and process evaluation through a set of toxicity bioassays, Water Research 43, 979–988.

Robert D., Malato S., (2002). Solar photocatalysis: a clean process for water detoxification, The science of the Total Environment 291, 85-97.

Roberts P., Thomas K., (2006). The occurrence of selected pharmaceuticals in wastewater effluent and surface waters of the lower Tyne catchment, Science of the Total Environment 356, 143-153.

Roig B., (2010). Pharmaceuticals in the environment: Current knowledge and need assessment to reduce presence and impact,Chapter 2, IWA Publishing.

Rosario-Ortiz F., Wert E., Snyder S., (2010). Evaluation of UV/H_2O_2 treatment for the oxidation of pharmaceuticals in wastewater, Water Research 44, 1440-1448.

Rosenfeldt E., Chen P., Kullman S., Linden K., (2007). Destruction of estrogenic activity in water using UV advanced oxidation, Science of The Total Environment 377, 105-113.

Ruiz-Reyes N., Vera-Candeasa P., Curpián-Alonso J., Cuevas-Martineza J., López-Ferreras F., (2006). RETRACTED: Matching pursuit-based approach for ultrasonic flaw detection, Signal Processing 86, 962-970.

Sacher F., Lange F., Brauch H., Blankenhorn I., (2001). Pharmaceuticals in groundwaters: Analytical methods and results of a monitoring program in Baden-Württemberg, Germany, Journal of Chromatography A 938, 199-210.

Sakkas V., Calza P., Medana C., Villioti A., Baiocchi C., Pelizzetti E., Albanis T., (2007). Heterogeneous photocatalytic degradation of the pharmaceutical agent salbutamol in aqueous titanium dioxide suspensions, Applied Catalysis B: Environmental 77, 135-144.

Sammartino P., Bellanti F., Castrucci M., Ruiu D., Visco G., Zoccarato T., (2008). Ecopharmacology: deliberated or casual dispersion of pharmaceutical principles, phytosanitary, personal health care and veterinary products in environment needs a multivariate analysis or expert systems for the control, the measure and the remediation, Journal of Microchemistry 88, 201–210.

Sanchez-Prado L., Barro R., Garcia-Jares C., Llompart M., Lores M., Petrakis C., Kalogerakis N., Mantzavinos D., Psillakis E., (2008). Sonochemical degradation of triclosan in water and wastewater, Ultrasonics Sonochemistry 15, 689-694.

Sancho J., Pozo O., Ibanez M., Hernandez F., (2006). Potential of liquid chromatography/time-of-flight mass spectrometry for the determination of pesticides and transformation products in water, Analytical and Bioanalytical Chemistry 386, 987-997.

Shemer H., Kunukcu Y., Linden K., (2006). Degradation of the pharmaceutical Metronidazole via UV, Fenton and photo-Fenton processes, Chemosphere 63, 269-276.

Shirgaonkar I., Pandit A., (1998). Sonophotochemical destruction of aqueous solution of 2,4,6-trichlorophenol, Ultrasonics Sonochemistry 5, 53–61.

Silva, A., M. T., Nouli, E., Xekoukoulotakis, N. P., Mantzavinos, D., (2007). Effect of key operating parameters on phenols degradation during H_2O_2-assisted TiO_2 photocatalytic treatment of simulated and actual olive mill wastewaters. Applied Catalysis B-Environmental 73, 11-22.

Sim W., Lee J., Oh J., (2010). Occurrence and fate of pharmaceuticals in wastewater treatment plants and rivers in Korea, Environmental Pollution 158, 1938-1947.

Sioi M., Bolosis A., Kostopoulou E., Poulios I., (2006). Photocatalytic treatment of colored wastewater from medical laboratories: Photocatalytic oxidation of hematoxylin, Journal of Photochemistry and Photobiology A: Chemistry 184, 18-25.

Sirtori C., Zapata A., Gernjak W., Malato S., Lopez A., Aguera A., (2011). Solar photo-fenton degradation of nalidixic acid in waters and wastewaters of different composition. Analytical assessment by LC-TOF-MS, Water Research 45, 1736-1744.

Skoumal M., Rodríguez R., Cabot P., Centellas F., Garrido J., Arias C., Brillas E., (2009). Electro-Fenton, UVA photoelectro-Fenton and solar photoelectro-Fenton degradation of the drug ibuprofen in acid aqueous medium using platinum and boron-doped diamond anodes, Electrochimica Acta 54, 2077-2085.

Soulet B., Tauxe A., Tarradellas J., (2002). Analysis of acidic drugs in Swiss wastewaters, International Journal of Environmental Analytical Chemistry 82, 659–667.

Spongberg A., Witter J., (2008). Pharmaceutical compounds in the wastewater process stream in Northwest Ohio, Science of the Total Environment 397, 148-157.

Statistical Service of Cyprus, (2005). Demographic Report.

Steene J., Stove C., Lambert W., (2010). A field on 8 pharmaceuticals and 1 pesticide in Belgium: Removal rates in waste water treatment plants and occurrence in surface water, Science of the Total Environment 408, 3448-3453.

Stolker AAM, Niesing W, Hogendoorn EA, Versteegh JFM, Fuchs R, Brinkman UAT, (2004). Liquid chromatography with triple-quadrupole or quadrupole-time of flight mass spectrometry for screening and confirmation of residues of pharmaceuticals in water, Analytical Bioanalytical Chemistry 378, 955–963.

Stuer-Lauridsen F., Birkved M., Hansen L. P., Lützhoft H.-C. H., Halling-Sùrensen B. (2000). Environmental risk assessment of human pharmaceuticals in Denmark after normal therapeutic use, Chemosphere 40, 783-793.

Stumpf M., Ternes T., Wilken D., Rodrigues V., Baumann W., (1999). Polar drugs residues in sewage and natural waters in the state of Rio de Janeiro, Brazil, Science Total Environment 225, 135-141.

Suri R., Nayak M., Devaiah U., Helmig E., (2007). Ultrasound assisted destruction of estrogen hormones in aqueous solution: Effect of power density, power intensity and reactor configuration, Journal of Hazardous Materials 146, 472–478.

Taghizadeh M., Abdollahi R., (2011). Sonolytic, sonocatalytic and sonophotocatalytic degradation of chitosan in the presence of TiO_2 nanoparticles, Ultrasonics Sonochemistry 18, 149-157.

Tanizaki T., Kadokami K., Shinohara R., (2002). Catalytic Photodegradation of Endocrine Disrupting Chemicals Using Titanium Dioxide Photosemiconductor Thin Films, Bulletin of Environmental Contamination and Toxicology 68, 732-739.

Ternes T. and J. Andriano, ed. (2007). "Human Pharmaceuticals, Hormones and Fragrances, The challenge of micropollutants in urban water management", IWA.

Ternes T., (1998). Occurrence of drugs in German sewage treatment plants and rivers, Water Research 32, 3245-3260.

Ternes T., (2001). Analytical methods for the determination of pharmaceuticals in aqueous environmental samples, Trends in Analytical Chemistry 20, 419-434.

Thompson H. and Doraiswamy K., (2009), Sonochemistry: Science and engineering, Industrial and Engineering Chemistry Research 38, 1215-1249.

Trovo A., Nogueira R., Agüera A., Sirtori C. Fernandez-Alba A., (2009). Photodegradation of sulfamethoxazole in various aqueous media: Persistence, toxicity and photoproducts assessment, Chemosphere 77, 1292-1298.

Unceta N., Sampedro M., Bakar N., Caballero A., Goicolea M., Barrio R., (2010). Multi residue analysis of pharmaceutical compounds in wastewaters by dual solid-phase microextraction coupled to liquid chromatography electrospray ionization ion trap mass spectrometry, Journal of Chromatography A, 1217, 3392-3399.

UNEP, (2000). Water and wastewater reuse – An environmentally sound approach for sustainable urban water management.

United Nations Environment Programme (UNEP), (2002a). 'State of the Environment and Policy Perspective: 1972-2002', Global Environment Outlook 3, pp. 150-179, Division of Early Warning and Assessment (DEWA), Kenya.

Vanderford B., Pearson R., Rexing D., Snyder S., (2003). Analysis of Endocrine Disruptors, Pharmaceuticals, and Personal Care Products in Water Using Liquid Chromatography/Tandem Mass Spectrometry, Analytical Chemistry 75, 6265-6274.

Vieno N., Tuhkanen T., Kronberg L., (2006). Analysis of neutral and basic pharmaceuticals in sewage treatment plants and in recipient rivers using solid phase extraction and liquid chromatography–tandem mass spectrometry detection, Journal of Chromatography A 1134, 101-111.

Vieno N., Tuhkanen T., Kronberg L., (2007). Elimination of pharmaceuticals in sewage treatment plants in Finland, Water Research 41, 1001-1012.

Vissers J., Kearney G., Major H., Leerdam J., (2001). Screening and identification of unknown contaminants in water with liquid chromatography and quadrupole-orthogonal acceleration-time-of-flight tandem mass spectrometry, Journal of Chomatography A 929, 63-74.

Vogna D., Marotta D., Andreozzi R., Napolitano A., Ischia M., (2004a). Kinetic and chemical assessment of the UV/H_2O_2 treatment of antiepileptic drug carbamazepine, Chemosphere 54, 497–505.

Vogna D., Marotta D., Napolitano A., Andreozzi R., Ischia M., (2004b). Advanced oxidation of the pharmaceutical drug diclofenac with UV/H_2O_2 and ozone, Water Research 38, 414-422.

Vogna D., Marotta D., Napolitano A., Ischia M., (2002). Advanced oxidation chemistry of paracetamol. UV/H_2O_2- induced hydroxylation/degradation pathways and 15N-aided inventory of nitrogenous breakdown products, Journal of Organic Chemistry 67, 6143-6151.

WHO and UNICEF (2010). Report of the JMP Technical Task Force Meeting Monitoring of drinking-water quality Villié-Morgon, France, 16-18 November.

William A. Arnold and Kristopher McNeill, Transformation of pharmaceuticals in the environment: Photolysis and other abiotic processes, Chapter 3.2.

World Health Organization (WHO) and United Nations Children's Fund (UNICEF) (2000). Global Water Supply and Sanitation Assessment, USA.

Xekoukoulotakis N., Xinidis N., Chroni M., Mantzavinos D., Venieri D., Hapeshi E., Fatta-Kassinos D., (2010). UV-A/TiO_2 photocatalytic decomposition of erythromycin in water: Factors affecting mineralization and antibiotic activity, Catalysis Today 151, 29-33.

Yamamoto S., Barnouin-Jha O., Toriumi T., Sugita S., Matsui T., (2009). An empirical model for transient crater growth in granular targets based on direct observations, Icarus 203, 310–319.

Yang H., Li G., An T., Gao Y., Fu J., (2011). Photocatalytic degradation kinetics and mechanism of environmental pharmaceuticals in aqueous suspension of TiO_2: A case of sulfa drugs, Catalysis Today 153, 200-207.

Yang L., Yu E., Ray B., (2008). Degradation of paracetamol in aqueous solutions by TiO_2 photocatalysis, Water Research 42, 3480-3488.

Yoon Y., Ryu J., Oh J., Choi B., Snyder S., (2010). Occurrence of endocrine disrupting compounds, pharmaceuticals, and personal care products in the Han River (Seoul, South Korea), Science of the Total Environment 408, 636-643.

Yu T., Bouwer J., Coelhan M., (2006). Occurrence and biodegradability studies of selected pharmaceuticals and personal care products in sewage effluent. Agricultural, Water Management 86, 72–80.

Yurdakal S., Loddo V., Augugliaro V., Berber H., Palmisano G., Palmisano L., (2007). Photodegradation of pharmaceutical drugs in aqueous TiO_2 suspensions: Mechanism and kinetics, Catalysis Today 129, 9-15.

Zhang X.,Wu F., Wu X., Chen P., Deng N., (2008). Photodegradation of acetaminophen in TiO_2 suspended solution, Journal of Hazardous Materials 157, 300-307.

Zhao X., Hou Y., Liu H., Qiang Z., Qu J., (2009). Electro-oxidation of diclofenac at boron doped diamond: Kinetics and mechanism, Electrochimica Acta 54, 4172–4179.

Zheng B., Zheng Z., Zhang J., Luo X., Wang J., Liu Q., Wang L., (2011). Degradation of the emerging contaminant ibuprofen in aqueous solution by gamma irradiation, Desalination xxx, xxx-xxx.

Zwiener C., Seeger S., Glauner T., Frimmel F., (2002). Metabolites from the biodegradation of pharmaceutical residues of ibuprofen in biofilm reactors and batch experiments, Analytical Bioanalytical Chemistry 372, 569–575.